

QATAR UNIVERSITY

COLLEGE OF ARTS AND SCIENCES

DEVELOPMENT OF A NOVEL POLYMER-MODIFIED GRAPHENE OXIDE  
NANOCOMPOSITES FOR CONTROLLING CALCIUM SULFATE SCALING AND  
BIOFOULING ON REVERSE OSMOSIS MEMBRANE: MECHANISTIC STUDY

BY

MOHAMMAD YOUSAF ASHFAQ

A Dissertation Submitted to  
the College of Arts and Sciences  
in Partial Fulfillment of the Requirements for the Degree of  
Doctorate in Philosophy in Biological and Environmental Sciences

June 2020

© 2020. Mohammad Yousaf Ashfaq. All Rights Reserved.

## COMMITTEE PAGE

The members of the Committee approve the Dissertation of  
Mohammad Yousaf Ashfaq defended on 05/05/2020.

---

Dr. Mohammad Al-Ghouti  
Thesis/Dissertation Supervisor

---

Prof. Nabil Zouari  
Co-Supervisor

---

Prof. Hazim Qiblawey  
Committee Member

Approved:

---

Ibrahim AlKaabi, Dean, College of Arts and Sciences

## ABSTRACT

ASHFAQ, MOHAMMAD, YOUSAF., Doctorate, June: 2020,

Biological and Environmental Science

Title: Development of a Novel Polymer-modified Graphene Oxide Nanocomposite for controlling Calcium Sulfate Scaling and Biofouling on Reverse Osmosis Membrane: Mechanistic Study

Supervisor of Dissertation: Dr. Mohammad A. Al-Ghouti.

Reverse Osmosis (RO) is a promising environment friendly desalination technology for clean water production. However, the performance of RO is getting affected by the mineral scaling and biofouling. During this research, various unknown interactions occurring in RO systems between minerals, microorganisms, antiscalants and antimicrobial nanomaterials were investigated.

The first goal of this dissertation was to understand and investigate the calcium sulfate scaling on reverse osmosis membranes in terms of effect of different concentrations of calcium ions and effect of temperature of feedwaterfeed water. It was noted that the mineral scaling tends to increase with the increase in temperature and concentration of ions. Moreover, the results showed that the functional groups of membranes such as hydroxyl and carboxyl, tend to interact with gypsum during scaling.

To investigate the interaction of seawater microorganisms with antiscalants and with calcium sulfate, various bacterial strains were isolated and identified from Gulf seawater. The identification results showed that the isolated bacteria include *Halomonas aquamarina*, *Pseudomonas fragi*, *Pseudomonas stutzeri* and others. It was noted that the bacterial strains have the capability to utilize antiscalants as a carbon and

energy source, thereby, degrading them and making them ineffective against scaling. Moreover, the isolated bacterial strains were also found to be capable of mediating/inducing calcium sulfate precipitation on RO membranes. The results of these interactions showed that microorganisms may enhance mineral scaling via (i) biodegradation of antiscalants and (ii) biomineralization of calcium sulfate. Therefore, it is important to modify RO membranes to tackle both mineral scaling and biofouling, simultaneously.

In this research, the polyamide RO membranes were modified with antimicrobial nanomaterial (graphene oxide) and polymer antiscalants to improve the surface characteristics of RO membranes and to give rise to antifouling characteristics in membranes. The results showed that the newly modified membranes have the capability to control calcium sulfate scaling. In addition, the antibiofouling tests performed through determining bacteriostasis rates also showed that the modified membranes inhibited the growth of bacteria. Overall, the results of this research provided in-depth information about various interactions occurring in RO systems and demonstrated the potential of membrane modification technique to control various types of membrane fouling, simultaneously.

## DEDICATION

*I would like to dedicate my thesis to my family members and my friends,  
especially to those who have been the motivation behind all my hard work,  
but are no longer with me.*

## ACKNOWLEDGMENTS

In the name of **Allah**, the most Gracious and the most Merciful who made me capable enough to do the work without being dispirited. I thank Allah for blessing me with the strength and patience.

I would love to pay my humble gratitude to **Dr. Mohammad Al-Ghouti** for providing me with the opportunity, supervision, guidance, continuous encouragement, and support throughout my PhD journey. I would also like to thank **Prof. Nabil Zouari** (as my Co-Supervisor) and **Prof. Hazim Qiblawey** (as a Committee member) for all their precious time, efforts, and guidance during this research. The inputs from my Supervisory committee has always guided me in my research and helped me in moving forward to achieve my objectives.

I would also like to thank all my Professors who taught me various courses which helped me to gain new knowledge and skills namely: Dr. Radhouane Ben Hamadou, Prof. Samir Jaoua, Dr. Allal Ouhtit, Dr. Perumal Balakrishnan, Dr. Haissam Abou Saleh, and Prof. Ayman Bakleezi. I am indeed humbly grateful to the Department of Biological and Environmental Sciences, Dr. Mohammed Abu-Dieyeh as a Head of Department for providing all the necessary facilities and to Mr. Abdol Ali, Mr. Abdul Mateen, Mr. Habib and Mr. Saeed as Laboratory Technicians for their assistants and support during research. I would also like to thank Ms. Dana A. Da'na, Ms. Randa Zedan, Ms. Shazia Bibi for her assistance during practical work and my colleagues Dr. Zulfa Al-Disi for her valuable inputs and suggestions. I am also thankful to Central Laboratory Unit and Center for Advanced materials for analyzing my samples. I would also like to pay my gratitude to Ms. Summaiya Arshad for her efforts and assistance during this research.

I am extremely grateful to Microbiology Laboratory, Department of Lab, Medicine and Pathology in Hamad General Hospital for their support throughout my PhD journey especially Ms. Fatma Al Mohannadi, and Ms. Khloud Al-Qadi as Supervisors and Dr. Emad Elmagboul as a Head of Department.

Finally, this would have not been possible without the moral support and love of my parents, wife, siblings and my in-laws. I thank them for being there; to support and encourage me during my hard times.

## TABLE OF CONTENTS

DEDICATION .....	v
ACKNOWLEDGMENTS .....	vi
LIST OF TABLES .....	xv
LIST OF FIGURES .....	xvii
CHAPTER 1: INTRODUCTION .....	25
1.1 Background .....	25
1.2 Physical-Chemical-Biological interactions in RO system .....	27
1.3 Research Rationale .....	34
1.4 Research Focus.....	35
1.4.1 Research Questions.....	35
1.4.2 Research Objectives .....	36
CHAPTER 2: LITERATURE REVIEW .....	38
2.1 Reverse Osmosis .....	38
2.2 Membrane Structures .....	39
2.3 Reverse osmosis process parameters.....	42
2.3.1 Percentage membrane rejection.....	42
2.3.2 Salt Passage % .....	43
2.3.3 Mass Balance .....	43
2.3.4 Recovery .....	43



2.3.5 Permeate Flux .....	44
2.3.6 Membrane Resistance .....	44
2.4 Membrane Fouling .....	48
2.4.1 Concentration Polarization (CP) and Fouling .....	50
2.4.2 Types of Fouling.....	51
2.5 Anti-Biofouling and Anti-Scaling.....	67
2.5.1 Membrane coating using polymers and nanomaterials for anti-biofouling.	68
2.5.2 Membrane coating using nanomaterials for anti-scaling.....	71
2.6 Analytical techniques used to characterize scaling. ....	74
2.6.1 Scanning Electron Microscopy (SEM).....	74
2.6.2 X-ray Diffraction (XRD).....	76
2.6.3 X-ray Fluorescence (XRF). ....	77
2.6.4 X-ray Photoelectron Spectroscopy (XPS). ....	78
2.6.5 Fourier Transform Infrared Spectroscopy (FTIR).....	79
2.6.6 Other Techniques.....	81
CHAPTER 3: METHODOLOGY .....	83
3.1 Investigating effect of calcium ions and temperature on scaling .....	83
3.1.1 Membranes used .....	83
3.1.2 Model scaling solutions .....	83
3.1.3 Membrane filtration experiments .....	85

3.1.4 Scaled membrane characterization .....	88
3.1.5 Contact angle measurements .....	88
3.1.6 Multivariate Analysis .....	89
3.2 Isolation, Identification and Differentiation of antiscalant degrading bacteria..	89
3.2.1 Seawater Samples Collection .....	90
3.2.2 Isolation of Microorganisms from Seawater .....	91
3.2.3 Screening of Antiscalant degrading Bacteria .....	92
3.2.4 Identification of isolates by MALDI-TOF MS.....	93
3.3 Interaction between microorganisms and antiscalants on RO membranes .....	95
3.3.1 Media Preparation.....	95
3.3.2 Inoculum preparation.....	95
3.3.3 RO Membrane .....	95
3.3.4 Biofilm growth assay .....	96
3.3.5 Qualitative analysis of biofilm .....	96
3.3.6 Quantitative analysis of bacterial cells in biofilm (Serial dilution).....	97
3.4 Interaction between Seawater Microorganisms and CaSO <sub>4</sub> scaling .....	98
3.4.1 Seawater microorganisms.....	98
3.4.2 Bacterial growth medium .....	98
3.4.3 Modified media for biomineralization studies.....	99
3.4.4 Biomineralization studies using solid media .....	99

3.4.5	Biom mineralization studies using liquid media .....	99
3.4.6	Effect of calcium and sulfate ions on bacterial growth .....	100
3.4.7	Protein profiles of biom mineralizing strains .....	101
3.4.8	Statistical analysis.....	102
3.5	Development of polymer modified graphene oxide coated RO membranes)..	102
3.5.1	Materials and Chemicals .....	102
3.5.2	Functionalization of RO membranes with Graphene oxide (GO) nanomaterials.....	103
3.5.3	Polymerization of acrylic acid or maleic acid on GO@RO membranes...	103
3.5.4	Membrane permeability and separation experiments .....	106
3.5.5	Membrane scaling experiments .....	106
3.5.6	Membrane biofouling studies .....	107
3.5.7	Inhibition of minerals precipitation and microbial growth, simultaneously .....	108
3.5.8	Membrane surface characterization.....	109
 CHAPTER 4 – OBJECTIVE 01: UNDERSTANDING EFFECTS AND MECHANISMS OF ANTI-MICROBIAL NANOMATERIALS (GO) ON CALCIUM SULFATE SCALING.....		
4.1	Effect of concentration of calcium and sulfate ions on gypsum scaling of RO and Graphene oxide (GO) coated RO membranes.....	111
4.1.1	Introduction .....	111

4.1.2 Results and Discussion .....	113
4.1.3 Conclusion .....	135
4.2 Effect of temperature on gypsum scaling of RO and GO coated RO membranes .....	136
4.2.1 Introduction .....	136
4.2.2 Results and Discussion .....	138
4.2.3 Conclusion .....	164
<b>CHAPTER 5 – OBJECTIVE 02: DEMONSTRATE AND DETERMINE BIODEGRADATION OF POLYMER ANTISCALANTS USED IN REVERSE OSMOSIS SYSTEMS .....</b>	<b>166</b>
5.1 Isolation, Identification and Differentiation of antiscalant degrading bacteria	166
5.1.1 Introduction .....	166
5.1.2 Results and Discussion .....	170
5.1.3 Conclusion .....	186
5.2 Investigating the effect of antiscalants on biofouling of RO membranes .....	187
5.2.1 Introduction .....	187
5.2.2 Results .....	191
5.2.3 Discussion.....	204
5.2.4 Conclusion .....	209
<b>CHAPTER 6 – OBJECTIVE 03: INVESTIGATING THE INTERACTIONS BETWEEN MICROORGANISMS AND CALCIUM SULFATE IN RO SYSTEM</b>	

.....	211
6.1 Introduction .....	211
6.2 Results .....	214
6.2.1 Formation of CaSO <sub>4</sub> crystals in solid medium (Light Microscopy investigation) .....	214
6.2.2 Precipitation of CaSO <sub>4</sub> on the RO membrane and in the biofilm .....	216
6.2.3 Kinetics and effect of calcium ions concentration on CaSO <sub>4</sub> biomineralization .....	222
6.2.4 Attachment of bacteria and biofilm formation on the surface of gypsum crystals .....	228
6.2.5 Role of proteins in biomineralization of CaSO <sub>4</sub> .....	229
6.2.6 Effect of calcium ions on bacterial growth .....	231
6.3 Discussion .....	232
6.4 Conclusion and Future Perspectives .....	239
 CHAPTER 7 – OBJECTIVE 04: DETERMINE WHETHER NEW COATINGS (GO-PAA, GO-PMA) WILL PREVENT BIOFOULING AND SCALING .....	 241
7.1 Introduction .....	241
7.2 Results and Discussion .....	244
7.2.1 Membrane surface characterization .....	244
7.2.2 Membrane scaling experiment .....	251
7.2.3 Biofouling tests .....	257

7.2.4 Simultaneous inhibition of mineral scaling and biofouling.....	258
7.3 Conclusion.....	261
CHAPTER 8: CONCLUSION AND FUTURE PERSPECTIVES.....	263
REFERENCES .....	266
APPENDIX A: PUBLICATION FROM LITERATURE REVIEW.....	313
APPENDIX B: PUBLICATION FROM OBJECTIVE 01.....	314
APPENDIX C: PUBLICATIONS FROM OBJECTIVE 2 .....	315
APPENDIX D: PUBLICATIONS FROM OBJECTIVE 3 .....	317

## LIST OF TABLES

Table 1. Known and Unknown phenomena/interactions in RO Systems.....	32
Table 2. Advantages and Disadvantages of Asymmetric and Composite Membranes	41
Table 3. Types of Membrane Resistance and their Measurement Methods .....	47
Table 4. Organic and Inorganic colloids involved in Colloidal Fouling .....	60
Table 5. Factors affecting Biofilm Formation (Nguyen et al., 2012; Flemming and Ridgway, 2009).....	65
Table 6. Comparison of Different Techniques used to Study Membrane Scaling .....	80
Table 7. Solution compositions and SI of different polymorphs of calcium sulfate at 30°C.....	85
Table 8. Effect of concentration of calcium ions on permeate flux, membrane resistances and % salt rejection.....	119
Table 9. Comparison of scale layer thickness and density with the literature at different conditions.....	124
Table 10. Peak Shifts through Comparison between the Pure Gypsum and the Gypsum Scaled Membrane.....	131
Table 11. Properties of RO and GO-RO membranes (Ashfaq et al., 2020a).....	139
Table 12. Effect of temperature on membrane resistance and percentage rejection (Ashfaq et al., 2020a).....	144
Table 13. Total mass of crystals and thickness of scaled layer on the membranes at different temperatures (Ashfaq et al., 2020a). .....	145
Table 14. Peak shifts through comparison between the pure gypsum and the gypsum scaled membrane (Ashfaq et al., 2020a) .....	160
Table 15. Identification of isolated strains from Seawater samples using MALDI-TOF-	

MS (Ashfaq et al., 2019a) .....	172
Table 16. Peak assignments to characterize biofilm layer (Boubakri and Bouguecha, 2008; Karime et al. 2008; Krishnamurthy et al. 2010; Xu et al. 2010; Rabiller-Baudry et al. 2012; Dixit et al. 2014) (Ashfaq et al., 2019b) .....	195



## LIST OF FIGURES

Figure 1. Schematic illustration of Physical-Chemical-Biological interaction in RO systems.....	31
Figure 2. Identification of "Research gaps" in physical-chemical-biological interactions in RO systems .....	33
Figure 3. Cross section of Thin Film Composite membrane (Akin and Temelli, 2011). .....	41
Figure 4. Schematic representation of different resistances during filtration (Shirazi et al., 2010) .....	46
Figure 5. Mechanism of membrane fouling.....	49
Figure 6. Contributing factors and steps in scale formation (adopted from Antony et al., 2011) .....	55
Figure 7. Conceptual representation of scaling (Shih et al., 2005).....	56
Figure 8. (a) Monoclinic gypsum crystal morphology (numbers in parenthesis represent crystal orientation); (b) SEM image of gypsum crystal on membrane (Shih et al., 2005) .....	59
Figure 9. Five steps of Biofilm formation (1: Initial attachment, 2: Irreversible attachment, 3: Initial growth, 4: Final growth, 5: Dispersion) (Monroe, 2007) .....	64
Figure 10. Example of some polymers and nanomaterials used recently for anti-biofouling research. (Chae et al. 2017, Chae et al. 2015, Ginic-Markovic et al. 2015, Shafi et al. 2015, Blok et al. 2014, Matin et al. 2014, Saeki et al. 2014a, Saeki et al. 2014b, Zhang et al. 2013) .....	70
Figure 11. Enhancement of permeate flux using some nanomaterials for RO anti-scaling research. (Chae et al. 2017; Kim et al. 2016; Bao et al. 2013; Chan et al. 2013; Yin et	

al. 2012; Fathizadeh et al. 2011; Zhang et al. 2011).....	73
Figure 12. Principle of X-ray diffraction, where d is the distance between crystalline planes (Atkins, 2002) .....	77
Figure 13. X-ray Photoelectron and X-ray Fluorescence Spectroscopy (Seltzer, 1993) .....	78
Figure 14. Process flow diagram of the membrane scaling experiments (Ashfaq et al., 2020a). .....	86
Figure 15. Seawater sampling locations map (A) 7 sampling locations; (B) Enhanced view showing two sampling sites situated near desalination plant (QONSW – Qatar Onshore seawater, QOFSW – Qatar offshore seawater) .....	91
Figure 16. Qualitative and Quantitative analysis of biofilm formation conducted in 24-wells microtiter plate (modified from Lutskiy et al. 2015; Jung et al. 2018) .....	97
Figure 18. Flux decline curves obtained at different concentration of Calcium ions (A) RO membrane, (B) GO-RO membrane, (C) Correlation between Flux decline and concentration of calcium ions, (D) PCA for flux decline over time;.....	118
Figure 19. SEM-EDX analysis for scaled membranes at concentrations of 20 and 30 mM.....	126
Figure 20. SEM-EDX analysis for scaled membranes at concentrations of 50 to 150 mM.....	128
Figure 21. XRD results of deposits on RO and GO-RO membranes (A) Low concentration of calcium ions (20 and 30 mM); (B) High concentration of calcium ions (50 – 150 mM). .....	129
Figure 22. FTIR spectra of the scaled membranes (A) $Ca^{+2} = 20$ mM; (B) $Ca^{+2} = 30$ mM (C) $Ca^{+2} = 50$ to 150 mM. The black colored arrows and texts refers to the	

functional groups of membrane and red-colored to the functional groups of gypsum. .....	133
Figure 23. Contact angle ( $^{\circ}$ ) for gypsum scaled membranes at different concentration of calcium ions in feedwater. ....	135
Figure 24. Flux decline curves for Solution 1 ( $\text{Ca}^{+2}=20$ mM) obtained using (a) RO membrane; (b) GO-RO membrane; and for Solution 2 ( $\text{Ca}^{+2}=50$ mM) obtained using (c) RO membrane; (d) GO-RO membrane; and PCA graphs for (e) Solution 1, $\text{Ca}^{+2}=20$ mM, (f) Solution 2, $\text{Ca}^{+2}=50$ mM (Ashfaq et al., 2020a). ....	142
Figure 25. Correlation between mass of scales on the membrane with temperature for RO membrane (a) Solution 1 ( $\text{Ca}^{+2}=20$ mM), (b) Solution 2 ( $\text{Ca}^{+2}=50$ mM) and for GO-RO membrane (c) Solution 1 ( $\text{Ca}^{+2}=20$ mM), (d) Solution 2 ( $\text{Ca}^{+2}=50$ mM) (Ashfaq et al., 2020a).....	146
Figure 26. SEM-EDX analysis of scaled membrane at different temperatures for Solution 1, $\text{Ca}^{+2}=20$ mM (Ashfaq et al., 2020a).....	153
Figure 27. SEM-EDX analysis of the scaled membrane at different temperatures for Solution 2, $\text{Ca}^{+2}=50$ mM (Ashfaq et al., 2020a).....	156
Figure 28. XRD spectra of $\text{CaSO}_4$ precipitates at different temperatures; (A) RO membrane (Solution 1, $\text{Ca}^{+2}=20$ mM); (B) GO - RO membrane (Solution 2, $\text{Ca}^{+2}=20$ mM); (C) RO membrane (Solution 2, $\text{Ca}^{+2}=50$ mM); (D) GO - RO membrane (Solution 2, $\text{Ca}^{+2}=50$ mM) (Ashfaq et al., 2020a) .....	157
Figure 29. FTIR results of (a) RO membrane, (Solution 1, $\text{Ca}^{+2}=20$ mM); (b) GO-RO membrane, (Solution 1, $\text{Ca}^{+2}=20$ mM); (c) RO membrane, (Solution 2, $\text{Ca}^{+2}=50$ mM); (d) GO-RO membrane, (Solution 2, $\text{Ca}^{+2}=50$ mM) (Ashfaq et al., 2020a) .....	160
Figure 30. Interaction of membrane functional groups with gypsum and effect of	

temperature on scaling (Ashfaq et al., 2020a) .....	161
Figure 31. Effect of gypsum scaling at different temperatures on wettability (Ca <sup>+2</sup> = 20mM, solution 1) (Ashfaq et al., 2020a) .....	164
Figure 32. Differentiation of isolated strains using PCA (A) <i>H. aquamarina</i> ; (B) <i>P. fragi</i> (Ashfaq et al., 2019a). .....	177
Figure 33. Biplot showing m/z loading values for (A) <i>H. aquamarina</i> and (B) <i>P. fragi</i> strains. The peaks of interest i.e. differentiating peaks are labelled and possible biomarkers are labelled and underlined (Ashfaq et al., 2019a). [ <b>A:</b> A - QONSW-1 (#2), B1 - QONSW-2 (#1), B2 - QOFSW-1 (#1). B3 - QOFSW-1 (#2), C1 - QOFSW-2 (#4), C2 - QOFSW-2 (#5), C3 - QOFSW-3 (#1), D1 - QOFSW-4 (#1), D2 - QOFSW-5 (#2)) and <b>B:</b> A - QONSW-1 (#3), B - QOFSW-1 (#3), C - QOFSW-2 (#2), D1 - QOFSW-3 (#2), D2 - QOFSW-3 (#3), E - QOFSW-5 (#1), F - QOFSW-4 (#2)]. .....	179
Figure 34. Mass spectra obtained for <i>P. fragi</i> strains (A) Main spectra (2000 – 13000 m/z); Magnified regions (B) 7400 – 7700 m/z (C) 8100 – 8400 m/z (D) 8700 – 8900 m/z, showing the differences of mass spectra among the strains (Ashfaq et al., 2019a). [a – QOFSW-1 (#3), b – QOFSW-2 (#2), c – QOFSW-3 (#2), d – QOFSW-3 (#3), e – QOFSW-5 (#1), f – QOFSW-4 (#2)]. .....	180
Figure 35. (A) Comparison of specific growth rates of isolated seawater bacteria in different antiscalant containing medium (B) Specific growth rates of <i>H. aquamarina</i> (QOFSW-4 (#1)) at different concentrations of poly acrylic acid and poly maleic acid (Ashfaq et al., 2019a). .....	183
Figure 36. Schematic diagram depicting the effect of antiscalant biodegradation on membrane scaling and biofouling (Ashfaq et al., 2019a) .....	186
Figure 37. FTIR spectra of RO membranes after exposure to different media in the	

presence of *H. aquamarina* (incubation for 48 hours at 30°C, Concentration – 1g/L) (Virgin RO – Pure RO membrane surface, Negative control – MSM (no carbon source) with bacteria and MSM + Carbon source (acrylic/maleic/poly acrylic acid/glucose) without bacteria, Positive control – Glucose in MSM, AA+MSM – Acrylic acid in MSM, PAA+MSM – Poly acrylic acid in MSM, MA+MSM – Maleic acid in MSM) (Ashfaq et al., 2019b)..... 193

Figure 38. Increase in absorbance for selected peaks representing: A. Fatty acids and phospholipids, B. Polysaccharides, C. Protein components of Biofilm layer (Neg. control – MSM (no carbon source) with bacteria, and MSM + Carbon source (acrylic/maleic/poly acrylic acid/glucose) without bacteria, Pos. control – Glucose in MSM, AA+MSM – Acrylic acid in MSM, PAA+MSM – Poly acrylic acid in MSM, MA+MSM – Maleic acid in MSM) (Ashfaq et al., 2019b)..... 197

Figure 39. Clustering of variables obtained through PCA using The Unscrambler (V10.5) (Ashfaq et al., 2019b)..... 199

Figure 40. Biplot obtained for A. Proteins, B. Fatty acids and phospholipids, C. Polysaccharides components of Biofilm using XLSTAT (V2016) (Ashfaq et al., 2019b) ..... 201

Figure 41. Clustering of biofilm components obtained in the presence of different carbon sources (Ashfaq et al., 2019b)..... 203

Figure 42. CFU Counts obtained from bio-fouled RO membranes (Ashfaq et al., 2019b) ..... 204

Figure 43. Formation of CaSO<sub>4</sub> crystals in the presence of bacteria at Ca<sup>+2</sup> and SO<sub>4</sub><sup>-2</sup> =50 mM after 14 days of incubation (a) *P. fragi* (QOFSW-3 (#2)), (b) *C. maltaromaticum* (QONSW-2 (#2)), (c, d) Adhesion and growth of *H. aquamarina*

(QOFSW-1 (#1)) on the surface of crystals after 21 days of incubation at 40x and 100x magnifications, and (e) Morphology of gypsum crystal (Ashfaq et al., 2020b).....215

Figure 44. Formation of CaSO<sub>4</sub> crystals at lower ions concentrations in the presence of *H. aquamarina* (QOFSW-1 (#1)) strain after 14 days of incubation (a) Ca<sup>+2</sup> and SO<sub>4</sub><sup>-2</sup> = 30 mM (LBM2), (b) Ca<sup>+2</sup> and SO<sub>4</sub><sup>-2</sup> = 20 mM (LBM1) (Ashfaq et al., 2020b).....216

Figure 45. CaSO<sub>4</sub> precipitates attached to the membrane in the presence of bacteria after 7 days of incubation at Ca<sup>+2</sup> and SO<sub>4</sub><sup>-2</sup> = 50 mM (a) *P. stutzeri* (QOFSW-2 (#3)), (b) *P. fragi* (QOFSW-5 (#1)), (c) *H. aquamarina* (QOFSW-1 (#1)), (d) *H. aquamarina* (dead), (e) *C. maltaromaticum* (QONSW-2 (#2)), (f) *P. fragi* (dead) (QOFSW-5 (#1)), (g) Control (without bacteria – no crystals formation) (Ashfaq et al., 2020b) .....220

Figure 46. Concentration of calcium ions remaining in the liquid medium after 14 days of incubation (medium used: LMB3 containing Ca<sup>+2</sup> and SO<sub>4</sub><sup>-2</sup> = 50 Mm, *H. aquamarina*: n = 3, *P. fragi*: n = 1, *C. maltaromaticum*: n = 1) (Ashfaq et al., 2020b) .....221

Figure 47. SEM-EDX analysis of precipitates formed in the biofilm of (a) *P. fragi* (QOFSW-4 (#2)), (b) *H. aquamarina* (QOFSW-1 (#1)) (medium used: LMB3 containing Ca<sup>+2</sup> and SO<sub>4</sub><sup>-2</sup> = 50 mM) (Ashfaq et al., 2020b) .....222

Figure 48. Kinetics and effect of calcium and sulfate ions concentration on CaSO<sub>4</sub> bio-precipitation (Strain used: *H. aquamarina* - (QOFSW-1 (#1)) (Ashfaq et al., 2020b) .....226

Figure 49. (A) EDX mapping of CaSO<sub>4</sub> and NaCl crystals formed in the presence of bacteria at low concentration (Ca<sup>+2</sup> and SO<sub>4</sub><sup>-2</sup> = 30 mM, LBM2) after 1-day incubation, (B) IC results showing quantitative analysis of CaSO<sub>4</sub> precipitation – kinetics and effect of calcium ions concentration (LBM3: Ca<sup>+2</sup> and SO<sub>4</sub><sup>-2</sup> = 50mM, LBM2: Ca<sup>+2</sup> and SO<sub>4</sub><sup>-2</sup>

$^{2-} = 30\text{mM}$ , LBM1: $\text{Ca}^{+2}$ and $\text{SO}_4^{-2} = 20\text{mM}$ , B: Bacteria i.e. <i>H. aquamarina</i> - (QOFSW-1 (#1))) (Ashfaq et al., 2020b) .....	227
Figure 50. Attachment of bacteria to gypsum crystals and formation of biofilm in LBM3 medium (a) <i>H. aquamarina</i> (QOFSW-1 (#1)), (b) <i>P. stutzeri</i> (QOFSW-2 (#3)), (c) <i>P. fragi</i> (QOFSW-3 (#2)), (d) <i>H. aquamarina</i> (QOFSW-5 (#2)) (Ashfaq et al., 2020b)	229
Figure 51. Discriminating the protein profiles of cells involved in biomineralization (a) Direct visual method (b) Through PCA (Strain used: <i>H. aquamarina</i> - (QOFSW-1 (#1), Medium used: LBM3, $\text{Ca}^{+2}$ and $\text{SO}_4^{-2} = 50 \text{ mM}$ ) (Ashfaq et al., 2020b) .....	231
Figure 52. Growth rates of bacteria in LB and LBM medium (LB – Luria Bertani, LBM3 – Luria Bertani medium supplemented with $\text{Ca}^{+2}$ ions = 50 mM, 2000 mg/L) [ <i>H. aquamarina</i> : QOFSW-1 (#1), <i>C. maltaromaticum</i> : QONSW-2 (#2) <i>P. fragi</i> : QOFSW-3 (#2)] (Ashfaq et al., 2020b) .....	232
Figure 53. Effect of microbes and minerals' foulant-foulant interactions on membrane fouling (Ashfaq et al., 2020b) .....	239
Figure 54. SEM images of the membrane surface (a) RO; (b) GO@RO; (c) PAA-GO@RO; (d) PAA-GO@RO*; (e) PMA-GO@RO; (f) PMA-GO@RO*; and AFM images of (g) RO; (h) GO@RO; (i) PAA-GO@RO; (j) PAA-GO@RO*; (k) PMA-GO@RO; (l) PMA-GO@RO* .....	246
Figure 55. Spectroscopic analysis of the membrane surface (a) Raman spectra; (b) FTIR spectra .....	248
Figure 56. Results of (a) Membrane permeability and % salt rejection; (b) water contact angle .....	251
Figure 57. Normalized flux obtained during scaling experiments .....	252
Figure 58. SEM-EDX analysis of the scaled membrane (a, b) RO; (c, d) GO@RO; (e,	

f) PAA-GO@RO; (g, h) PAA-GO@RO*; (i, j) PMA-GO@RO); (k, l) PMA-GO@RO*	.....255
Figure 59. (a) FTIR spectra of the scaled membrane both in high saturated zone (HSZ); (b) less saturated zone (LSZ) on membranes, (c) XRD spectra of the scale layer ....	257
Figure 60. Anti-biofouling performance of membranes after functionalization.....	258
Figure 61. Simultaneous reduction of biofilm growth and CaSO <sub>4</sub> precipitation after functionalization (a) RO; (b) GO@RO; (c) PAA-GO@RO; (d) PAA-GO@RO*; (e) PMA-GO@RO; (f) PMA-GO@RO* .....	261



## CHAPTER 1: INTRODUCTION

### *1.1 Background*

Qatar is an arid country. It is characterized with hot temperature during summer crossing 40°C with average rainfall as low as 46.71 mm during the time period of 2008-2013 (Ministry of Development, Planning and Statistics, 2016). In addition, the average annual evaporation rate is as high as 2200 mm (Darwish and Mohtar, 2012). Thus, due to its harsh and fragile environment together with limited renewable water resources, the country has been categorized with the group of countries that are at “extremely high-water risk” by Aqueduct Water Risk Atlas (Water Resource Institute).

In Qatar and other Gulf Cooperation Council (GCC) countries, the concepts of water security, water stress and water resources sustainability are interrelated and are major hurdle for the economic growth and social development. Water stress concept is the situation in which water is not available enough to satisfy all needs related to agricultural, domestic and industrial activities. On the other hand, reliable access to clean and safe water for every person for healthy and productive living and for social and economic growth without polluting the environment is known as water sustainability and water security (UN-Water, 2013).

It is difficult to define the threshold for water stress in terms of available water per capita. Nevertheless, it has been proposed that the boundary line in terms of annual per capita renewable water resource availability is 1000 cubic meters. Below this, the country is considered under water stress and it begins to hamper social and economic development (World Business Council for Sustainable Development, 2006). In comparison, the annual

water resource availability per capita in Qatar was 71 cubic meters in 2005 (Darwish and Mohtar, 2012). This was further reduced to 25.78 cubic meter in 2014 (Index Mundi) which makes the country under severe water stress condition.

Moreover, there are several pressures and stressors that are increasing the demand of water resources. The economic and population growth are most significant forces pressurizing the water resources of Qatar which is further exacerbated by unsustainable consumption of water by the residents of the country. Qatar has witnessed an increase of as much as 726% in GDP from 1990 to 2013 (MDPS, 2016). The increase in GDP strengthens the economy of country which ultimately leads to the improved income of the inhabitants of the country. The increase in income then leads to the increased spending on resource consumption and utilization. It has been estimated that there is 376% increase in Qatar's population from 1990 to 2013 (MDPS, 2016). Such an increase will lead to the increase in per capita water demand and reduction in per capita water availability.

To cope with the rising demands of water due to economic and population growth, Qatar utilizes the services of desalination industry to provide potable water resources. Thus, 99% of the country's domestic demand is fulfilled by desalination industry. The GCC region in general and Qatar in particular, utilize Multi-Stage Flash (MSF) technique in Desalination plants. However, because MSF technique requires huge amount of thermal and electrical energy and releases greenhouse gases (through consumption of fossil fuels); it is not considered as an environment friendly technology for desalination (Lior, 2017, Darwish et al., 2013). Therefore, Reverse osmosis (RO) membrane technology is recommended as an environment friendly and energy efficient technology for future desalination industries (Ashfaq et al., 2018).

### *1.2 Physical-Chemical-Biological interactions in RO system*

Reverse Osmosis (RO) membrane technology is widely used in seawater desalination, brackish water treatment and wastewater treatment. RO is currently the most energy-efficient technology for desalination, with energy cost about 1.8 kWh/m<sup>3</sup>, which is much lower than that of other technologies (Xu et al., 2013). RO membrane has the ability to reject both dissolved and suspended substances from water. The rejected substances then interact with each other and with the membrane surface which often results in membrane fouling. Membrane fouling is defined as a process in which particles/solutes present in wastewater gets deposit on the surface of the membrane partially or completely blocking the membrane pores. The process results in decline in flux with time and increase in operating cost of a system. There are different types of fouling based on foulants that are participating in membrane fouling. However, each type does not occur individually. Instead, they occur together most of the time and interact with each other to affect the membrane's performance (Tang et al., 2011; Tang et al., 2009). The types of fouling include organic, inorganic, particulate (chemical) and biological fouling (biofouling) (Chian et al., 2007). The major issues of RO operations are mineral scales and biofoulants that clog and reduce the overall performance and lifetime of the membranes (Xu et al., 2013; Al-Shammiri et al., 2000; Lee et al., 2013; Baker and Dudley, 1998; Li et al., 2007). Therefore, the simultaneous prevention of mineral scaling and biofouling on RO membranes are essential in RO operations. However, the complex physical-chemical-biological interactions in the RO system are not fully understood and therefore biofouling and scaling prevention remains a challenge.

In RO operations, typical mineral scales are calcium carbonate, calcium sulfate,

silicate, and barium sulfate (Al-Shammiri et al., 2000; Lee et al., 2013; Li et al., 2007; Shiha et al., 2006). Carbonate fouling can be prevented by adjusting the pH of the water (Al-Shammiri et al., 2000; Lee et al., 2013; Li et al., 2007; Shiha et al., 2006). In most inland water sources, barium concentrations are typically very low ( $\leq 0.5$  mg/L) as opposed to  $\text{Ca}^{2+}$  that are generally high. That is the reason,  $\text{BaSO}_4$  precipitates in RO system would be less than 2% of the mass of  $\text{CaSO}_4$  (Lee et al., 2013; Li et al., 2007). Therefore,  $\text{CaSO}_4$  is most significant scalant in membrane filtration. To prevent mineral scaling on RO membranes, antiscalants are added to suppress mineral scale formation. The most common antiscalants for  $\text{CaSO}_4$  include phosphonates and organic polymers (Shiha et al., 2006). In RO systems, phosphonates, however, tend to hydrolyze to orthophosphate and react with calcium ions to form calcium orthophosphate, which is insoluble (Antony et al., 2011). Hence, nowadays, most of the commercial antiscalants for RO membranes are organic polymer-based chemicals, such as polyacrylic acid (PAA), polymethacrylic acid (PMAA), and polymaleic acid (PMA).

The use of polymer inhibitors has shown satisfactory performance in preventing  $\text{CaSO}_4$  scaling (Shiha et al., 2006). However, it is not well studied that these inhibitors are biodegradable or not. In the case of biofouling prevention, disinfectants, such as chlorine, are added to the feed water. However, chlorine addition can deteriorate the membranes (Ahmad et al., 2013). Furthermore, it was found that chlorination might not be as effective in controlling biofouling as previously thought. Recently, some microorganisms have been shown to be resistant to chlorine by exuding large amounts of extracellular polysaccharides (EPS) for protection, which enhances biofilm formation on membranes (Shih et al., 2005). As an alternative, anti-microbial nanomaterial coated membranes have been showing

excellent anti-biofouling properties (Chesters, 2009). Dr. Rodrigues' research group has demonstrated that poly(N-vinylcarbazole) chemically modified graphene oxide (PVK-modified graphene oxide (GO)) coated on microfiltration membranes can successfully prevent microbial growth (Rodrigues et al., 2013; Musico et al., 2014). Lee et al. (2013) recently have also demonstrated that GO can prevent biofouling on membrane bioreactors. Hence, membrane fouling, and anti-fouling strategies are being thoroughly investigated. Some statistics have revealed that there were more than 3000 research papers published in the area during the last 25 years which indicates the researcher's interest in the area (Jiang et al., 2017).

In addition to the interaction of different type of foulants at the RO membrane surface, some physical factors influence those interactions. These physical factors include temperature, pH, cross flow velocity, pressure etc. These physical factors can contribute to increase or decrease of membrane fouling. For example, Ashfaq et al., (2017) investigated the effect of cross flow velocity on membrane flux for the treatment of laundry wastewater. It was found that increasing the crossflow velocity will lead to the increase of membrane flux which reflects decrease in fouling. This could be because of increased shear rates at higher cross flow velocities, which will reduce the formation of concentration polarization and membrane fouling. Similarly, it has also been shown that the organic foulants acts as a nutrient source for microorganisms and thus promotes biofouling. Alternatively, microorganisms present at the RO membrane surface can also secrete carbohydrates, extracellular polymeric substances (EPS) which in turn enhances the organic fouling. That is why, 60% of the constituents in biofilm were found to be organic substances (Butt et al., 1997). As shown in Figure 1, most of these interactions between physical-chemical-

biological are known. However, there are some complex interactions such as those, which include calcium sulfates and microorganisms, are still unknown and therefore, it is an interesting area of research. The membrane fouling results due to these interactions is being thoroughly investigated. Some statistics have revealed that there were more than 3000 research papers published in the area of RO membrane fouling during the last 25 years, which indicates the researcher's interest in the area (Jiang et al., 2017).

In addition to the physical-chemical-biological interactions, the characteristics of membranes themselves also influence these interactions. Thus, the membrane properties and surface features such as porous structure, charge, characteristics of polymer, membrane roughness and hydrophilicity/hydrophobicity (Bellona et al., 2004; Hirose et al., 1996; Vrijenhoek et al., 2001) also plays key role in determining the extent of membrane fouling and its constituents. For example: the hydrophilic membranes are less prone to fouling caused by microorganisms, organic substances and some inorganic substances due to their less interaction with membrane surface (Liu et al., 2006; Hilal et al., 2005). Similarly, it was noted that the permeate flux decreased with increase in membrane hydrophobicity during filtration of bovine serum albumin solution (Nabe et al. 1997). Therefore, there is a direct correlation between membrane flux (membrane fouling) and membrane hydrophilicity.

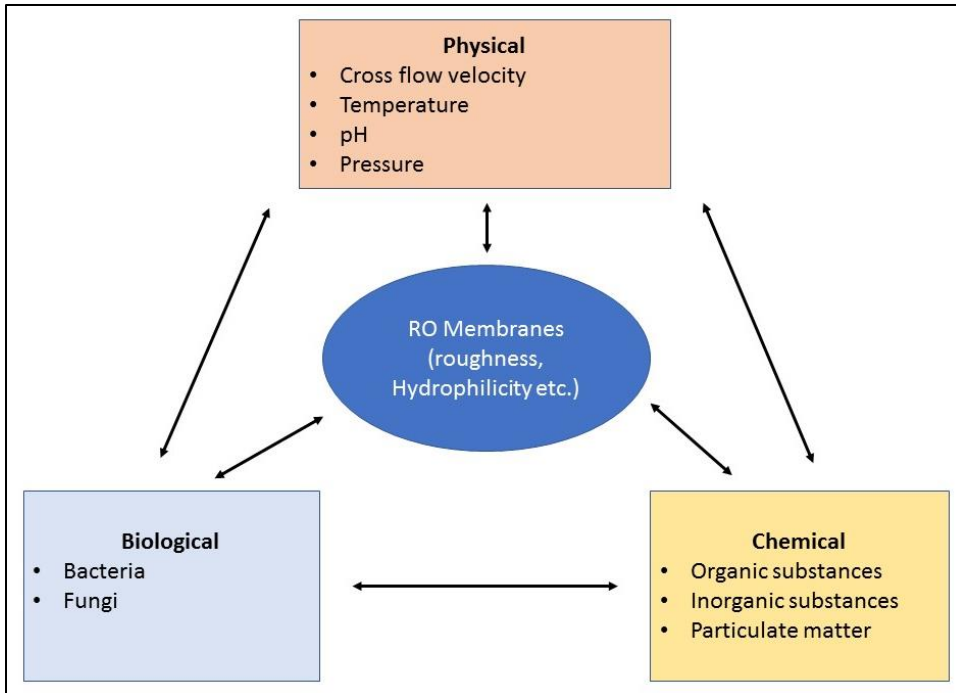


Figure 1. Schematic illustration of Physical-Chemical-Biological interaction in RO systems

However, it is not clearly known that the antiscalants used in RO systems to prevent scaling can also interact with the microorganisms present there. It is possible that some antiscalants can prevent mineral scaling, but they might serve as energy sources for the microorganisms present in the RO system and therefore, the antiscalants could potentially enhance microbial growth and biofouling. Additionally, if the antiscalant are indeed biodegraded, they would no longer effectively inhibit  $\text{CaSO}_4$  scaling. Such behavior is expected since researchers have found that the polymer inhibitor, polyacrylic acid (PAA), can be degraded by mixed microbial communities in activated sludge (Kavitha et al., 2014). However, nothing is known about the specific microorganisms involved in the polyacrylic acid (PAA) or polymaleic acid (PMA) degradation as well as their degradation pathways. Hence, it is essential to investigate whether the polymer antiscalants can be degraded by

common microorganisms existing in RO systems or not.

Similarly, no previous studies have investigated the interactions between the microorganisms in RO system and the CaSO<sub>4</sub>. Li's recent research reported that the fouling of biopolymers on RO membrane can be influenced by the presence of Ca<sup>+2</sup> (Li et al., 2007). Other studies have demonstrated that microorganisms can induce calcium carbonate precipitation (Onal and Rodriguez, 2014; Mortensen et al., 2011; Okwadha and Li, 2010). However, it is unknown if the microorganisms, used in these studies, exist in RO system. Therefore, the question is whether the co-presence of microorganism in RO systems and CaSO<sub>4</sub> will promote scaling and biofouling, i.e., can Ca<sup>+2</sup> promote microbial growth and bio-enhance CaSO<sub>4</sub> mineral formation?

Furthermore, as discussed in detail, many polymers and antimicrobial nanomaterials have been used in membrane coating to prevent biofouling. But these researches have not deal with the interaction of these modified membranes with the mineral scaling. In addition, most studies focus on either to prevent the biofouling or the scaling, but no studies have deal with preventing both type of fouling simultaneously. Table 1 summarizes the known and unknown interactions in RO systems.

Table 1. Known and Unknown phenomena/interactions in RO Systems

Known interaction/phenomena	Un-known interaction/phenomena
Interaction between organic foulants and Microorganisms (Butt et al., 1997)	Interaction between inorganic foulants like calcium ions and microorganism present in RO system
Role of antiscalants in reducing inorganic fouling or mineral scaling (Antony et al., 2011)	Interaction between antiscalants and microorganisms



Known interaction/phenomena	Un-known interaction/phenomena
Effect of physical parameters such as pH, temperature, cross flow velocity on membrane fouling (or membrane flux) as a whole (Ashfaq et al., 2017)	Effect of physical parameters such as temperature on type of scalants (e.g. polymorphs of calcium sulfates)
Role of membrane coatings (polymers and nanomaterials) in enhancing membrane features (smoothness, hydrophilicity) to reduce biofouling or scaling (Chae et al., 2017)	Simultaneous reduction of both biofouling and scaling through modified membranes
Role of antimicrobial coatings on reducing biofouling (Antony et al., 2011)	Interaction between antimicrobial coatings with scaling (e.g. CaSO <sub>4</sub> )

By keeping into consideration, the unknown interactions and knowledge gaps in the literature, Figure 2 summarizes the unknown interactions and research gaps that will be studied in this research project and research objectives will be formulated accordingly.

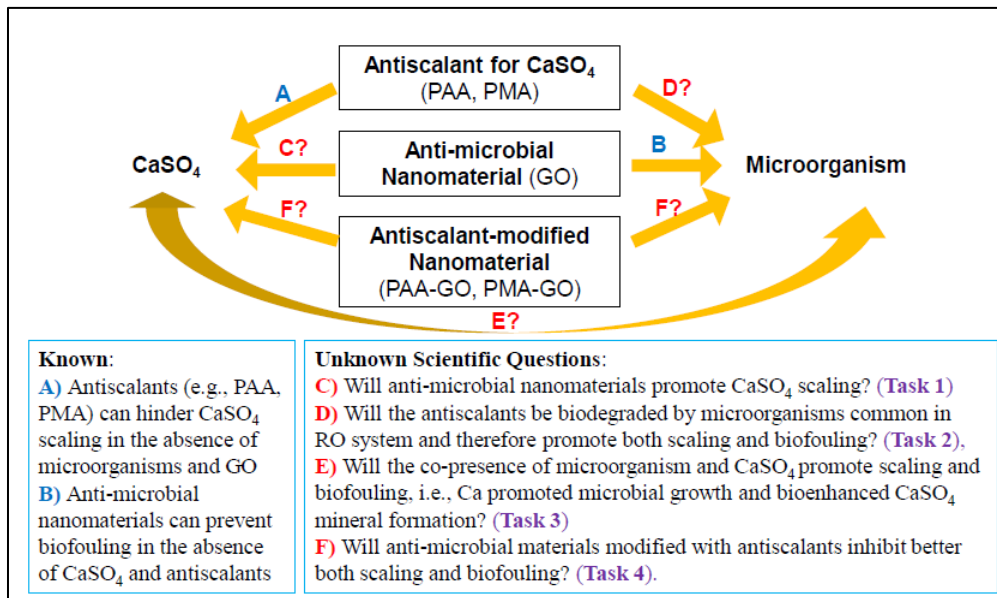


Figure 2. Identification of "Research gaps" in physical-chemical-biological interactions in RO systems

### *1.3 Research Rationale*

The Qatar Environment and Energy Research Institute has declared that Qatar's residents consume about 500 liters of water per day. This amount makes Qatar one of the largest water consumers in the world. The reason for such large water consumption is the dry climate and the population lifestyle. One solution for this high-water consumption is the development or improvement of desalination technologies with little or no negative effect on the environment. Reverse Osmosis has been described as the most suitable and environmentally friendly desalination technology and in the past 25 years this technology has been evolving and able to separate product waters from 90% to 98% from total dissolved solids (TDS) concentrations ranging from 1500 mg/L to 3000 mg/L. This was mainly possible due to research focusing on improving the membrane quality and finding alternative methods to prevent membrane fouling. Initially, RO systems used polyamide and cellulose acetate membranes, today membranes are made of thin composites and can withstand higher temperatures and wider range of pH values. Overall, the RO desalination plants are extremely effective to produce clean water from marine water; however, fouling is still a major issue in these systems. The understanding of fouling (biological and chemical) is essential for the development of more effective desalination technologies that will prevent membrane fouling.

The project will benefit the Qatari society's clean water supply and reduce membrane maintenance costs, by providing important scientific information to prevent scaling and biofouling on RO membranes. The project will advance our scientific understanding on the complex problem of simultaneous scaling and biofouling on RO membranes. At the same time, a transformative approach will be used to improve the

efficiency of preventing scaling and biofouling in RO water treatment processes. By investigating the complex interactions among  $\text{CaSO}_4$ , polymer antiscalants, microorganisms, antimicrobial nanomaterials, and polymer-modified antimicrobial nanocomposites, the project will fill out important information gaps (as shown in Figure 6), and contribute greatly to the scientific basis for efficiently preventing both scaling and biofouling on RO membranes. This project will be the first one investigating biofouling and scaling simultaneously in RO systems. PAA-GO (Poly acryl amide – Graphene oxide) is a newly synthesized material that has seen increasingly used in material science and biomedical engineering; the proposed project will establish its value for RO systems. By adopting these advanced materials and novel techniques, the proposed project will allow new scientific and transformative findings and will advance discovery across disciplines of environmental science, chemistry, biology, and materials science by addressing the questions mentioned in the Figure 2.

#### *1.4 Research Focus*

The overarching research objective is to understand the synergistic interactions of preventing  $\text{CaSO}_4$  scaling and biofouling in the presence of *polymer-modified graphene oxide* (PAA-GO and PMA-GO) on RO membranes.

##### *1.4.1 Research Questions*

During the course of research, the answer to the following important research questions will be investigated:

1. Will anti-microbial nanomaterials promote  $\text{CaSO}_4$  scaling?

2. Will the antiscalants be biodegraded by microorganisms common in RO system and therefore promote both scaling and biofouling?
3. Will the co-presence of microorganisms and  $\text{CaSO}_4$  promote scaling and biofouling i.e. Ca promoted microbial growth and bio-enhanced  $\text{CaSO}_4$  mineral formation?
4. Will anti-microbial materials modified with antiscalants inhibit better both scaling and biofouling?

#### *1.4.2 Research Objectives*

Specific objectives and associated hypotheses are:

**Objective 1:** Understand effects and mechanisms of anti-microbial nanomaterials (GO) on  $\text{CaSO}_4$  scaling.

Hypothesis 1.1 Anti-microbial nanomaterial (e.g., graphene oxide) coatings on RO membranes will change the membrane surface properties and affect  $\text{CaSO}_4$  scaling on membranes.

Hypothesis 1.2 Both the membrane surface physicochemical properties and the  $\text{CaSO}_4$  precipitation will depend on the coating used on the membrane, solution compositions, and temperatures.

**Objective 2:** Demonstrate and determine biodegradation of polymer antiscalants used in RO systems.

Hypothesis 2.1 The polymer antiscalants (PAA, PMA) can be degraded by microorganisms found in RO systems and it will promote microbial growth and biofouling.

Hypothesis 2.2 PAA and PMA may have varied microbial degradation rates and pathways.

**Objective 3:** Investigate the interactions between microorganisms and  $\text{CaSO}_4$  in RO

system.

Hypothesis 3.1 The presence of  $\text{CaSO}_4$  can promote the growth of microorganisms found in RO systems.

Hypothesis 3.2 The microorganisms existing in RO systems will promote  $\text{CaSO}_4$  scaling on membrane.

**Objective 4:** Determine whether new coatings (GO-PAA, GO-PMA) will prevent biofouling and scaling.

Hypothesis 4.1 The antimicrobial nanomaterials (e.g., GO) can be modified with polymer antiscalants (PAA and PMA) to form PAA-GO and PMA-GO.

Hypothesis 4.2 PAA-GO and PMA-GO will be antimicrobial and non-biodegradable in RO systems.

Hypothesis 4.3 PAA-GO and PMA-GO will inhibit both  $\text{CaSO}_4$  scaling and biofouling on RO membranes.

## CHAPTER 2: LITERATURE REVIEW<sup>1</sup>

### *2.1 Reverse Osmosis*

The Osmosis is a naturally occurring process in which the water from a diluted solution tends to move towards the concentrated solution. The Reverse Osmosis (RO) is the same process but in reverse direction. In RO systems, water is pushed through a semipermeable membrane thereby retaining the dissolved and suspended substances. Thus, the RO membrane is a semipermeable membrane that allows only water molecules to pass through it and withholding majority of dissolved salts, microorganisms, viruses, organic compounds, and dissolved ions. Nonetheless, the pressure of 20 - 80 MPa is needed to push the water molecules through the membrane (Saleem and Zaidi, 2020).

There are several mechanisms of mass transfer in RO systems such as size or charge exclusion, solution-diffusion mechanism, and physico-chemical interactions between water (solvent), dissolved and substances (solute) and membrane (Malaeb and Ayoub, 2011).

The most common application of RO is its utilization in the purification and filtration of seawater to produce drinking water, thereby, removing all the contaminants, salts and other substances. Similarly, RO can also be utilized for the treatment of wastewater coming from a wide variety of industries such as textile, chemical, food, pulp

---

<sup>1</sup> Contents of this chapter have been published. Reference: Ashfaq, M.Y., Al-ghouti, M.A., Qiblawey, H., Zouari, N. Rodrigues, D.F., Hu, Y. 2018. Use of DPSIR Framework to Analyze Water Resources in Qatar and Overview of Reverse Osmosis as an Environment Friendly Technology. *Env. Prog. Sustain.* 38, 1–13.

and paper, petroleum and petrochemical industries and from domestic sources. This is mainly because of RO's ability to provide higher percentage salt rejection and higher removal efficiencies. (Lee et al., 2011). RO can be used in combination with other techniques such as Ultrafiltration - RO (UF-RO), or Microfiltration - RO (MF-RO) to develop a hybrid process and gives better efficiency and higher rejection (Ang et al., 2015).

The RO concept has been known for many years, but it became practical to be utilized at industrial level after 1960s when cellulose acetate asymmetric membranes were produced which possess both higher water flux and removal efficiency (Greenlee et al., 2009). Later, the new generation membranes were developed such as Thin Film Composite (TFC) membrane which is resistant to high temperature, wide pH range and severe chemical environments and has higher water flux and percentage salt rejection. The development of such new generation membranes enhances their applications at industrial scale. It has developed over the past 50 years to a 44% share in world desalination capacity in 2009, and 80% share in the total number of desalination plants installed worldwide (Greenlee et al., 2009). In addition to the traditional seawater and brackish water desalination processes, RO membranes have found uses in wastewater treatment, production of ultrapure water, water softening, and food processing as well as many others.

## *2.2 Membrane Structures*

Membrane structures are of different kinds and are integral part of RO systems. These are critical in determining the performance, cost and sensitivity to temperature, pH, pressure and other environmental factors. The types of membrane structures include symmetric membranes, asymmetric membranes and composite membranes.

**Symmetric membrane:** These membranes are always made using single material (homogenous) with uniform pore structure (US EPA 2005).

**Asymmetric membrane:** In asymmetric membranes, there are two or more structural layers (filtration layer and support layer) of different morphologies i.e. filtration layer is denser than support layer and is used for solute rejection. Asymmetric membranes may also possess porous material of varying density from feed to permeate side. (US EPA 2005). The asymmetric membrane is made up of one polymer usually cellulose acetate. It is formed by forming a thin film of acetone-based solution of cellulose acetate polymer. In 1962, the first RO membrane of this type for commercial application was developed (Loeb and Sourirajan, 1962).

**Composite membrane:** These membranes are made up of three different layers with materials of structurally or chemically distinct characteristics. The three layers include upper most ultra-thin selective layer made up of polyamide polymer, micro porous interlayer made up of polysulfonic material and polyester support layer. The composition of the composite membranes is heterogenous and is widely utilized in Membrane filtration systems. Polyamide TFC (Thin film composite) is the example of widely used RO membrane (US EPA 2005). The thickness of upper most layer in TFC is of 0.2  $\mu\text{m}$ , intermediate layer of around 40  $\mu\text{m}$  and a support layer of about 120 – 150  $\mu\text{m}$  (Figure 3) (Akin and Temelli, 2011).

The top layer of polyamide material act as a barrier layer which is made by interfacial polymerization between two monomers such as amine and acid chloride. The thickness of top barrier layer is reduced to suppress its resistance to transport of permeate and to achieve higher rejection. The intermediate layer is added in between to enhance the



thin topmost layer's resistance to higher pressure.

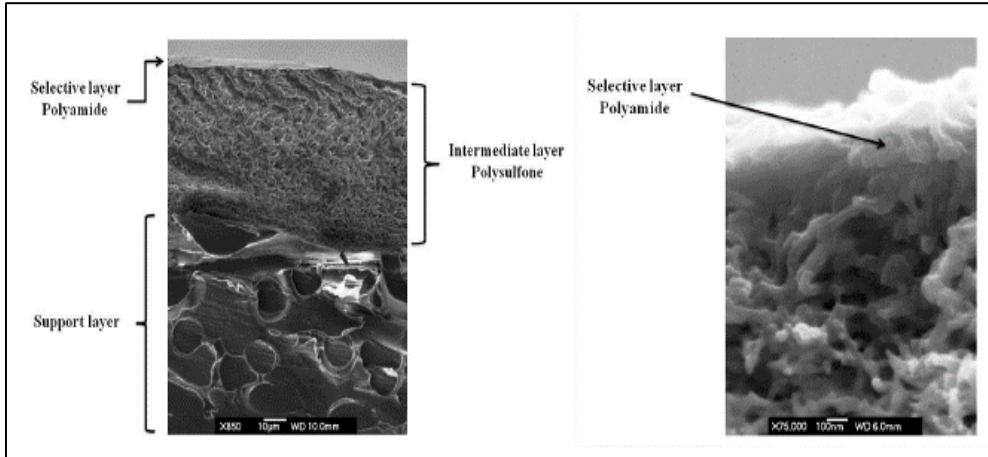


Figure 3. Cross section of Thin Film Composite membrane (Akin and Temelli, 2011).

The most popular RO membrane materials are cellulose acetate (CA) and thin film composite polyamides (PA). For a complete study of RO membrane materials for desalination, a review on RO membrane materials is reported by Lee and his coworkers (Lee et al., 2011). The advantages and disadvantages of both types of RO membranes are summarized in Table 2. In general, PA based RO membranes formed by interfacial polymerization exhibit better performance than CA based membranes due to higher water flux, enhanced physical and chemical resistance and wider range of processing pH and temperature conditions.

Table 2. Advantages and Disadvantages of Asymmetric and Composite Membranes

Structure	Material	Advantages	Disadvantages
Asymmetric	Cellulose acetate	<ul style="list-style-type: none"> <li>• Resistance to chlorine</li> <li>• Resistance to adsorption of natural organic matter</li> </ul>	<ul style="list-style-type: none"> <li>• Biodegradable</li> <li>• Severe flux decline</li> </ul>

Structure	Material	Advantages	Disadvantages
<b>Composite</b>	Polyamides (top layer), Polysulfone (interlayer)	<ul style="list-style-type: none"> <li>• Better water flux, % rejection,</li> <li>• Resistant to wider temperature and Ph range</li> </ul>	<ul style="list-style-type: none"> <li>• Susceptible to chlorine</li> <li>• Sensitive to fouling</li> </ul>

### 2.3 Reverse osmosis process parameters

#### 2.3.1 Percentage membrane rejection

The percentage rejection (percentage R) is one of the performance indicators for RO and is defined as the amount of material or salts being rejected by the membrane from the feed water. Thus, it can be calculated for any specific contaminant in feed water or by using overall characteristic such as turbidity or conductivity. (Crittenden et al., 2005, Greenlee et al., 2009). The percentage R can be calculated using following formula (Crittenden et al., 2005):

$$R = 1 - \frac{C_p}{C_f} \text{-----} (1)$$

Where, R is rejection,  $C_p$  and  $C_f$  are permeate and feed water concentrations respectively (mole/L or mg/L),

Alternatively, following formula can also be used:

$$\text{Salt Rejection (\%)} = \frac{\text{Feed water conductivity} - \text{Permeate water Conductivity}}{\text{Feed water conductivity}} \times 100 \text{--(2)}$$

### 2.3.2 Salt Passage %

The percentage of salt passage is the amount of salt that has passed through the membrane into the permeate water. The increase in percentage of salt passage shows the decrease in performance of RO membrane system.

$$\text{Salt Passage \%} = 1 - \text{Salt Rejection \%} \text{-----}(3)$$

### 2.3.3 Mass Balance

The Mass balance is done to check if the system is running and giving the reading correctly. In order to do the Mass balance, flow rate of feed, permeate and concentrate should be known. Furthermore, the data related to conductivity of feed, permeate and concentrate needs to be collected.

The Equation for mass balance is given by:

$$\text{Feed flow} \times \text{Feed Conductivity} = (\text{Permeate flow} \times \text{Permeate conductivity}) + (\text{Concentration flox} \times \text{Concentrate conductivity}) \text{-----} (4)$$

### 2.3.4 Recovery

The fraction of feed water that becomes permeate after the filtration run is called as Recovery. The following equation is sued to calculate the Recovery (Crittenden et al., 2005).

$$Rw = \frac{Qp}{Qf} \text{-----} (5)$$

Where,  $R_w$  represents recovery and  $Q_p$  signifies permeate flow rate ( $m^3/s$ ), and  $Q_f$  represents feed flow rate ( $m^3/s$ ).

### 2.3.5 Permeate Flux

The volume of water treated by the membrane per unit time per square meter of the membrane is called as membrane permeate flux. The most used parameter to investigate membrane performance and it is given by the following Equation.

$$J = \frac{Q_p}{A} \text{-----} (6)$$

Where,  $J$  denotes permeate flux ( $l/m^2/h$ ),  $Q_p$  represents permeate flow rate ( $l/h$ ) and  $A$  denotes the active membrane surface area ( $m^2$ ).

### 2.3.6 Membrane Resistance

Membrane resistance is an important feature that needs to be monitored in order to understand the fouling mechanisms. Each type of resistance such as Resistance due to cake layer formation, due to membrane or due to concentration polarization provides in-depth knowledge about the phenomena of fouling. Furthermore, it also provides important information required for scale-up studies for Industrial implementation. It is also important to know about the type of resistances occurring in order to develop techniques for improvement in membrane rejection and overall membrane performance (Rezaei et al., 2014).

2.3.6.1 Darcy's law and Resistance in Series Model. In membrane filtration systems, Darcy's law can be used to model water flow through the semi-permeable membrane. The following equation shows how the water flux is related to the total membrane resistance under Darcy's law (Hassan et al., 2013):

$$J = \frac{TMP}{\mu \cdot R_t} \text{-----} (7)$$

Where,

$$TMP = \frac{P_f + P_r}{2} - P_p \text{-----} (8)$$

J is flux, TMP is transmembrane pressure,  $\mu$  is dynamic viscosity of the feed water,  $R_T$  is total resistance,  $P_f$  is feed pressure,  $P_r$  is retentate pressure and  $P_p$  is permeate pressure

Rearranging the equation,

$$R_t = \frac{TMP}{\mu \cdot J} \text{-----} (9)$$

Thus, the equation can be used to find out the total resistance of the membrane. However, the above equation does not provide in depth knowledge about different types of resistances occurring in a membrane filtration system. Therefore, the Resistance in Series

model can be used for this purpose. The Resistance in Series model is used to quantify each type of resistance occurring due to different type of fouling mechanisms (Figure 4).

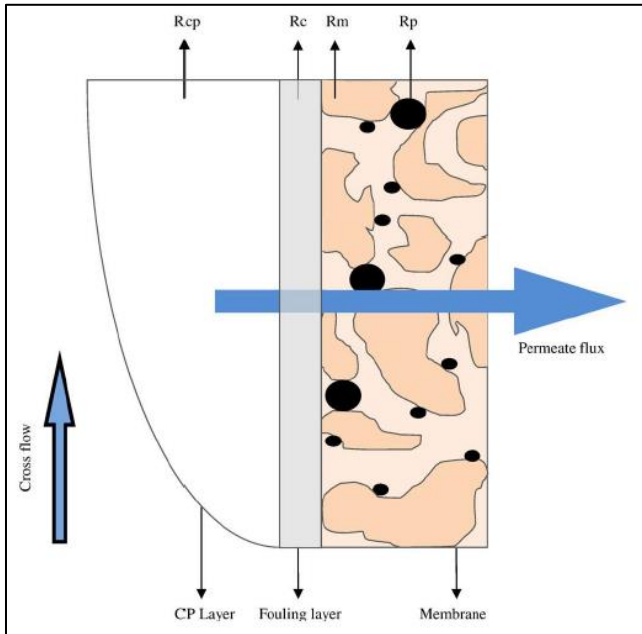


Figure 4. Schematic representation of different resistances during filtration (Shirazi et al., 2010)

Thus, the total resistance ( $m^{-1}$ ) can also be expressed using the following Equation:

$$R_t = R_m + R_C + R_{c.p} + R_{if} \text{ -----(10)}$$

$R_m$  is membrane resistance,  $R_c$  is resistance due to cake layer formation,  $R_{c.p}$  is resistance due to concentration polarization and  $R_{if}$  is resistance due to irreversible fouling.

All these parameters can be measured as following (Rezai et al., 2011):

Table 3. Types of Membrane Resistance and their Measurement Methods

Type of Resistance	Measurement Method
$R_m + R_c + R_{c.p.} + R_{if}$	Permeate flux measurement at the end of the run
$R_m + R_{if} + R_c$	Water flux measurements in situ at the end of the run
$R_m + R_{if}$	After mechanical removal of the deposited cake layer on the membrane surface, gently with a sponge and a 20-minute water flushing
$R_m$	Water flux measurement on a clean membrane.

In some cases, the membrane resistance due to each fouling mechanism is not required to be calculated. Since,  $R_c$ ,  $R_{c.p}$  and  $R_{if}$  represents resistance due to fouling ( $R_f$ ). The equation can also be simplified to give the following:

$$R_T = R_m + R_f \text{-----} (11)$$

Since, there is no resistance due to fouling ( $R_f$ ) for clean membrane, the Darcy's law can be used to calculate the membrane resistance ( $R_m$ ) as following:

$$R_m = \frac{TMP}{\mu \cdot J_0} \text{-----} (12)$$

Where  $J_0$  represents the initial membrane flux of clean water at the start of filtration experiment (Kumar et al., 2007). Thus, by combining the two equations, the membrane resistance due to fouling can be calculated as:

$$Rf = \frac{TMP}{\mu \cdot J} - Rm \text{-----} (13)$$

The flux loss after the filtration experiment can be calculated using:

$$\Delta J = \frac{J_0 - J_s}{J_0} \times 100 \text{-----} (14)$$

Where  $J_0$  is initial filtration flux and  $J_s$  is the stabilized filtration flux during the experiment (Hassan et al., 2013).

#### *2.4 Membrane Fouling*

The major problem associated with the widespread use of membrane technology is Membrane fouling. It is a process in which particles/solutes present in feed water gets deposit on the surface of the membrane partially or completely blocking the membrane pores. The process results in decline in flux with time and increase in operating cost of a system. Membrane fouling can be of two major types i.e. Reversible and Irreversible fouling. As the name indicates, reversible fouling can be removed using different physical and chemical cleaning methods. On the other hand, irreversible fouling refers to the condition when membranes cannot be cleaned using either physical or chemical methods or thus permanent blockage results (Mansoor and Toraj, 2007). According to Brans et al. (2004), there are four mechanisms of membrane fouling i.e. 1) pore blockage, 2) formation of cake layer, 3) in-depth fouling and 4) adsorption (as shown in Figure 5).



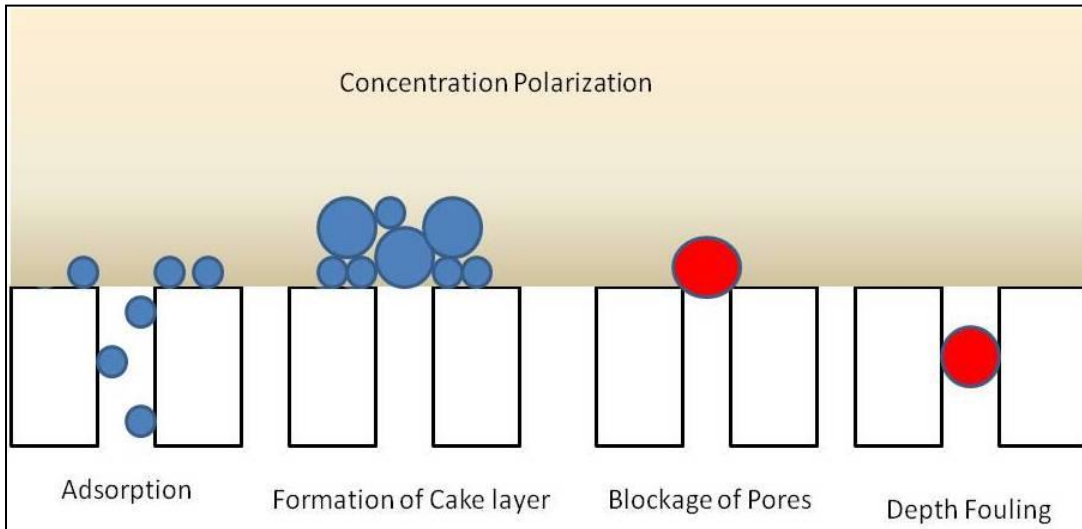


Figure 5. Mechanism of membrane fouling

International Union of Pure and Applied Chemistry (IUPAC) defines membrane fouling as a process that results in loss of membrane's performance which could be because of dissolved or suspended solids' deposition at the surface or inside the pore or at the pore opening (Aptel et al., 1996). In case of RO membrane, the possibility of pore blockage or depth fouling is less because of its pore-less structure. Therefore, fouling in RO usually occurs due the formation of cake layer (solids deposition) above the membrane surface. The membrane fouling causes decrease in flux, percentage rejection and deterioration of membrane structure and material (Flemming, 1997). The phenomenon of membrane fouling is complex and dynamic as it is affected and modified due to several factors such as the quality of feed water, pretreatment of feed water, operating conditions etc. Furthermore, type and nature of substances also dictate the fouling type and its kinetics. There are different types of fouling based on foulants that are participating in membrane fouling. However, each type does not occur individually. Instead, they occur together most

of the time and interact with each other to affect the membrane's performance (Tang et al., 2009 and Tang et al., 2011).

#### *2.4.1 Concentration Polarization (CP) and Fouling*

In addition to membrane fouling, concentration polarization is another phenomenon which results in decline in flux. The concentration polarization refers to the accumulation of solids near the surface of membrane with time. This accumulation of solids give rise to a boundary layer (called as gel layer) below which is the super-saturation of rejected substances from the membrane. However, the loss of flux due to this process can be partially restored by decreasing the pressure or feed concentration and also by increasing the crossflow velocity (Cheryan, 1998).

In pressure driven membrane treatment systems such as RO, NF; the rejection of suspended and dissolved substances results at the feed waterside results in the accumulation of these rejected substances above the membrane surface, which eventually leads to the concentration gradient. Thus, the particles will move towards the membrane under the influence of pressure called as convective transport and there will be back diffusion of substances from the region above membrane surface to the bulk solution. Due to high pressure, convective transport rate will be higher than back diffusion rate, which leads to the formation of dense layer that contains significantly higher concentration of rejected substances. This phenomenon of formation of dense layer or boundary layer is called as Concentration polarization (abbreviated as CP) (Baker, 2004). The concentration polarization has a major influence on the membrane fouling. If the concentration of salts of calcium or magnesium such as calcium sulfates increases its solubility limit in the

boundary layer, they will precipitate on the membrane surface causing membrane scaling. Furthermore, the concentration of nutrients are high at boundary layer. The concentration polarization provides optimum conditions for microbial growth causing biofouling (Paul and Abanmy, 1990).

However, the increase in cross flow velocity generates turbulence above the membrane surface, which in turn reduces the concentration polarization and membrane fouling. Similarly, pressure affects the concentration polarization as increasing the pressure will enhance the convective transport of solutes towards the membrane.

In some membrane modules, feed spacers are used to enhance the turbulence near the membrane surface and reduce the influence of CP (Paul and Abanmy, 1990, Sudak, 1990). The ratio of concentration of solute at the surface of membrane to that in the bulk solution is called as concentration polarization factor and is given by the following equation:

$$CP = \frac{C_m}{C_o} \text{-----} (15)$$

#### 2.4.2 Types of Fouling

The general classification of membrane fouling includes organic fouling, inorganic fouling or scaling, colloidal fouling and biofouling (Chian et al., 2007). Membrane fouling usually occurs as a result of combination of different type of foulants. However, it is also possible that one foulant might be dominant over the other. It has been reported based on several fouling experiments that biofouling is the most common type of fouling constituting 48% as compared to other types (Khedr, 2002).

#### *2.4.2.1 Organic Fouling*

The fouling that results due to the deposition of organic substances present in sea and wastewater is called as Organic fouling. They also act as a nutrient source for biofilm growth (Spyres et al., 2000). Although, the concentration of natural organic matter (NOM) present in seawater is less as compared to other substances, the fouling caused by NOM is generally harder than others (Shon et al., 2009). It has been shown that humic substances represent as much as 30% of the dissolved organic carbon content in seawater (Simon et al., 2012). The biochemical substances such as amino acids, lipids and carbohydrates also constitute nearly 30% of the dissolved organic matter and as much as 80% of the particulate organic matter (Ogawa and Tanoue, 2003). Organic fouling in RO can be reduced by pretreating the seawater. Thus, total organic carbon should be present in amount not more than 0.5 mg/l to avoid organic fouling.

Generally, the total organic carbon content ranges from 1-10 mg/l in seawater that usually results from algal bloom. The major problem of organic foulants is that they comprise a major constituent in the biofilm and become a carbon source for microorganisms. Thus, organic content was found to be 60% of the biofilm layer by weight (Butt et al., 1997).

#### *2.4.2.2 Inorganic Fouling/Scaling*

Inorganic fouling is caused by inorganic constituents of feed water and is also called as scaling. Due to an increase in % recovery of RO membranes, the concentration of sparingly soluble inorganic salts such as calcium sulfates, calcium carbonates etc increases

above saturation level on the feed side of the membrane. As a result, these salts crystallize on the membrane causing membrane scaling (Shih et al., 2005). The scaling causes decline in flux and reduction in membrane life. Although various salts have been associated with membrane scale formation such as sulfates (SO<sub>4</sub>) and carbonates (CO<sub>3</sub>) of calcium, aluminum, magnesium and iron; calcium carbonate and calcium sulfate dihydrate (also called as gypsum) are the most common scalants found during desalination of water (Shih et al., 2005). The most common calcium sulfate scale minerals include anhydrite (CaSO<sub>4</sub>), hemihydrate (CaSO<sub>4</sub>·1/2H<sub>2</sub>O) and gypsum (CaSO<sub>4</sub>·2H<sub>2</sub>O) (Kan et al., 2005; Schausberger et al., 2009). The pH adjustment can help to reduce the scaling caused by calcium carbonate, whereas, it does not affect the precipitation of calcium sulfate (gypsum) (Shih et al., 2005). If a solution is supersaturated with respect to one or more calcium sulfate minerals, precipitation can occur according to the reaction:



Concentration polarization also enhances the precipitation of inorganic salts as their concentration often exceeds the solubility limit near the membrane surface. Therefore, the extent of scaling depends upon the concentration of salts present in feed water e.g. sea water which is an aqueous solution of salts possess higher potential for scaling in RO membrane. These inorganic foulants such as nitrogen, phosphorus etc present in sea water also act as nutrients for microorganisms and therefore enhance the formation of biofilm on the membrane surface (Song et al., 2008, Van de Lisdonk et al., 2000).

It has been noted that the amorphous solids comprised of alumino-silicates caused

scaling in hollow fiber RO membranes (Butt et al., 1995). In addition, it was also noted that scaling resulted due to the formation of calcium or magnesium phosphonates by the antiscalants themselves (Butt et al., 1995). Sometimes, the calcium ions ( $\text{Ca}^{+2}$ ) present in feed water may also create bonds with carboxylic functional groups and produce macromolecules which has potential for scaling and reducing the flow of permeate (Ang et al., 2006). Another research has also shown the involvement of calcium ions in the formation of scales with humic substances during sea water reverse osmosis (SWRO) (Monruedee et al., 2012).

*2.4.2.2.1 Stages in Scale Formation.* The process of scaling can be divided into different stages. The first step is Induction in which nucleation occurs. The process of nucleation involves the complex organization of ions / molecules. The deposition step is then followed in which the nuclei thus formed will start depositing on the surface (Figure 6). The adhesion / deposition step results due to Van der Waals and electrostatic forces as well as other type of interactions such as hydrophobic or ion bridging interactions. At the end, the aging period starts during which changes in crystal structure occurs (Antony et al., 2011).

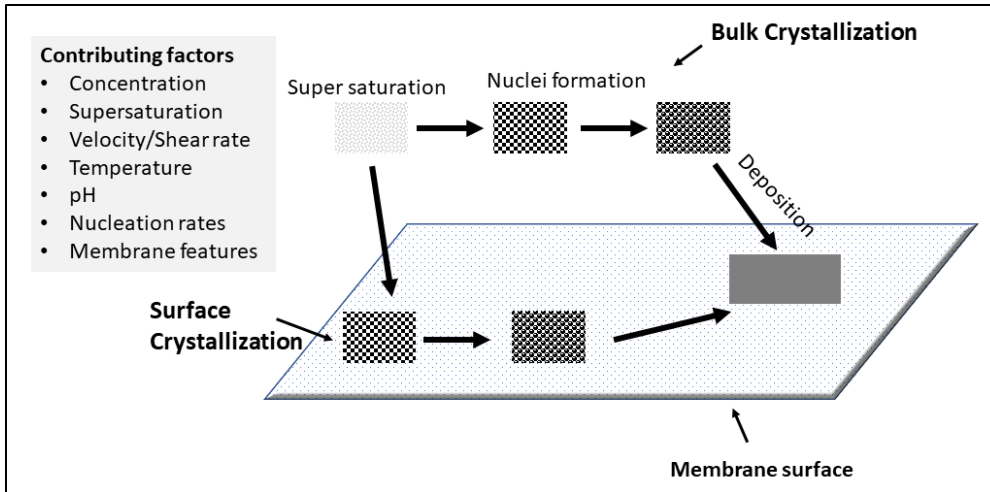


Figure 6. Contributing factors and steps in scale formation (adopted from Antony et al., 2011)

*2.4.2.2.2 Surface and Bulk Scaling.* Surface scaling occurs near the membrane surface as a result of supersaturation or due to the presence of substances responsible for crystals formation in the solution or due to the presence of conditions responsible for nucleation (Lee and Lee, 1999). Such conditions lead to the formation of scale at the membrane surface. When the supersaturation occurs in the bulk solution i.e. away from membrane surface, crystals will form away from membrane surface in the bulk solution and then settles on the membrane surface (Hasson et al., 1996). It is now accepted that mineral salt scaling occurs by both the deposition of bulk formed crystals onto the membrane surface and direct surface crystallization on the membrane surface (Figure 7) (Shih et al., 2005).

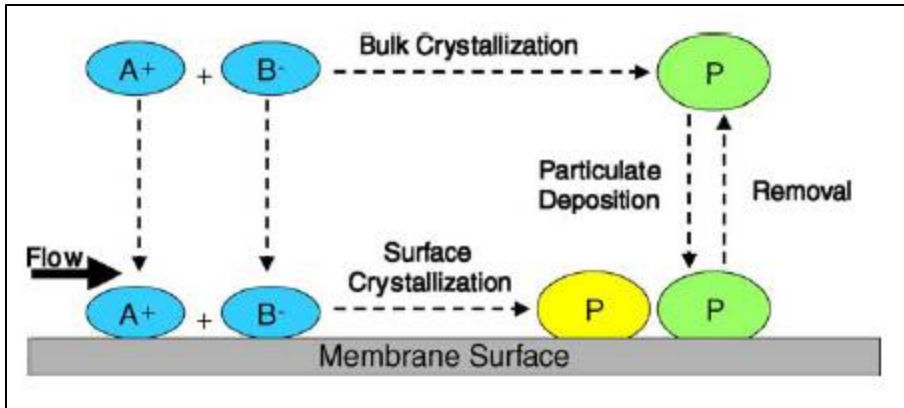


Figure 7. Conceptual representation of scaling (Shih et al., 2005)

2.4.2.2.3 *Factors Affecting Scaling.* There are several factors that affects the formation of scale such as temperature, pH, membrane materials, geometry and roughness (Sheikholeslami and Ng, 2001; Hamrouni and Dhahbi, 2001). In addition, presence of other substances also enhances crystal growth and membrane scaling via providing nucleation sites.

- **Supersaturation.** As discussed above, the main cause of scaling is the supersaturation of salts. Due to the increase of solubility product of calcium carbonate and calcium sulfate above the saturation value, their precipitation results on the membrane surface (Lee and Lee, 1999).
- **Velocity and Shear Rate.** The velocity of feed water affects the boundary layer formation. Because the turbulence induced by increased cross flow velocity will wash away the accumulated solutes from the membrane surface and thus the concentration polarization and nucleation will not result. Other researchers (Alventosa-deLara et al, 2012; Nghiem et al, 2008) also reported similar results and they also linked the reduction in concentration polarization and membrane fouling



with rise in velocity. Thus, the scaling usually occurs in dead end zones where water flow velocity is low.

- **pH and Ionic Strength.** The pH and ionic strength affect the supersaturation and rate of crystallization. The solubility of deposits such as calcium carbonate and magnesium hydroxide increase with the increase in pH (Sheikholeslami and Ng, 2001). Therefore, the deposition of such minerals can be controlled through pH adjustment. However, other deposits such as calcium sulfate's (gypsum) solubility is not pH dependent and therefore, the pH adjustments will not help to control gypsum's scaling.
- **Nucleation.** The nucleation rate also affects the scale formation on membrane. The ions interact with each other to form clusters which act as a platform for more deposition of ions. However, for nucleation to occur, the barrier of activation energy of the nuclei should be overcome (Stumm and Morgan, 1981).
- **Temperature.** The solubility of some salts such as calcium carbonate, calcium sulfate, calcium phosphate and magnesium carbonate, magnesium hydroxide etc is inversely proportional to temperature and thus, the solubility decreases with increase in temperature. However, at lower temperatures, the solubility of these salts will increase, and rate of crystallization will rise.

*2.4.2.2.4 Calcium Sulfate Scaling.* The most common scalant found in seawater desalination is calcium sulfate. The scaling caused by calcium sulfate deposition is also called as non-alkaline scale (Patel and Finan, 1999). The calcium sulfate is white in color and is quite like calcium carbonate in appearance. It mainly exists in three forms i.e.

calcium sulfate anhydrite ( $\text{CaSO}_4$ ), calcium sulfate hemihydrate ( $\text{CaSO}_4 \cdot 0.5\text{H}_2\text{O}$ ) and calcium sulfate dihydrate or gypsum ( $\text{CaSO}_4 \cdot 2\text{H}_2\text{O}$ ). The solubility of these forms of calcium sulfates are more than calcium carbonate (Patel and Finan, 1999). The most commonly occurring form of calcium sulfate is gypsum and it has a monoclinic prismatic crystal structure containing either four or eight molecules in the unit cell (Figure 8) (Shih et al., 2005).

The phenomenon of gypsum crystallization is complex and various factors such as temperature and pressure affect the rate of crystallization and crystal growth. Furthermore, the presence of other minerals and dissolved substances can also affect the formation of calcium sulfate or gypsum crystals (Trivedi et al., 2014). The solubility of gypsum decreases with temperature and possess maximum solubility at temperature range of 30-40°C. In reverse osmosis applications, the gypsum is commonly found deposit where temperature is about 50°C. In other applications where temperature is higher, the calcium sulfate hemihydrate and anhydrite are more common (Amjad, 2013; Muryanto et al., 2013). The precipitation of calcium sulfate is not pH sensitive unlike other scalants like calcium carbonate (Shih et al., 2005). The crystals of calcium sulfate can be as hard rock or soft granules depending upon the conditions at the time of precipitations. Like other scalants, presence of other dissolved substances can affect the gypsum scaling. It has been shown that organic compounds containing carboxylate as functional group severely affected the formation of gypsum deposits on the membrane surface (Liu and Mi, 2014).

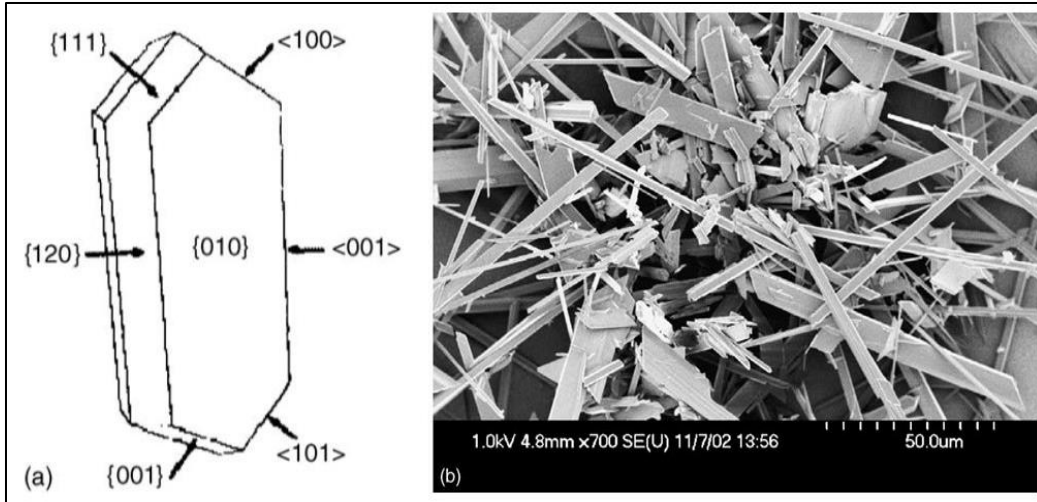


Figure 8. (a) Monoclinic gypsum crystal morphology (numbers in parenthesis represent crystal orientation); (b) SEM image of gypsum crystal on membrane (Shih et al., 2005)

#### 2.4.2.3. Colloidal/Particulate Fouling:

The type of fouling that result due to the presence of colloidal or suspended particles is called as Colloidal or particulate fouling. The colloidal particles can be categorized as following in order of increase in their size:

- Dissolved solids (<0.001  $\mu\text{m}$ )
- Colloidal solids (0.001  $\mu\text{m}$  to 1 $\mu\text{m}$ )
- Supra-colloidal solids (1  $\mu\text{m}$  to 100  $\mu\text{m}$ )
- Settle able solids (>100  $\mu\text{m}$ )

The colloidal substances could be of organic or inorganic nature (Yiantsios et al., 2005). Table 4 shows some examples of both organic and inorganic colloids (Yiantsios et al., 2005, and Ning, 1999).

Table 4. Organic and Inorganic colloids involved in Colloidal Fouling

<b>Organic colloids</b>	<b>Inorganic colloids</b>
Fats,	Iron and manganese oxides
Proteins,	Calcium carbonate
Oil,	Sulfur and sulfides
Carbohydrates	Aluminum silicates
Lipoproteins (secretions)	Silica
Kerogen (aged polysaccharides, marine snow)	
Humic-like substances	
Biological debris (plant and animal)	
Polysaccharides (gums, slime, plankton, fibrils)	
Microorganisms	

Membrane fouling results when these particles agglomerate and form a cake layer on the surface of membrane. The particulate colloids either already presents in feed water or they are formed because of concentration polarization. The colloids then agglomerate and settle down on the membrane surface forming a cake layer thereby causing membrane fouling. Several factors such as salinity, increase in concentration, flocculation, interaction with membrane surface and other physicochemical aspects affect the cake layer formation.

The inorganic colloids such as Aluminum silicates undergo polymerization reaction and by interacting with other organic and inorganic matter to form fouling layer. Similarly, organic colloids such as proteins, oils and polysaccharides also enhance membrane fouling. Therefore, it is not easy to differentiate between fouling caused by organic and inorganic colloids (Yiantsios et al., 2005). Same as other type of fouling; the colloidal fouling also depends upon the quality of feed water, membrane roughness etc. Therefore, if the membrane surface is smooth, the colloidal fouling rate will be less (Zhu and Elimelech, 1997).

#### 2.4.2.4. Biofouling

Biofouling refers to the formation of biofilm by the attachment and subsequent microbial growth on membrane surface (Chen et al., 2006). The Microorganisms can survive at wide temperature (-12°C to 110°C) and pH (0.5-13) ranges (Baker and Dudley, 1998). Biofouling is major problem in RO plants especially in Middle East countries like Qatar where temperature of seawater entering the plants exceeds 25°C which is optimum temperature for microbial growth (Al-Ahmad et al., 2000). It has been found that biofouling is most frequently occurring type of membrane fouling in membrane filtration plants. Thus, 82% RO plants in USA (Ridgway and Flemming, 1996) and 70% of RO plants treating sea water worldwide suffer from the problem of biofouling (Khedr, 2002).

The microorganisms are usually present in water systems. Therefore, they affect the membranes irrespective of type of feed water (Rodriguez and Penate 2012, Pang et al., 2005). It has been shown that the gram-negative bacteria are most common in causing biofouling in membrane systems such as *Proteobacteria* or *Bacteroidetes* (Ivnitskya et al., 2010). It is also reported that the living bacterial cells causes the flux decline more than the biofilm made by dead cells. Furthermore, the EPS secreted by bacteria causes more hydraulic resistance than the bacteria themselves. The EPS are comprised of polysaccharides and proteins linked to functional groups such as phenolic alcohols (OH), methoxycarbonyls (CH<sub>3</sub>-O-CO) and carboxylic acids (COOH) (Tsuneda et al., 2003). The balance between the rate of attachment of microbial cells, their growth rate and their detachment rate govern the formation of biofilm (Wang et al., 2013).

Biofilm formation affects the RO performance in several ways. It increases the

hydraulic resistance for the feed stream flow and reduces the transmembrane pressure. This will ultimately result in decline of membrane's permeate flux and membrane rejection (Wang et al., 2013). Alternatively, the biofilm formation sometimes acts as an additional barrier to the salt passage through the membrane, which enhances the membrane salt rejection.

During the initial stage of biofilm formation and growth, if the growth conditions are favorable, bacteria will grow rapidly which causes steep decline in permeate flux within the starting few days of membrane filtration operation. After reaching the threshold, the biofilm growth gets stable, which causes fewer declines in flux compared to initial days of operation. In membrane filtrations, the biofilm mostly results in the first membrane element of multi-elements membrane system or in the feed spacer of the membrane system.

2.4.2.4.1 Steps in Biofilm formation. Typically, a biofilm develops through a series of following five phases.

- **Development of conditioning film:** The biofilm formation starts with the development of conditioning film. This step involves adsorption and deposition of different substances (both organic and inorganic in nature). These organic and inorganic species are either present in water or released from microorganisms. The deposition of these substances helps in the attachment of living cells present in water. This step takes place before the attachment of cells (Ghayeni et al., 1998). The conditioning of membrane surface occurs within few minutes (Melo et al., 1988)

In literature, there is no information related to the characterization of the substances forming conditioning layer on the membranes in desalination plants. However,

researchers have studied the phenomenon in different materials such as glass and steel and found that substances like humic acids (Loeb and Neihof, 1975) proteins (Compere et al., 2001) and carbohydrates (Garg et al., 2009) constitutes major part of conditioning film. The formation of the layer changes both physical and chemical properties of the membrane such as hydrophobicity, roughness and surface tension. The changes in membrane properties thus also aids in cells attachment to the surface.

- **Transport of Microorganisms to the membrane surface:** Several factors play a role in bringing the microorganisms near the membrane surface and enhancing their contact with the surface. The factors include motility of microbes, permeate drag forces and diffusion. The operating conditions such as pressure and flow rate also play important role in bringing microorganisms near the membrane surface and consequently their attachment and growth on the membrane (Mansouri et al., 2010).
- **Microorganisms adhesion to the surface:** In order to grow and form a biofilm layer, bacteria need to adhere to the surface of the membrane. Thus, it is the primary step in biofilm formation (Costerton et al., 1994). The bacterial attachment can be reversible and irreversible. During reversible adhesion, the bacteria gets detaches due to shear forces generated by feed stream. However, during irreversible adhesion, the bacteria secretes extracellular polymeric substances (EPS) which helps them to anchor the surface of the membrane (Subramani and Hoek, 2010).
- **Microbial growth:** The main step of biofilm formation is microbial cells growth that results following microbial cells adhesion. The nutrients availability and operating conditions affect the growth of bacteria. The step usually occurs within days to weeks.

Some bacteria also release EPS, which helps them to protect the bacterial colonies thus formed.

- **Detachment and Dispersion.** The final step is the detachment of bacteria and their dispersion into the feed stream. This takes place over weeks and months and depends upon hydrodynamic conditions and biofilm physiology.

In literature, the process of biofilm formation has also been described in slightly different way as shown in Figure 9 (Monroe, 2007). This shows that the biofilm formation starts with initial (reversible) attachment followed by irreversible attachment, initial and final growth and then dispersion. However, the mechanism remains same as the process starts with the reversible and irreversible attachment of microorganisms followed by their growth and dispersion. As previously explained, there are several factors affect the formation such as flow rate of feed stream, nutrients availability and temperature.

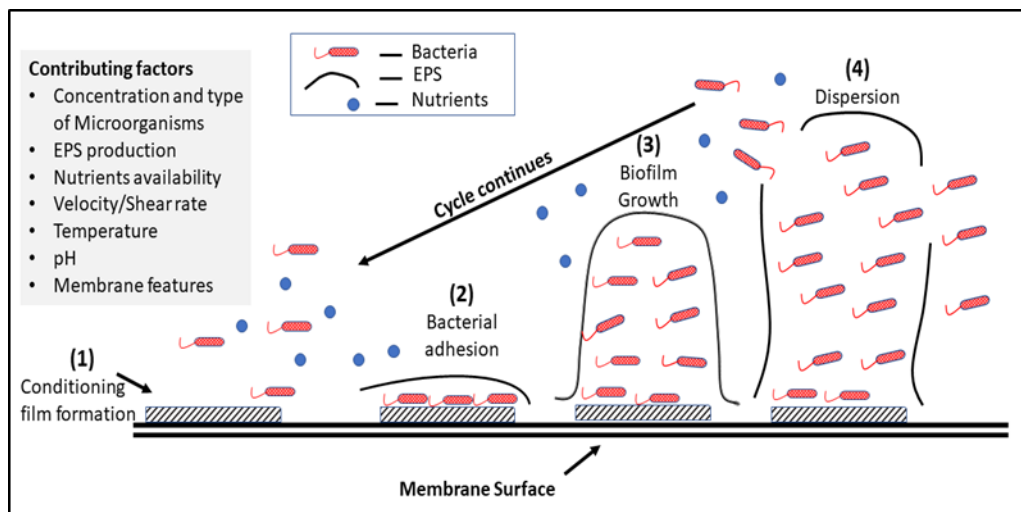


Figure 9. Five steps of Biofilm formation (1: Initial attachment, 2: Irreversible attachment, 3: Initial growth, 4: Final growth, 5: Dispersion) (Monroe, 2007)



2.4.2.4.2 *Factors affecting Biofilm formation.* There are several factors that play a role in biofilm formation pertaining to surface of membrane, feedwater characteristics and type of microorganisms (Table 5). The electrostatic and Vander Waal forces govern the attachment of bacteria to the surface. Furthermore, the type of membrane material (Flemming and Ridgway, 2009) and characteristics such as hydrophobicity (Daniels, 1980; Ridgway et al, 1985) and electrostatic charge (Daniels, 1980) also affects this step. It has been shown that the increase in ionic strength enhances attachment of bacteria. According to Mceldowney et al. (1986) increase in ionic strength increases the microbial adhesion. The effect of pH was also studied on three species of *Pseudomonas* on NF and RO membranes and it was shown that there was an increase in rate of attachment with increase in ionic strength of the medium (Ghayeni et al., 1998). Other factors such as cross flow velocity and back diffusion also affects the process of bacterial attachment to surface of membrane (Kang et al., 2004). The inorganic substances present in feed stream form crystalloids that settles on the membrane surface. These inorganic crystalloids enhance membrane roughness which is favorable for bacterial attachment and adhesion (Han and Lin, 2009).

Table 5. Factors affecting Biofilm Formation (Nguyen et al., 2012; Flemming and Ridgway, 2009)

Membrane Surface	Feed water conditions	Microorganisms
Conditioning film	Flow rate / shear rate	Type (Bacteria / Fungi)
Hydrophobicity/Hydrophilicity	Nutrients availability	Species
Surface roughness	Temperature	EPS production
Membrane Porosity	pH	Concentration of microbes

Membrane Surface	Feed water conditions	Microorganisms
Surface charge	Dissolved substances	Adaptability / Physiological responses
Membrane material/ configuration	-	-

The composition of feed stream also affects the biofilm formation. It was reported that the feed stream despite having high substrate composition but with lack of phosphate substances caused less biofouling. Thus, antiscalants used in RO membranes may contain phosphate substances which will enhance the biofilm formation (Vrouwenvelder et al., 2010).

Due to the ability of microorganisms to grow and multiply at a much faster rate, even 99.9% removal of microorganisms does not prevent biofouling (Flemming, 1997). In terms of membrane materials, polysulfone and polyamide membranes promote more microbial growth than other materials (Flemming and Ridgway, 2009). Furthermore, the membrane configuration also affects the biofouling. It has been noted that spiral wound membrane configuration promotes higher bacterial growth as the environment inside the spiral wound membrane has optimum growth conditions in terms of temperature and low cross flow velocity and turbulence (Al-Ahmad et al., 2000).

The water flow rate affects the biofilm formation by increasing the loading rate of nutrients to the microorganisms and by increasing the shear rate (Dreszer et al., 2013). The shear rate also affects the biofilm morphology. It was found that the low shear rate causes the biofilm more filamentous and compact as compared to high shear rate (Vrouwenvelder et al., 2010).

Several researches have focused on the kinetics and dynamics of biofilm formation

on membranes. It was found that *Gammaproteobacteria* and *Betaproteobacteria* are the groups of bacteria that form biofilm on NF membrane despite the presence of less nutrients in feed stream (Horsch et al., 2005). Similarly, Bereschenko et al. (2010) analyzed the biofilm layer formed after 4, 8, 16 and 32 days in membranes and found that the biofilm was mainly formed by *Sphingomonads* (class *Alphaproteobacteria*). The techniques utilized in the study include both molecular (denaturing gradient gel electrophoresis, fluorescence in situ hybridization and cloning) and microscopic (field emission scanning electron microscopy and confocal laser scanning microscopy). Furthermore, the technique of 16s rRNA T-RFLP (terminal restriction fragment length polymorphism) was also utilized to characterize the biofilm on membrane and it was found that *Leucothrix mucor* (*Gammaproteobacteria*) was about 30% of the clone library (Zhang et al., 2011).

## 2.5 Anti-Biofouling and Anti-Scaling

Several techniques have been introduced and implemented to avoid biofouling and mineral scaling on RO membranes. Since many factors play a role in formation of mineral scales as discussed in previous sections; different treatment techniques are designed to tackle those factors and ultimately to reduce the RO scaling. The pretreatment techniques may include changes in feed water composition by addition of coagulants (coagulation) to remove scalants before RO step, softening of feed water through ion-exchange technique and changes in pH to enhance solubility of scales. In addition, other techniques such as addition of antiscalants, limiting product recovery etc have also been proposed and tested (Antony et al. 2011). Similarly, techniques to reduce biofouling may include removal of microorganisms from feed water and several disinfection techniques such as chemical,

thermal, UV light electrical and ultrasound techniques (Al-Juboori and Yusaf, 2012).

In addition, efforts have also been made to improve the membranes through membrane coating and making them resistant to fouling. The techniques used for membrane coating may include physical coating, grafting (using techniques such as free radical, plasma/redox induced technique, photochemical technique (Bhattacharya and Misra, 2004)) or during membrane synthesis / fabrication (Louie et al. 2006). Most of the membrane coating techniques targets to enhance the membrane surface properties to make them resistant to fouling/scaling. However, modifying the characteristics of RO membrane may sometimes lead to other problems such as net negative charge on the surface will attract positively charged other fouling substances leading to enhanced fouling due to those substances. Similarly, hydrophilic membrane will have enhanced fouling due to hydrophilic compounds present in feed water (Kwon et al. 2004).

#### *2.5.1 Membrane coating using polymers and nanomaterials for anti-biofouling*

Since, biofouling occurs in a sequence of steps explained in Section 2.5.2.4.1; the anti-biofouling strategies focus on to stop biofouling by preventing one or more of these stages to happen such as preventing the bacterial adhesion to membrane surface or biofilm growth. This is achieved by modifying membrane surface to improve the features that are linked with membrane fouling potential such as surface roughness and charge, hydrophobic/hydrophilic properties etc. Since, the bacterial surfaces have negative charge in water (Hori and Matsumoto, 2010); the negative charge on the membrane introduced through coating helps to create repulsion between membrane and bacteria and avoids microbial attachment. Similarly, the hydrophilicity of membrane surfaces enhances its

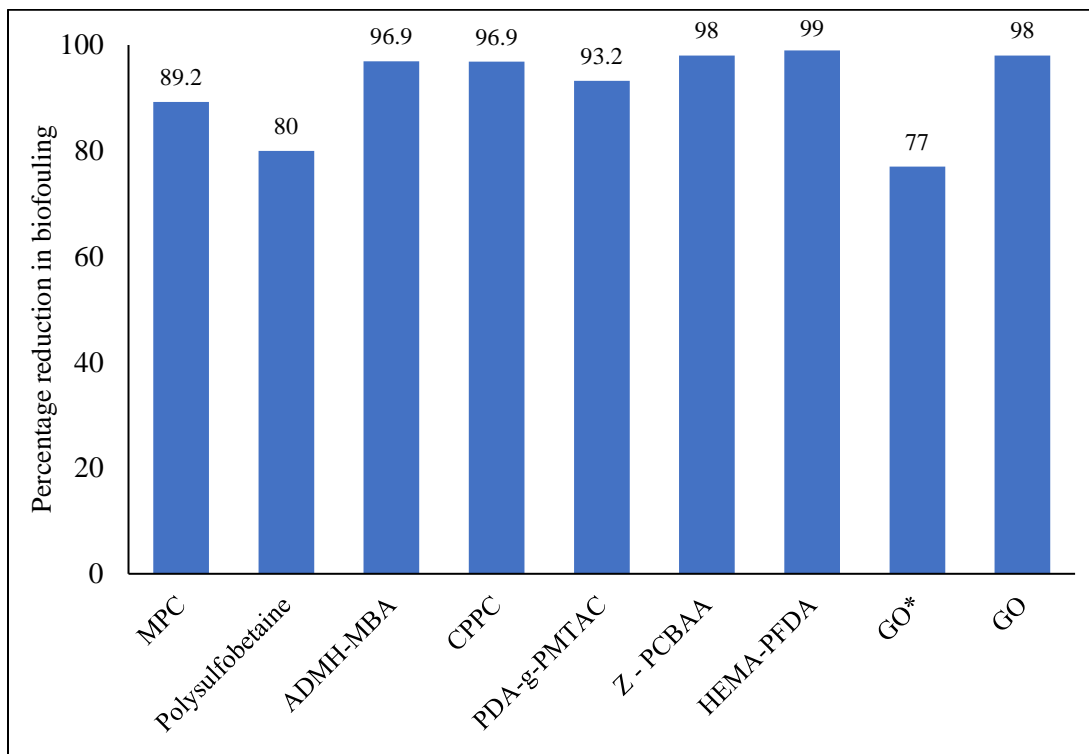
interaction with water molecules instead of microorganisms and therefore, inhibits their attachment and growth (Al-Juboori and Yusaf, 2012).

Different polymers have been used for membrane coating to impart anti- biofouling properties into the RO membrane. Figure 10 shows the comparison of different polymers' performance against biofouling of RO membranes. For example, 80% reduction in biofouling result (Figure 10) when the polyamide RO membrane was coated with polysulfobetaine (Ginic-Markovic et al. 2015). This was achieved by increasing the hydrophilicity and surface smoothness of the membrane. Water contact angle analysis showed that the contact angle reduced from  $62 \pm 1^\circ$  to  $16.8 \pm 2^\circ$  after coating. Furthermore, transmission electron microscopy showed that the membrane surface smoothness has significantly enhanced after modification of membrane surface with polysulfobetaine polymer.

Similarly, Blok et al. (2014) modified the polyamide RO membrane via polymerization process in two steps i.e. the layer of 2-bromoisobutyryl bromide initiator-polydopamine (BiBBr-initiator-PDA) was formed on the membrane surface followed by grafting of polymer chains of [2-(methacryloyloxy) ethyl-trimethylammonium chloride (MTAC). The results showed that modified membrane (abbreviated as PDA-g-PMTAC) had relatively higher hydrophilicity than unmodified membranes. Furthermore, the results clearly show that the modified membrane possess promising anti-biofouling properties as shown in Figure 10.

Thus, it can be concluded from Figure 10 that several polymers have been used against biofouling and showed satisfactory performance. However, to the best of our knowledge, there is no research done related to polymer coating to reduce scaling. Instead,

antiscalant polymers such as poly acrylic acid and poly maleic acid have been used in feed water to reduce scaling.



**MPC:** 2-methacryloyloxyethyl phosphorylcholine; **ADMH-MBA:** 3-allyl-5,5-dimethylhydantoin (ADMH) crosslinked by N,N'-Methylenebis(acrylamide) (MBA); **CPPC:** Cationic phosphorylcholine polymer; **PDA-g-PMTAC:** Poly [2-(methacryoyloxy) ethyl]trimethylammonium chloride; **Z – PCBAA:** Zwitterionic structures containing polycarboxybetaine acrylic acetate (PCBAA); **HEMA-PFDA:** Hydrophilic hydroxyethyl methacrylate (HEMA) and the hydrophobic perfluoro decylacrylate (PFDA); **GO\*:** Graphene oxide layer in both polyamide active and polysulfone support layer; **GO:** Graphene oxide embedded TFC membrane

Figure 10. Example of some polymers and nanomaterials used recently for anti-biofouling research. (Chae et al. 2017, Chae et al. 2015, Ginic-Markovic et al. 2015, Shafi et al. 2015, Blok et al. 2014, Matin et al. 2014, Saeki et al. 2014a, Saeki et al. 2014b, Zhang et al. 2013)

Other than modifying the membrane surface features using polymers, antimicrobial

agents in the form of nanomaterials have also been used in membrane coating such as graphene oxide (Chae et al. 2017), zwitterion functionalized carbon nanotubes (Chan et al. 2016) and silver nano-particles (Rahman et al. 2014) into the RO membrane. Among these antimicrobial nanomaterials, graphene oxide has been given importance due to their unique properties in terms of mechanical strength, high surface area (Ong et al. 2016) and antimicrobial properties (Chen et al. 2014; Yu et al. 2013). The GO inhibits biofilm formation by producing reactive oxygen species or by removing lipid contents from bacteria thereby deactivating them or by changing the membrane surface charge (Ong et al. 2016). Recently a novel approach was adopted by embedding GO layer into both polyamide active layer and polysulfone support layer (Chae et al. 2017). The resulted membrane showed 77% improvement in antibiofouling capabilities and 17% increase in permeability. This is because of changes in surface charge, roughness, and hydrophilicity of the modified membrane. The CLSM images of the modified membranes in comparison with bared membranes clearly showed that the biofilm formed on modified membranes was significantly less than bared membranes.

### *2.5.2 Membrane coating using nanomaterials for anti-scaling.*

Nanomaterials have also been used in membrane coating to enhance the membrane flux and thereby enhancing antiscaling capabilities such as graphene oxide (Chae et al. 2017), silica (Bao et al. 2013 and Yin et al. 2012), carbon nanotubes (Zhang et al. 2011), titanium dioxide (Kim et al. 2016) and zwitterionic structures (Chan et al. 2013) (Figure 11). The increase in permeability was achieved through providing water transport network structures in the membrane. Titanium dioxide is famous for membrane coating due to their

properties such as chemical stability, photocatalytic activity, high membrane flux and low cost. Therefore, these materials are used for membranes to reduce fouling (Buonomenna, 2013). Recently, Kim et al. (2016) proposed a novel sol gel-derived spray coating method for coating titanium dioxide nano particles on reverse osmosis membranes. The coating resulted in negative charge on the membrane surface with hydrophilic properties. Thus, the coated membrane showed 25% increase in flux as compared to non-coated membrane which showed its enhanced resistance to fouling/scaling.

The comparison shown in Figure 11 reveals that nanotubes such as zwitterion functionalized carbon nanotubes and multiwalled carbon nanotubes have shown tremendous improvement in terms of membrane permeability and antiscaling properties as compare to other materials. Thus, the ability of carbon nanotubes (CNTs) to reject substances simultaneously providing path for water flow through the membrane has made these nanomaterials successful in membrane technology. The research group of Chan et al. (2013) showed that incorporation of zwitterion functionalized CNTs into polyamide membrane increased the membrane flux from 6.8 to 20.7 gallons/ft<sup>3</sup>/day (more than 2-fold) with just slight increase in percentage rejection. In addition to CNTs, zeolite nanomaterials are another type of nanomaterials that have shown their potential to improve RO membranes. Due to their ability to enhance molecular sieving mechanism and adsorption through providing cation exchange sites; the zeolite has shown to improve permeability more than 75% as well as increase in percentage rejection by about 5 % (Fathizadeh et al. 2011).



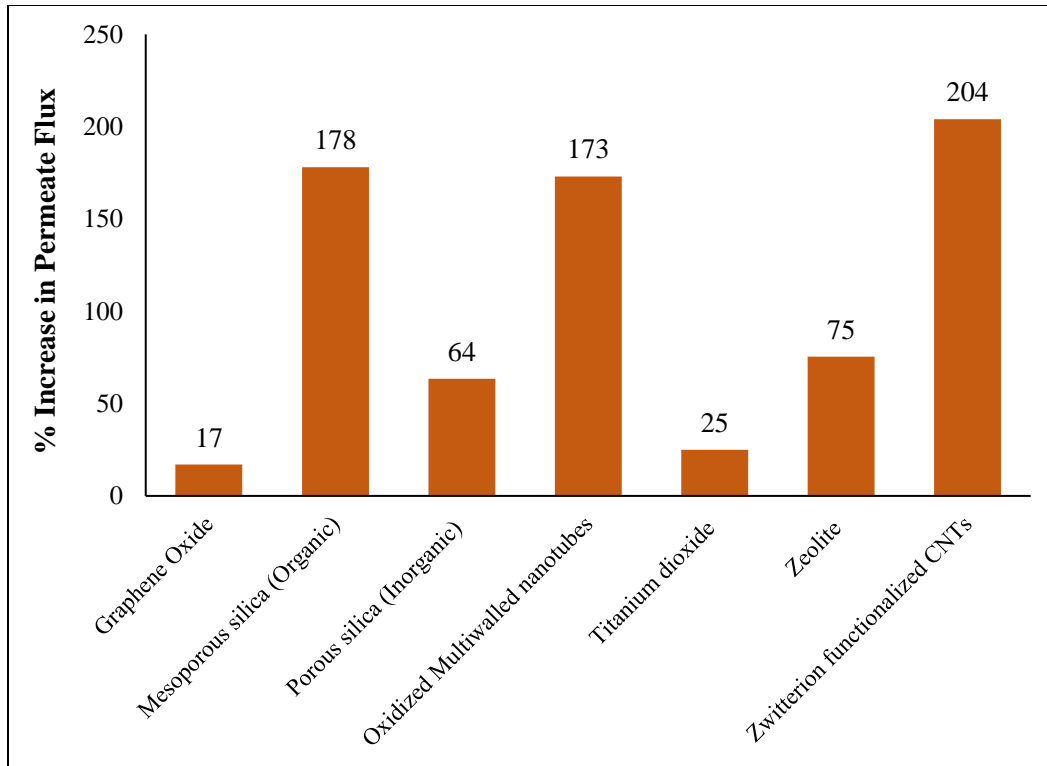


Figure 11. Enhancement of permeate flux using some nanomaterials for RO anti-scaling research. (Chae et al. 2017; Kim et al. 2016; Bao et al. 2013; Chan et al. 2013; Yin et al. 2012; Fathizadeh et al. 2011; Zhang et al. 2011)

Although membrane modifications using nanomaterials and polymers have achieved great attention and considerable success have been achieved in terms of reduction in mineral scaling and biofouling. However, there are some issues related to their widespread usage at larger scale. The issues related to economic feasibility, complicated operation and maintenance process, time consuming membrane modification process, mechanical strength and durability are some key issues associated with their use at large scale (Ong et al. 2016). In addition, statistics have shown that 500 research papers haven't been published to address the issue of biofouling during last 10 years. Similarly, researchers have also put efforts on to reduce scaling caused by carbonates and sulphates.

However, it can be deduced that the researchers have tried to resolve one of the two problems (biofouling and scaling) at a time. Since, the two problems often co-exist in RO systems and may also help to promote each other such as microbial mediated precipitation; there is need to look for solutions to tackle both issues together. Therefore, novel materials such as combination of both or individual polymers and nano materials needs to be introduced and tested for their ability to reduce both scaling and biofouling simultaneously.

### *2.6 Analytical techniques used to characterize scaling.*

There are several techniques used for the characterization of scaling. By knowing the chemical composition of the deposits, it helps to understand different processes that are involved in scale formation. There are two types of techniques i.e. Destructive and Non-Destructive. The Nondestructive techniques provides information about the chemical composition of the deposits as well as the links between the scalants and other substrates. Whereas, the destructive techniques provide information about the elemental profiles of the deposits and their degree of reactivity. Visual techniques help to explain the structure of the scales formed and their characteristics such as hardness and porosity. In addition, information about degree of crystallinity, the size of crystals and their morphologies can also be obtained using these techniques. The detailed analysis of the deposits helps the investigator to develop the best antiscaling strategy, its mechanism of action, its effectiveness and cleaning protocols for the membrane (East et al., 2015).

#### *2.6.1 Scanning Electron Microscopy (SEM)*

SEM offers more quantitative approach as compared to light microscopy, which

relies on qualitative analysis of deposits. In SEM, elemental analysis is done including images that are collected from secondary electrons and back scattered electrons from the specimen. Back scattered electrons show about the density differences in the area, which is based on the atomic number of atoms in the sample. Whereas, secondary electrons help to generate image of high resolution that shows topography of scales and deposits with details up to 100 nm scale. In order to avoid the charge buildup in the sample and its damage, the specimen should be coated with gold or carbon as a conductive material. However, coating is not required for backscattered imaging for elemental analysis as the coating itself may become the source of contamination. However, carbon coating can be done which does not affect the results of elemental analysis significantly (East et al., 2015).

The working principle of SEM relies on striking the beam of electrons on the surface of the specimen and then detecting the interactions of electron beam with the surface. After the electrons beam hits the surface, it will eject electrons from the (electron orbital of) atom on the surface. These ejected electrons are called as Secondary electrons, which is used to generate an image on the computer. The electron, thus, emitted from the inner orbital will be replaced by the electron from the outer orbital releasing x-ray. The energy of the x-ray depends upon the atom and therefore, it is called as characteristic x-ray. These radiations are then detected using x-ray detector to perform the elemental analysis of the foulants which tells both the nature of foulants as well as their amounts present. This is called as Energy dispersive spectroscopy (EDS).

The atoms present in the deposits may also scatter the electron beam without losing energy. When this electron beam reflected from the sample, it is detected using backscatter detector. The atoms with higher atomic number reflect more electrons leading to brighter

image of these atoms. Thus, the image from these backscattered electrons is used to understand and know about the density differences in the area.

It is important to obtain information about the elemental profile of the scales and deposits. The techniques such as ICP and XRF do provide such information. However, sample preparation processes for these techniques causes loss of structural information of scales and therefore, EDS-SEM technique is useful for this purpose. The drawback for EDS technique is that the sample preparation is a time-consuming process.

Elemental mapping; a form of EDS is another technique that can be used for the analysis of elements in scales. It analyzes each point separately and then produces a profile, which provides information about the elements present in scale as well as their distribution throughout the specimen. Thus, combining all these techniques in SEM will be helpful for the analysis of scales and deposits.

### *2.6.2 X-ray Diffraction (XRD)*

This technique is used for the mineral's identification in deposits and scales. Both powder diffraction and surface techniques are used. In these techniques, the x-ray of known wavelength strikes on the surface and its diffraction pattern is then recorded as shown in Figure 10. The pattern is the product of the incident and reflection angle from the surface, the distance between crystal planes within the sample. When the x-ray will incident on the sample, some rays will be reflected from the surface while some travels into the crystal planes and then reflected (Atkins and De Paula, 2002) (Figure 12). Since, the crystalline materials have their own characteristic distances between their crystal planes; this information is used for the identification of crystalline phases in the sample. Thus, X-ray

diffraction technique is useful in getting the details about the crystalline phases of the sample. Furthermore, it can also be used to estimate the non-diffracting content (i.e. amorphous part) of the sample.

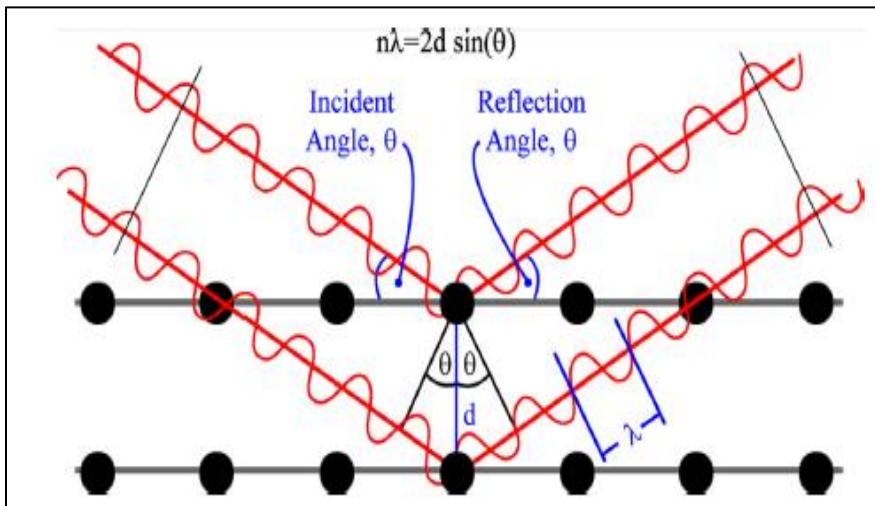


Figure 12. Principle of X-ray diffraction, where  $d$  is the distance between crystalline planes (Atkins, 2002)

### 2.6.3 X-ray Fluorescence (XRF).

This technique is used to perform the elemental analysis of the scales / deposits. The principle is same as Energy dispersive spectroscopy in SEM. However, the only difference is that XRF uses X-rays instead of electron beams. Thus, the X-rays are used to emit the electron from the inner orbital (lower energy orbital i.e. K-shell) which is then replaced by the electrons from outer orbitals (higher energy orbital i.e. M-shell or L-shell). The electrons from the outer orbital releases the energy (x-ray fluorescence) upon moving to inner orbitals (as shown in Figure 13) which is then detected to perform elemental analysis of the scale. The technique depends upon the penetration capability of the X-rays

and fine details are difficult to obtain since the size of sample is usually in mm range (Seltzer, 1993). The requirement of sample preparation is less in XRF techniques. However, it is important to ensure that the sample fits in the sample holder.

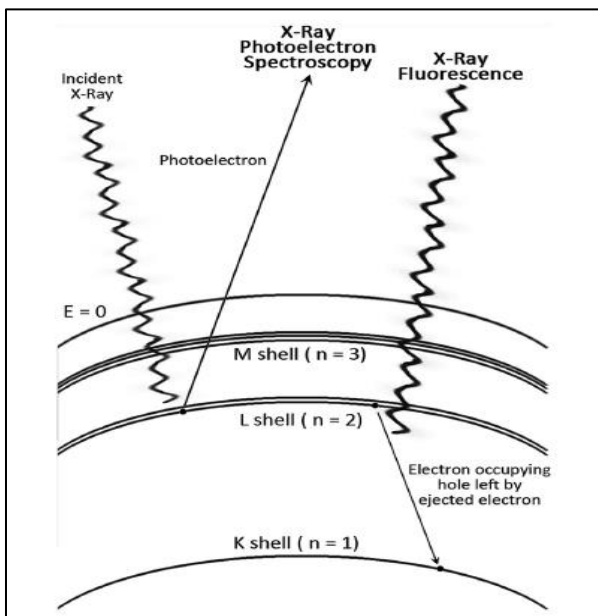


Figure 13. X-ray Photoelectron and X-ray Fluorescence Spectroscopy (Seltzer, 1993)

It has been shown that the XRF is useful technique for scale analysis. This technique has been utilized to characterize the amorphous deposits as well which cannot be detected by other techniques such as XRD. Thus, the identification of aluminosilicates, calcium / magnesium phosphonates have been done on RO membranes using XRF technique (Butt et al., 1995). It can also be used in combination with SEM and XRD to confirm the elemental analysis of deposits and scales.

#### 2.6.4 X-ray Photoelectron Spectroscopy (XPS).

XPS; also called as Energy spectroscopy for Chemical analysis; is a technique to

analyze the atomic structure, the electronic structure of an atom and ionization energies. This is done by irradiating the atoms/elements/sample with X-rays to eject the electrons and then measuring the kinetic energy of the ejected electrons and number of electrons ejected from the sample. This helps to know about the chemical elements of the materials and about the nature of chemical bonds exist in the material. It is a non-destructive surface analysis technique (Briggs and Seah, 1990).

The energy of the ejected photoelectrons is measured using electron detector and information is given in terms of intensity against binding and kinetic energy. The energy is usually expressed in eV.

$$BE = h\nu - KE \text{ ----- (16)}$$

Where, BE is the binding energy of an electron core electron, h is Planck's constant,  $\nu$  is the frequency of the exciting radiation, and KE is the kinetic energy of an emitted electron.

#### *2.6.5 Fourier Transform Infrared Spectroscopy (FTIR).*

FTIR is another technique that can also be used for analyzing scales and deposits. Infrared Spectroscopy helps to gather information about the functional groups and chemical species present in scales. The technique does not only detect the presence of CaCO<sub>3</sub> in scales but it can also differentiate between the presence of CaCO<sub>3</sub> in calcite, vaterite, aragonite and amorphous forms due to difference in the vibrational frequencies of C-O bonds in these substances (Al-Hamzah et al., 2014). In organic chemistry, FTIR is widely used technique

and is mainly suitable for detection of humic substances in deposits (Al-Amoudi and Lovitt, 2007, Melian-Martel et al., 2012).

Attenuated Total Reflectance- Fourier Transform Infrared spectroscopy (ATR-FTIR) is also used for determining the functional groups present in scale surface. In this technique, infrared radiations are reflected from the surface made from diamond (Tay and Kazarian, 2007), germanium (Tang et al., 2007) or zinc selenide (Xu et al., 2010) crystal and the sample. Consequently, radiations with wavelengths corresponding to the molecular vibrations of substances present will be absorbed while reflecting the radiations of different wavelength which will help to obtain reflectance spectra.

Table 6. Comparison of Different Techniques used to Study Membrane Scaling

Technique	Analysis Type	Technique Type	Detection Limit	Information type
Visual inspection and Light Microscopy	Scaling surface layer and cross section	Qualitative Non-destructive	w100 mm for visual, 100 nm for light	Surface morphology and layering
SEM - Secondary electron	Surface, cross-section	Quantitative Non-destructive	>50 nm	Surface morphology
SEM - Backscattered electrons	Surface, cross-section	Quantitative Non-destructive	>50 nm	Density distribution
SEM – Energy Dispersive Spectroscopy (EDS)	Bulk, surface, cross-section	Semi quantitative	0.1 wt%	Elemental analysis
SEM - Elemental mapping	Bulk, surface, cross-section	Semi quantitative	0.1 wt%	Elemental analysis
Fourier Transform Infra-red Spectroscopy (FTIR)	Bulk, surface	Destructive		Chemical composition, chemical mapping
X-ray fluorescence (XRF)	Bulk and surface	Quantitative	Bulk samples >500 mg	Elemental analysis



Technique	Analysis Type	Technique Type	Detection Limit	Information type
X-ray diffraction (XRD)	Bulk and surface	Quantitative and Qualitative	Variable depending on crystallinity and composition.	Quantitative crystalline phase determination or qualitative crystalline phase detection.
X-ray Photoelectron Spectroscopy (XPS)	Surface	Quantitative	Lesser amounts	Elemental analysis and Chemical bonding
Raman Spectroscopy	Bulk, Surface, Cross-section		>1 $\mu\text{m}$	Chemical composition and mapping
Thermogravimetric analysis	Bulk	Quantitative	5-50 mg	Phase determination
ICP – MS	Bulk (digested scale)	Quantitative	In ppm, ppb, ppt,	Elemental analysis
HPLC	Bulk	Quantitative		Organic content (carbohydrates, organic acids)
Tof-SIMS	Surface	Quantitative		Organic content on the surface (amino acid, polymers)

#### 2.6.6 Other Techniques.

There are several other techniques that are used for characterization of scales such as Raman spectroscopy, ICP-MS, Thermogravimetric analysis etc. In Raman spectroscopy, the sample will scatter the monochromatic light in-elastically resulting in the loss or gain of energy in frequencies that are specific to the molecular vibrations of the sample (Table 6). Thus, the Raman spectroscopy is the form of vibrational spectroscopy and it uses smaller wavelengths which is suitable for mapping surfaces that can be done at a resolution of around 5  $\mu\text{m}$ . This technique is good for exploring and investigating inorganic surfaces and can easily differentiate between scales of carbonates and sulfates. However, this technique is not as efficient as FTIR for resolving specific chemical species (Siozos et al., 2013).

In scaling studies, Thermogravimetric analysis is used for quantifying the changes in mass due to change in temperature. The changes in mass occur due to the loss of water content and formation of gases like CO<sub>2</sub> loss from carbonate scales. Thus, mass loss is quantified to determine the changes in scales as a function of temperature.

The ICP-MS is a bulk analysis technique that can be used for identifying and determining the concentration of elements after dissolving scale samples in acid. Furthermore, it can also be used to analyze the feed solution itself to determine its scaling potential and mechanism of scaling. However, the drawback of ICP is that the sample should be analyzed in the form of solution.

Similarly, there are several other techniques that can be utilized for the deposit's analysis such as HPLC (high performance liquid chromatography), atomic spectroscopy and Tof-SIMS (time of flight – Secondary ion mass spectrometry). HPLC is used in scaling studies for determining the organic content (such as carbohydrates and organic acid) of scales and deposits whereas, Tof-SIMS being a surface technique; can be used to determine organic content such as amino acids and polymers with atomic mass unit up to 10,000 on the surface of the scales with depth of about 5 – 10 nm.

## CHAPTER 3: METHODOLOGY<sup>2</sup>

### *3.1 Investigating effect of calcium ions and temperature on scaling<sup>3</sup>*

#### *3.1.1 Membranes used*

Thin film composite RO polyamide membranes (ESPA – Energy saving polyamide) were obtained from Hydranautics Inc. (USA). The graphene oxide (GO) functionalized RO membranes were obtained from our collaborators (Cao et al., 2018), to carry out initial studies during Objective 1. However, the GO functionalization was also done as part of research during Objective 4.

#### *3.1.2 Model scaling solutions*

In seawater of Arabian Gulf, the concentration of calcium ions varies from 225 - 500 mg/L (Matin et al., 2019). Considering the percentage RO recovery of 30-70%, the concentration of calcium ions can exceed 130 mM (Hasson et al., 2001; Rahman, 2013). All the scaling experiments were performed using different solution compositions chosen to represent the expected conditions of calcium ions in feedwater and to ensure that the solution is supersaturated with respect to different polymorphs of calcium sulfate: anhydrite ( $\text{CaSO}_4$ ), bassanite ( $\text{CaSO}_4 \cdot 1/2\text{H}_2\text{O}$ ) and gypsum ( $\text{CaSO}_4 \cdot 2\text{H}_2\text{O}$ ). In this research,  $\text{CaCl}_2$  and  $\text{Na}_2\text{SO}_4$  salts were used to prepare solutions with  $\text{Ca}^{+2}$  and  $\text{SO}_4^{-2}$

---

<sup>2</sup> Contents of this chapter have been published in various International Journals.

<sup>3</sup> This content has already been published. Reference: Ashfaq, M.Y., Al-Ghouti, M., Qiblawey, H., Zouari, N. 2020. Investigating the effect of temperature on calcium sulfate scaling of reverse osmosis membranes using FTIR, SEM-EDX and multivariate analysis. *Sci. Total Environ.* 703, 134726.

concentrations between 20 mM and 150 mM (Table 7). The prepared  $\text{CaCl}_2$  and  $\text{Na}_2\text{SO}_4$  solutions were allowed to equilibrate for 24 h with the atmospheric  $\text{CO}_2$  before being mixed. After mixing, the ionic strength (IS), pH, and saturation indices ( $\text{SI} = \log ([\text{Ca}^{+2}] [\text{SO}_4^{-2}]/K_{\text{sp}})$ , where  $[\text{Ca}^{+2}]$  and  $[\text{SO}_4^{-2}]$  are the activities of calcium and sulfate ions, respectively and  $K_{\text{sp}}$  is the solubility product) of the solutions with respect to gypsum, bassanite, and anhydrite were calculated using geochemists' workbench (GWB, V11.0). The calculations at 30 °C are shown here in Table 7. Solution with 30 mM  $\text{Ca}^{+2}$  and  $\text{SO}_4^{-2}$  (#2, Table 7) will be saturated with respect to only gypsum; while solutions with 50 and 100 mM  $\text{Ca}^{+2}$  and  $\text{SO}_4^{-2}$  (#3 and #4, Table 7) will be saturated with both gypsum and anhydrite. Based on classical nucleation theory (CNT) (Lee et al., 1999), bulk mineral precipitation in solution is likely to occur for highly supersaturated solutions, while surface precipitation is more dominant for slightly supersaturated solution. For example, for solution #5, bulk gypsum precipitation in solution is likely to occur as the solution is highly supersaturated to gypsum ( $\text{SI} = 0.83$ ); while bassanite is likely to precipitate on RO membrane surfaces, since the solution is only slightly supersaturated with respect to bassanite ( $\text{SI} = 0.08$ ). Hence, it is expected that different polymorphs of  $\text{CaSO}_4$  on RO membrane will result due to membrane scaling at all these different concentrations (Table 7, Solution #1 to #5). Different morphologies of  $\text{CaSO}_4$  polymorphs will have different effects on the performance and properties of the membranes. The membrane performance was monitored in terms of salt rejection, flux decline over time and changes in terms of membrane resistance. The presence of different polymorphs was analyzed using XRD, FTIR, and SEM-EDX. To investigate the effect of temperature on membrane scaling, the operating temperature of feedwater was varied as 5, 15, 25, and 35°C for Solution 1 and 3.

Table 7. Solution compositions and SI of different polymorphs of calcium sulfate at 30°C.

Solution #	Concentration of ions (mM)				pH	SI	SI	SI
	Na <sup>+</sup>	Cl <sup>-</sup>	Ca <sup>+2</sup>	SO <sub>4</sub> <sup>-2</sup>		bassanite	anhydrite	gypsum
1	40	40	20	20	5.68	-0.8898	-0.2608	-0.1329
2	60	60	30	30	5.69	-0.6852	-0.0561	0.0712
3	100	100	50	50	5.70	-0.4349	0.1946	0.3208
4	200	200	100	100	5.72	-0.1037	0.5263	0.6499
5	300	300	150	150	5.73	0.0878	0.7185	0.8395

### 3.1.3 Membrane filtration experiments

The membranes were cut into appropriate sizes and were rinsed using deionized (DI) water thoroughly before use. The bench-scale membrane filtration setup was constructed (Figure 14) to carry out membrane scaling experiments. The feedwater was supplied from 20 L tank using high pressure feed pump (Baldor Reliance Industrial Motor) to the inlet situated at the base of the crossflow membrane filtration cell (CF042, Sterlitech Corporation, USA). The transmembrane pressure (TMP) was controlled through valves at the feedwater and concentrate water lines. The temperature in the feed water was controlled by recirculating the concentrate water line through the circulating water chiller to the feed tank. To maintain the feed water conditions, the experiments were performed in total recycle mode. To investigate the effect of temperature and concentration of ions, the operating conditions were fixed at 35 bars (TMP), 3 LPM (flow rate), 55.74 cm per second (crossflow velocity) and 30 °C (temperature). Whereas, to investigate the performance of RO and modified RO membranes (prepared during this project), the operating conditions were varied as 20 bars (TMP), 1 LPM (flow rate), and 25 °C (temperature).

The experiments were performed in two steps. In first step, the membranes were

conditioned at desired operating conditions for 1-2 h using ultrapure water. In second step, the feed water was switched to model scaling solution (Table 7) and the resulting effect on flux decline over time was monitored until stable permeate flux was obtained. The effect of membrane scaling on salt rejection was calculated by measuring the conductivity of permeate and feed water samples using an electrical conductivity meter (HACH, HQ440d, multi). The membrane permeate flux, normalized permeate flux, %salt rejection, total membrane resistance and resistance due to fouling were calculated using Equations provided in Section 1.2.

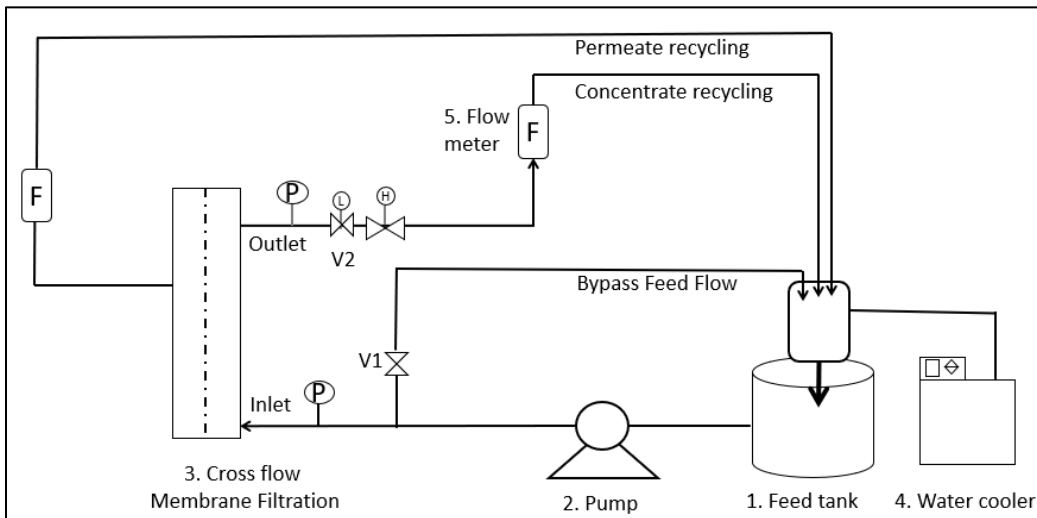


Figure 14. Process flow diagram of the membrane scaling experiments (Ashfaq et al., 2020a).

Furthermore, the mass of crystals formed on the membrane surface ( $M_t$ ) can be calculated using the following mass balance Equation (17):

$$M_t = C_f V_f - C_r V_r - C_p V_p \text{ -----(17)}$$

Where,  $C_f$ ,  $V_f$ ,  $C_r$ ,  $V_r$ ,  $C_p$  and  $V_p$  are the concentration and volume of solutes in feed, retentate and permeate water samples, respectively (Lee et al., 1999), which was measured using ion chromatography (850 Professional IC, Metrohm).

Using thin film model, the degree of concentration polarization (CP) can be calculated using Equation (18) (Zydney, 1997)

$$CP = \frac{c_m}{c_b} = \exp\left(\frac{J}{k}\right) \text{-----(18)}$$

$$R_o = 1 - \frac{c_p}{c_f} \text{-----(19)}$$

Where,  $C_m$  and  $C_b$  are the concentration of solutes near the membrane surface and in the bulk solution, respectively. The solute mass transfer coefficient is denoted by  $k$  which was calculated from Sherwood relations which is given by Equation (20).

$$Sh = k \cdot (L/D) \text{-----(20)}$$

Where  $L$  is the length of the channel (9.207 cm) and  $D$  is the solute diffusion coefficient ( $1.23 \times 10^{-5} \text{ cm}^2/\text{s}$ ). Sherwood number was calculated using Leveque solution for laminar wall mass transfer in a rectangular channel using Equation (21).

$$Sh = 1.47 \left(\frac{L}{H}\right)^{2/3} (\mu \cdot Hv)^{1/3} (v/D)^{1/3} \text{-----(21)}$$

Where,  $H$  is the height of the channel (0.23 cm),  $\mu$  is the average crossflow velocity of the membrane cell frame (55.4 cm/s),  $\nu$  represents solution kinematic viscosity (0.007 cm<sup>2</sup>/s).

#### *3.1.4 Scaled membrane characterization*

After the second step of filtration experiment was completed i.e. recirculation of model scaling solution, the membrane was removed and was subsequently air-dried for 1 h before subsequent analysis. To characterize the precipitates on the scaled membrane, Fourier Transform Infra-red (FTIR) spectroscopy, X-ray diffraction (XRD) and Scanning Electron Microscopy (SEM) – Energy-dispersive X-ray (EDX) spectroscopy techniques were used.

During FTIR analysis, the spectra of 400-4000 cm<sup>-1</sup> was obtained using Perkin Elmer 400 spectrum instrument (UATR – Universal Attenuated Total Reflectance) and the spectra of the scaled membrane was compared with that of pure gypsum and virgin membrane (as blank). Through XRD analysis, the polymorphs of calcium sulfates were identified using PANalytical (Empyrean / Netherland). The SEM-EDX analysis was done using Nova™ NanoSEM 50 Series (FEI Company) and the images of the scaled membrane were captured at different magnifications.

#### *3.1.5 Contact angle measurements*

The changes in the hydrophilic properties of the membrane due to scaling was investigated through contact angle analysis which was measured using sessile drop method.



The water droplet of 2  $\mu$ l was released onto the membrane surface placed in contact angle device (OCA15Pro, Germany). The contact angle was measured using SCA20 software after 5 seconds, at the minimum of 10 locations and the average water contact angle was then calculated.

### *3.1.6 Multivariate Analysis*

Different mathematical and statistical methods known as Chemometric, are developed for the extraction of important information from the data obtained from chemical measurements. PCA is one of the technique for multivariate analysis that can serve the purpose of extracting useful information and interpreting the variance in multivariate data set (Ashfaq et al., 2019a). In this research, PCA was used for the categorization of flux decline over time data obtained, which aided in differentiating effect on permeate flux decline in response to different solution conditions. Hence, the variables were the two type of membranes (RO and GO-RO) and five different concentrations of ions in feedwater (Table 1), whereas, the observations were the normalized permeate flux values obtained. PCA was carried out using The Unscrambler (v10.4, Camo Analytics, Magnolia, TX, USA) using Singular value decomposition (SVD) algorithm.

### *3.2 Isolation, Identification and Differentiation of antiscalant degrading bacteria<sup>4</sup>*

---

<sup>4</sup> This content has already been published. Reference: Ashfaq, M.Y., Al-ghouti, M.A., Qiblawey, H., Rodrigues, D.F., Hu, Y., Zouari, N. 2019a. Science of the Total Environment Isolation, identification and biodiversity of antiscalant degrading seawater bacteria using MALDI-TOF-MS and multivariate analysis. *Sci. Total Environ.* 656, 910–920.

### 3.2.1 Seawater Samples Collection

Samples were collected from both onshore and offshore marine environment (Figure 15A) including locations nearby a desalination plant (Figure 15B). The sample containers were autoclaved before use. Sample bottles were labelled after collection as per sample location and date of collection. The samples were then stored at 2 – 8 °C before subsequent analysis.

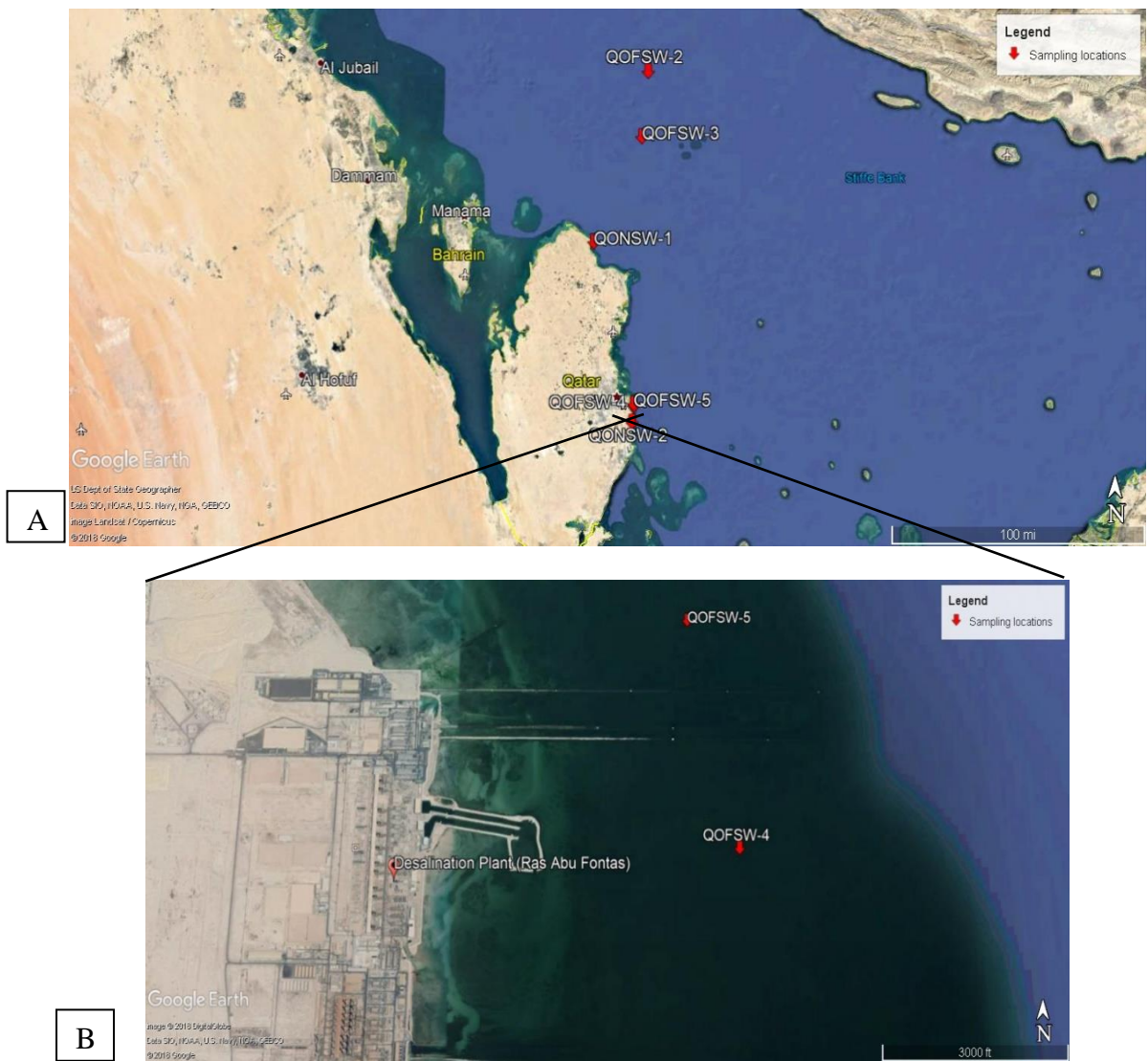


Figure 15. Seawater sampling locations map (A) 7 sampling locations; (B) Enhanced view showing two sampling sites situated near desalination plant (QONSW – Qatar Onshore seawater, QOFSW – Qatar offshore seawater)

### *3.2.2 Isolation of Microorganisms from Seawater*

#### *3.2.2.1 Media Preparation.*

Two types of media (mineral salt medium (MSM) and Luria Bertani (LB)) were prepared for the isolation of seawater microorganisms. MSM media was prepared as (g/L) 4 ammonium nitrate, 2 disodium hydrogen phosphate, 0.53 potassium dihydrogen phosphate, 0.17 potassium sulphate, 0.1 Mg.SO<sub>4</sub>.7H<sub>2</sub>O, 20 Agar, 35 NaCl and 2 Glucose as carbon source. Trace element solutions (1 mL in 1 L media) was prepared as (g/L) 0.1 EDTA, 0.042 ZnSO<sub>4</sub>, 0.178 MnSO<sub>4</sub>, 0.05 H<sub>3</sub>BO<sub>3</sub>, 0.1 NiCl<sub>2</sub>. Luria Bertani (LB) medium was prepared as (g/L): 10 tryptone, 5 yeast extract, 10 NaCl and 15 Agar.

#### *3.2.2.2 Membrane Filtration.*

Seawater samples were filtered through 0.45 µm membrane filters. The filters were subsequently placed in LB and MSM media. Filtration was repeated thrice for each media and the sample volumes were 10, 20, and 30 mL. Plates were incubated for 24 to 72 h at 30 °C. Results were collected using colony counter instrument (SC6plus, Stuart colony counter, Bibby Scientific Ltd., Staffordshire, UK). Each type of colony was sub-cultured into new LB / MSM media for further analysis.

### *3.2.3 Screening of Antiscalant degrading Bacteria*

#### *3.2.3.1 Initial screening using monomer antiscalant.*

Initial screening was carried out using antiscalant monomers i.e. acrylic acid (molecular weight: 72.06 g/mol from Sigma-Aldrich, South Korea) and maleic acid (molecular weight: 116.07 g/mol from Sigma-Aldrich, St. Louis, Missouri, USA). MSM media was used as described in Section 2.2.1. Glucose, used as carbon source, was replaced with respective antiscalants with concentration of 20 mg/L. During each experiment, glucose containing media was also used as a positive control. Fresh cultures were sub-cultured in monomer antiscalant containing solid medium and incubated for 7 days at 30 °C.

#### *3.2.3.2 Bacterial Growth Kinetics.*

To study the growth kinetics of bacteria in antiscalant containing medium, five types of liquid MSM media as per the carbon source i.e. glucose/acrylic acid/maleic acid/poly acrylic acid/poly maleic acid (at 1 g/L) were used. The poly acrylic acid (molecular weight: 1800 g/mol) was obtained from Sigma-Aldrich (St. Louis, Missouri, USA) and poly maleic acid was supplied by 2A Biotech, (Lisle, Illinois, USA). The pH of the media was maintained at 7 + 0.5 by adding appropriate amount of 0.1M NaOH (Sodium hydroxide). The isolates were freshly cultured in solid LB medium. After 24 h incubation at 30 °C, colonies were then harvested in sterile water and the calculated volume was transferred to all liquid MSM media to obtain the OD of 0.1. These liquid cultures were incubated at 37°C and 180 rpm in shaking incubator (Innova40, New Brunswick Scientific,

Connecticut, USA) until analysis is complete. Microbial growth was monitored through optical density (OD) at 600 nm using UV/Vis. spectrophotometer (Model: 6715, Thermo fisher scientific, Staffordshire, UK) and through serial dilution for the colony forming unit “CFU” determination. The specific growth rate was calculated through determining the slope of the exponential phase of bacterial growth curve.

### *3.2.4 Identification of isolates by MALDI-TOF MS*

#### *3.2.4.1 Sample Preparation.*

The ethanol/formic acid method for protein extraction was adopted as reported by Bibi et al., (2018), as commonly used and generally recommended method by the manufacturer for identification through MALDI-TOF MS (Model: microflex LT/SH from Bruker Daltonics, Germany). Briefly, loop full of freshly grown bacterial cultures in solid LB medium were suspended in water (300 µl) and then in ethanol (900 µl) followed by centrifugation at 13,000 rpm for 2 min. The pellet obtained was then mixed with equal volume of formic acid (70%) and acetonitrile (100%). The resultant supernatant (extracted bacterial proteins) after centrifugation was then used for the identification and protein profiling using MALDI-TOF MS technique.

#### *3.2.4.2 Identification of Microorganisms.*

For identification, 1 µL of the sample was deposited on MALDI biotarget plate and was subjected to dry at room temperature. The dried sample spot was then overlaid with 1 µL of CHCA (α-cyanohydroxycinnamic acid) matrix provided by the manufacturer for

crystallization of proteins in the sample. The MALDI biotarget plate was then loaded into the MALDI-TOF instrument. The sample spots were labeled in MALDI Biotyper Real Time Classification and identification process was initiated. The identification score from 0 to 3 on a logarithmic scale was then used to express the level of mass spectral concordance with the database.

#### *3.2.4.3 Mass Spectra Acquisition.*

Bruker Flex Control software was used to acquire protein profiles of the isolated strains. Two sample spots for each strain were used and three protein profiles were obtained for each spot to obtain six profiles per strain. These profiles were then analyzed and processed using Flex Analysis and Biotyper RTC 3 software.

#### *3.2.4.4 Differentiation of Microorganisms (MALDI-TOF MS and PCA).*

Differentiation of isolated strains was carried out through combining the techniques of MALDI-TOF-MS and PCA. The raw peak spectra were processed through baseline subtraction, smoothing and then peak detection using default algorithms in Flex Analysis 3.4. Briefly, the protein spectra with relative peak intensities (2000 – 20,000m/z) of isolated strains were divided into 3600 classes, each class with the width of 5 m/z. This is done to accommodate the mass accuracy of database-matching algorithm i.e. 0.08% (Kehramann et al., 2016). The relative peak intensities were calculated through the ratio of peak intensity to the base peak (the peak with highest intensity) and multiplying by 100. The data about the m/z classes with the relative peak intensities from different strains was then fed to PCA using singular value decomposition (SVD) algorithm in The Unscrambler x 10.5 software.

### 3.3 Interaction between microorganisms and antiscalants on RO membranes<sup>5</sup>

#### 3.3.1 Media Preparation

Mineral salt medium (MSM) was prepared as (g.l<sup>-1</sup>) namely, 4 ammonium nitrate, 2 disodium hydrogen phosphate, 0.53 potassium dihydrogen phosphate, 0.17 potassium sulfate, 0.1 Mg.SO<sub>4</sub>.7H<sub>2</sub>O, 20 Agar, and 35 NaCl. Trace element solutions (1 mL in 1 L media) were prepared as (g.l<sup>-1</sup>), 0.1 EDTA, 0.042 ZnSO<sub>4</sub>, 0.178 MnSO<sub>4</sub>, 0.05 H<sub>3</sub>BO<sub>3</sub>, and 0.1 NiCl<sub>2</sub>. Four carbon sources were used separately as (1g.l<sup>-1</sup>); glucose (G+MSM), acrylic acid (AA+MSM), maleic acid (MA+MSM), and poly acrylic acid (PAA+MSM).

#### 3.3.2 Inoculum preparation

The strain of *H. aquamarina* strain was inoculated in Luria Bertani (LB) medium containing (g.l<sup>-1</sup>); 10 tryptone, 5 yeast extract, 10 NaCl and 15 Agar. After 24 h of incubation at 37°C in shaker set at 250 rpm, the bacterial culture was used for inoculum preparation in sterile distilled water.

#### 3.3.3 RO Membrane

Polyamide TFC (thin film composite) RO (Energy Saving Polyamide – ESPA 2) membrane was acquired from Hydranautics Inc. – USA. Membranes were stored at 4-8°C in deionized (DI) water. The membrane samples were cut into desired sizes, thoroughly

---

<sup>5</sup> This content has already been published. Reference: Ashfaq, M.Y., Al-ghouti, M.A., Qiblawey, H., Zouari, N. 2019b. Evaluating the effect of antiscalants on membrane biofouling using FTIR and multivariate analysis. *Biofouling* 35 (1), 1–14.

washed with running DI water and then stored in DI water at room temperature for 24 hours before experiment. Initial characteristics of the membrane include pure water flux ( $5.1 \pm 0.1 \text{ L m}^{-2} \text{ h bar}^{-1}$ ), surface roughness ( $74.98 \pm 5.60 \text{ nm}$ ), and salt rejection ( $99.0 \pm 0.1 \%$ ).

#### *3.3.4 Biofilm growth assay*

Polyamide TFC RO membranes (approx. 1.5 x 0.8 cm) were first rinsed with 70% ethanol and distilled water and were subsequently placed at the bottom of the 24-wells microtiter plate in a way that the active polyamide surface faces the medium. Four MSM liquid mediums were prepared as explained in Section 2.1 with different carbon sources i.e. glucose / acrylic acid / maleic acid / poly acrylic acid. MSM liquid medium without any carbon source was also prepared. 2 mL of each medium was added into each well followed by the addition of 40  $\mu\text{l}$  of inoculum to finally achieve  $\text{OD}_{600 \text{ nm}} = 0.1$ . The microtiter plate was then incubated for 48 hours at 30°C at 180 rpm (Figure 16). The negative controls included MSM (no carbon source) with Bacteria and MSM (containing either acrylic or maleic or polyacrylic acid or glucose) without Bacteria. The positive control included MSM with glucose as carbon source and bacteria.

#### *3.3.5 Qualitative analysis of biofilm*

Qualitative analysis of biofilm formed on RO membranes was done through Fourier transform Infra-Red (FTIR) spectroscopy (Perkin Elmer 400 FTIR instrument). RO membranes were transferred to sterile petri dishes and were subjected to oven drying for 2 hours at 35°C. The membranes were then subsequently subjected to FTIR analysis (Spectrum 400 FTIR from PerkinElmer using UATR) and spectra from 4000-400  $\text{cm}^{-1}$



were obtained.

### 3.3.6 Quantitative analysis of bacterial cells in biofilm (Serial dilution)

Quantitative analysis of the bacterial cells in biofilm formed on RO membranes was done through measuring CFU counts as previously described by Lutskiy et al. (2015). Briefly, RO membranes after incubation, were transferred to centrifuge tubes containing 5 mL of sterile water. The tubes were subjected to sonication for 2 minutes followed by vortexing for few seconds. This step was done to ensure biofilm detachment from RO membranes. The detached bacterial cells were then serially diluted and plated on LB medium. After incubation for 48 hours at 30 °C, colony forming units (CFU) were counted and viable number of bacteria were then determined.

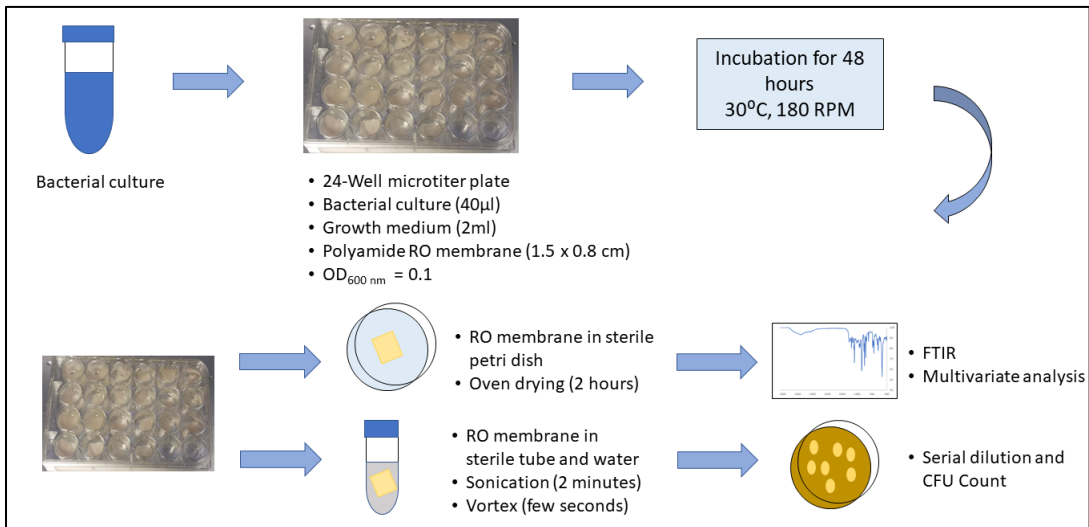


Figure 16. Qualitative and Quantitative analysis of biofilm formation conducted in 24-wells microtiter plate (modified from Lutskiy et al. 2015; Jung et al. 2018)

### 3.4 Interaction between Seawater Microorganisms and CaSO<sub>4</sub> scaling<sup>6</sup>

#### 3.4.1 Seawater microorganisms

In this research, three isolates of *Pseudomonas fragi* (*P. fragi*), and *Halomonas aquamarina* (*H. aquamarina*) and one isolate of *Pseudomonas stutzeri* (*P. stutzeri*) and *Carnobacterium maltaromaticum* (*C. maltaromaticum*) were used to investigate their ability to induce calcium sulfate precipitation. These strains were previously isolated in the framework of their ability to biodegrade antiscalants used in RO systems (Objective 2). However, *C. maltaromaticum* was newly isolated and identified through Matrix assisted laser desorption ionization – time of flight mass spectrometry (MALDI-TOF MS) following same protocol as described above. *C. maltaromaticum* was identified with the score of 2.43 in MALDI-TOF MS, which is considered as highly probable species level identification. All the strains were stored in 30% glycerol at – 80 °C in Microbial strains bank at Qatar University and were revived before experimentation.

#### 3.4.2 Bacterial growth medium

For the growth and preparation of fresh and pure cultures, Luria Bertani (LB) medium was used. LB medium was prepared as (g/L): 10 tryptone, 5 yeast extract, 10 NaCl and 15 Agar. The strains were routinely cultured by surface streaking on solid LB medium to obtain fresh, viable cells before each experiment.

---

<sup>6</sup> This content has already been published. Reference: Ashfaq, M.Y., Al-Ghouti, M.A., Al-Disi, Z., Zouari, N. 2020. Investigating the microorganisms-calcium sulfate interaction in reverse osmosis systems using SEM-EDX technique. J. Env. Chem. Eng. 8, 103963.

### *3.4.3 Modified media for biomineralization studies*

LB medium was modified to investigate the biomineralization of calcium sulfate. For this purpose, salts of sodium sulfate ( $\text{Na}_2\text{SO}_4$ ) and calcium chloride ( $\text{CaCl}_2$ ) were added to LB medium. To investigate the effect of calcium and sulfate ions, the concentration of  $\text{Ca}^{+2}$  and  $\text{SO}_4^{-2}$  were varied as 20, 30 and 50 mM in the “modified LB medium”. The modified LB media were then designated as LBM1 ( $\text{Ca}^{+2}$  and  $\text{SO}_4^{-2} = 20$  mM, 800 mg/L), LBM2 ( $\text{Ca}^{+2}$  and  $\text{SO}_4^{-2} = 30$  mM, 1200 mg/L), and LBM3 ( $\text{Ca}^{+2}$  and  $\text{SO}_4^{-2} = 50$  mM, 2000 mg/L). Since, the concentration of  $\text{Ca}^{+2}$  and  $\text{SO}_4^{-2}$  are same in each media type, therefore, the concentration is referred with  $\text{Ca}^{+2}$  only during the discussion.

### *3.4.4 Biomineralization studies using solid media*

Modified LB media plates were inoculated with selected bacterial strains by surface streaking and were then incubated aerobically for 3 weeks at 30 °C. The formation of crystals in the plates were monitored through light microscopy at alternate days. All the experiments were carried out in triplicates and modified LB media plates without inoculated bacteria were used as controls.

### *3.4.5 Biomineralization studies using liquid media*

Modified LB liquid media were used to investigate the formation of calcium sulfate crystals in suspended growth cultures. Briefly, 25 mL of freshly prepared autoclaved modified LB medium (LBM3) were added to 50 mL sterile centrifuge tube. The medium was then inoculated with appropriate volume of freshly prepared bacterial inoculum to

achieve the initial optical density at 600 nm ( $OD_{600}$ ) equal to 0.1.

Polyamide RO membranes obtained from (Hydranautics Inc. USA) were sterilized by thoroughly washing with running distilled water several times before soaking them in ethanol for 30 min. After soaking, the membranes were washed again with autoclaved distilled water to remove residual ethanol from their surface. Two pieces of membrane (1 cm x 1 cm) were then added to the cultures to investigate the interaction of microorganisms and calcium sulfate at the membrane surface. Then the cultures were incubated for up to 14 days at 30 °C and 150 rpm in shaking incubator (SSI10R-2, Sheldon Manufacturing Inc., USA). After the end of experiment, membrane pieces were removed, dried and then immediately analyzed using scanning electron microscopy – energy dispersive x-ray spectroscopy (SEM-EDX) (Nova™ NanoSEM 50 Series, FEI Company). The liquid cultures were then filtered through 0.2 µm membrane filter to recover any crystals formed in the liquid medium and the filters were subsequently analyzed through SEM-EDX. To calculate the amount of calcium ions precipitated as  $CaSO_4$ , the filtrate was also analyzed through Ion chromatography (850 Professional IC, Metrohm). The biofilm layer formed at the bottom of the centrifuge tubes was also analyzed. All the experiments were performed in triplicates. Modified LB medium without bacteria as well as mixture of  $Na_2SO_4$  and  $CaCl_2$  were used as controls.

To investigate the kinetics of precipitation and effect of different concentrations of ions, similar protocol was adopted but the incubation times were varied as 1, 3 and 7 days and all the three modified LB media (LBM1, LBM2, and LBM3) were used.

#### *3.4.6 Effect of calcium and sulfate ions on bacterial growth*

To investigate the effect of calcium and sulfate ions on bacterial growth, freshly prepared cultures of isolates were first harvested in LB to make an inoculum. Then, the specific volume of the inoculum required to reach OD<sub>600</sub> equal to 0.1 was transferred to centrifuge tubes containing 25 mL of the freshly prepared and autoclaved LBM3 (Ca<sup>+2</sup> and SO<sub>4</sub><sup>-2</sup> = 50 mM, 2000 mg/L) and LB media, the latter being used as control. The liquid cultures were then incubated at 30 °C and 150 rpm in shaking incubator (SSII10R-2, Sheldon Manufacturing Inc., USA). The growth of strains was estimated through OD<sub>600</sub> measurements using UV/Vis. spectrophotometer (Model: 6715, Thermo fisher scientific, Staffordshire, UK) and also through spreading serial dilutions on LB solid plates for the colony forming unit “CFU” determination (Bibi et al. 2018). The specific growth rates were calculated through determining the slope of the exponential phase of bacterial growth curve.

#### *3.4.7 Protein profiles of biomineralizing strains*

To investigate the role of bacterial proteins in formation of calcium sulfate crystals, the protein profiles of bacteria growing in LB (used as control) and LBM3 (used as biomineral forming) media were analyzed and compared. Briefly, one selected strain of *H. aquamarina* (QOFSW-1 (#1)) was freshly cultured on LB and LBM3 solid plates. The plates were checked periodically for formation of minerals using light microscopy. After incubation for 4-7 days, the formation of crystals in LBM3 solid plates were noted. Then, as many as 10 colonies of bacteria were deposited to MALDI Biotarget plate as spots. Once air-dried, the spots were overlaid with 1 µL of CHCA (α-cyanohydroxycinnamic acid) matrix provided by the manufacturer for crystallization of proteins in the sample. The

MALDI biotarget plate was then loaded into the MALDI-TOF instrument (Model: microflex LT/SH from Bruker Daltonics, Germany). The protein profiles were then obtained using Bruker Flex Control software available in the instrument.

#### *3.4.8 Statistical analysis*

Principle component analysis (PCA), a type of multivariate analysis, was used to discriminate protein profiles obtained for bacteria growing in LB and LBM3 medium. The protein profiles were directly subjected to PCA using Flex Analysis and Biotyper RTC 3 software available in MALDI-TOF MS. Inferential statistics such as t-test was performed, where needed, using MS Excel 2016.

### *3.5 Development of polymer modified graphene oxide coated RO membranes*

#### *3.5.1 Materials and Chemicals*

Thin film composite RO polyamide membranes (ESPA – Energy saving polyamide) were obtained from Hydranautics Inc. (USA). Graphene oxide sheets (Code: 763713-250MG) and other chemicals used during GO functionalization which includes i.e. N-hydroxysuccinimide (NHS, 98%), Ethylenediamine (ED, BioXtra), HEPES (4-(2-hydroxyethyl)-1-piperazineethanesulfonic acid) N-(3-Dimethylaminopropyl)-N'-ethylcarbodiimide hydrochloride (EDC, 98%), and MES monohydrate (>99.0%, BioXtra), were obtained from Sigma Aldrich, USA. Acrylic acid (molecular weight: 72.06 g/mol) used as antiscalant was also acquired from Sigma-Aldrich, South Korea.

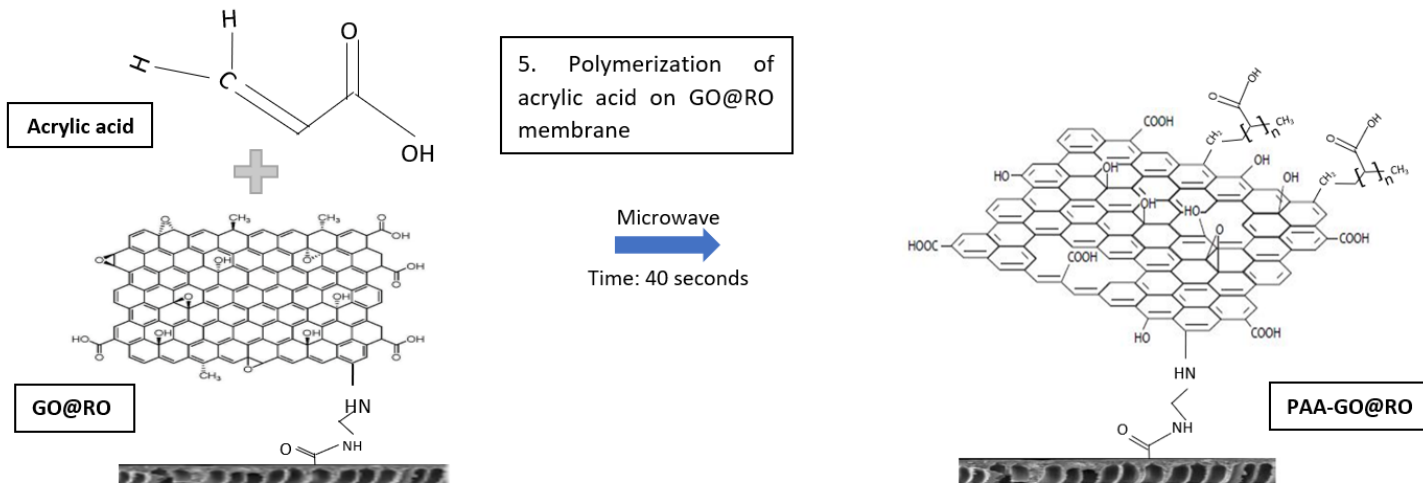
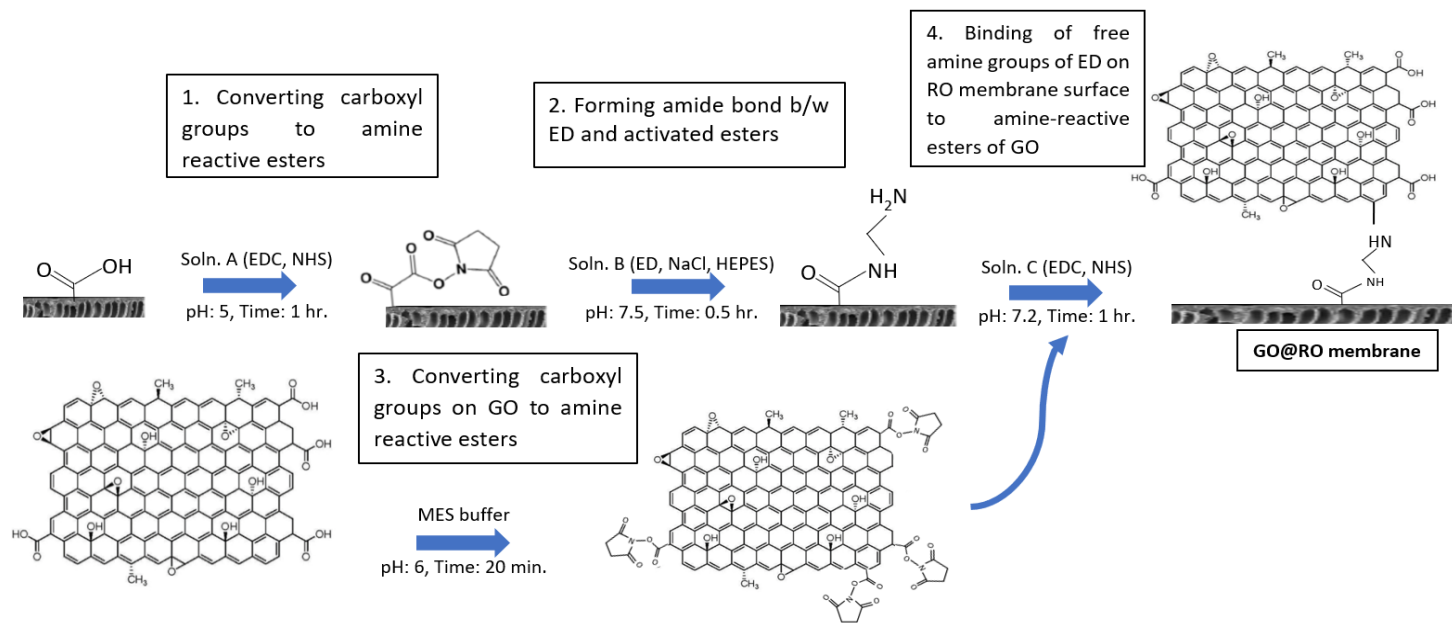
### *3.5.2 Functionalization of RO membranes with Graphene oxide (GO) nanomaterials*

The functionalization of RO membrane with GO was done using previously reported procedure (Cao et al., 2018; Perrault et al., 2013) (Figure 17). In brief, the carboxyl groups on the membranes were converted to amine-reactive esters by exposing the membrane surface to coating solution “A” which contained 4 mM of N-(3-Dimethylaminopropyl)-N'-ethylcarbodiimide hydrochloride (EDC, 98%), 10 mM of N-hydroxysuccinimide (NHS, 98%) and 0.5 M Sodium chloride (NaCl) prepared in 10 mM MES monohydrate (>99.0%, BioXtra) at pH = 5 for one hour. The amide bond between ethylenediamine (ED, BioXtra) and activated esters were then formed by reacting the membrane with coating solution “B” which contained 10 mM of ED, 0.15 M NaCl prepared in 10 mM of HEPES(4-(2-hydroxyethyl)-1-piperazineethanesulfonic acid) buffer at pH=7.5 for 0.5 hour. To convert the carboxyl groups of the commercially available GO to amine-reactive esters, GO was first dispersed in MES buffer at pH = 6, and probe sonicated for 20 minutes to ensure good suspension. Then, centrifugation was done for 30 minutes and the supernatant was diluted in MES buffer. 2 mM of EDC and 5 mM of NHS were then added to the solution (named as coating solution “C”) and the reaction was allowed to proceed for 15-20 minutes. The free amine groups of ED on RO membrane surface were then bonded to amine-reactive esters of GO by exposing the membrane surface to coating solution “C” for 1 hour at pH = 7.2. At the end, the membrane was washed with DI water twice and bath sonicated for two minutes to detach any non-reacted GO nanoparticles.

### *3.5.3 Polymerization of acrylic acid or maleic acid on GO@RO membranes*

The acrylic acid (AA) or maleic acid (MA) of 0.01 and 0.02 wt% were prepared and poured on the GO coated RO membrane. Immediately after pouring, the membrane was exposed to irradiation powers (Medium H1, 600W) for 40s time. The reaction was then allowed to proceed for 60 minutes. The excess solution was then disposed of and the membrane was exposed to hot air (at 70°C) for 5 minutes (Figure 17). Upon completing the procedure, the membrane was washed thoroughly to remove excess unreacted AA solution. The modified membranes were designated as PAA-GO@RO and PMA-GO@RO for 0.01 wt% and PAA-GO@RO\* and PMA-GO@RO\* for 0.02 wt%, respectively.





### 3.5.4 Membrane permeability and separation experiments

The pure water permeability (PWP) and percentage salt rejection was measured for both RO and modified RO membranes. The crossflow membrane filtration setup was used to carry out all filtration experiments. Briefly, the feedwater from high-pressure feed pump (Baldor Reliance Industrial Motor) was supplied to the inlet of membrane filtration cell (CF042, Sterlitech Corporation, USA). The temperature of feedwater was maintained by passing the concentrate water line through recirculating water chiller to the feed tank. The experiments were performed at fix operating conditions i.e. trans-membrane pressure (25 bars), flow rate (1 L/h) and temperature (25 °C) and in total recycle mode. The PWP (L/m<sup>2</sup>/h/bar) was measured using Equation 22.

$$PWP = \frac{Q_p}{\Delta P \cdot A} \text{-----(22)}$$

Where,  $Q_p$  represents permeate water flow rate (L/h),  $A$  is the effective membrane area (m<sup>2</sup>), and  $\Delta P$  is the trans-membrane pressure (bar).

### 3.5.5 Membrane scaling experiments

The membrane scaling experiments were performed in calcium sulfate solution as reported above. Briefly, the salts of CaCl<sub>2</sub> and Na<sub>2</sub>SO<sub>4</sub> were prepared to have concentration of Ca<sup>+2</sup> and SO<sub>4</sub><sup>-2</sup> ions equal to 800 mg/L (20 mM) (Table 7). The scaling experiment was carried out in two steps. First step was pre-conditioning in which the membrane was subjected to 20 bars pressure and 1 L/min flow rate using pure water for 2 hours. Then the pure water was replaced with calcium sulfate solution to start the scaling experiment. The bench-scale membrane filtration setup was used (Figure 14) to carry out these experiments. The feed water (pure water or calcium sulfate solution)

was supplied from 20 L tank using a high-pressure feed pump (Baldor Reliance Industrial Motor) to the inlet situated at the base of the crossflow membrane filtration cell (CF042, Sterlitech Corporation, USA). The temperature of feed water was controlled by recirculating the concentrate through the water chiller to the feed tank. To maintain the saturated conditions, the experiments were performed in total recycle mode at operating conditions outlined in Table 1. The transmembrane pressure (TMP) was controlled through valves at the feedwater and concentrate water lines.

### 3.5.6 Membrane biofouling studies

In this research, the *Halomonas aquamarina* (*H. aquamarina*) strain isolated previously from Gulf seawater (Ashfaq et al., 2019a) was used. This strain has demonstrated its ability to use antiscalants as a source of carbon and energy and cause biofouling. The bacterial strain was preserved in 30% glycerol at  $-80\text{ }^{\circ}\text{C}$  in Microbial strains bank at Qatar University and reviving was done before biofouling studies. To confirm the purity and identity of strain, the fresh bacterial culture was re-identified using Matrix assisted laser desorption ionization – time of flight Mass spectrometry (MALDI-TOF MS) following same protocol as previously reported (Ashfaq et al., 2019a; Bibi et al., 2018). The bacterium was again identified as *H. aquamarina* ruling out any contamination/impurity during preservation.

The antibacterial activity of membranes can be determined through bacteriostasis rate determination as it is commonly used technique in the literature (Duan et al., 2015; Yu et al., 2013). Briefly, both modified and unmodified RO membranes were weighted to obtain 0.05 g of membrane samples, which were then washed thoroughly with running distilled water followed by soaking them in 70% ethanol. After 30 min, the membranes were washed again with autoclaved distilled

water to ensure removal of residual ethanol from their surfaces.

Luria Bertani (LB) medium was freshly prepared comprising (g/L): 5 yeast extract, 10 tryptone and 10 NaCl. Then, 10 mL of LB liquid medium was added to 50 mL sterile centrifuge tube and was inoculated with appropriate volume of freshly prepared bacterial inoculum to reach initial OD<sub>600</sub> (optical density at 600 nm) equal to 0.1. The membranes samples were then added to this centrifuge tube to investigate their impact on bacterial growth following incubation for 18 hours at 30 °C. The actual number of cells at t = 0 (beginning of experiment) and at t = 18 h (end of experiment) were calculated using standard serial dilution method. The antibacterial activity (bacteriostasis rate, BR) of the membranes was then calculated using Equation 23:

$$BR = \frac{n_o - n_1}{n_o} \times 100 \text{-----(23)}$$

Where  $n_o$  is the number of colonies on the plates treated with control membrane (unmodified RO), while  $n_1$  is the number of colonies on the plates treated with modified membranes.

### *3.5.7 Inhibition of minerals precipitation and microbial growth, simultaneously*

The inhibition of both minerals precipitation and growth of bacteria was done using modified LB medium. Thus, LB medium was prepared as described in section 2.4 and was then supplemented with salts of Na<sub>2</sub>SO<sub>4</sub> and CaCl<sub>2</sub> to attain the concentration of Ca<sup>+2</sup> and SO<sub>4</sub><sup>-2</sup> equal to 800 mg/L in the “supplemented LB medium”. This supplemented growth medium helped to explore the formation of calcium sulfate crystals in suspended growth cultures. Briefly, 25 mL of freshly prepared autoclaved growth medium was added to 50 mL sterile centrifuge tube followed by addition of

bacterial inoculum to obtain initial OD<sub>600</sub> equal to 0.1. As mentioned in section 2.4; the membrane samples were sterilized by soaking them in ethanol for 30 min followed by washing them with autoclaved distilled water to remove residual ethanol from their surfaces. The membranes samples were then added to the cultures and the incubation was done for 3 days at 30 °C in shaking incubator (SSI10R-2, Sheldon Manufacturing Inc., USA) at 150 rpm. At the end of experiment, the membrane samples were subsequently removed, dried and analyzed using SEM-EDX for the formation of biofilm and calcium sulfate precipitates. After the end of experiment, membrane pieces were removed, dried and then immediately analyzed using SEM-EDX (Nova™ NanoSEM 50 Series, FEI Company) for the formation of biofilm and calcium sulfate precipitates.

#### *3.5.8 Membrane surface characterization*

To investigate the effect of coating on membrane surface properties, various techniques like SEM-EDX, AFM, Raman and FTIR spectroscopic techniques were used. Moreover, the hydrophilicity tests were performed using sessile drop method through contact angle instrument (OCA15Pro, Germany). Briefly, the water droplet of 2 µL was released onto the membrane surface placed inside the instrument and the contact angle was subsequently measured using SCA20 software after 5 seconds. The measurements were taken at the minimum of 10 locations across the membrane surface and the average water contact angle was then calculated. The SEM-EDX analysis was done using Nova™ NanoSEM 50 Series (FEI Company) and the images of the membrane surface were captured at different magnifications. The AFM was done in conjunction with a Nano indenter (AFM-MFP-3D, Asylum Research). The values of root mean square roughness (RMS) and average roughness (Ra) were determined from

various locations on the membrane surface and reported as average. During FTIR analysis, the spectra of 400-4000  $\text{cm}^{-1}$  was obtained using Shimadzu FTIR spectrum instrument, while, Raman spectroscopy was carried out through Raman Microscope (Thermo Fisher, DXR Dispersive Raman) using wavelength of 532 nm, and laser power of 10.

In addition to SEM-EDX and FTIR techniques, XRD analysis using PANalytical, Empyrean / Netherland was also done for the scaled membrane to identify polymorphs of calcium sulfate precipitated on the membranes. Before scale layer characterization, the membrane was removed from the crossflow cell and was subsequently air-dried for 1 h. During sampling, the samples were taken from various locations across the membrane surface to investigate the formation of precipitates at both less saturated zone, LSZ (water flow entry region) and high saturated zone, HSZ (water flow exit regions).

CHAPTER 4 – OBJECTIVE 01: UNDERSTANDING EFFECTS AND  
MECHANISMS OF ANTI-MICROBIAL NANOMATERIALS (GO) ON CALCIUM  
SULFATE SCALING

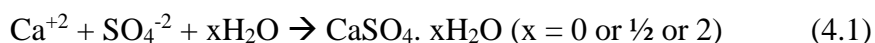
*4.1 Effect of concentration of calcium and sulfate ions on gypsum scaling of RO and  
Graphene oxide (GO) coated RO membranes*

*4.1.1 Introduction*

In arid countries like Qatar, seawater desalination industry has faced rapid growth to fulfil increase in water demands resulted from both population and economic growth. Due to the environmental impacts caused by the thermal desalination techniques, seawater reverse osmosis (SWRO) is being recommended to be utilized for new desalination industries (Ashfaq et al., 2018; Qiblawey et al., 2009). Nevertheless, membrane fouling (organic, inorganic, colloidal and biofouling) is affecting the widespread application of SWRO (Ashfaq et al., 2019a).

The inorganic fouling or mineral scaling is mainly caused by calcium carbonates, calcium sulfates, barium sulfates and silicates in reverse osmosis (RO) technique (Ashfaq et al., 2019b; Wang et al., 2019). Due to the increase in percentage of recovery by RO membranes, the concentration of sparingly soluble inorganic salts such as calcium sulfates, and carbonates increases above saturation level on the feed side of the membrane. As a result, these salts crystallize on the membrane causing membrane scaling (Karabelas et al., 2011; Mitrouli et al., 2013). The scaling causes decline in flux and reduction in membrane life (Vatankhah et al., 2018). Since, the scaling caused by calcium carbonates can be controlled by pH adjustments, therefore, calcium sulfate scaling is expected to be most dominant as compared to others (Benecke et al., 2018). If a solution is supersaturated with respect to one or more calcium sulfate

minerals, precipitation can occur according to the reaction 4.1:



Concentration polarization also enhances the precipitation of inorganic salts as their concentration often exceeds the solubility limit near the membrane surface. Therefore, the extent of scaling depends upon the concentration of salts present in feedwater e.g. seawater which is an aqueous solution of salts possess higher potential for scaling in RO systems. Various previous studies have focused on calcium sulfates scaling on membranes to investigate the effect of operating pressure and cross flow velocity (Lee et al., 1999), effect of organic macromolecules in forward osmosis (Liu and Mi, 2014), effect of antiscalants (Ali et al., 2015), kinetics of precipitation (Alimi et al., 2003), diagnostic characterization of calcium sulfate (Rahardianto et al., 2006), antagonistic gypsum and calcium carbonate scaling (Rahardianto, 2008), analysis of the onset of scaling (Shmulevsky et al., 2017) and calcium sulfate adhesion on different membranes (Su et al., 2018). Since, the concentration of calcium ions may vary widely in seawater such as from 225 to 500 mg/L in the case of Arabian Gulf (Matin et al., 2019), it is important to investigate the effect of calcium ions on membrane scaling of different RO membranes.

Graphene oxide has been catching attention in the field of research and industries due to its unique properties such as antimicrobial activity, hydrophilicity, smoothness, negative charge, and its functionalization with carboxyl, hydroxyl, epoxy, and ether groups (Inurria et al., 2019; Sun and Li, 2018). Recent research by Cao et al., (2018) has shown that the presence of high number of -COOH functional groups on GO-coated RO membrane resulted in increase in calcium ions adsorption on the



membrane which was subsequently hard to remove during the cleaning process with fresh water circulation. Therefore, both RO and GO-coated RO membranes were studied in this research.

Hence, in this research, the effect of different concentration of calcium ions on membrane scaling was investigated on bare RO and GO coated RO membranes. The effect of membrane scaling at different conditions on membrane flux, resistance, and solute rejection was explored. The mechanism of membrane scaling at different conditions was studied through combining the techniques of SEM-EDX, FTIR and XRD. Furthermore, PCA was applied on the results of flux decline data to explore its ability to differentiate membrane performance at different conditions.

#### *4.1.2 Results and Discussion*

##### *4.1.2.1 Initial characterization of membranes*

To initially characterize the RO and GO-RO membranes, parameters such as pure water flux, salt rejection, membrane hydrophilicity and roughness were investigated. The membrane transport and rejection characteristics were studied in terms of pure water permeability and percentage of salt rejection. After coating with GO, pure water permeability increased from  $5.0 \pm 0.2$  to  $5.2 \pm 0.4$ . Additionally, the percentage rejection of sodium ions was found to be  $98.6 \pm 0.1\%$  and  $98.4 \pm 0.4$  for RO and GO-RO membranes, respectively. Such changes in membrane transport and rejection properties after coating with GO has also been noted in previous studies (Cao et al., 2018; Faria et al., 2017).

GO nanosheets have been found to be hydrophilic with smooth surface (Inurria et al., 2019; Sun and Li, 2018), which helped to improve the hydrophilic and surface smoothness properties of the RO membrane. The water contact angle of RO membrane

was  $80.1 \pm 1.6$ , which was reduced to  $46.8 \pm 1.3$  after functionalizing with GO. The membrane roughness was measured through Atomic force microscopy (AFM), and it was found that the surface roughness reduced from  $75.0 \pm 8.0$  (RO) to  $62.8 \pm 1.2$  nm (GO-RO). The solid-liquid interfacial energy ( $-\Delta G_{SL} = \gamma_L [1 + \cos \Theta/\Delta]$ ,  $\gamma_L$  denotes surface tension of pure water) which relies on the water contact angle ( $\Theta$ ) and relative surface area ( $\Delta$ ) of the membrane was found to be 72.2 and 98.0 ( $\text{mJ}\cdot\text{m}^{-2}$ ) for RO and GO-RO membranes, respectively.

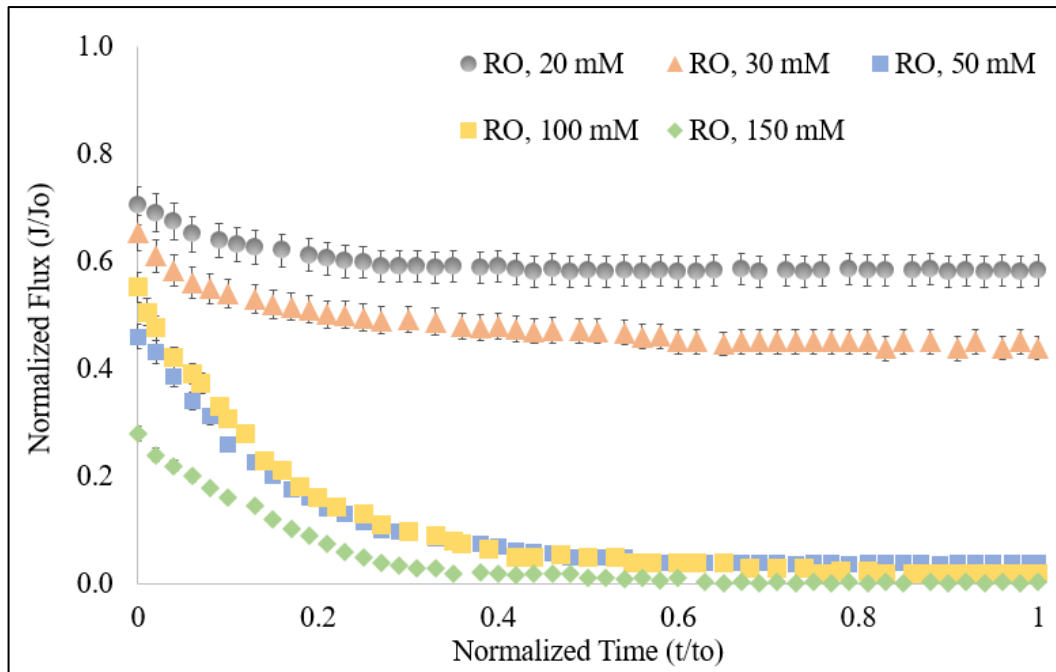
#### *4.1.2.2 Effect of Calcium ions concentration on membrane scaling and performance.*

For each set of experiment, there were two steps. Initial preconditioning of membrane for 1-2 h at 30°C, 3LPM with DI water. Once, the stable flux was obtained, the second step was initiated in which the mixture of  $\text{CaCl}_2$  and  $\text{Na}_2\text{SO}_4$  solutions (#1 - #5 as outlined in Table 7) were used as feed water. The effect of concentration on membrane scaling was evident from the results of flux analysis as shown in Figure 18. It was noted that the extent of flux decline increased with the increase in concentration of ions in the feed water (Figure 18A and 18B). Hence, as the concentration of calcium ions increased in the solution to 100 and 150 mM; the membrane flux decreased by more than 99% due to the membrane surface blockage by the precipitates (Gilron and Hasson, 1987). This is in line with the previous findings, which conclude that the intensity of calcium sulfate scaling increases with increasing the saturation conditions of feed water (Dydo et al., 2004; Uchymiak et al., 2008). Since, the feed water was undersaturated; the flux decline can be attributed to the saturated conditions near the membrane surface as a result of concentration polarization. The percentage decline in flux obtained is plotted against the initial concentration of calcium ions in the feedwater. Figure 18C shows that if the concentration of calcium ion will exceed 30

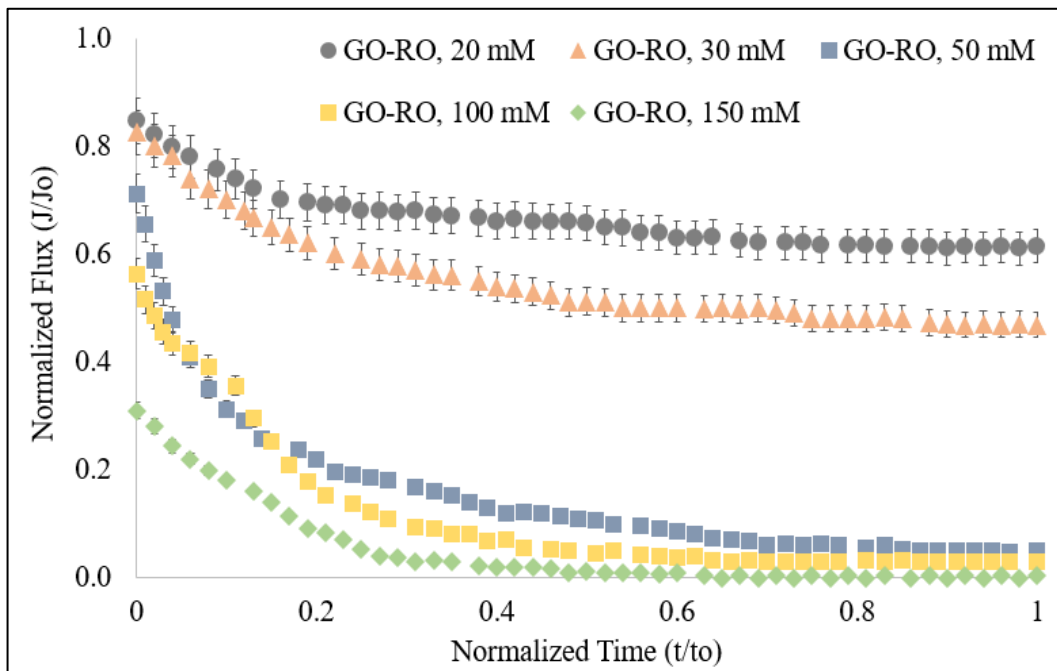
mM in feed water, the % flux decline will increase sharply from around 45 % at 30 mM to more than 90% at 50 mM. While studying the effect of gypsum precipitation on flux decline of RO membrane, 50 – 80 % decline in flux was also noted at low concentration of 16.4 mmol/l but after long experimental time period of 4-6 days ( Brusilovsky et al., 1992). This shows that the membrane scaling becomes highly intense at certain concentration of ions (above 30 mM) and therefore, the pre-treatment of feed water should ensure that the concentration does not exceed certain limit within the RO systems.

PCA was used to elucidate the differences between the flux decline curves over time at different concentrations obtained using RO and GO-RO membranes. Using two principle components (PC-1 and PC-2), PCA showed 99% variability in the data set and helped to cluster the similar data together. Hence, through PCA, 3 clusters were obtained (Figure 18D). Since, PC-1 shows 96% of the variability, the distance between the two points on x-axis shows higher variability as compared to the distance on y-axis. Therefore, cluster 1 i.e. flux decline curve obtained for both RO (RO, 20) and GO-RO (GO-RO, 20) membranes at lowest concentration ( $\text{Ca}^{+2} = 20 \text{ mM}$ ) was significantly different from the flux decline curve obtained at 30 mM concentration of  $\text{Ca}^{+2}$  (cluster 2). Furthermore, since, flux declined sharply over time when higher concentration of calcium was used, the cluster 3 comprising points belonging to RO and GO-RO at  $\text{Ca}^{+2}$  concentration equal to 50, 100, 150 mM is located far from both cluster 1 and 2. The distance between the points within the same cluster are shows that the flux decline curves were different for the two membranes tested. In fact, it was found that less severe decline in flux was obtained for GO-RO membrane as compared to RO membrane (Figure 18A and 18B). Thus, PCA helped to elucidate the differences related to the extent of membrane scaling at the studied conditions. Such an application of PCA in

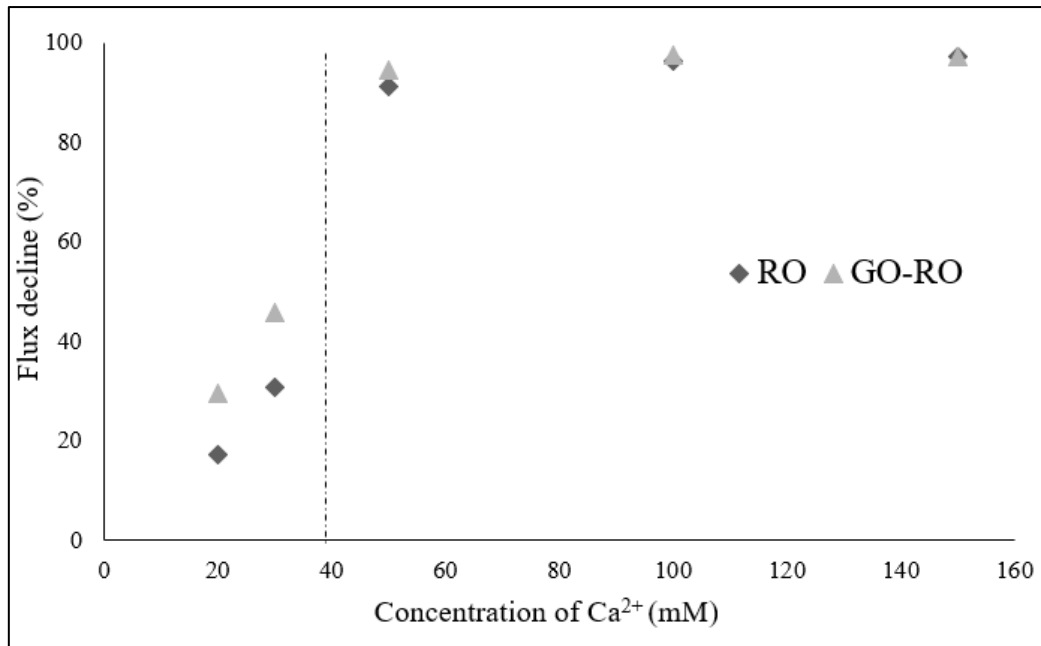
membrane fouling studies is seldom reported. Previously, the bio-film layer formed on RO membranes in the presence of different antiscalants was categorized using PCA (Ashfaq et al., 2019). The technique helped to differentiate the biofouling intensity and composition for various antiscalants, which subsequently aided in determining their fouling potential. SIMCA (Soft independent modeling of class analogy) models, another type of multivariate analysis, was also utilized by Gelaw et al., (2011, 2014), and was combined with FTIR technique to demonstrate the differences between the fouled and cleaned membranes which helped to determine best cleaning practice. Hence, it can be concluded that the multivariate analysis such as PCA and SIMCA helps to provide various insights into the fouling mechanisms, their type and intensity (such as using flux decline curves). In addition, fouling mitigation studies such as through the addition of antiscalants or membrane coating or changing operating conditions can also employ PCA to differentiate among the flux decline curves obtained with and without mitigation strategy, which can help to decide best fouling mitigation technique in membrane sciences.



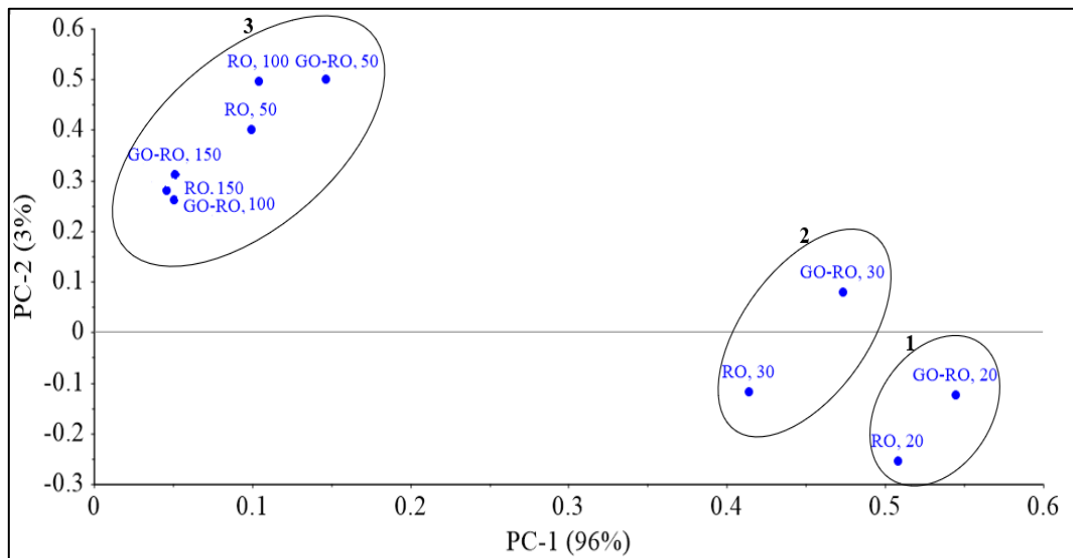
(A)



(B)



(C)



(D)

Figure 17. Flux decline curves obtained at different concentration of Calcium ions (A) RO membrane, (B) GO-RO membrane, (C) Correlation between Flux decline and concentration of calcium ions, (D) PCA for flux decline over time;

The estimation of membrane resistance mainly depends upon the stabilized flux obtained at the end of scaling experiments. It was noted that at low initial concentration, the increase in membrane resistance was minimal (Table 8). For example, the initial

membrane resistance of the RO membrane ( $R_m$ ) i.e.  $6.65 \times 10^{13}$  doubled to  $12.96 \times 10^{13}$  ( $R_t$ ) due to additional resistance imposed by the scaling layer ( $R_f$ ), which was calculated to be  $6.31 \times 10^{13}$ . However, at higher initial concentrations, the membrane resistance increased manifolds due to more intense scaling as the  $R_f$  surged to as much as  $1823.28 \times 10^{13}$ . Similar increase in membrane resistance was noted for GO-RO membranes. It was also noted that the percentage rejection of solutes decreased markedly with the increase in concentration which could be due to the formation of porous scale layer on the membrane and its interaction with the functional groups of the membranes as will be discussed in preceding sections. Since, more functional groups were involved in interaction with the scale layer, their interaction with the solutes would have decreased. Furthermore, it can also be deduced that the scale layer deposited on the membrane altered the porous structure of the membrane affecting its rejection capabilities.

Table 8. Effect of concentration of calcium ions on permeate flux, membrane resistances and % salt rejection

Concentration of $Ca^{+2}$ (mM)	$R_t$ ( $m^{-1}$ ) ( $10^{13}$ )		$R_f$ ( $m^{-1}$ ) ( $10^{13}$ )		%R		CP	
	RO	GO-RO	RO	GO-RO	RO	GO-RO	RO	GO-RO
20	12.96	12.45	6.31	5.31	99.50	99.60	1.15	1.16
30	17.27	16.32	10.62	9.60	99.00	99.08	1.12	1.12
50	189.84	162.07	183.18	155.36	95.00	95.25	1.02	1.02
100	424.19	366.84	417.54	360.12	81.12	81.58	1.01	1.01
150	1829.93	1674.19	1823.28	1667.48	43.50	43.61	1.00	1.00

**%R** was calculated using Equation 19 and Membrane resistance terms i.e.  **$R_t$** ,  **$R_m$** ,  **$R_f$**  were calculated through Equation (11, 12, and 13) using mean permeate flux values. The  $R_m$  for RO and GO-RO was  $6.65 \times 10^{13}$  and  $6.61 \times 10^{13}$  respectively, at the experimental conditions.

The time required from reaching supersaturation stage to the time when the first crystal deposit is detected is known as Induction time ( $t_{ind}$ ). It is the sum of the time

required for the nucleus to form ( $t_n$ ) and the time taken for the nucleus to grow into the visible size ( $t_g$ ). The increase in temperature as well as supersaturation decreases the induction time. The time at which the membrane permeability starts declining can be correlated with the  $t_{ind}$  (Hasson et al., 2009; Shmulevsky et al., 2017). As shown previously in Figure 18A and 18B, the membrane flux started decreasing immediately after the start of experiment, which showed that the induction times initiated immediately after mixing of  $\text{CaCl}_2$  and  $\text{Na}_2\text{SO}_4$ . It has been noted previously that the induction times decreased from  $10^5$  to 100 seconds when the supersaturation with respect to calcium sulfate in the feed water increased from 2 to 12 (Alimi et al., 2003). Furthermore, it was also found that the activation energy reduces with the increase in supersaturation which is related to the  $t_{ind}$  through the following Equation (24).

$$\text{Log } 1/t_{ind.} = A - \frac{E}{2.303 RT} \text{-----(24)}$$

Where A is a constant, E is the activation energy for the nucleation (J/mol), R is the universal gas constant (8.31 J/K. mol) and T is the temperature (°K).

In addition to the supersaturation conditions in the bulk and at the membrane surface, the presence of external body can also decrease the activation energy significantly. The activation energy for calcium sulfate precipitation has been found to be in the range of 51 – 160 kJ/mol for the concentration between 0.01 – 0.05 mol/L. Nevertheless, the activation energy was found to be lower i.e. 42.4 – 48.2 kJ/mol for the concentration between 0.05 – 0.075 mol/L (Hoang et al., 2007). This shows that the membrane surface can act as a nucleating site for calcium sulfate crystallization causing heterogeneous nucleation which require much less activation energy as compared to homogenous nucleation, forming scale layer and reducing the membrane flux.



#### *4.1.2.3 Characterization of membrane scale layer.*

The morphology of the crystals formed after the experiment was investigated using SEM. The SEM images also helped to obtain information about the surface coverage of membrane by deposits. Figures 19 and 20, shows the morphology and surface coverage of crystals on the surface of RO and GO-RO membranes at both lower (20 to 30 mM) and higher (50 to 150 mM) concentrations, respectively. It is evident from these Figures that the surface coverage by scales increased with increase in concentration. Thus, membrane surface was fully covered with the scales when the concentration of calcium was more than 50 mM.

There are two pathways of scale formation i.e. bulk crystallization (homogenous or heterogenous nucleation) and surface crystallization (heterogenous nucleation). Surface scaling occurs near the membrane surface as a result of supersaturation or due to the presence of substances responsible for crystals formation in the solution or due to the presence of conditions responsible for nucleation (Lee et al., 1999). Such conditions lead to the formation of scale at the membrane surface. When the supersaturation occurs in the bulk solution i.e. away from the membrane surface, nucleation will occur in the bulk solution on the nano-particles which are almost always present in water (Popov et al., 2019), and the resulting crystals then settles on the membrane surface, forming a cake layer (Hasson et al., 1996). It is now accepted that mineral salt scaling occurs by both the deposition of bulk formed crystals onto the membrane surface and direct surface crystallization on the membrane surface. The membrane materials can also affect the mechanism of scaling as it was noted that the gypsum scaling occurred as a result of surface crystallization on polyamide membranes, while, bulk crystallization was dominant mechanism in the case of cellulose acetate

membranes (Mi and Elimelech, 2010).

Thus, in this research, it was also noted that the solutions that are less concentrated (20, 30 and 50 mM); the surface crystallization resulted as also evident from needle like crystals protruding into the membrane surface in SEM images (Figure 19 and 20A, 20B). However, from Figures 20C to 20F of RO and GO-RO membranes, it can be concluded that both the bulk crystallization as well as surface crystallization occurred at higher saturated conditions (100 and 150 mM) which resulted in cake layer formation on the membrane surface causing more severe decline in Flux as noted previously in Figure 18. The EDX analysis confirmed the crystals on the membrane belong to calcium sulfates as the ions of calcium, sulfur and oxygen were found to be present in abundance.

Furthermore, it was also noted that the increase in concentration altered the morphology of crystals. The needle-like structures were noted at lower saturation conditions on both membranes. However, at higher concentrations, the crystal growth increased which resulted in orthorhombic or hexagonal prismatic shapes causing floral structures at these conditions. In general, typical needle like structure is for gypsum precipitates as previously reported in the literature (Antony et al., 2011; Rahman, 2013; Shih et al., 2005). Karabelas et al., (2014) investigated the incipient CaSO<sub>4</sub> scaling in narrow spacer filled channel using SEM. It was also noted that the needle like structures appeared at lower saturation conditions, while, broader, rosette-like structures were visible at higher saturation conditions. The kinetic model for gypsum crystallization explain this trend as follows (Lee et al., 2000; Ozkar, 2001; Shih et al., 2005):

$$\frac{d_m}{d_t} = k (C_m - C_s)^n \text{-----}(25)$$

$C_m$  and  $C_s$  is the gypsum concentration at the membrane surface, and the calcium sulfate solubility at the experimental conditions, respectively and  $k$  is the growth rate constant. Whereas,  $n$  represents the kinetic order, in which value of 1 describes the diffusion-controlled process, and 2 defines the surface reaction mechanism.

Hence, the increase in concentration of calcium sulfate at the membrane surface ( $C_m$ ) at higher saturation conditions caused the increase in rate of scale formation ( $dm/dt$ ) which modified the crystal structures at higher concentrations. In previous research (Shih et al., 2005), which deals with the axial development of gypsum crystals on the membrane surface, it was noted that the rod shaped structures were present at the entrance region of the feed water where the  $C_m$  is usually low. Whereas, towards the exit region, the crystals appeared were of rosette structures where the  $C_m$  is high. In addition to the changes in crystal morphology, more intense scaling resulted due to higher saturation conditions has also been demonstrated through scale layer thickness and mass density ( $g/cm^2$ ) measurements (Table 9). Previous researches (An et al., 2011; Chai et al., 2007), has shown that the mass density ( $g/cm^2$ ) increases at regions characterized with higher saturation conditions in spiral wound modules. For instance, membrane coverage by  $CaSO_4$  increased from 0.00025 to 0.00426  $g/cm^2$  along the direction of feed flow, corresponding to higher saturation conditions and concentration polarization near the exit region (An et al., 2011) (Table 9). Similarly, in terms of scale layer thickness, Rahardianto et al., (2006) estimated the thickness of scale layer to be 15  $\mu m$  formed on RO membrane at concentration of 16.4 mM. In this research, the scale layer thickness was also found to increase from 40 to 246  $\mu m$  when the concentration of calcium ions was increased from 20 to 150 mM (Table 9).

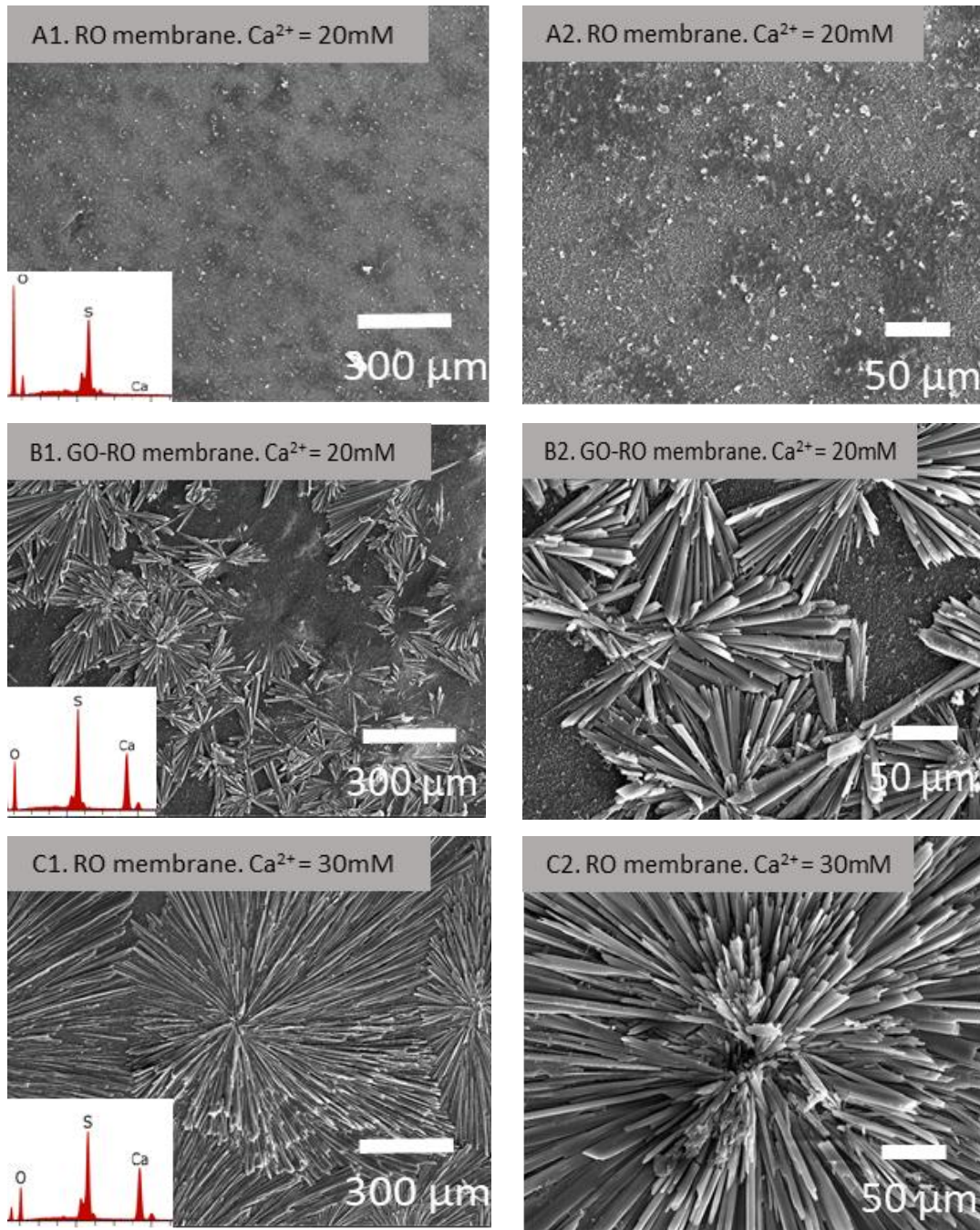
Table 9. Comparison of scale layer thickness and density with the literature at different conditions

Concentration	Scale layer measurements	Operating conditions	Reference
16.4 mmol	Thickness: 15 $\mu\text{m}$	Polyamide composite membrane, Fully recycle mode	Rahardianto et al. 2006
39.92 mmol/L	Mass density: 0.00132 - 0.0216 $\text{g}/\text{cm}^2$	Spiral wound membrane, Fully recycle mode Pressure: 0-28 bar	Chai et al., 2007
12.5 mmol/L	Thickness: 2-29 $\mu\text{m}$	Polyamide/Polysulfone composite membrane, Partial recycle mode (retentate recycling) Pressure: 41.4 bar	Matral et al., 2000
50 mmol/L	Mass density: 0.000256 - 0.004 $\text{g}/\text{cm}^2$	Spiral wound membrane, Fully recycle mode Pressure: 10 bar	An et al., 2011
17 mmol/L	Density: 0.001 $\text{g}/\text{cm}^2$	Spiral wound membrane, Pressure: 25 bar	Benecke et al., 2018
20-150 mmol	Density: 0.01-0.05 $\text{g}/\text{cm}^2$ Thickness: 40-246 $\mu\text{m}$	Polyamide composite membrane, Fully recycle mode	This research

Average thickness of the scaled layer was calculated from mass of crystals ( $M_t$  estimated using Equation 18) per membrane surface area and average density of gypsum (2320  $\text{kg}/\text{m}^3$ ).

Uchymiak et al., 2008 studied the kinetics of gypsum scaling on RO membranes and found that the crystal number density (CND) temporal profiles were similar to logistic growth model, in which, CND ( $\#/ \text{cm}^2$ ) increased rapidly initially until limiting SND was reached. At that point, additional increase in crystals was depending upon the availability of free surface area, while, existing crystals grew further to rosette structures occupying more surface area. In addition to the concentration of ions in feedwater, other operating parameters such as cross flow velocity and pressure has also been shown to modify the morphology of gypsum crystals (Lee et al., 1999). On the other hand, it has also been demonstrated that the presence of microorganisms

(Thompson et al., 2012) and organic macromolecules (Liu and Mi, 2014) also plays role in enhancing gypsum scaling by reducing induction times and modifying crystal morphologies. The results also show that the morphology of crystals did not change significantly after coating the RO membrane with GO.



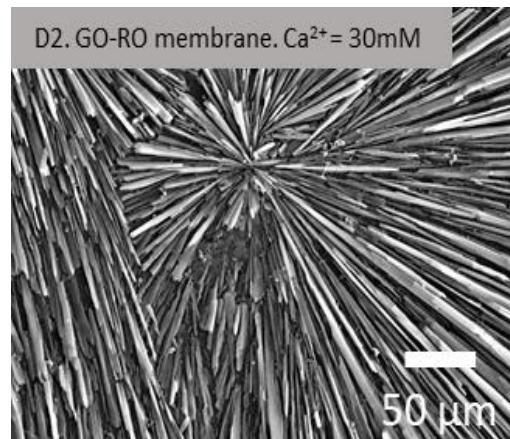
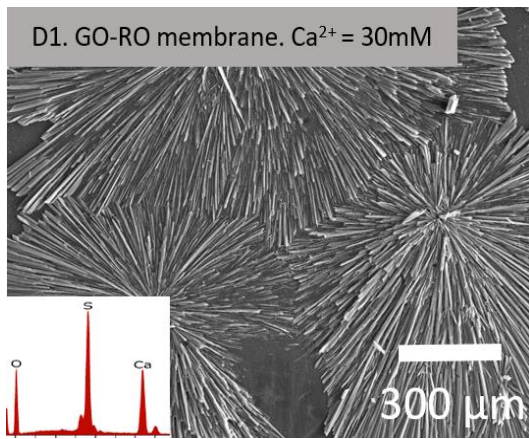
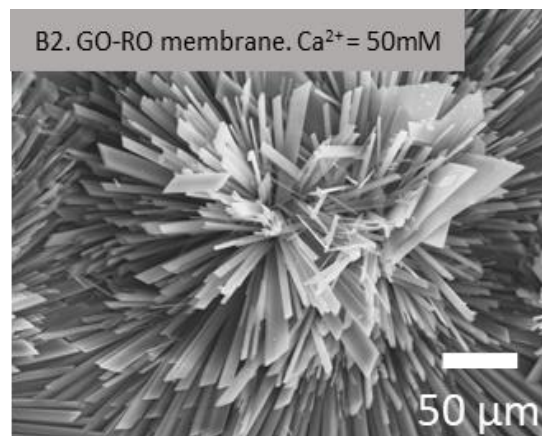
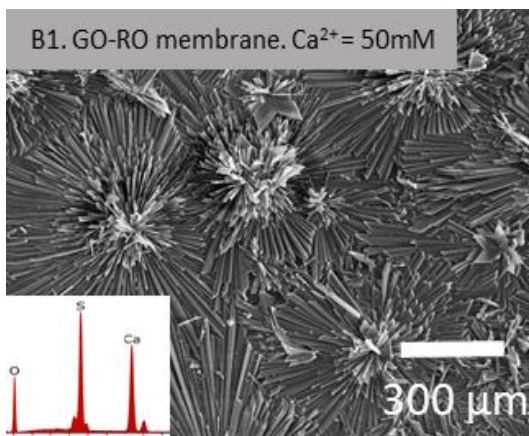
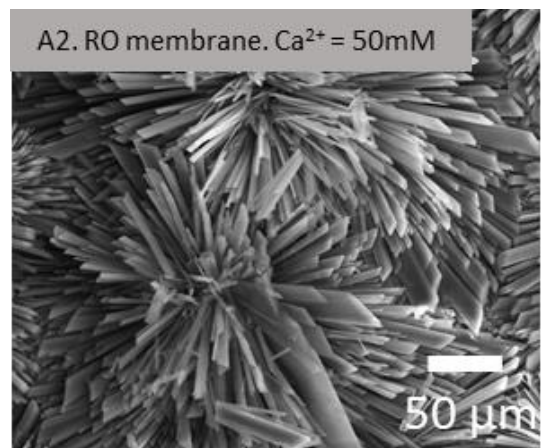
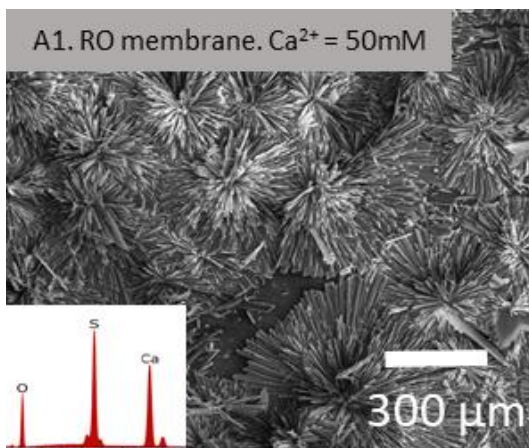


Figure 18. SEM-EDX analysis for scaled membranes at concentrations of 20 and 30 mM.



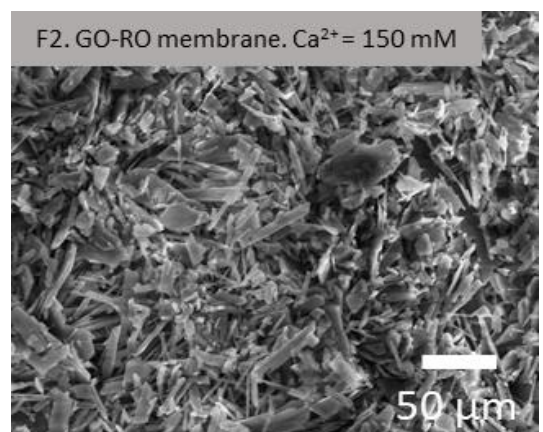
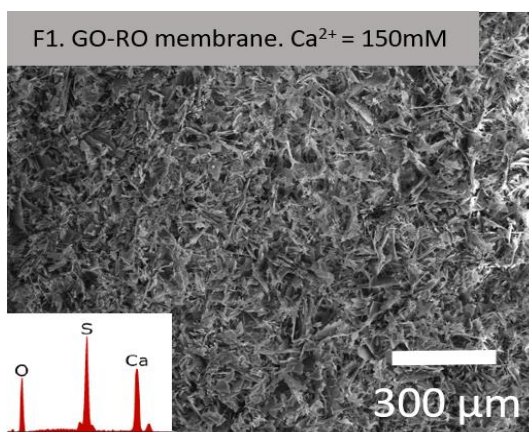
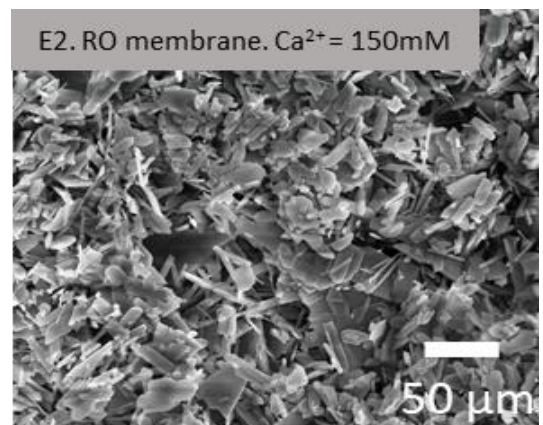
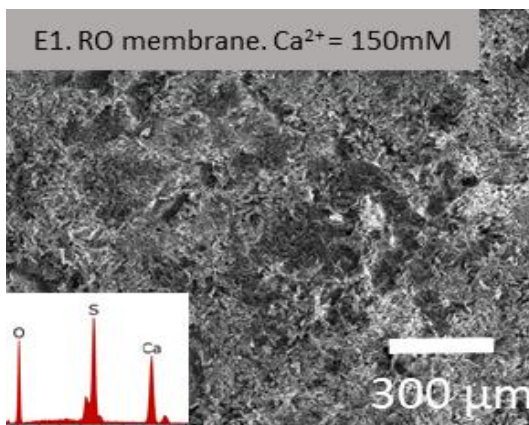
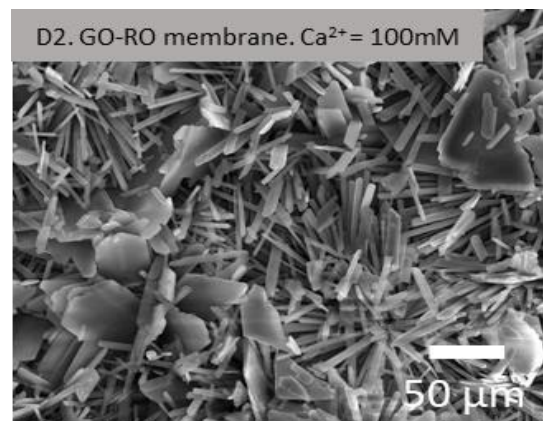
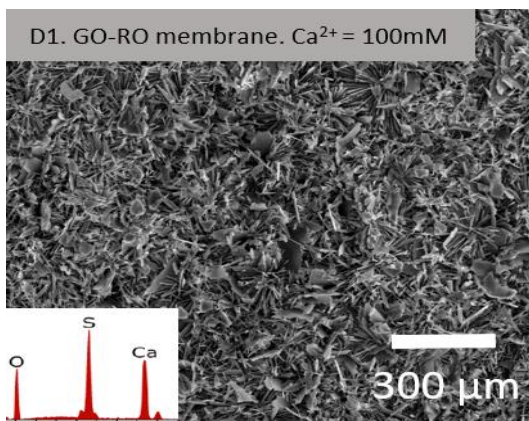
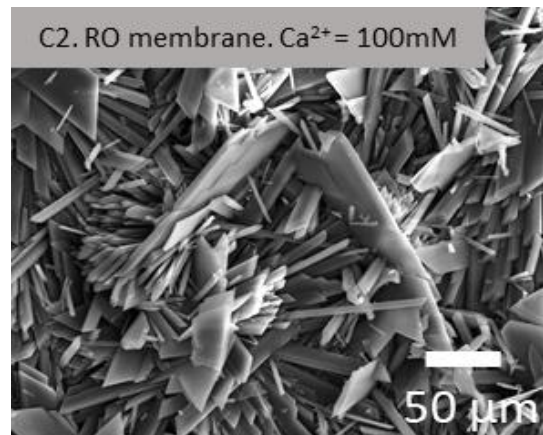
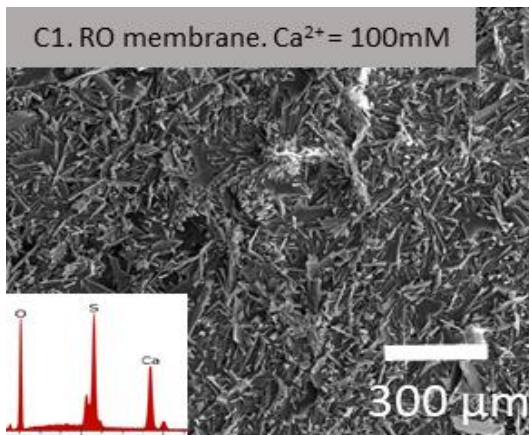


Figure 19. SEM-EDX analysis for scaled membranes at concentrations of 50 to 150 mM.

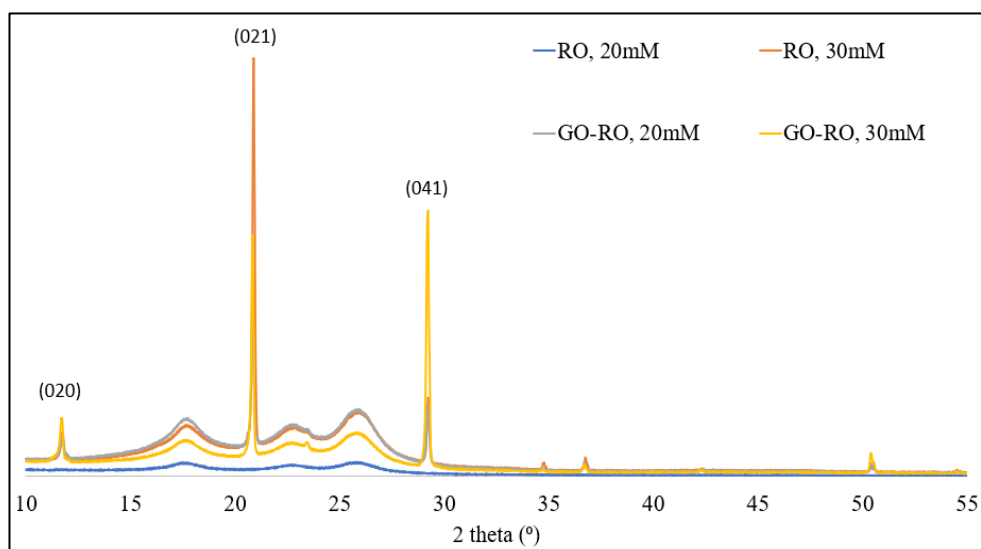
To identify the polymorph of precipitates on the scaled membrane, XRD technique was used. In all the experimental and solution conditions investigated in this research, the precipitate formed on the membrane was found to be only gypsum ( $\text{CaSO}_4 \cdot 2\text{H}_2\text{O}$ ) and no other polymorphs were formed. The peaks at 11.5, 20.6, 23.1, 29.0° (Farrah et al., 2004) demonstrates the presence of gypsum on the membrane (Figure 21). The strong intense peaks showed the formation of well crystalline gypsum structures at higher concentration. Whereas, at lower concentration, the amorphous form of gypsum was found as indicated by the presence of broader less intense peaks. This was further confirmed by calculating the degree of crystallinity using the Equation 26.

$$\text{Crystallinity} = \frac{\text{Area of crystalline peaks}}{\text{Area of all peaks (Crystalline+Amorphous)}} \times 100 \text{ -----(26)}$$

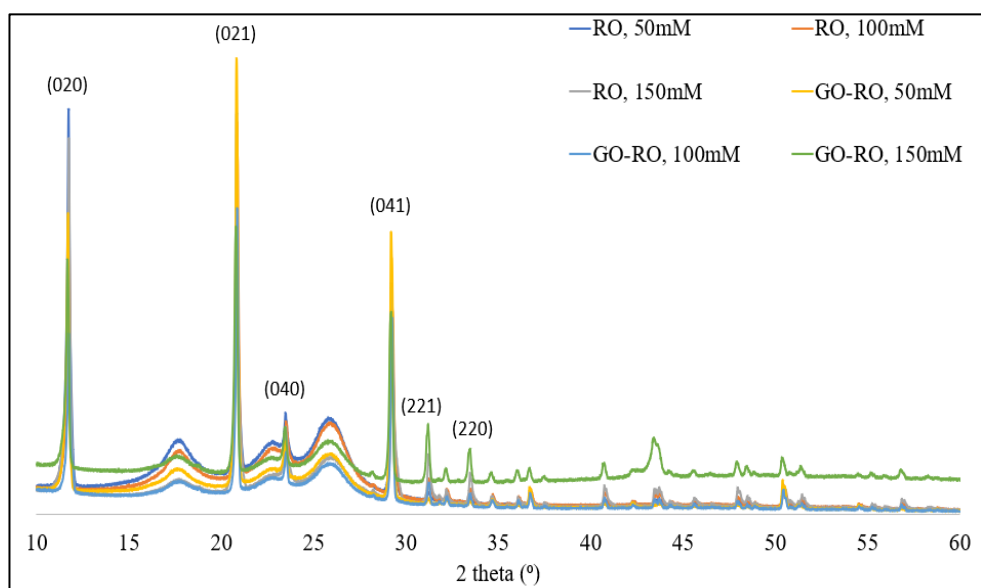
Where, the area under the peaks was calculated using Origin Pro 8 software. It was found that the degree of crystallinity increased with the increase in concentration of calcium ions. Hence, at low concentration i.e. RO membrane at 30 mM concentration, the degree of crystallinity was just around 12% as there were smaller number of sharp intense crystalline peaks noted in the XRD spectrum. Whereas, at high



concentration i.e. at 150 mM, degree of crystallinity increased to 37%.



(A)



(B)

Figure 20. XRD results of deposits on RO and GO-RO membranes (A) Low concentration of calcium ions (20 and 30 mM); (B) High concentration of calcium ions (50 – 150 mM).

#### *4.1.2.4 Mechanism of interaction between gypsum and membrane surface at different feedwater conditions.*

To understand the interaction between the gypsum at various concentrations with the membrane surface, FTIR spectra of the scaled membrane was used and was compared with the reference spectra of pure gypsum and pure membrane. Figure 22 shows the FTIR spectra obtained for the scaled and virgin GO-RO and RO membranes. Since the scaling progressed with the increase in concentration, Figures 22 (A, B, and C) provides interesting transition or stepwise interaction of gypsum ( $\text{CaSO}_4 \cdot 2\text{H}_2\text{O}$ ) with the membrane surface. At lower initial concentration ( $\text{Ca}^{+2} = 20 \text{ mM}$ , Figure 22A), the OH groups that typically appears around  $3400 \text{ cm}^{-1}$  as broad bands transitioned to the less broad and stronger bands which showed their interaction with the water molecules of gypsum. This is in consistent with the literature (Bo, 2004; Dabbas et al., 2014), that the water molecules in the gypsum appears at the peaks of  $3580$  and  $3430 \text{ cm}^{-1}$  and their interaction with OH groups has also been previously noted in forward osmosis during surface crystallization of gypsum on polyamide membranes (Xie and Gray, 2016). Furthermore, as the scaling progressed further when the higher concentration of calcium ions was used ( $\text{Ca}^{+2} = 30 \text{ mM}$ , Figure 22B), the C-H stretching of carboxyl groups of the polyamide layer which typically appears at  $2970 \text{ cm}^{-1}$  (Tang et al., 2007) disappeared completely possibly due to its interaction with the calcium ions. However, when the initial concentration of 50 to 150 mM of calcium ions were used and the scaling got intense on the membrane, then the presence of sulfate groups from gypsum was evident in the FTIR spectra ( $\text{Ca}^{+2} = 50$  to  $150 \text{ mM}$ , Figure 22C). In general, the strong bands centered around  $1140 \text{ cm}^{-1}$  splitting into two components at around  $1146$ ,  $1116 \text{ cm}^{-1}$  and  $669$ ,  $662 \text{ cm}^{-1}$  represents stretching and bending modes of  $\text{SO}_4$  from pure gypsum (Bo, 2004; Dabbas et al., 2014). Hence, the possible interaction of amide bands

(NH<sub>2</sub>) which appears at 1542, 1609, 1662 cm<sup>-1</sup> from polyamide RO membrane surface (Tang et al., 2009) with SO<sub>4</sub> groups resulted in the disappearance of these peaks in the scaled membrane.

Through comparing the FTIR spectra of pure gypsum and gypsum scaled membranes, these interactions of water molecules and sulfate group from gypsum with these functional groups (-OH, -COOH, -NH<sub>2</sub>) of the membrane were also evident in the form of peak shifts. For example; the stretching vibration of water molecules from gypsum, which usually appears at 3580 and 3430 cm<sup>-1</sup> shifted to 3518 and 3400 cm<sup>-1</sup> in the scaled membrane due to its interaction with the OH groups of the membrane that appear in this region (Table 10).

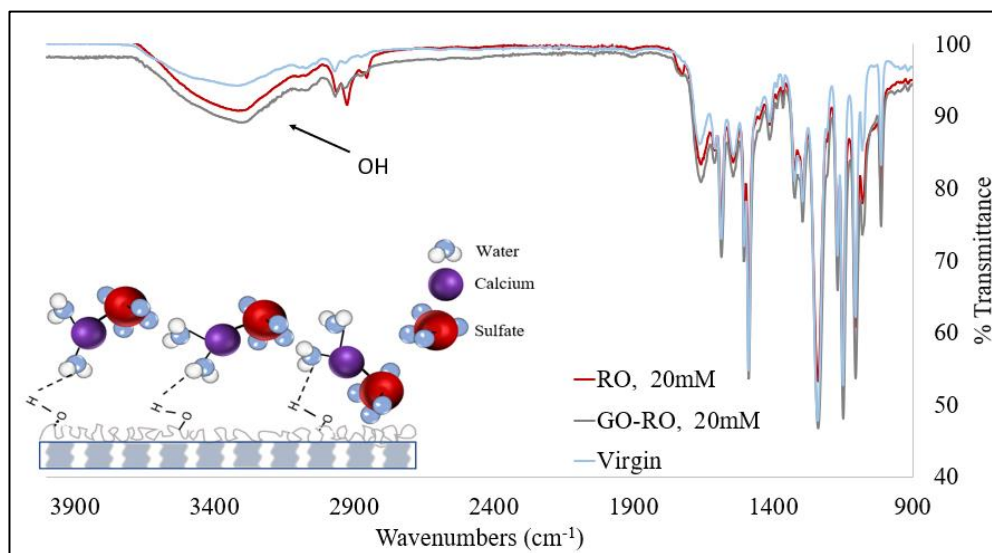
Table 10. Peak Shifts through Comparison between the Pure Gypsum and the Gypsum Scaled Membrane

#	Peak assignments (Gypsum)	Pure gypsum (cm <sup>-1</sup> )*	Gypsum scaled membrane (cm <sup>-1</sup> )	Peak shifts (Difference) (cm <sup>-1</sup> )
01	Stretching vibration of water molecules	3580	3518	62
02		3430	3400	30
03	Stretching and bending modes of SO <sub>4</sub> group	1146	1108	38
04		1116	1108	8
05		669	667	2
06		602	595	7

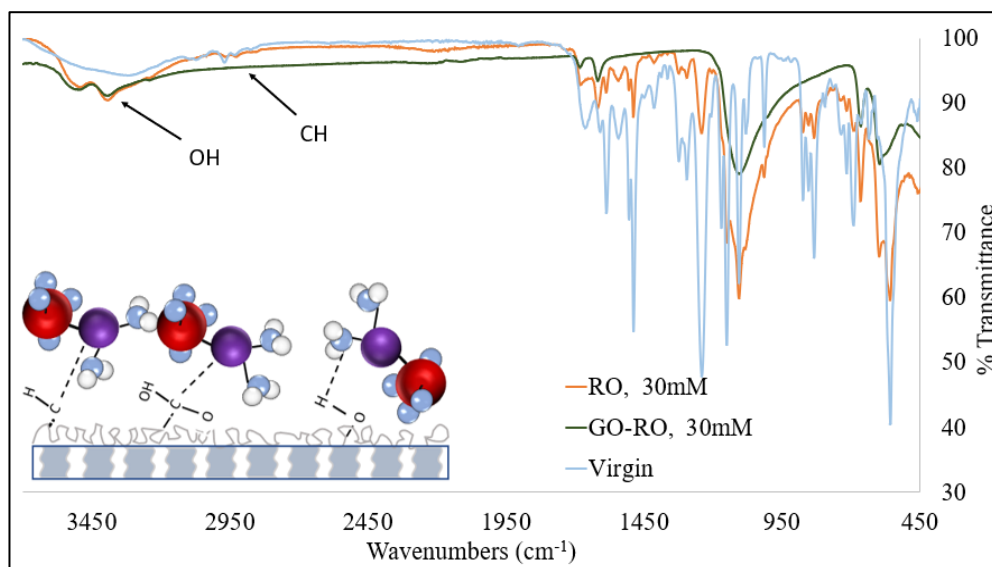
\* Bo, 2004; Dabbas et al., 2014

In addition to provide insights about the mechanism of scaling, FTIR spectra also provided useful information about the extent of scaling. The peaks of polysulfone support layer of the membrane such as 1587, 1541, 1504, 1488, and 1055 cm<sup>-1</sup> (Tang et al., 2009) were present at lower saturation conditions (Figure 22A, 22B), but gradually disappeared in Figure 22C which showed that the infrared radiations were not able to travel down to the support layer as the scaling layer was thicker and was

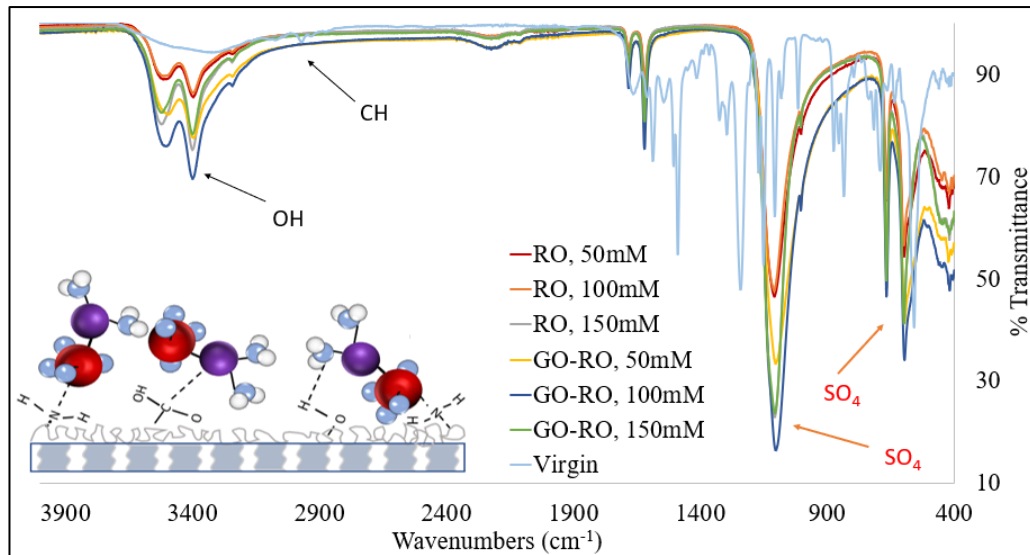
fully covering the membrane surface at higher saturation conditions. This is also in consistent with the SEM-EDX results that the membrane surface coverage by gypsum crystals increased with the concentration of calcium ions.



(A)



(B)



(C)

Figure 21. FTIR spectra of the scaled membranes (A)  $\text{Ca}^{+2} = 20 \text{ mM}$ ; (B)  $\text{Ca}^{+2} = 30 \text{ mM}$  (C)  $\text{Ca}^{+2} = 50 \text{ to } 150 \text{ mM}$ . The black colored arrows and texts refers to the functional groups of membrane and red-colored to the functional groups of gypsum.

#### 4.1.2.5 Effect of scaling on membrane hydrophilicity.

The foulant – foulant and membrane - foulant interactions are important in membrane sciences to predict and understand the interaction of foulants with other foulants and with membrane. Previous research investigated the effect of hydrophilicity of pure membrane on scaling by gypsum. It was found that the hydrophilic membranes of cellulose acetate ( $50.0^\circ$ ) and nylon ( $44.9^\circ$ ) polymer showed highest adhesion energy to gypsum crystals measured through interaction energy ( $E_{in}$ ). The research concluded that the polymers containing various carboxylic, hydroxyl and other functional groups demonstrated enhanced interaction with gypsum crystals as they can form hydrogen bonds with water molecules of gypsum crystals (Su et al., 2018). Therefore, hydrophilic membranes with higher wettability possesses higher surface energy, which results in increased affinity to gypsum crystals.

In terms of foulant-foulant interaction, the hydrophilicity is a property of the

foulant which can have a profound effect on membrane fouling by altering its interaction with other foulants and now this area is receiving extensive attention in membrane fouling research (Mu et al., 2019). Since, the membrane fouling is caused by organic, inorganic (mineral scaling), colloidal and microorganism, the hydrophilicity of the scaled membrane can determine its interaction with other foulants. If the scaled membrane becomes more hydrophobic, it is expected that its interaction with the organic foulants will increase resulting in enhanced membrane fouling. Previous research has shown that the hydrophobicity of the dissolved organic matter caused the fouled membrane surface more hydrophobic, which caused the severe decline in flux. Hence, the membrane fouled with more hydrophobic DOM had lowest permeate flux as compared to the membrane fouled with less hydrophobic (or hydrophilic) DOM (Mu et al., 2019). Furthermore, it was also noted that the organic fouling caused by sodium alginate, and humic acid enhanced gypsum crystallization on the membrane by acting as a nucleus for crystals formation (Liu and Mi, 2014). The research concluded that the density of carboxyl groups of organic foulants will determine their interaction with gypsum scaling (Liu and Mi, 2014). Various factors such as the hydrophilicity of the virgin membrane, the foulants involved and the extent of scaling will determine the hydrophilicity of the scaled membrane (Mu et al., 2019). In this research, it was found that the hydrophilicity of the scaled membrane increased with the extent of scaling. As shown in Figure 22, as the concentration of calcium ions increased from 20 mM to 150 mM, the water contact angle of the scaled membranes decreased to the extent that it was non-measurable at the experimental conditions. Thus, the water droplet of 2  $\mu$ L dispersed in less than 3 seconds after it was placed on the extensively scaled membrane. Therefore, the foulant-membrane interactions and inter/intra foulant interactions are very important to understand, in order to predict the

behavior of membrane fouling in both single and mixed foulant environments. Hence, further research is being done to investigate the intra-foulant interactions between gypsum and microorganisms in membrane filtration systems.

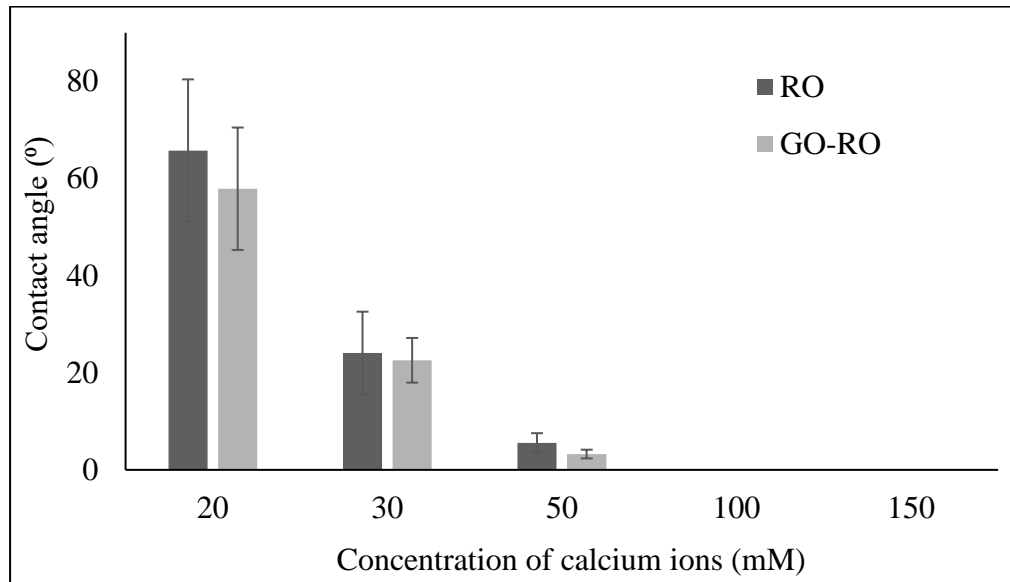


Figure 22. Contact angle (°) for gypsum scaled membranes at different concentration of calcium ions in feedwater.

#### 4.1.3 Conclusion

In this research, the effect of concentration of calcium ions in feed water was investigated on scaling of RO and GO-RO membranes. The effect of GO coating on RO membrane did relatively reduce the severity of flux decline due to membrane scaling. In general, it was found that the intensity of membrane scaling increased with the increase in concentration as reflected by the increase in intensity of flux decline over time as well as mass density of crystals formed on the membrane surface. As a result, the membrane resistance increased due to fouling ( $R_f$ ) and was found to be highest at highly concentrated solution conditions (i.e. 150 mM). The membrane surface coverage by the scales also increased at higher concentrations as shown by

SEM-EDX and FTIR results. The morphology of the crystals varied from thin needle like structures to broader floral structures when the concentration was increased. FTIR results showed that the mechanism of interaction of gypsum with membrane surface also varied with the extent of scaling as hydroxyl groups were found to be involved when the scaling was less intense. Whereas, interaction of carboxyl and amide groups were also found when the scaling was more intense. The results of XRD confirmed that the gypsum ( $\text{CaSO}_4 \cdot 2\text{H}_2\text{O}$ ) was the only polymorph formed on the membrane. The water contact angle analysis showed that the gypsum scaling on the membrane enhanced its hydrophilicity, which may develop its inter- / intra- foulant interactions with other ions present in water. Since, the presence of other foulants such as microorganisms may also alter the mechanism and extent of membrane scaling as a result of foulant – foulant interactions between them, further research is being done on the effect of microorganism on gypsum scaling.

#### *4.2 Effect of temperature on gypsum scaling of RO and GO coated RO membranes<sup>7</sup>*

##### *4.2.1 Introduction*

Recent estimations of World Health Organization (WHO) has shown that in every 10 individuals, one does not have access to clean drinking water (Ashfaq et al., 2019). With the increase in population and growth in economy, countries are increasingly relying on seawater desalination industry to fulfil rising water demands. Due to the bigger environmental and economic footprint, it is recommended that the thermal desalination techniques need to be replaced by membrane desalination systems

---

<sup>7</sup> This content has already been published. Ashfaq, M.Y., Al-ghouti, M.A., Qiblawey, H., Zouari, N. 2020. Investigating the effect of temperature on calcium sulfate scaling of reverse osmosis membranes using FTIR, SEM-EDX and multivariate analysis. *Sci. Total. Environ.* 703, 134726.



such as seawater reverse osmosis (SWRO) for the new desalination industries (Banat et al., 2009). However, the issue of membrane fouling especially biofouling is affecting the widespread use of SWRO in the desalination industry.

The inorganic fouling or mineral scaling is also a type of membrane fouling which is mainly caused by the precipitation of calcium sulfates, calcium carbonates, barium sulfate and silicates (Ashfaq et al., 2019). There are two pathways proposed for mineral scaling: 1) homogeneous process as bulk crystallization followed by deposition and 2) heterogeneous process of surface crystallization (Mi and Elimelech, 2013). However, recent research has shown that the bulk crystallization is also a heterogeneous process as the nucleation takes place on the nanoparticles which are almost always present in water (Popov et al., 2019). The operating conditions such as cross flow velocity and pressure can affect which mechanism (bulk or surface crystallization) dominates the membrane scaling. It was noted that increase in operating pressure enhances the surface crystallization, whereas the increase in cross flow velocity reduces the surface crystallization. Hence, the extent of concentration polarization will be a dominant factor in this case. On the other hand, intermediate cross flow velocity with high pressure enhances the chances of bulk crystallization followed by deposition (Lee et al., 2000; Lee et al., 1999). The presence of organic macromolecules also affects the membrane scaling. It was noted that humic acid and alginate conditioning on the membrane surface enhances the gypsum scaling in forward osmosis by shortening the nucleation time and increasing the flux decline (Liu and Mi, 2014). Similarly, the temperature is another factor that can influence the membrane scaling through altering activation energy (Hoang et al., 2007). Previous research has shown that the precipitation of calcium sulfate in pipes increased at higher temperatures. It was concluded that higher temperature provided additional energy for molecules to

overcome activation energy for the precipitation reaction and fasten the transportation of ions from bulk solution to the surface (Hoang et al., 2007). However, effect of membrane scaling on membrane performance (flux, resistance, solute rejection) and scale layer characteristics (crystals morphology, layer thickness etc.) at different temperatures has not been investigated in detail. The application of antiscalants is shown to be effective in controlling mineral scaling, however, their dosage may also need to consider the variation in intensity of scaling as a result of different operating conditions such as temperature.

Hence, in this research, the effect of temperature on membrane scaling was investigated on bared RO and GO coated RO membranes using two initial solution conditions. The effect of temperature on permeate flux decline, total mass of crystals precipitated on the membrane, morphology, and polymorphs of scales formed was explored. Furthermore, PCA was applied on the results of flux decline over time data to explore its ability to differentiate membrane scaling at different conditions and establish its significance and use in membrane fouling studies.

## *4.2.2 Results and Discussion*

### *4.2.2.1 Characterization of RO and GO-RO membranes.*

Initial characterization of RO and GO-RO membranes was done in terms of membrane roughness, pure water flux, hydrophilicity and salt rejection. Due to the hydrophilic and smoothness of GO (Inurria et al., 2019; Sun and Li, 2018), the GO functionalized membrane was found to be more hydrophilic as the water contact angle was reduced from  $80.1 \pm 1.6$  (bared RO membrane) to  $46.8 \pm 1.3$ . Furthermore, the membrane roughness characterized through Atomic Force Microscopy (AFM) showed that the surface roughness of the membrane also reduced as shown in Table 11 after

modification with GO. The solid-liquid interfacial energy ( $-\Delta G_{SL} = \gamma_L [1 + \cos \Theta/\Delta]$ ) was also calculated (Wang et al., 2018) (Table 11), in which,  $\Delta$  is the relative surface area obtained from atomic force microscopy,  $\gamma_L$  is the surface tension of pure water (at 25 °C: 72.8 mJ.m<sup>-2</sup>). The membrane transport and salt rejection properties measured in terms of pure water flux and percentage sodium rejection were also changed slightly, which is in consistent with the previous researches (Cao et al., 2018; Faria and Perreault, 2017)

Table 11. Properties of RO and GO-RO membranes (Ashfaq et al., 2020a).

Properties	RO membrane	GO-RO membrane
Water permeability (L.m <sup>-2</sup> .h.bar <sup>-1</sup> ) at 25 °C, 35 bars	5.0 ± 0.2	5.2 ± 0.4
Average Na <sup>+</sup> rejection (%) (25 °C, 35 bars, 0.04 M NaCl)	98.6 ± 0.1	98.4 ± 0.4
Contact angle (Θ)	80.1 ± 1.6	46.8 ± 1.3
Surface roughness (nm)	75.0 ± 8.0	62.8 ± 1.2
Solid-liquid interfacial energy ( $-\Delta G_{SL}$ ) (mJ.m <sup>-2</sup> )	72.2	98.0

Solid-liquid interfacial energy was calculated as:  $-\Delta G_{SL} = \gamma_L [1 + \cos \Theta/\Delta]$  (Wang et al., 2018). Where,  $\Delta$  is the relative surface area obtained from atomic force microscopy,  $\gamma_L$  is the surface tension of pure water (at 25 °C: 72.8 mJ.m<sup>-2</sup>).

#### 4.2.2.2 Effect of Temperature on membrane scaling and performance

In general, the solubility of calcium sulfate polymorphs decreases with temperature. Nevertheless, the solubility of gypsum (CaSO<sub>4</sub>.2H<sub>2</sub>O) slightly increases from 2.02 to 2.18 and then to 2.10 g/L when the temperature increases from 20 to 30 and then to 40 °C, respectively. When the temperature further exceeds to 50 and 60°C, the solubility starts decreasing to 2.07 and 2.01 g/L, respectively. That is why, the gypsum is commonly found deposit at temperature about 50°C. In other applications

where temperature is higher, the calcium sulfate hemihydrate and anhydrite are more common (Muryanto et al., 2013).

In general, increase in temperature results in an increase in permeate flux (Ashfaq et al., 2017; Gönder et al., 2011) which can be attributed to the decrease in viscosity of water, increase in diffusion coefficient and thermal expansion of membrane pores (Kowalska et al., 2006; Tsai et al., 2006). In this research, it was also noted that the stable permeate flux ( $J_f$ ) obtained at the end of experiment was highest at 35°C and lowest at 5°C. To investigate the rate of flux decline due to scaling, normalized flux ( $J_n = J_f/J_o$ , where  $J_o$  is the pure water membrane flux at a specific temperature) was calculated and depicted in Figure 24 (a-d). The initial membrane flux ( $J_o$ ) for RO membrane was found to be (LMH):  $98 \pm 3$  (5 °C),  $129 \pm 6$  (15 °C),  $178 \pm 8$  (25 °C) and  $245 \pm 10$  (35 °C). While, the initial membrane flux ( $J_o$ ) for GO-RO membrane was found to be slightly higher than RO i.e. (LMH):  $102 \pm 4$  (5 °C),  $136 \pm 5$  (15 °C),  $182 \pm 5$  (25 °C) and  $250 \pm 8$  (35 °C). It was noted that  $J_n$  decreased with increase in temperature indicating more intense scaling. It can be deduced that increase in permeate flux brought more solutes towards the membrane surface, intensifying concentration polarization and causing more severe scaling at higher temperatures which ultimately resulted in more intense flux decline at these temperatures. In addition, higher feed water temperature also provided enough energy to the molecules to overcome the barrier of activation energy of the precipitation reaction (Hoang et al., 2007; Ashfaq et al., 2019) resulting in more intense scaling. It can also be deduced from Fig. 2a that the permeate flux was higher when initial concentration was lower ( $Ca^{+2} = 20mM$ , solution 1) as compared to higher initial concentration conditions ( $Ca^{+2} = 50mM$ , solution 2). This could be attributed to the higher saturation conditions in the latter as outlined in Table 7. Furthermore, the concentration polarization effect is also expected to be more

intense at higher concentration as compared to lower concentration.

The results of flux decline over time for different temperatures and membrane was also analyzed using PCA to elucidate the differences of flux decline at different conditions. Figure 24e and 24f shows that the flux behavior was significantly different at different temperatures, but the difference between the two membranes (RO and GO-RO) was lesser. At lower initial concentration ( $\text{Ca}^{+2} = 20\text{mM}$ , solution 1), the principle components (PC1 and PC2) together shows 99% of the variability in the data (Fig. 25e). It is worth noting that the distance between the two points along x-axis is much more significant than the distance along y-axis as 97% variability is shown in the former as compared to 2% in the latter. Hence, PCA graph showed that the flux decline due to membrane scaling got intense as the temperature was increased from 5 and 15°C to 25°C and then to 35°C. Similar trend was also noted for the case of higher initial concentration ( $\text{Ca}^{+2} = 50\text{mM}$ , solution 2) as shown in Figure 24f. The separation of points resulting from two different membranes (RO and GO-RO) at the same temperature also accounts for variation in the trend due to the two different membranes, which was not clear from flux decline graphs alone (Figure 24a-d). In this way, PCA can help to provide insights into the data set of flux decline over time in membrane fouling studies and can aid in differentiating the flux response to different conditions/foulants/membranes etc. Such an application of PCA in membrane fouling studies is seldom reported. PCA was utilized in our previous research to differentiate the bio-film layer on RO membranes formed in response to different antiscalants (Ashfaq et al., 2019). Gelaw et al., 2011 and Gelaw et al., 2014, combined SIMCA (Soft independent modeling of class analogy models) models with FTIR to differentiate the fouled and cleaned membranes, which helped them to identify best cleaning protocol. Thus, use of multivariate analysis in membrane fouling studies can help to

provide various insights into the fouling mechanisms, type, and extent at different conditions. In addition, it can also help in determining and differentiating the effectiveness of various antiscalants to diminish membrane scaling.

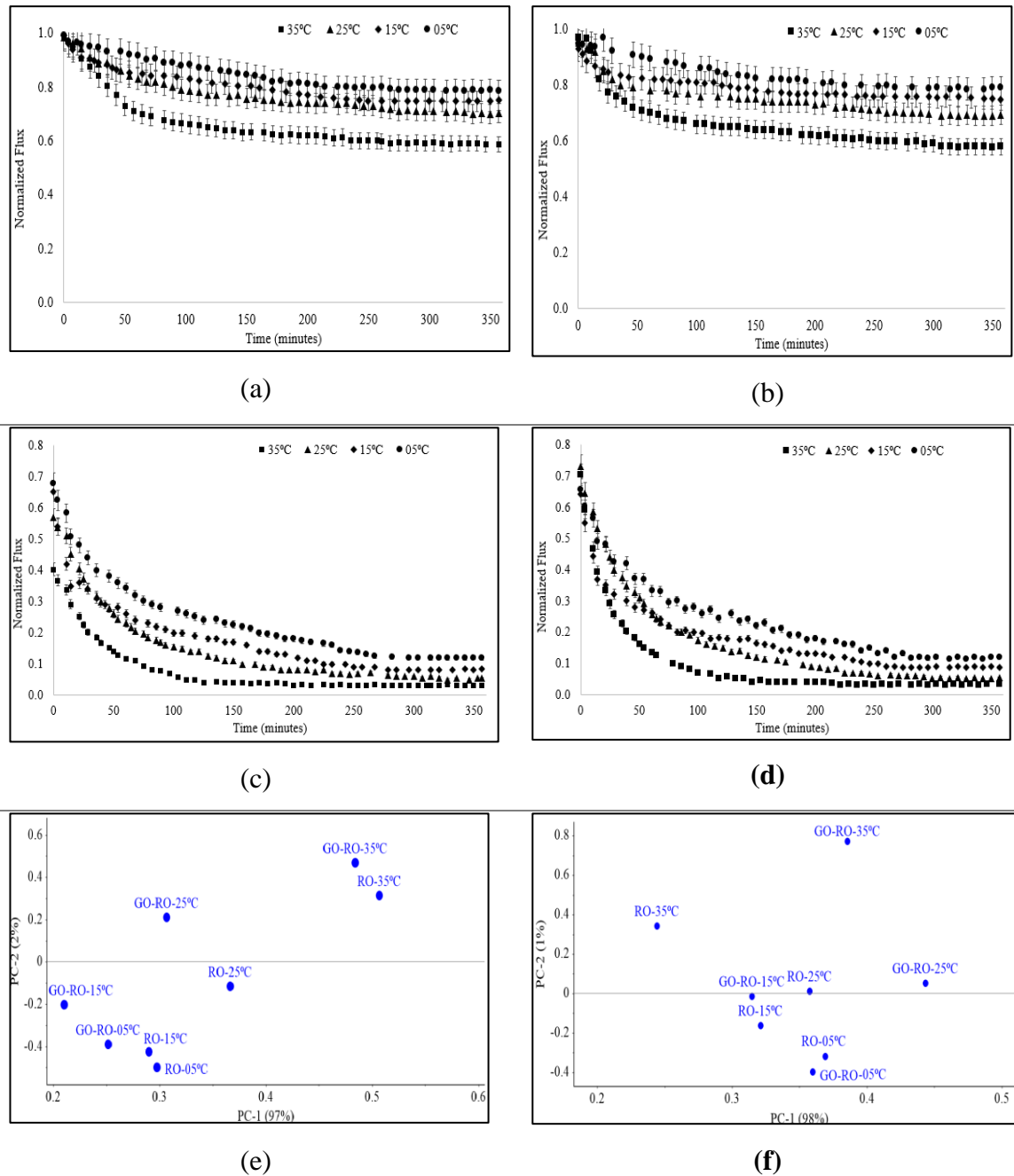


Figure 23. Flux decline curves for Solution 1 ( $\text{Ca}^{+2}=20$  mM) obtained using (a) RO membrane; (b) GO-RO membrane; and for Solution 2 ( $\text{Ca}^{+2}=50$  mM) obtained using

(c) RO membrane; (d) GO-RO membrane; and PCA graphs for (e) Solution 1,  $\text{Ca}^{+2}=20$  mM, (f) Solution 2,  $\text{Ca}^{+2}=50$  mM (Ashfaq et al., 2020a).

The estimation of membrane resistance mainly depends upon the stabilized flux obtained at the end of scaling experiments. It was noted that at low initial concentration, the increase in membrane resistance was minimal (Table 12). For example, the membrane resistance increased from  $8.12 \times 10^{13} \text{ m}^{-1}$  ( $R_m$ ) to  $9.83 \times 10^{13} \text{ m}^{-1}$  ( $R_t$ ) due to additional resistance caused by the scale layer/concentration polarization ( $R_f$ ) which was estimated to be  $1.71 \times 10^{13} \text{ m}^{-1}$  at 5 °C for GO-RO membrane. Due to the decline of flux over time at higher temperatures, the  $R_f$  increased further to  $5.39 \times 10^{13} \text{ m}^{-1}$  at 35 °C. Nevertheless, this increase in membrane resistance was more severe at higher concentrated solution as the  $R_f$  increased from  $60.4 \times 10^{13} \text{ m}^{-1}$  (at 5 °C) to  $215.23 \times 10^{13} \text{ m}^{-1}$  (at 35 °C). Decrease in percentage rejection with increase in temperature was also noted especially at higher saturation conditions (Table 12) for both RO and GO-RO membranes, possibly due to the thermal expansion of membrane pores as discussed previously (Kowalska et al., 2006; Tsai et al., 2006).

Table 12. Effect of temperature on membrane resistance and percentage rejection (Ashfaq et al., 2020a).

Solution	Temp. (°C)	$R_m$ ( $m^{-1}$ ) ( $10^{13}$ )		$R_t$ ( $m^{-1}$ ) ( $10^{13}$ )		$R_f$ ( $m^{-1}$ ) ( $10^{13}$ )		%R	
		RO	GO-RO	RO	GO-RO	RO	GO-RO	RO	GO-RO
Ca <sup>+2</sup> = 20 mM	5	8.45±0.42	8.12±0.41	10.22±0.51	9.83±0.49	1.77±0.09	1.71±0.09	98.7±0.6	98.6±0.4
	15	8.67±0.39	8.21±0.37	10.93±0.49	10.32±0.46	2.26±0.10	2.11±0.09	99.2±0.2	99.1±0.2
	25	7.95±0.38	7.77±0.37	11.19±0.54	11.11±0.53	3.24±0.16	3.34±0.16	98.7±0.1	98.7±0.3
	35	7.24±0.28	7.09±0.27	12.52±0.48	12.48±0.47	5.28±0.20	5.39±0.20	98.9±0.3	99.1±0.2
Ca <sup>+2</sup> = 50 mM	5	8.45±0.33	8.12±0.32	67.84±2.65	68.52±2.67	59.39±2.32	60.40±2.36	96.6±0.8	98.2±0.7
	15	8.67±0.43	8.21±0.41	96.63±4.83	89.75±4.49	87.97±4.40	81.54±4.08	95.5±0.5	97.8±0.8
	25	7.95±0.52	7.77±0.51	146.15±9.50	142.89±9.29	138.20±8.98	135.12±8.78	94.5±0.7	96.8±0.6
	35	7.24±0.44	7.09±0.43	228.82±13.96	222.32±13.56	221.59±13.52	215.23±13.13	91.5±0.7	91.4±0.5

%R was calculated using Equation (19) and Membrane resistance terms i.e.  $R_t$ ,  $R_m$ ,  $R_f$  were calculated through Equation (11, 12, and 13) using mean permeate flux values.



#### 4.2.2.3 Membrane Scale layer characterization

Table 13 shows the increase in mass crystals and scale layer thickness with temperature calculated using mass balance equation (8) mentioned in Section 2.3. It should be noted that this method of calculating mass of crystals and scale layer thickness does not consider variability in the scale morphology. The thickness of the scale layer obtained in this research is higher than previously obtained (Matral et al., 2000; Rahardianto et al., 2006), which could be due to relatively lower initial concentration of calcium ions in the feed water adopted in those researches (4 and 16.4 mM, respectively) and difference in operating conditions such as crossflow velocity and temperature.

Table 13. Total mass of crystals and thickness of scaled layer on the membranes at different temperatures (Ashfaq et al., 2020a).

Solution	Temp. (°C)	Total mass of crystals on the membrane, $M_t$ (g)		Average thickness of scaled layer ( $\mu\text{m}$ )	
		RO	GO-RO	RO	GO-RO
$\text{Ca}^{+2} = 20 \text{ mM}$	5	$0.32 \pm 0.01$	$0.32 \pm 0.01$	$32.40 \pm 1.60$	$32.35 \pm 1.65$
	15	$0.35 \pm 0.01$	$0.35 \pm 0.01$	$35.95 \pm 1.62$	$35.45 \pm 1.60$
	25	$0.38 \pm 0.02$	$0.37 \pm 0.02$	$38.49 \pm 1.85$	$38.30 \pm 1.85$
	35	$0.41 \pm 0.02$	$0.40 \pm 0.02$	$41.58 \pm 1.60$	$41.45 \pm 1.55$
$\text{Ca}^{+2} = 50 \text{ mM}$	5	$0.98 \pm 0.04$	$0.95 \pm 0.04$	$100.58 \pm 3.90$	$97.55 \pm 3.80$
	15	$1.02 \pm 0.05$	$1.02 \pm 0.05$	$104.17 \pm 5.20$	$105.20 \pm 5.30$
	25	$1.06 \pm 0.07$	$1.04 \pm 0.05$	$108.50 \pm 7.05$	$107.10 \pm 7.10$
	35	$1.13 \pm 0.07$	$1.11 \pm 0.07$	$115.82 \pm 7.07$	$113.90 \pm 7.95$

$M_t$  was calculated using Equation (17), the average thickness of the scaled layer was calculated from mass of crystals per membrane surface area and average density of gypsum ( $2320 \text{ kg/m}^3$ ).

The correlation between the temperature and the mass of scale formed on the

membrane was estimated by plotting the inverse of temperature with scale mass (log) in MS Excel (Figure 25). The curves obtained were linear which showed that the exponential correlation exists between the scale mass and the temperature i.e. mass of scales on the membrane will rise exponentially in response to the temperature. Such a correlation was also previously obtained for precipitation of calcium sulfates in pipes at concentration of 50 and 75 mM (Hoang et al., 2007).

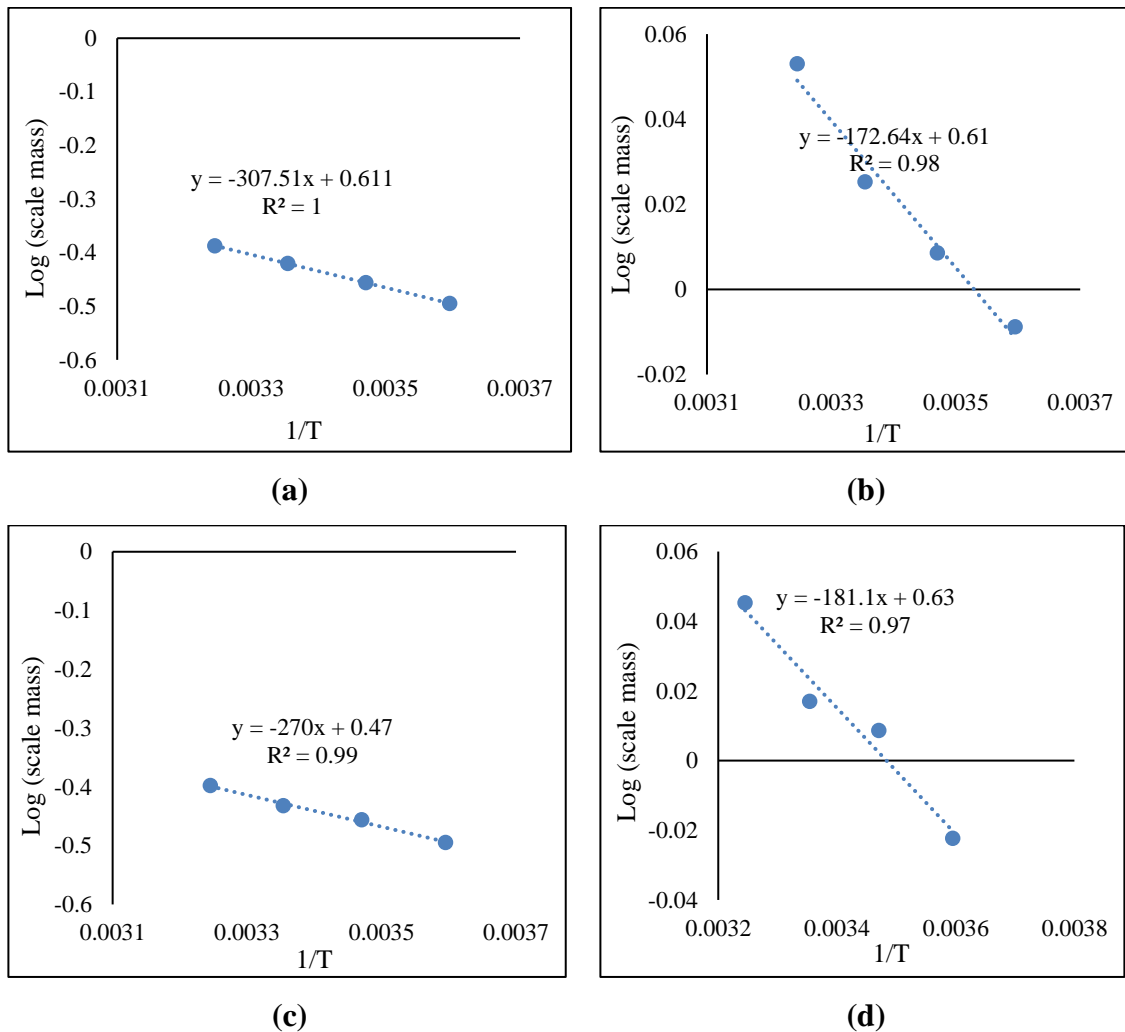


Figure 24. Correlation between mass of scales on the membrane with temperature for RO membrane (a) Solution 1 ( $Ca^{+2}=20$  mM), (b) Solution 2 ( $Ca^{+2}=50$  mM) and for GO-RO

membrane (c) Solution 1 ( $\text{Ca}^{+2}=20$  mM), (d) Solution 2 ( $\text{Ca}^{+2}=50$  mM) (Ashfaq et al., 2020a).

Induction time ( $t_{\text{ind.}}$ ) is the time taken from achieving supersaturation to the detection of first crystal deposit on the membrane. It is the sum of the time required for the nucleus to form ( $t_n$ ) and the time taken for the nucleus to grow into the visible size ( $t_g$ ). It has been noted that both the increase in supersaturation and temperature decreases the induction time (Alimi et al., 2003). Previous researches have shown the correlation between the effect of  $t_{\text{ind.}}$  with the initiation of the decline in permeability (Shmulevsky et al., 2017; Hasson et al., 2009). In this research, it was noted that the permeability decreased immediately after the start of experiments (Fig. 25a-d) which showed that the induction times initiated immediately and therefore, it was difficult to detect the induction times in these conditions. Furthermore, the solutions of  $\text{CaCl}_2$  and  $\text{Na}_2\text{SO}_4$  were mixed before introducing the solution to the feed tank, which means that the  $t_n$  may have started before the start of scaling runs. The effect of temperature is related to the  $t_{\text{ind.}}$  by the Equation (27), which is similar to the Arrhenius equation for dependence of rate constants on temperature,

$$\text{Log } 1/t_{\text{ind.}} = A - \frac{E}{2.303 RT} \text{-----}(27)$$

Where A is a constant, E is the activation energy for the nucleation (J/mol), R is the universal gas constant (8.31 J/K. mol) and T is the temperature ( $^{\circ}\text{K}$ ).

Thus, activation energy can be determined from the slope of the curve obtained by plotting the log of inverse  $t_{\text{ind.}}$  data against  $1/T$ . It has been noted that the presence of

external body can significantly reduce the activation energy. For solution conditions in the range of 0.01 to 0.05 mol/L; the activation energy has been calculated to be in the range of 51 to 160 kJ/mol. However, the presence of nucleation site reduced the activation energy to 42.4 – 48.2 kJ/mol for 0.05 – 0.075 mol/L (hoang et al., 2007). This shows that the presence of nucleation site affects the mechanism of crystallization of CaSO<sub>4</sub> on the membrane. Perhaps, the membrane surface can act as a nucleating site causing heterogenous nucleation, which require much less activation energy than the homogenous nucleation. Furthermore, increase in temperature will provide additional energy to overcome activation energy for nucleation, reducing induction times and promoting crystallization and membrane scaling.

#### *4.2.2.4 Morphological characterization of the precipitates.*

To demonstrate the effect of temperature on morphology of precipitates, micrographs of the crystals were obtained at different temperature and solution conditions, using SEM-EDX. The needle-like crystals seen in SEM images (Figure 26 and 27) can be regarded as gypsum due to their similarity to previously reported morphology of gypsum (Rahman et al., 2013; Antony et al., 2011). Since, the solubility of gypsum is lowest as compared to other polymorphs (bassinite and anhydrite) between the temperatures 0 - 40°C. Therefore, gypsum was the only polymorph obtained in this study. The EDX analysis (Figure 26 and 27) indicated that the ions of calcium, sulfur and oxygen are present in high abundance on the membrane confirming that the precipitates are mainly comprised of CaSO<sub>4</sub>.

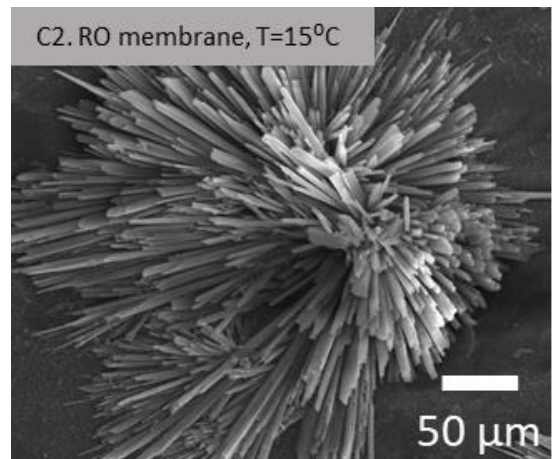
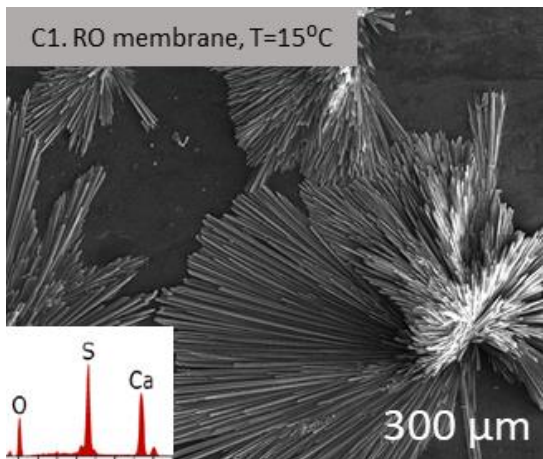
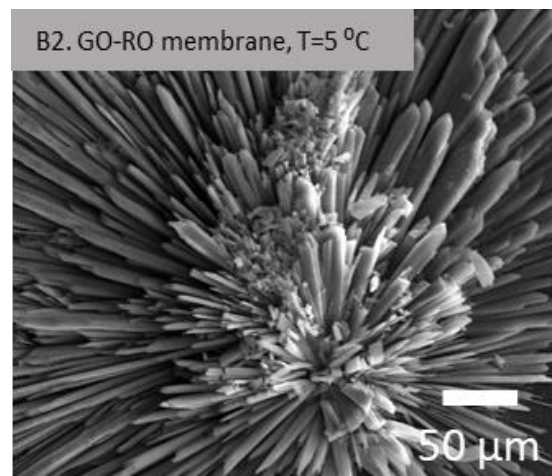
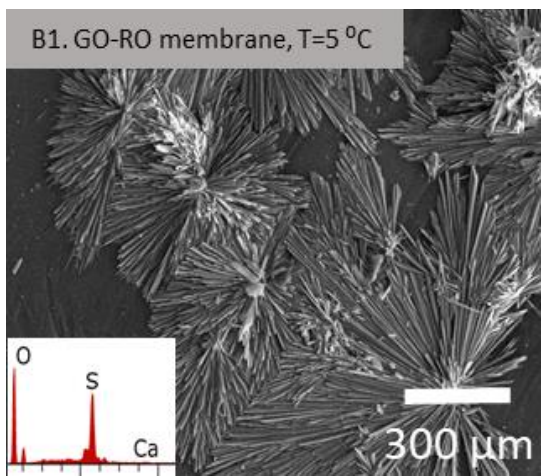
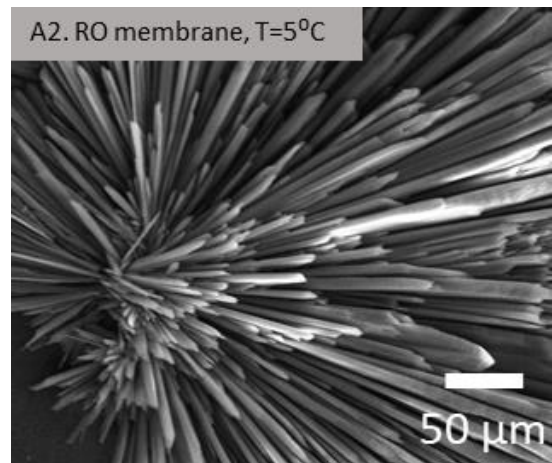
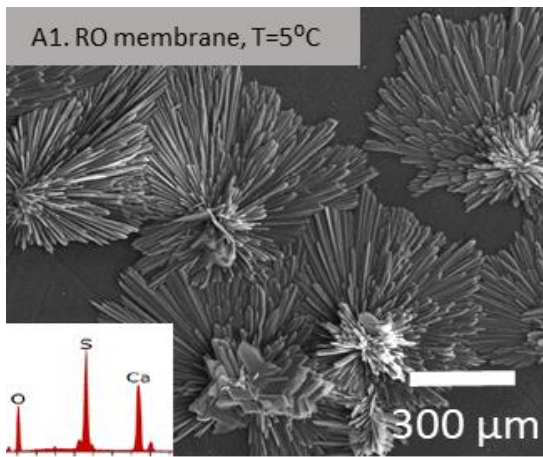
In this research, it was noted that the crystalline shapes of gypsum varied with the

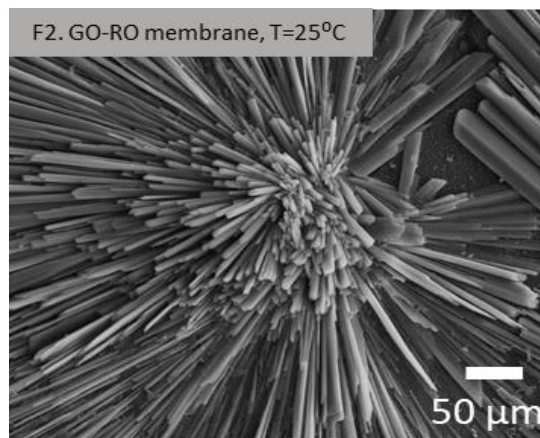
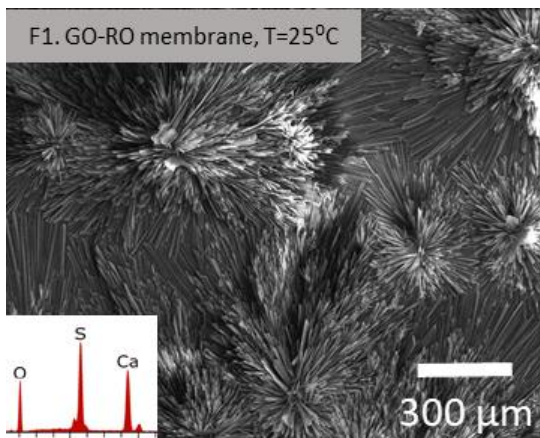
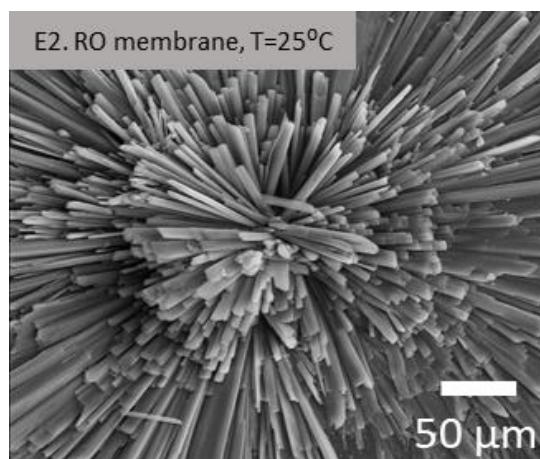
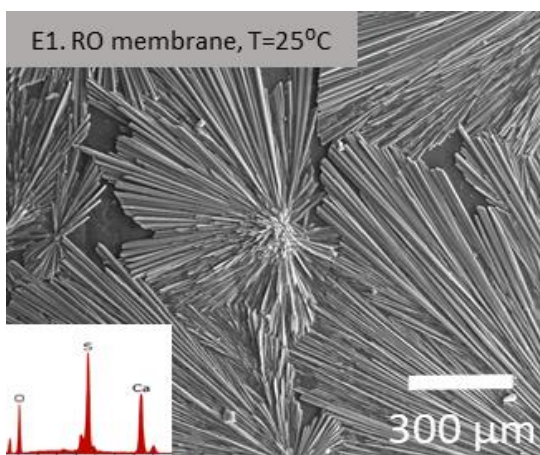
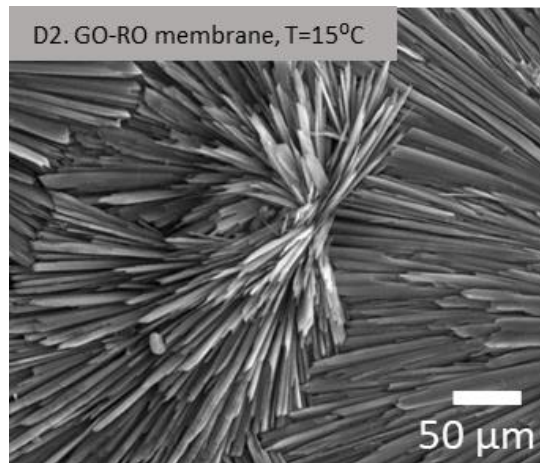
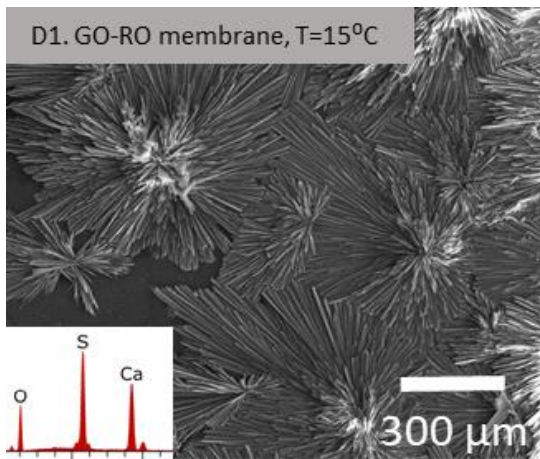
temperature. This trend is more visible in Figure 27 when more concentrated solution (solution 2) was used. At lower temperatures (05°C and 15°C), the crystals are in small needle like structures protruding into the surface of the membrane which also shows that the contact nucleation of gypsum (surface crystallization) was dominant mechanism in membrane scaling as previously reported in the literature (Gryta, 2009; Xie and Gray, 2016). However, at higher temperatures, the crystal growth increased which resulted in orthorhombic or hexagonal prismatic shapes causing floral structures, which may have caused additional resistance to the flow of water reducing membrane flux and membrane performance. Similar trend was also noted when GO-RO membrane was used, demonstrating similar mechanism behind gypsum scaling in both membranes. The development of rod and needle like structures to rosettes can be attributed to the higher concentration polarization and subsequently higher concentration of gypsum at the membrane surface as previously reported by Antony et al., (2011) and Rahman et al., (2013). Recent research by Stawski et al. (2016), has demonstrated the four stages of  $\text{CaSO}_4$  precipitation at different temperature and supersaturation conditions. It was noted that crystallization starts with formation of well-defined domains of primary species (sub-3nm size) (stage I and II) followed by aggregation and self-assembly to form large surface fractal morphologies (stage III) and then growth of species in all dimensions eventually forming larger morphologies similar to what was noted in SEM results (Figure 26 and 27). The kinetic model for gypsum crystallization can explain the trend of formation of rod to rosette structures as follows [Lee et al., 1999; Ozkar, 2001; Shih et al., 2005]:

$$\frac{dm}{dt} = k (C_m - C_s)^n \text{-----(28)}$$

$C_m$  is the concentration of gypsum at the membrane surface,  $C_s$  is the calcium sulfate solubility at the experimental conditions and  $k$  is the growth rate constant. The kinetic order is represented by  $n$ ; in which value of 1 and 2 shows the diffusion-controlled and surface reaction mechanisms, respectively.

Hence, the increase in concentration polarization ( $C_p$ ) and increase in concentration of calcium sulfate at the membrane surface ( $C_m$ ) at higher temperature and saturation conditions caused the increase in rate of scale formation ( $dm/dt$ ) (or reduction in induction times, as previously discussed) which subsequently transformed the gypsum crystals from rod shaped to rosette structures. Such a phenomenon has also been noted in the axial development of crystal structures along the membrane surface, where the rod-shaped structures were noted at the entrance region referring to lower  $C_p$  and  $C_m$ , and the rosette structures were obtained at the exit region demonstrating the effect of higher  $C_p$  and  $C_m$  (Shih et al., 2005). In addition to the temperature, the variation in pressure and crossflow velocity has also been demonstrated to affect the morphology of gypsum crystals (Lee et al., 1999). Furthermore, in RO systems, variety of inorganic, organic and biological constituents of feed water can interact with each other and cause membrane fouling (Ashfaq et al., 2018). That is why, the presence of organic macromolecules (Liu and Mi, 2014) and microorganisms (Thompson et al., 2012) has been found to enhance gypsum scaling through decreasing induction times, thereby, altering crystal morphologies.







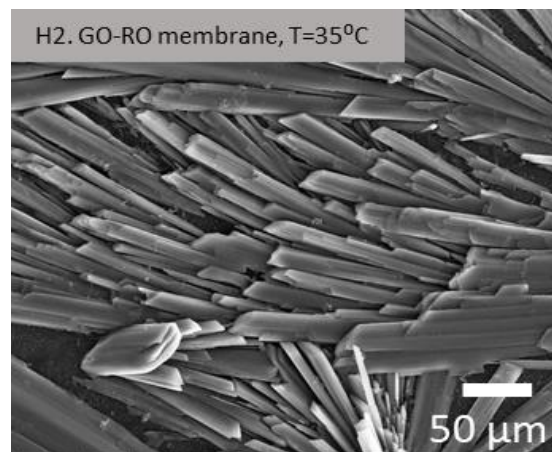
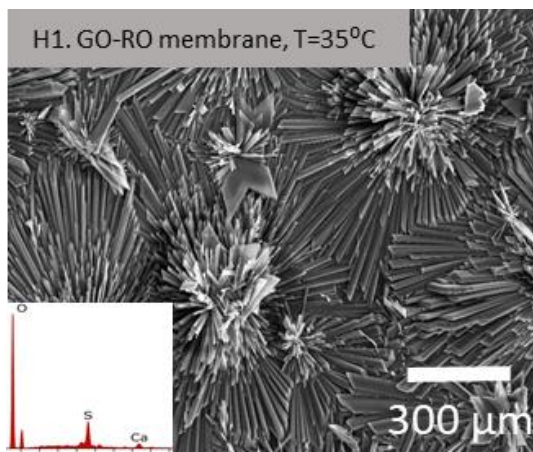
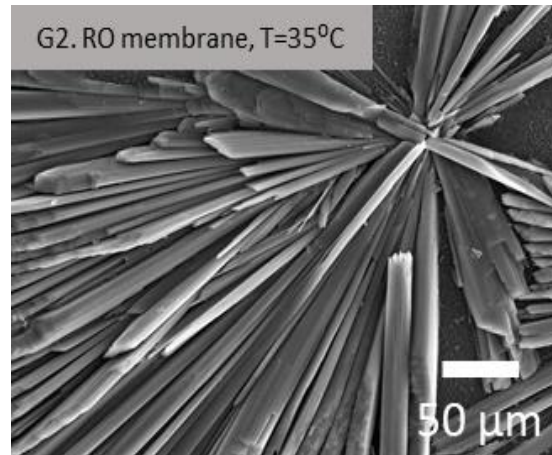
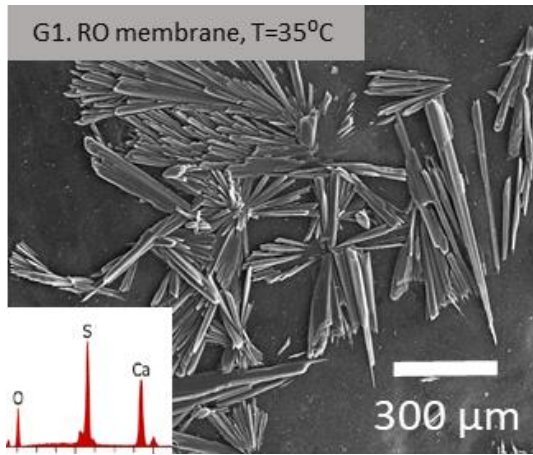
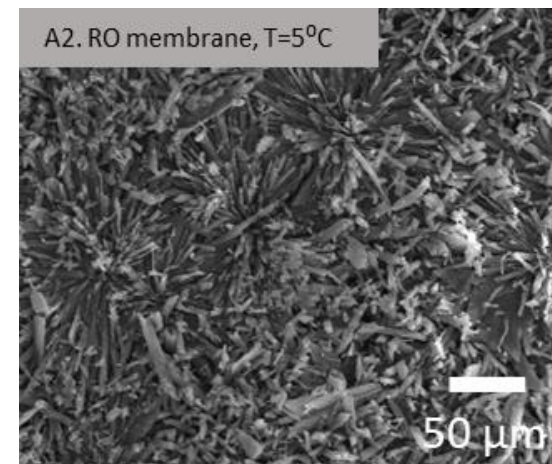
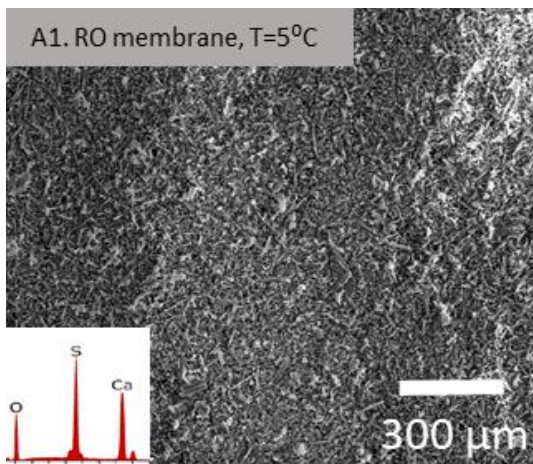
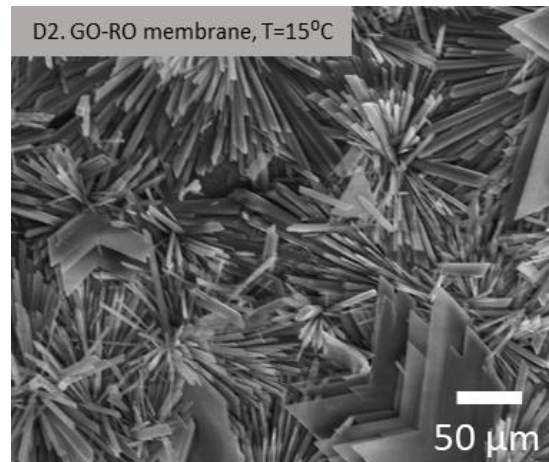
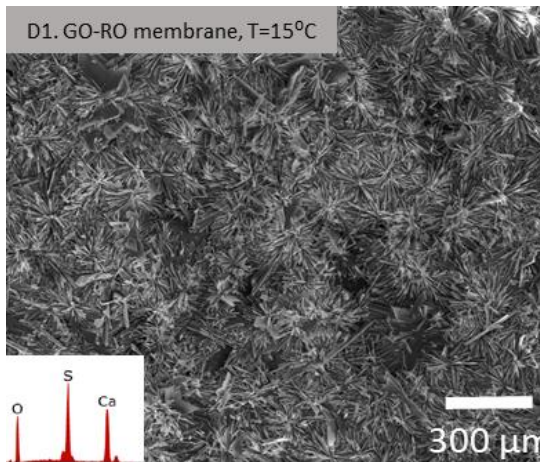
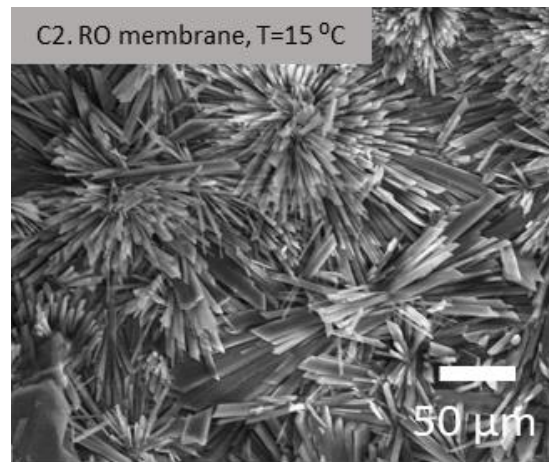
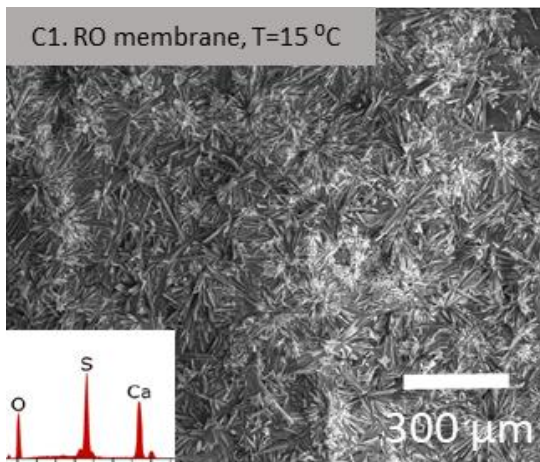
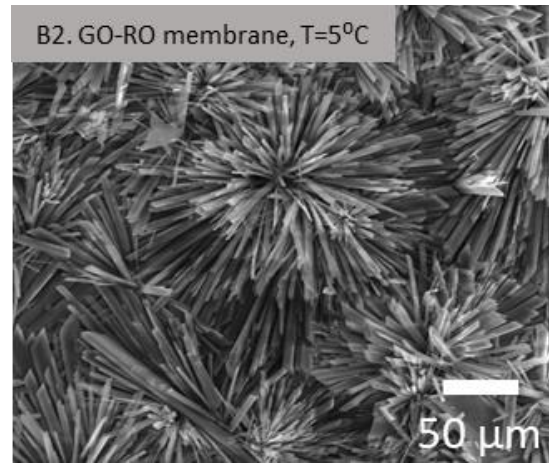
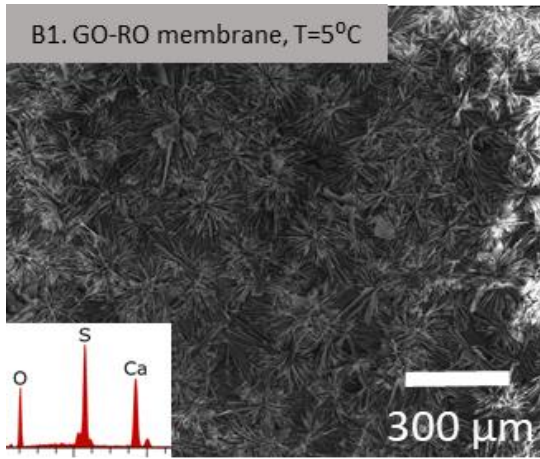
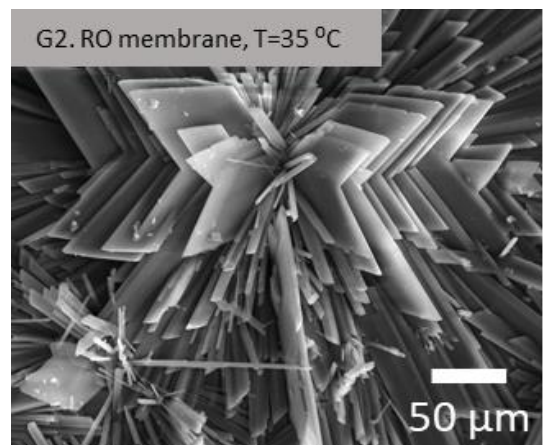
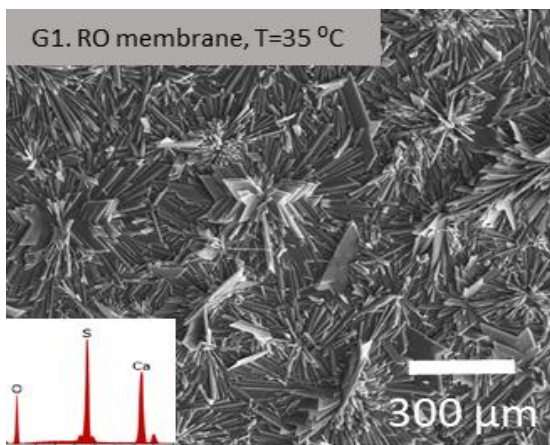
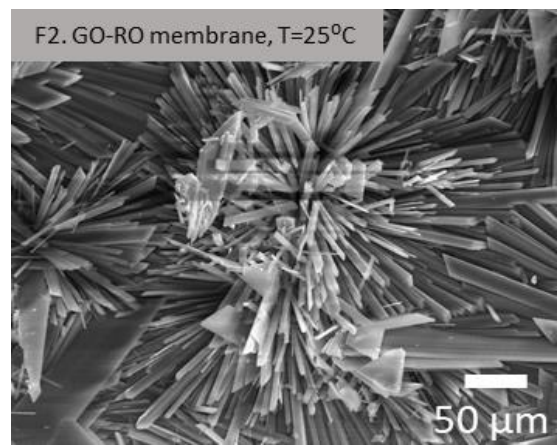
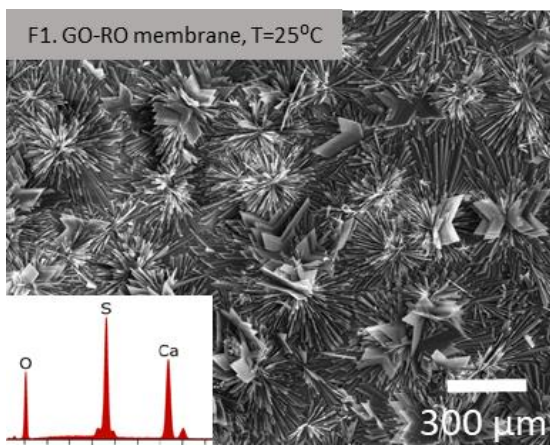
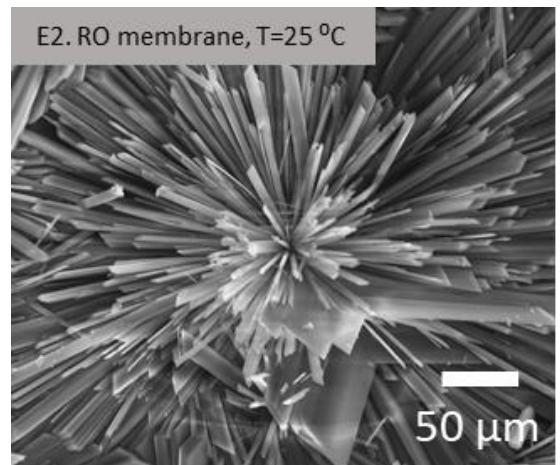
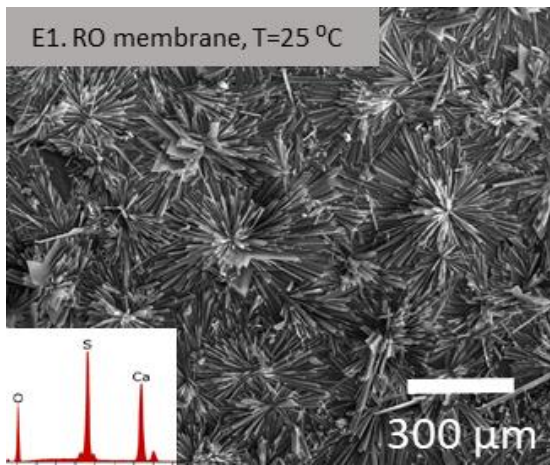


Figure 25. SEM-EDX analysis of scaled membrane at different temperatures for Solution 1,  $\text{Ca}^{+2}=20 \text{ mM}$  (Ashfaq et al., 2020a)







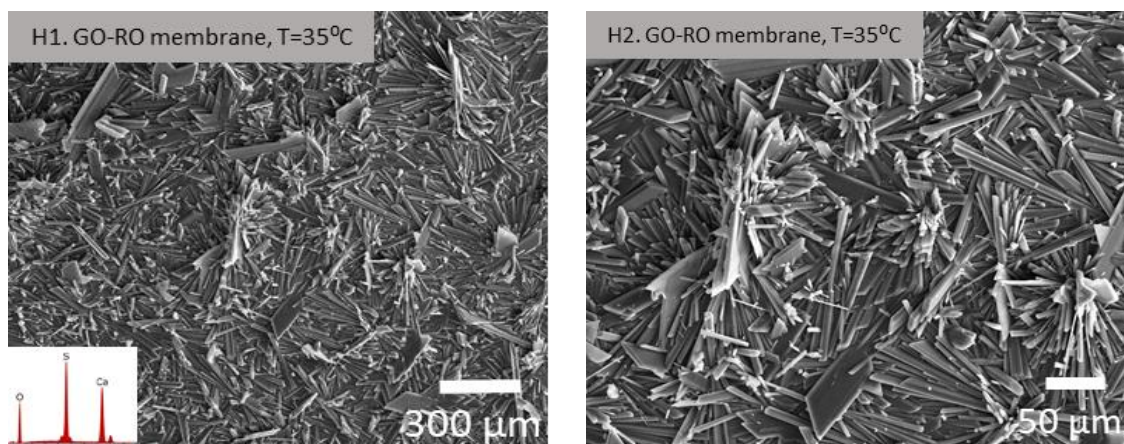


Figure 26. SEM-EDX analysis of the scaled membrane at different temperatures for Solution 2,  $\text{Ca}^{+2}=50 \text{ mM}$  (Ashfaq et al., 2020a).

The XRD results shown in Figure 28 confirmed that the precipitates were mainly gypsum ( $\text{CaSO}_4 \cdot 2\text{H}_2\text{O}$ ) and no other polymorphs (anhydrite or hemihydrate) were formed in the experimental conditions. The peaks at  $11.5^\circ$ ,  $20.6^\circ$ ,  $23.1^\circ$ ,  $29.0^\circ$  represents the presence of gypsum (Farrah et al., 2004) which are evident in Figure 28. The peaks were clearer at higher initial concentration as compared to lower concentration. The minor changes in the spectra at different temperatures could be associated with different needle, plate-like and floral structures obtained as indicated by SEM results. Other broad peaks obtained around  $18^\circ$  and in the range of  $22 - 28^\circ$  could have resulted from the polyamide membrane surface.

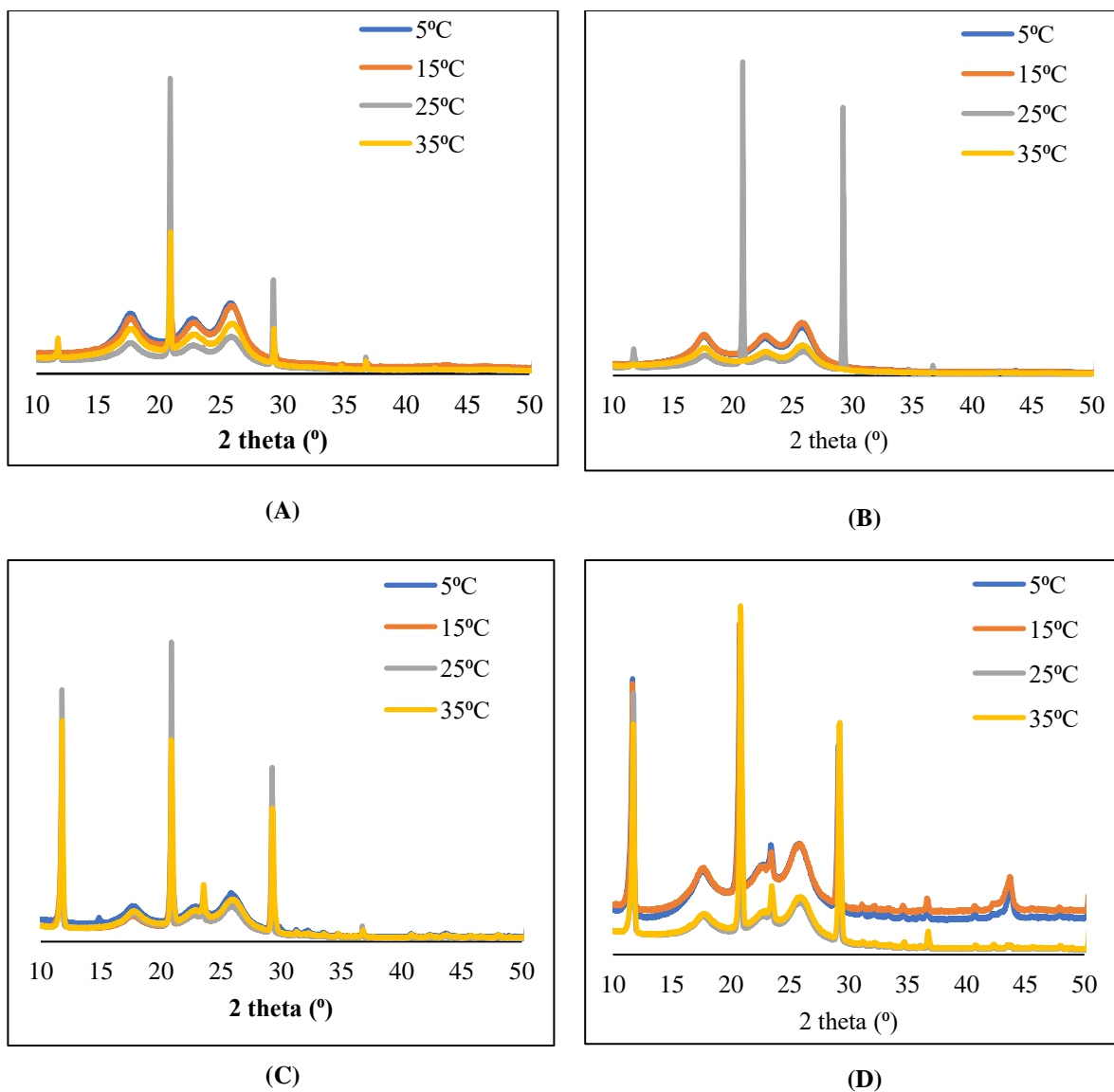


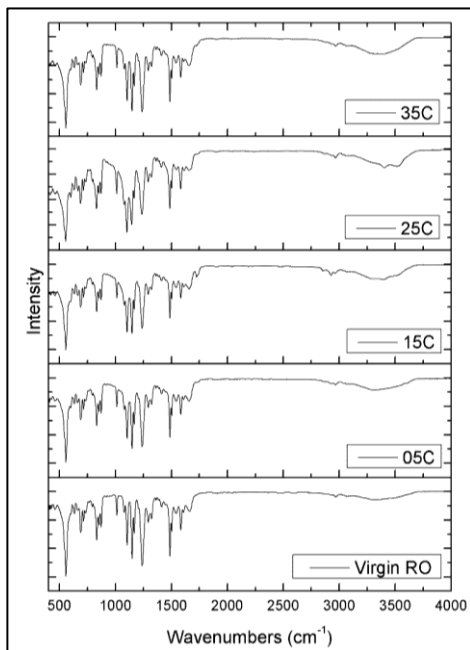
Figure 27. XRD spectra of  $\text{CaSO}_4$  precipitates at different temperatures; (A) RO membrane (Solution 1,  $\text{Ca}^{+2}=20$  mM); (B) GO - RO membrane (Solution 2,  $\text{Ca}^{+2}=20$  mM); (C) RO membrane (Solution 2,  $\text{Ca}^{+2}=50$  mM); (D) GO - RO membrane (Solution 2,  $\text{Ca}^{+2}=50$  mM) (Ashfaq et al., 2020a)

#### 4.2.2.5 Mechanism of interaction of gypsum with membrane.

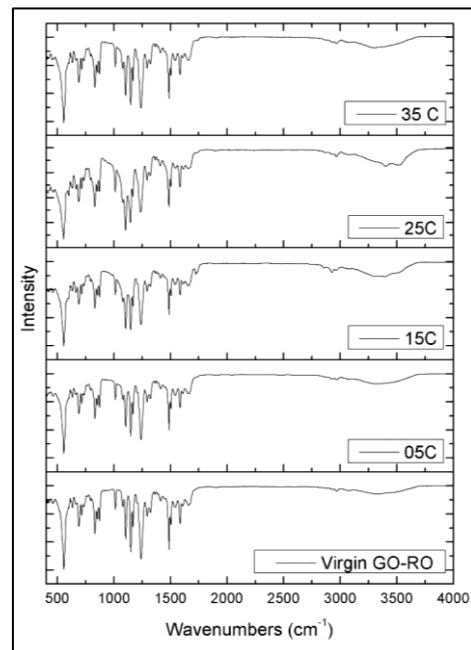
The FTIR spectra of the scales were used to identify the functional groups involved

in the interaction between gypsum and membrane surface. These spectra were compared with spectra of pure gypsum and pure membrane surface to investigate peak shifts and appearance of new peaks/disappearance of peaks. Figure 29 shows the FTIR spectra obtained for the scaled RO and GO-RO membranes. According to the literature (Bo, 2004; Al Dabbas et al., 2014), the water molecules in the gypsum appears at the peaks of 3580, 3430 and 1600  $\text{cm}^{-1}$ . The strong band centered around 1140  $\text{cm}^{-1}$  splitting into two components at around 1146, 1116  $\text{cm}^{-1}$  and 669, 662  $\text{cm}^{-1}$  represents stretching and bending modes of  $\text{SO}_4$ . However, the comparison between the gypsum scaled membrane, virgin membrane and spectra of pure gypsum showed that the peaks either shifted or disappeared completely (mainly in the case of virgin membrane) which can potentially reveal the involvement of functional groups in the adsorption of gypsum on the RO and GO-RO membranes as well as provide insights about the extent of gypsum scaling. The peaks around 3400 and 2970  $\text{cm}^{-1}$  in the spectra of membrane represents stretching vibration of carboxylic and C-H groups of the polyamide layer as well as other O-H groups of the coating layer (Tang et al., 2007). The interaction of water molecules and calcium from gypsum with these groups shifted the peaks from 3580 and 3430  $\text{cm}^{-1}$  (pure gypsum) to 3518 and 3400  $\text{cm}^{-1}$  (scaled membrane) (Table 14). Similar interaction of carboxylic and hydroxyl groups with gypsum as a result of surface crystallization has also been reported in forward osmosis through FTIR analysis, which was also confirmed through X-ray photoelectron spectroscopy (XPS) results (Xie and Gray, 2016). Furthermore, there were differences in the peaks showing  $\text{SO}_4$  vibrations (1146, 1116, 669, 602  $\text{cm}^{-1}$  in pure gypsum), when compared with gypsum scaled membrane as shown in the Table 14. These differences may have resulted from the interaction of  $\text{SO}_4$  group with the C-O bonds

present in the virgin membrane and appears at  $1150\text{ cm}^{-1}$ . The peaks at  $1663$ ,  $1609$ , and  $1541\text{ cm}^{-1}$  represent C=O stretching of amide I band and N-H in-plane bending and N-C stretching vibration of amide II bands of polyamide surface layer were present in virgin membrane but disappeared in scaled membrane (Figure 29c and 29d). Other peaks of polysulfone support layer of the membrane such as  $1587$ ,  $1541$ ,  $1504$ ,  $1488$ , and  $1055\text{ cm}^{-1}$  (Tang et al., 2009) also disappeared (Figure 29c and 29d); which can be attributed to the surface coverage and thickness of the scale layer as the infra-red radiations could not travel to the support layer despite having a penetration depth of  $300\text{ nm}$  at these wavenumbers. Nevertheless, the spectra obtained at lower feed water concentration ( $\text{Ca}^{+2} = 20\text{mM}$ , solution 1) (Figure 29a and 29b) did not show the disappearance of all the peaks in this region. This could be attributed to the less scaling resulted at these conditions and therefore, the membrane surface was not fully covered with the gypsum scales.



(a)



(b)

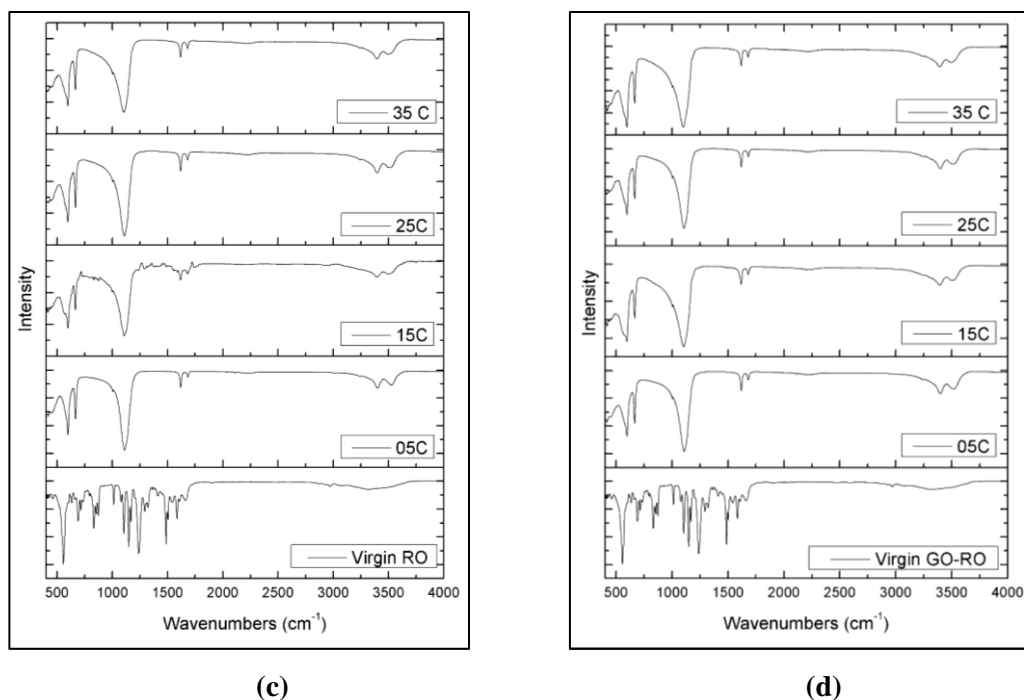


Figure 28. FTIR results of (a) RO membrane, (Solution 1,  $\text{Ca}^{+2}=20$  mM); (b) GO-RO membrane, (Solution 1,  $\text{Ca}^{+2}=20$  mM); (c) RO membrane, (Solution 2,  $\text{Ca}^{+2}=50$  mM); (d) GO-RO membrane, (Solution 2,  $\text{Ca}^{+2}=50$  mM) (Ashfaq et al., 2020a)

Table 14. Peak shifts through comparison between the pure gypsum and the gypsum scaled membrane (Ashfaq et al., 2020a)

Peak Assignments (Gypsum)	Pure Gypsum* ( $\text{cm}^{-1}$ )	Gypsum scaled RO ( $\text{cm}^{-1}$ )	Differences ( $\text{cm}^{-1}$ )
Stretching vibrations of water molecules	3580	3518	62
	3430	3400	30
	1146	1108	38
Stretching and bending modes of $\text{SO}_4$	1116	1108	8
	669	667	2
	602	595	7

\*(Bo, 2004 and Al Dabbas et al., 2014)

Hence, FTIR is a powerful tool to elucidate the functional groups involved in the process of adsorption (Figure 30), thereby helping in understanding the adsorption



mechanisms (Iqbal et al., 2009; Elsehly et al., 2018). As per the results of FTIR, the functional groups of the membrane surface such as OH<sup>-</sup>, COO<sup>-</sup> and NH<sub>2</sub> groups were found to be involved in gypsum scaling. This also shows that the membrane with high hydrophilicity and polar groups are more susceptible to gypsum scaling as compared to hydrophobic membranes with smaller number of functional groups.

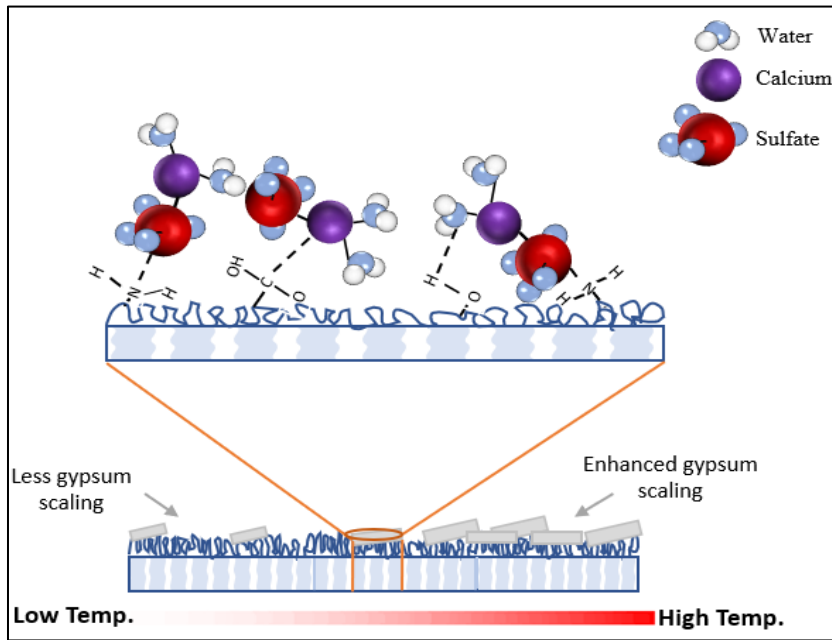


Figure 29. Interaction of membrane functional groups with gypsum and effect of temperature on scaling (Ashfaq et al., 2020a)

#### 4.2.2.5 Effect of scaling on membrane surface properties.

The hydrophilicity test of the scaled membrane was carried out to help in predicting its behavior during foulant-foulant interactions. The hydrophilicity is a property of the foulant which has profound effect on membrane fouling by altering membrane-foulant and foulant-foulant interactions and it has received extensive attention in membrane fouling

research (Mu et al., 2019). If the scaled membrane becomes more hydrophobic, it is expected that its interaction with the organic foulants will increase resulting in enhanced membrane fouling. Previous research has shown that the hydrophobicity of the dissolved organic matter caused the fouled membrane surface more hydrophobic which caused the severe decline in flux. Hence, the membrane fouled with more hydrophobic DOM had lowest permeate flux as compared to the membrane fouled with less hydrophobic (or hydrophilic) DOM (Mu et al., 2019) The interaction of calcium sulfate with organic fouling layer (i.e. sodium alginate, bovine serum albumin and humic acid) has already been investigated and it was noted that the humic acid and sodium alginate fouled membranes enhanced the surface crystallization of gypsum by acting as a nucleus for crystallization. It was concluded that the density of carboxylic groups play an important role in determining organic foulants' interaction with gypsum (Liu and Mi, 2014). The water contact angle of the fouled/scaled membrane depends upon the hydrophilicity of the virgin membrane, and of the foulant/scalant itself and the extent of scaling layer on the membrane (Mu et al., 2019). In this research, it was noted that the scaling increased the hydrophilicity of membranes. Therefore, at lower feed water conditions ( $\text{Ca}^{+2} = 20\text{mM}$ , solution 1), the water contact angle decreased with the increase in scaling caused by increase in temperature, demonstrating increase in hydrophilicity of the scaled membrane (Figure 31). Furthermore, at higher feed water conditions, since the scaling was intense as shown by the results of flux decline, SEM and FTIR results, the hydrophilicity increased to the extent that the water contact angle could not be measured in the experimental conditions. The water droplet (2  $\mu\text{L}$ ) dispersed immediately (within 3 seconds) after its release to the scaled membrane surface. Hence, it can be concluded that the gypsum scaling on the membrane increases the

hydrophilicity of the membrane enhancing its inter- and intra- foulant interactions. The effect of pure membrane hydrophilicity on gypsum scaling was investigated and it was found that hydrophilic membranes such as cellulose acetate and nylon with contact angle of  $50.0^\circ$  and  $44.9^\circ$ , respectively showed highest adhesion (or interaction,  $E_{in}$ ) energy to gypsum crystals ( $E_{in} = -586.68$  kJ/mol for cellulose acetate and  $-212.60$  kJ/mol for nylon). This is mainly because these polymers are polar molecules with various carboxylic, hydroxyl and other functional groups which can easily form hydrogen bonds with water molecules in gypsum crystals (Su et al., 2018). In this research, the total mass of crystals on the GO-RO membrane was not found to be significantly higher than that on RO membrane, however, previous research has shown that the adhesion of gypsum crystals to hydrophilic GO membrane was so strong that it was subsequently hard to detach them through ultrapure water cleaning (Cao et al., 2018). Therefore, higher wettability of the GO membrane resulted in higher surface energy which in turn increased the affinity to the gypsum crystals. That is why, several researchers tried to increase the hydrophobicity of the membrane and consequently, proved reduction in mineral scaling (Gryta, 2016; Song et al., 2007). Hence, the understanding of inter/intra foulant interactions in addition to the foulant-membrane interactions are very important to understand and predict the behavior of membrane fouling in both single and mixed foulant systems. Therefore, further research is on-going to investigate the intra-foulant interaction of calcium sulfate with microorganisms to demonstrate their effect on each other.

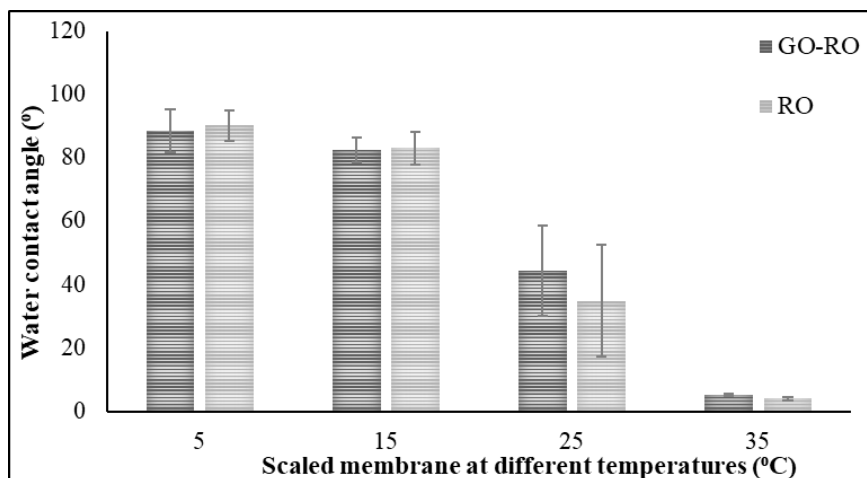


Figure 30. Effect of gypsum scaling at different temperatures on wettability ( $\text{Ca}^{+2} = 20\text{mM}$ , solution 1) (Ashfaq et al., 2020a)

#### 4.2.3 Conclusion

In this research, the effect of temperature on calcium sulfate scaling of RO and GO-RO membrane was investigated. The results of flux decline over time, mass of crystals and thickness of scaled layer showed that the increase in temperature enhances the activation energy for the precipitation reaction leading to severe membrane scaling and increase in membrane resistance. Between the temperatures of 5 – 35 °C, gypsum was the only polymorph formed on the membrane as confirmed by the XRD and SEM-EDX results. In addition, the morphology of the crystals also varied under the influence of temperature as the crystals structure changed from rod shape to rosette structures as the temperature was increased. The results of SEM and FTIR explained that surface crystallization of gypsum was the dominant mechanism in scaling. Overall, results did not show significant difference in terms of scaling intensity and crystals morphology between the two membranes used. The measurement of water contact angle of the scaled membranes

showed that the hydrophilicity increased with the increase in membrane scaling. This showed that the gypsum layer on the membrane will have enhanced inter/intra foulant interactions with other hydrophilic substances in combined foulant systems. The results of this research show that in harsh cold climate areas of the World such as Canada, China and USA, the intensity of membrane scaling will be less as the feed water temperature stays low. Whereas, in warm areas of the World such as Qatar and other Arabian countries, the membrane scaling will be more intense as the feed water temperature is often high. Therefore, there is a need to consider the temperature of feed water entering into the RO system while deciding the antiscaling measures and antiscalant dosages.

CHAPTER 5 – OBJECTIVE 02: DEMONSTRATE AND DETERMINE  
BIODEGRADATION OF POLYMER ANTISCALANTS USED IN REVERSE  
OSMOSIS SYSTEMS<sup>8</sup>

*5.1 Isolation, Identification and Differentiation of antiscalant degrading bacteria*<sup>9</sup>

*5.1.1 Introduction*

As per the recent estimates of WHO (WHO UNICEF Joint monitoring program, 2017), one in every 10 individuals do not have access to clean drinking water. With the rise in worlds' population, this number is expected to increase further. For arid countries like Qatar and other Middle Eastern countries there is a severe shortage of renewable water resources such as groundwater and consequently, the countries are increasingly relying on seawater desalination to fulfil rising demands. Due to the population and economic growth in Qatar, there is rapid expansion in the desalination industry through increased construction of desalination plants. Although, Middle Eastern countries have been historically relying extensively on the thermal desalination technology (Darwish et al., 2013). Nevertheless, seawater reverse osmosis (SWRO) has been catching attention recently owing to its lesser environmental footprint and economic viability. The major hurdle for the widespread use of reverse osmosis (RO) technology is the membrane scaling and biofouling. In RO operations, typical mineral scales are calcium carbonate, calcium

---

<sup>8</sup> The contents of this chapter have already been published.

<sup>9</sup> This content has been published. Reference: Ashfaq, M. Y., Al-ghouti, M.A., Qiblawey, H., Rodrigues, D.F., Hu, Y., Zouari, N. 2019a. Isolation, identification and biodiversity of antiscalant degrading seawater bacteria using MALDI-TOF-MS and multivariate analysis. *Sci. Total Environ.* 656, 910–920.

sulfate, silicate, and barium sulfate (Al-Shammiri et al., 2000; Lee et al., 2013; Li et al., 2007; Shih et al., 2006). Antiscalants such as organic polymers and phosphonates are generally used to reduce mineral scaling (Shih et al., 2006). Phosphonates-based antiscalants can hydrolyze to orthophosphates and result in insoluble calcium orthophosphate precipitation in membrane systems (Antony et al., 2011). Polymer-based antiscalants like poly maleic acid (PMA) and poly acrylic acids (PAA) are commercially being used in membrane systems.

These antiscalants have been performing satisfactorily against membrane scaling (Shih et al., 2006). They have played significant role in maintaining the efficiency of RO plants with maximum recovery rates, reducing the consumption of harmful substances, decreasing the consumption of energy and reducing the frequency of plant shutdown for cleaning (Greenlee et al., 2009; Darton, 2000). Nevertheless, the biodegradability of these antiscalants is rarely reported. The presence of microorganisms in feed water with ability to biodegrade antiscalants or use them as a source of energy will not only reduce the antiscalants' efficiency to combat membrane scaling but it will also become a source of enhanced biofouling due to microbial growth. Previous works have shown that the bacterial attachment and subsequent biofouling by model microorganisms (*Pseudomonas fluorescens*) has increased due to the addition of various poly acrylate and poly phosphate based antiscalants (Sweity et al., 2015, Sweity et al., 2013). Nevertheless, the information related to biodiversity of microorganisms in seawater capable of biodegrading these antiscalant monomers and polymers is not yet reported. The seawater of Arabian Gulf is relatively polluted due to rapid industrialization and oil spills in the past and the microbial population in seawater is adapted to survive in such harsh environment. The presence of

antiscalant biodegrading microorganisms in the seawater will therefore raise the concern on the efficiency of these antiscalants to inhibit membrane scaling and the performance of SWRO in the region.

Dereplication is a process of grouping identical strains together at a certain taxonomic level (Popovic et al., 2017; Ghyselinck et al., 2011). Since, isolation of large number of strains using different growth media and their identification using conventional microbiological and molecular techniques is a time-consuming and complicated process. Therefore, categorization of environmental strains from unknown sources is now important to obtain information about biodiversity and to reduce the need to adopt other procedures. Nowadays, Matrix assisted laser desorption ionization – time of flight mass spectrometry (MALDI-TOF MS) is being used for dereplication of isolates using protein spectra of the strains. The protein profiles are differentiated mostly using algorithms that are based on the absence/presence of peaks or the peak intensities (Spitaels et al., 2016). The technique has been used for differentiation of strains from marine (Dieckmann et al., 2005) and hypersaline (Munoz et al., 2011) environments. Dereplication of isolates also helps to group microorganisms based on their specific characteristics like resistance/sensitivity or sources like clinical and environmental and therefore, reduces the workload for screening larger number of isolates. MALDI-TOF MS technique is relatively rapid and cost effective as compared to its counterparts such as 16s rRNA technique (Almuzara et al., 2015; Caretto et al., 2013; Jamal et al., 2013). However, its application in environmental microbiology is still limited. Many investigators have attempted to compare the efficiency, reliability and accuracy of MALDI-TOF MS with other conventional microbiological techniques (Almuzara et al., 2015; Caretto et al., 2013; Jamal et al., 2013; Fang et al., 2012; Meex et



al., 2012; Zangenah et al., 2012). Recently, the technique is gaining attention of researchers and is being recommended for environmental samples over molecular techniques (Koubek et al., 2012). Using MALDI-TOF MS, various bacterial strains such as *V. furnissii* and *V. fluvalis* (Schirmeister et al., 2014) and 30 closely related *Vibrio* isolates (Eddabra et al., 2012) have been differentiated for wide variety of applications. Similarly, Telesmanich et al., (2014) performed interspecific differentiation of *Vibrio* strains isolated from ballast waters, which helped them to detect both pathogenic and non-pathogenic bacterial strains. Otherwise, the use of conventional molecular techniques would have been much more labor intensive and time consuming.

Principle component analysis (PCA) is a type of multivariate analysis that helps to reduce redundancy in the data set (Kehrmann et al., 2016). It gives rise to new coordinates by linear combination of the actual ones i.e.  $m/z$  in the case of MALDI-TOF-MS, which represents principal components (PCs). These newly produced PCs are numbered as per the amount of variability they explain in the original data set. Mostly, first 2 or 3 PCs are used to analyze the data variability. Although, PCA has been widely used for its applications in various fields (Li et al., 2018; Kamijo et al., 2017; Kasban et al., 2016); its application in combination with MALDI-TOF-MS is limited. Kehrmann et al., (2016) combined PCA with MALDI-TOF-MS proteins spectral data to discriminate *Mycobacterium abscessus* subspecies for clinical significance. It was concluded that the PCA is a robust and easy method for microbial subspecies level differentiation.

Thus, the aim of this research was to investigate the biodiversity of microorganisms in Qatar's seawater with the ability to biodegrade organic antiscalants used in membrane systems. MALDI-TOF MS technique was combined with PCA to demonstrate the

biodiversity of isolated antiscalant degrading bacteria. The objectives of this research include (1) isolation and identification of antiscalant degrading bacteria using MALDI-TOF MS; (2) investigating the biodiversity of antiscalant degrading bacteria through combining MALDI-TOF MS with PCA; (3) estimation of specific growth rates of selected strains in antiscalants containing medium. The antiscalants selected for this research include monomers and polymers of acrylic and maleic acids. The results of this research will help to understand the outcome and fate of using these polymer antiscalants in SWRO. To the best of our knowledge, this study is first of its kind to demonstrate the interaction of antiscalants used in SWRO with seawater microorganisms using multidisciplinary approach.

### *5.1.2 Results and Discussion*

#### *5.1.2.1 Screening of isolated bacteria for monomer antiscalant degradation*

Seawater samples from both offshore (QOFSW) and onshore (QONSW) were used to isolate the endogenous bacteria from Qatar's seawater and study their potential to biodegrade antiscalant monomers. Seven samples from different locations across Qatar's marine environment were collected to isolate and test a wide variety of bacteria for this purpose. The evaluation of monomers' biodegradation was based on the estimation of colony size formed by each isolate by using them as carbon and energy source in comparison to the growth in glucose containing medium. It was noted that all strains were able to grow in maleic acid medium after 5 days of incubation. In general, all strains showed heavy growth in glucose medium (after 48 hours), moderate in maleic acid medium

(after 5 days), and there was no growth noted in acrylic acid medium even after 7 days of incubation. This showed that the two antiscalant monomers requires different biodegradation pathways and most of the bacteria lack the necessary catabolic pathways to use acrylic acid as a carbon and energy source in solid media.

#### 5.1.2.2 Identification of Antiscalant degrading bacteria using MALDI – TOF MS

MALDI – TOF MS technique was used to identify seawater microorganisms. The technique is being used frequently to identify clinical isolates (Fang et al., 2012; Meex et al., 2012; Zangenah et al., 2012; Caretto et al., 2013; Jamal et al., 2013; Almuzara et al., 2015), but it is not yet widely used to study aquatic microorganisms. Emami et al., (2012) used this technique to identify *Vibrio species*, *P. aeruginosa*, *Enterococci species* and coliforms in ballast waters. Hence, diversity of bacteria isolated from Qatari seawater, identified using MALDI – TOF MS include *H. aquamarina*, *H. elongata*, *P. fragi*, *V. alginolyticus*, and *V. fluvalis* (Table 15). The score between 2.3-3.00 shows highly probable species level identification and between 2.0 – 2.29 represents genus level identification and probable species level of identification. A score between 1.7 – 1.99 indicates probable genus level identification. As shown in Table 15, only 5 out of 20 strains had scores in the lower (1.7 – 1.99) range which means that 75% of the strains were identified up to species level.

*Halomonas* species belonging to the family of proteobacteria, have been reported to be less frequent in Gulf waters (Sorkhoh et al., 2010). However, it was noted that the species of *Halomonas* were found in most of the offshore and onshore samples tested in this research. *Halomonas* bacteria are of ecologically importance due to their oil degrading

capabilities (Sorkhoh et al., 2010), biomineralization potential through ureolytic activity (Arias et al., 2017), EPS production and surface adhesion (Rodriguez-Calvo et al., 2017), biofouling potential and biofilm formation (Zhang et al., 2011; Ivnitsky et al., 2010; Bereschenko et al., 2010). These bacteria have also been studied to test the antibiofouling potential of different nanomaterials and polymers (Sathya et al., 2016; Inbakandan et al., 2013). Thus, the occurrence of *Halomonas* species in Qatar’s seawater should have significant ecological significance as they can potentially cause biofouling in RO membranes in desalination industry.

*Pseudomonas fragi*; another bacteria obtained frequently from different seawater samples, is a psychrophilic Gram-negative Bacillus commonly found in temperate waters (Wang et al., 2017). Their ecological importance includes their ability to produce biofilm (Wirtanen, and Mattila-Sandholm, 1994) and food spoilage especially meat, fishes and other marine organisms (Ercolini et al., 2007; Tryfinopoulou et al., 2002). Moreover, the complete genome sequence of *P. fragi* has shown their ability to biodegrade toxic compounds (Yanzhen et al., 2016). Therefore, showing the occurrence of *P. fragi* in Qatar’s seawater is important and relevant to the objectives of this research.

Table 15. Identification of isolated strains from Seawater samples using MALDI-TOF-MS (Ashfaq et al., 2019a)

#	Station #	Isolate code	Identification	Score
1	QONSW-1	QONSW-1 (#1)	<i>Halomonas elongata</i>	1.854
		QONSW-1 (#2)	<i>Halomonas aquamarina</i>	1.78
		QONSW-1 (#3)	<i>Pseudomonas fragi</i>	1.93
2	QONSW-2	QONSW-2 (#1)	<i>Halomonas aquamarina</i>	2.07

#	Station #	Isolate code	Identification	Score
3	QOFSW-1	QOFSW-1 (#1)	<i>Halomonas aquamarina</i>	2.08
		QOFSW-1 (#2)	<i>Halomonas aquamarina</i>	2.04
		QOFSW-1 (#3)	<i>Pseudomonas fragi</i>	2.4
		QOFSW-1 (#4)	<i>Vibrio fluvalis</i>	1.75
4	QOFSW-2	QOFSW-2 (#1)	<i>Vibrio alginolyticus</i>	2.04
		QOFSW-2 (#2)	<i>Pseudomonas fragi</i>	2.39
		QOFSW-2 (#3)	<i>Pseudomonas stutzeri</i>	2.47
		QOFSW-2 (#4)	<i>Halomonas aquamarina</i>	2.07
		QOFSW-2 (#5)	<i>Halomonas aquamarina</i>	2.02
5	QOFSW-3	QOFSW-3 (#1)	<i>Halomonas aquamarina</i>	1.96
		QOFSW-3 (#2)	<i>Pseudomonas fragi</i>	2.36
		QOFSW-3 (#3)	<i>Pseudomonas fragi</i>	2.34
6	QOFSW-4	QOFSW-4 (#1)	<i>Halomonas aquamarina</i>	2.01
		QOFSW-4 (#2)	<i>Pseudomonas fragi</i>	2.33
7	QOFSW-5	QOFSW-5 (#1)	<i>Pseudomonas fragi</i>	2.32
		QOFSW-5 (#2)	<i>Halomonas aquamarina</i>	2.04

#### 5.1.2.2 Differentiation of Isolated Bacterial community using MALDI – TOF MS and PCA

The protein profiles were established for all the isolates using MALDI-TOF MS for their subtyping. Even though, this technique is widely used for identification of bacteria at species and genus level, its potential for subtyping microorganisms was also proved (Rizzardi et al., 2013; Emami et al., 2012). The subtyping of strains is quite difficult since the strains are usually quite similar in terms of both phenotype and genotype. However, subtyping of strains like *Vibrio alginolyticus*, *Pseudomonas sp.* and *Enterococcus faecalis* (Emami et al., 2012); Methicillin-resistant *Staphylococcus aureus* lineages (Wolters et al., 2011), *Salmonella enterica* (Dieckmann and Malorny, 2011), *Yersinia enterocolitica* (Rizzardi et al., 2013) and *Streptococcus agalactiae* (Lartigue et al., 2009) have been done

using MALDI-TOF MS.

The strain differentiation is generally carried out based on the absence and presence of protein peaks at specific mass to charge ratio. The mass signals obtained between 2000 to 20,000 m/z are used to produce profile spectra, which comprises series of peaks that are conserved at genus, species and even subspecies levels (Barbuddhe et al., 2008). In this work, PCA was used to process MALDI-TOF-MS protein spectral data. Previously, Kehrmann et al., (2016) used combination of MALDI-TOF-MS and PCA to characterize the *Mycobacterium* species i.e. *M. abscessus*, *M. bolletii* and *M. massillense*. However, its utilization in literature is rarely reported. Hence, the results of PCA for the differentiation of *H. aquamarina* and *P. fragi* strains isolated from several locations in Qatar's seawater are presented in Figure 32A. It is evident from Figure 32A that the isolated strains possessed wide biodiversity at proteins level. The three principle components i.e. PC-1 (35%), PC-2 (27%) and PC-3 (16%) together showed 78% of the variance in the data. Using PCA, *H. aquamarina* strains can be distinguished into four categories. One major group encircled (in Figure 32A) contains several closely related strains i.e. B2 (QOFSW-1 (#1)), C1 (QOFSW-2 (#4)), C2 (QOFSW-2 (#5)), D1 (QOFSW-4 (#1)), D2 (QOFSW-5 (#2)). All strains belonging to this group were positively correlated to both PC1 and PC2 representing 35 and 27% variance in the data, respectively. While all strains in this group were negatively correlated to PC3 (representing 16% of the variance). The case of D1 (QOFSW-4 (#1)) is exceptional as it is situated on the boundary line (towards y negative axis) and thus is slightly negatively correlated to PC-2. Another group comprising B1 (QONSW-2 (#1)) and B3 (QOFSW-1 (#2)) were found to be negatively correlated to PC-1 and PC-3, but positively correlated to PC-2. The two uncategorized strains were A

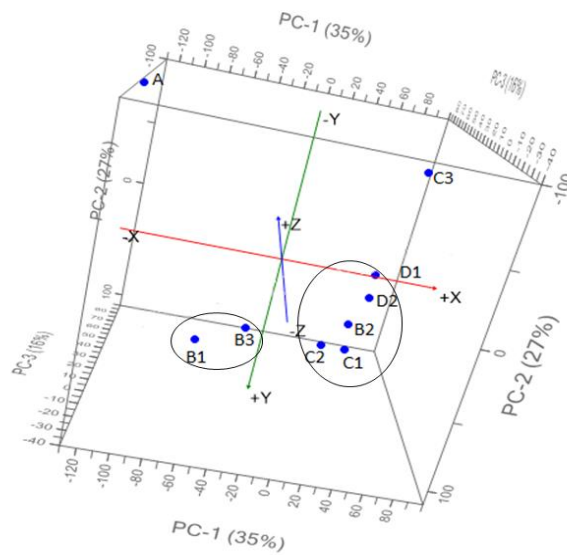
(QONSW-1 (#2)) and C3 (QOFSW-3 (#1)). As shown in Figure 32A, the strain A was highly negatively correlated to both PC-1 and PC-2 and highly positively correlated to PC-3. On the other hand, the strain C3 was highly positively correlated to PC-1 and PC-3 but highly negatively correlated to PC-2.

The isolated strains of *P. fragi* were found to be widely diverse and therefore, not many categories were obtained through PCA. The first three principle components together represent only 57% of the variance in the data, which shows that the isolated strains are widely different from each other at protein level. The strains D1 and D2 isolated from the same location i.e. QOFSW-3 (QOFSW-3 (#2), QOFSW-3 (#3) respectively) were found to be positively correlated to all the three components and thus can be categorized together. On the other hand, the strains E (QOFSW-5 (#1)) and F (QOFSW-4 (#2)) isolated from two different offshore sampling locations were found to be negatively correlated to all the three components and thus can be grouped together. Other strains A (QONSW-1 (#3)), B (QOFSW-1 (#3) and C (QOFSW-2 (#2)) can be easily differentiated from each other and from the two groups as shown in Figure 32B. Thus, it can be concluded that PCA is a useful method for differentiation of environmental bacterial isolates using MALDI-TOF MS spectral information.

Ghyselinck et al., (2011) compared MALDI-TOF MS with repetitive element sequence-based Polymerase Chain Reaction (rep-PCR) for differentiation of bacterial strains. It was noted that MALDI-TOF MS is more promising in terms of cost and time efficiency and high throughput analysis. In addition, the technique can differentiate till strains level and therefore, it is useful for differentiation of strains. PCA has also been applied to construct dendrograms through MALDI-TOF MS, which was able to

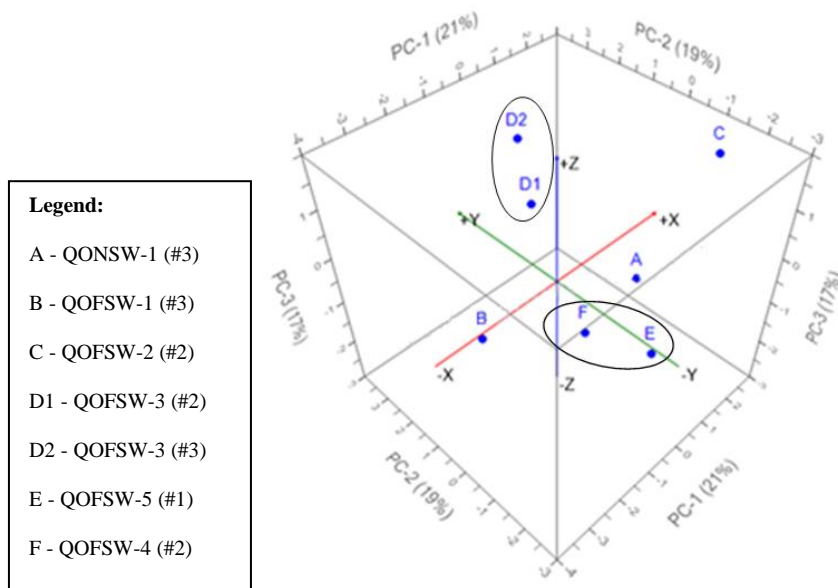
discriminate several *Vibrio parahaemolyticus* strains (Malainine et al., 2013). The combination of MALDI-TOF MS with PCA is a powerful tool for rapid categorization of strains. Niyompanich et al., 2014 classified strains of *Burkholderia pseudomallei* based on clinical and environmental sources. It remains unknown that if this tool can differentiate strains based on their environmental/ecological significance such as pollutant degrading strains and non-degrading strains. If it is achievable, then larger number of bacterial isolates can be easily screened for their potential to exhibit certain activity, which is of ecological, environmental, or biotechnological significance.

Legend:	
A	- QONSW-1 (#2)
B1	- QONSW-2 (#1)
B2	- QOFSW-1 (#1)
B3	- QOFSW-1 (#2)
C1	- QOFSW-2 (#4)
C2	- QOFSW-2 (#5)
C3	- QOFSW-3 (#1)
D1	- QOFSW-4 (#1)
D2	- QOFSW-5 (#2)



(A)





(B)

Figure 31. Differentiation of isolated strains using PCA (A) *H. aquamarina*; (B) *P. fragi* (Ashfaq et al., 2019a).

Using PCA, biplot showing both the scores (strains) and loadings (m/z values) can be used to obtain information about the m/z of proteins playing significant role in strains differentiation. As evident from the Figure 33A, protein peak at m/z 5120 had higher intensities for all the isolated strains, except strain A (QONSW-1 (#2)), in which it was found to be completely missing. That is why, it is located far from strain A (QONSW-1 (#2)) in Figure 33A. On the other hand, the protein peak at m/z 7345 was present at highest intensity in strain A (QONSW-1 (#2)) but was absent from strain B1 (QONSW-2 (#1)). Similarly, protein peaks at m/z 6055 (situated closely to strain C3) and 7350 (situated closely to strain B1) were only present in these respective strains and were absent from all other strains. Thus, biplot helps to obtain information about the presence and absence of

different protein peaks among strains. Furthermore, protein peaks at  $m/z$  3025, 3140, 3680, 4470, 4710, 4830, 5145, 6285, 6300, 8715, 8940, and 10185 were found to be present in all the strains and thus can be used as possible biomarkers. The peaks that are differentiating among the strains are labelled, while, the peaks that can be possibly used as biomarkers are labelled as well as highlighted in Figure 33 (A and B).

In the case of *P. fragi*, biplot (Figure 33B) shows that the protein profiles of strains were highly variable from each other and it is difficult to obtain information about the presence and absence of the protein peaks using only two components (PC-1 and PC-2). The protein peak at  $m/z$  5065 was present in all strains at higher intensities. The protein peak at  $m/z$  4430 was present in all strains at the relative intensity of more than 50, except in strain A (QONSW-1 (#3)) in which it was shifted to  $m/z$  4440. Such a protein shift slightly affecting the  $m/z$  value of protein could be due to the replacement of one or few amino acids in this strain. Similarly, a shift of protein peak was also noted at  $m/z$  of 5090 where the peak was present at a relative intensity in between 20-35 for all strains, except strain A (QONSW-1 (#3)). This peak was shifted to 5095 at a relative intensity of 23.26 in strain A (QONSW-1 (#3)). The peaks at  $m/z$  2530, 3020, 3295, 3590, 3615, 3800, 4125, 4400, 4420, 5065, 5670, and 11340 were present in all strains. Figure 34A shows the MALDI spectra obtained for *P. fragi* strains with enhanced views (Figure 34B, 34C and 34D) showing some differences in peaks among the strains.

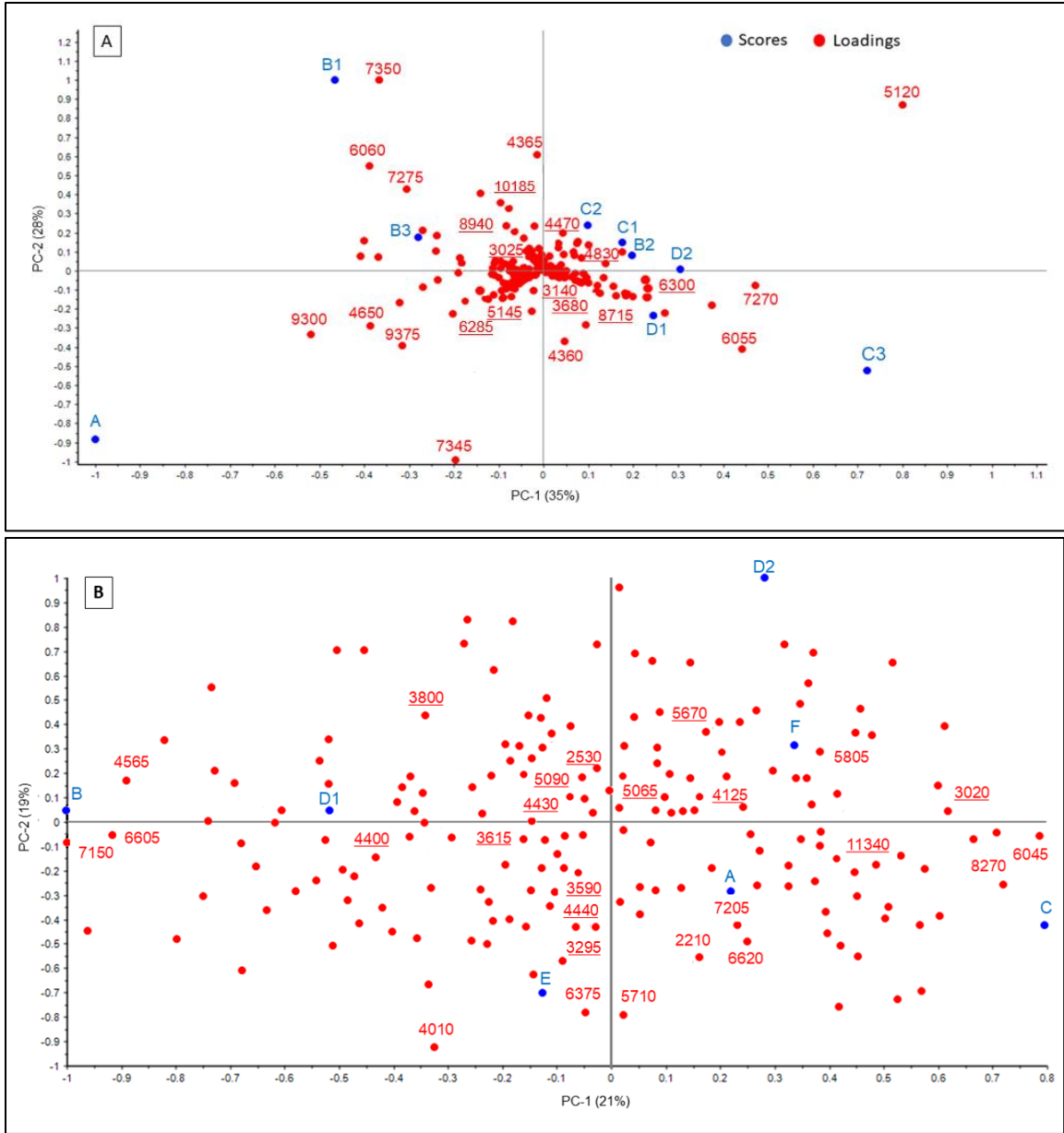


Figure 32. Biplot showing m/z loading values for (A) *H. aquamarina* and (B) *P. fragi* strains. The peaks of interest i.e. differentiating peaks are labelled and possible biomarkers are labelled and underlined (Ashfaq et al., 2019a). [A: A - QONSW-1 (#2), B1 - QONSW-2 (#1), B2 - QOFSW-1 (#1), B3 - QOFSW-1 (#2), C1 - QOFSW-2 (#4), C2 - QOFSW-2 (#5), C3 - QOFSW-3 (#1), D1 - QOFSW-4 (#1), D2 - QOFSW-5 (#2) and B: A - QONSW-1 (#3), B - QOFSW-1 (#3), C - QOFSW-2 (#2), D1 - QOFSW-3 (#2), D2 - QOFSW-3 (#3), E - QOFSW-5 (#1), F - QOFSW-4 (#2)].

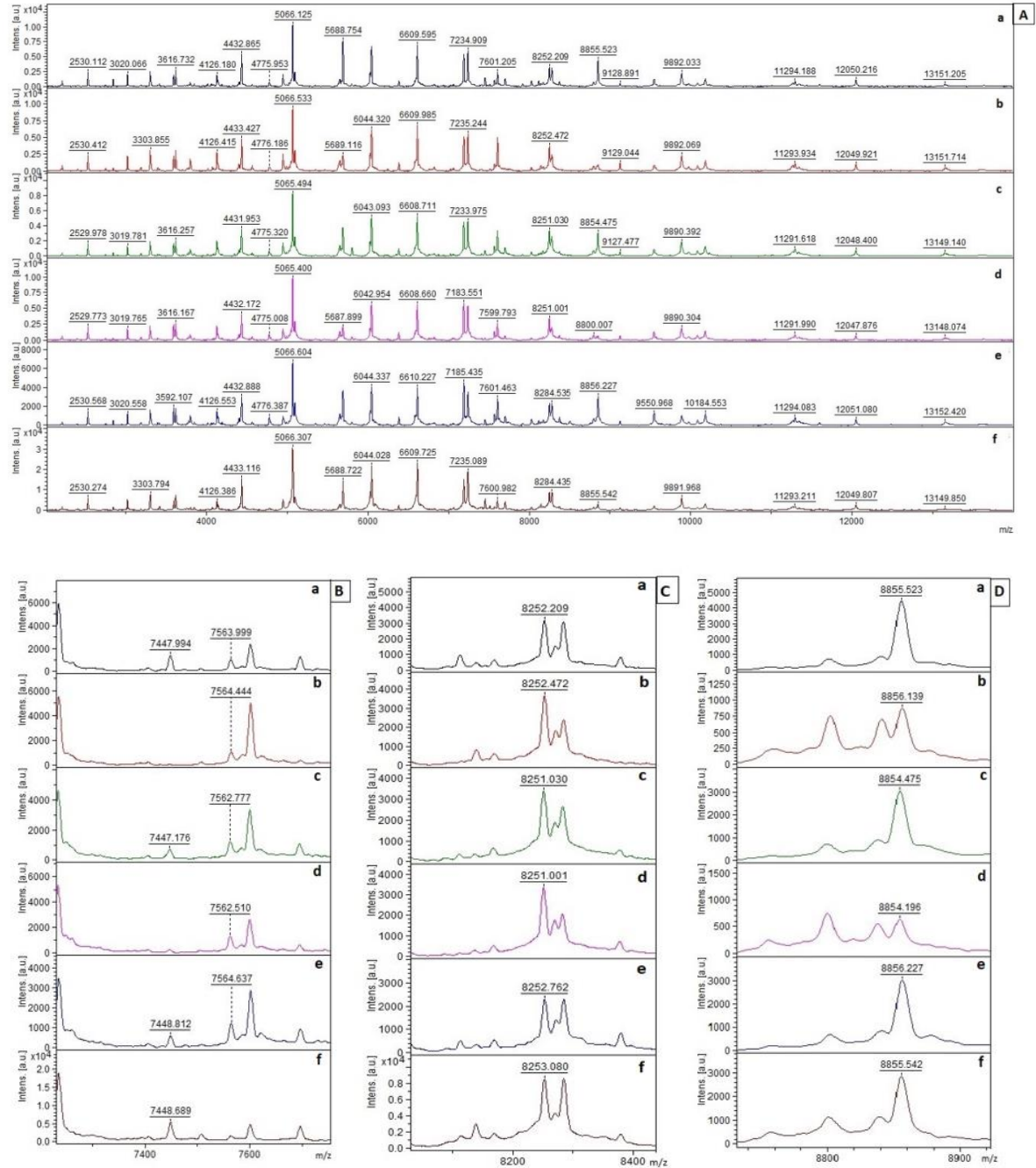


Figure 33. Mass spectra obtained for *P. fragi* strains (A) Main spectra (2000 – 13000 m/z); Magnified regions (B) 7400 – 7700 m/z (C) 8100 – 8400 m/z (D) 8700 – 8900 m/z, showing the differences of mass spectra among the strains (Ashfaq et al., 2019a). [a – QOFSW-1 (#3), b – QOFSW-2 (#2), c – QOFSW-3 (#2), d – QOFSW-3 (#3), e – QOFSW-5 (#1), f – QOFSW-4 (#2)].

### 5.1.2.3 Growth kinetics of Antiscalant degrading bacteria

Initial screening for antiscalant degrading bacteria showed that the strains were able to grow in antiscalant containing media, especially in maleic acid media. The specific growth rates of antiscalant degrading bacteria were then investigated. It was noted that the growth rates vary for each antiscalant as well as with the bacterial strain used. As expected, the specific growth rates in glucose medium, used as positive control, were the highest as compared to antiscalant based media. The average specific growth rates of bacteria in glucose media were  $1.467 \pm 0.79$  (*H. aquamarina*),  $1.02 \pm 0.79$  (*H. elongata*),  $1.03 \pm 0.21$  (*P. fragi*),  $0.84 \pm 0.04$  (*P. stutzeri*),  $0.63 \pm 0.03$  (*V. alginolyticus*), and  $0.75 \pm 0.36$  (*V. fluvalis*). The average specific growth rates for each type of isolated bacteria in antiscalants media are depicted in Figure 35A. By comparison, it is obviously clear that *H. aquamarina* strains isolated across various locations are characterized with the highest growth rates in antiscalant media as compared to other strains. It was also noted that the isolated strains were able to grow faster in poly maleic and poly acrylic acids as compared to their respective monomers.

The process of microbial biodegradation occurs through different enzymatic activities and cleavage of bonds. Accordingly, the biodegradation of polymers occurs through the sequence of energy generating steps. It starts with breaking the bonds in polymer (biodeterioration and bio-fragmentation or digestion), obtaining energy and producing oligomers, dimers and monomers. All these macromolecules are then again used as carbon/energy source (assimilation and mineralization) for further microbial growth (Pathak and Navneet, 2017 and Lucas et al. 2008). Due to the stepwise degradation and assimilation of the polymer, the concentration of monomers remains below certain limit,

which reduces the chance of toxicity/growth inhibition induced by high substrate concentration. Moreover, it is also possible that relatively higher concentration of monomers in the medium could induce the phenomenon of carbon catabolite repression (Cecilia et al. 2019), affecting microbial growth. Further research is therefore needed to obtain information about the biodegradation pathways, the intermediate and end products of biodegradation and factors affecting the microbial growth rates and biodegradation rates. On the other hand, the difference of growth rates between poly acrylic and poly maleic acid media can be attributed to their different molecular structures. Thus, maleic acid was found to be easily assimilable carbon and energy source as compared to acrylic acid. Moreover, previous research of Larson et al. (1997) showed that the mixed microbial community from activated sludge was able to use acrylic acid as a carbon and energy source. Hence, the obtained results clearly show that the organic chemicals used to prevent scaling differ greatly in their ability to promote growth of microorganisms. Since, these organic antiscalants were found to be biodegradable by seawater microorganisms; their potential to promote biofouling in SWRO is highly expected. These observations conform with previous observations about potentialities of antiscalants to promote microbial growth and biofouling (Vrouwenvelder et al., 2000; Sweity et al., 2015, 2013).

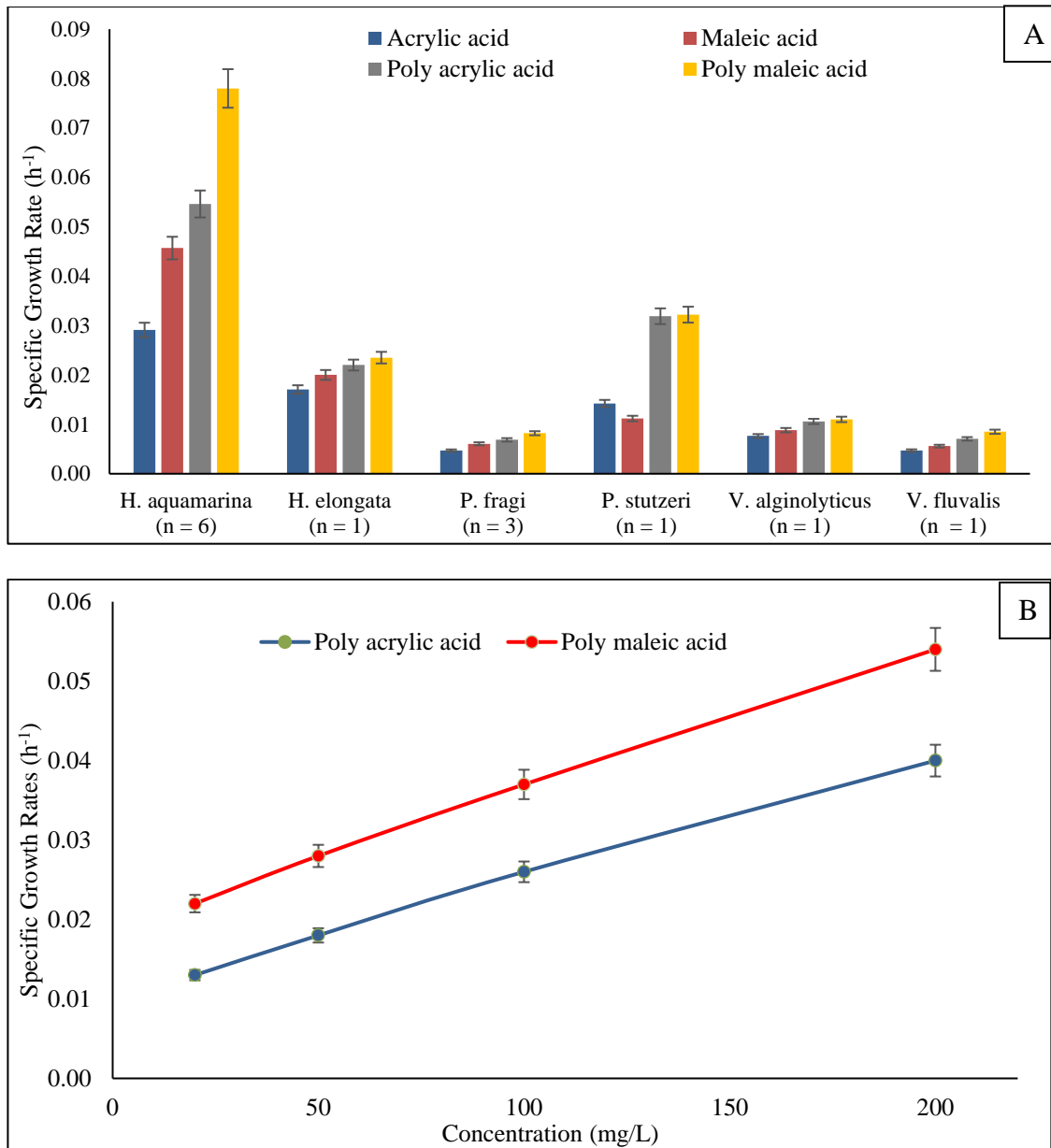


Figure 34. (A) Comparison of specific growth rates of isolated seawater bacteria in different antiscalant containing medium (B) Specific growth rates of *H. aquamarina* (QOFSW-4 (#1)) at different concentrations of poly acrylic acid and poly maleic acid (Ashfaq et al., 2019a).

The antiscalants are generally used at low concentration of 2-4 mg/L in RO systems

(Sweity et al., 2015). Depending upon the extent of concentration polarization, the concentration at the membrane surface will rise further. Therefore, dose-effect relationship of poly acrylic and poly maleic acid was also studied at 20, 50, 100, 200 mg/L. Figure 35B shows that the increase in concentration resulted in linear increase in microbial growth and there was no growth inhibition or toxicity effect of antiscalant within the dose range tested. Thus, it is expected that as the intensity of concentration polarization rises in RO systems; the concentration of antiscalants near the membrane surface will increase which will result in higher bacterial growth near/on the membrane surface.

In the work of Vrouwenvelder et al, (2000), there were two different types of growth tests adopted to investigate the growth promoting properties of antiscalants. These tests include the assessment of assimilable organic carbon (AOC) and biomass production potential (BPP). The researchers successfully evaluated several antiscalants for their potential to cause biofouling and proposed the classification based on their AOC and BPP values. However, it was also concluded that these tests are complicated to assess the biofouling potential of antiscalants. On the other hand, the growth tests performed in this research relied on ensuring the antiscalants as the only source of carbon, which helped to investigate directly the growth promoting properties of antiscalants.

The biofouling results in series of steps, which include (1) formation of conditioning film, (2) bacterial adhesion, (3) feeding of microorganisms on available nutrients and organic compounds in feed water, which subsequently leads to biofilm formation and growth. Thus, formation of conditioning film and source of energy (nutrients/carbon sources) are major pre-requisites for membrane biofouling. Previous researches have shown that the addition of antiscalants enhance biofouling through



increased organic fouling (Sweity et al., 2014; Surrat et al., 2000), which can also act as a conditioning layer for biofouling (step 1) and through altering membrane surface characteristics i.e. hydrophobicity (Sweity et al., 2013, 2015), which subsequently enhances bacterial attachment (step 2). Furthermore, it has also been demonstrated that the poly phosphates-based antiscalants can become a source of phosphorus for bacterial growth (step 3). It can also be concluded from this research and from the work of Vrouwenvelder et al., (2000, 2010), that the antiscalants can also be used as a source of energy and carbon by microorganisms subsequently promoting the biofouling and there is variety of such bacteria present in seawater. Thus, the effect of antiscalants on membrane fouling is explained in Figure 36. In the absence of microorganisms, **(1)** antiscalants will effectively reduce membrane scaling by delaying the nucleation time of salts or by distorting the crystals shape and making them soft and non-adherent. Furthermore, sometimes antiscalants adsorb on the crystals and impart anionic charge, which keep them separated from each other and from the membrane surface. Nevertheless, **(2)** the microorganisms present in feed water will biodegrade these antiscalants and use them as an energy/carbon source, which will ultimately **(3)** neutralize the effect of antiscalants causing both membrane scaling and biofouling. The membrane fouling will result in reduced water flux, decreased percentage rejection, higher energy requirements due to increased transmembrane pressure. To recover membrane performance; frequent cleaning would be needed which will lead to reduction in operational period and increase in cost of RO desalination plant. Therefore, it is now important to develop certain screening methods to investigate the potential of organic antiscalants to cause membrane biofouling before their application at the industrial level. Furthermore, inorganic polymers/nanomaterials need to

be prepared to modify RO membranes that are resistant to microbial biodegradation and can help to reduce both membrane scaling and biofouling.

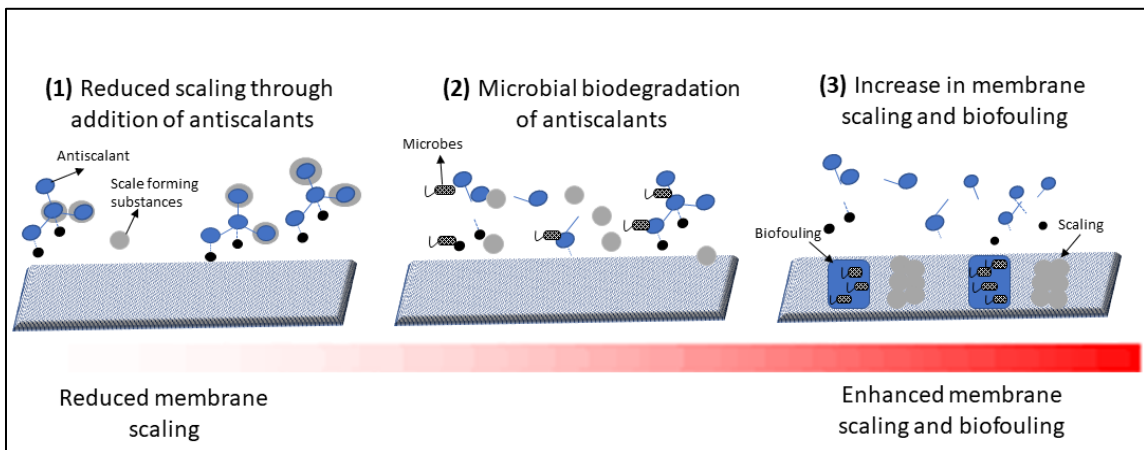


Figure 35. Schematic diagram depicting the effect of antiscalant biodegradation on membrane scaling and biofouling (Ashfaq et al., 2019a)

### 5.1.3 Conclusion

In this research, it was found that the microorganisms isolated from Qatar seawater has the ability to use antiscalants as a carbon and energy source for their growth. The isolated microorganisms were identified as *H. aquamarina*, *H. elongata*, *P. fragi*, *P. stutzeri*, *V. alginolyticus* and *V. fluvalis* using MALDI-TOF MS. By combining the techniques of MALDI-TOF MS with PCA, the isolated strains of *H. aquamarina* and *P. fragi* were categorized into several groups based on their differences in protein spectra showing the biodiversity of such antiscalant degrading bacteria in seawater. Hence, the combination of MALDI-TOF MS and PCA also has a potential to differentiate strains based on their environmental / biotechnological roles, which can reduce time and cost of

screening larger number of microorganisms isolated from different environments. It was also noted that the growth rates vary with type of antiscalant and bacteria used. Highest growth rates were obtained for poly maleic followed by poly acrylic acid media.

Our study showed that there is wide variety of seawater bacteria possessing ability to biodegrade antiscalants used in SWRO. The biodegradation of these organic antiscalants will reduce their efficiency to combat membrane scaling and will become source of enhanced microbial growth causing membrane biofouling. Therefore, it is now a need to develop polymers/nanomaterials that are resistant to biological degradation and can be used to reduce both membrane scaling and biofouling in SWRO.

## *5.2 Investigating the effect of antiscalants on biofouling of RO membranes<sup>10</sup>*

### *5.2.1 Introduction*

Membrane filtration technique is being adopted worldwide as an environment friendly and energy efficient technique in desalination industry as compared to thermal desalination techniques (Tang et al. 2009, 2011; Sun et al. 2016). However, the performance of membranes, which includes permeate flux and rejection is affected by the membrane fouling and scaling. To prevent mineral scaling on reverse osmosis (RO) membranes, antiscalants are added to suppress mineral scale formation. The most common antiscalants for calcium sulfate ( $\text{CaSO}_4$ ) include phosphonates and organic polymers (Shih

---

<sup>10</sup> This content has been published. Reference: Ashfaq, M.Y., Al-ghouti, M.A., Qiblawey, H. Zouari, N. 2019b. Evaluating the effect of antiscalants on membrane biofouling using FTIR and multivariate analysis. *Biofouling* 35 (1), 1–14.

et al. 2006). In RO systems, phosphonates, however, tend to hydrolyze to orthophosphate and react with calcium ions to form calcium orthophosphate, which is insoluble (Antony et al. 2011). Therefore, most of the commercial antiscalants for RO membranes are organic polymer-based chemicals, such as poly acrylic acid (PAA), polymethacrylic acid (PMAA), and poly maleic acid (PMA).

The use of polymer-based inhibitors has shown satisfactory performance in preventing membrane scaling (Shih et al. 2006). However, little research has been performed on their biodegradability. Due to the presence of microorganisms in seawater, these antiscalants may act as an energy/carbon source and their biodegradation will not only reduce their efficiency to control membrane scaling, but they will also become a source of enhanced microbial growth causing membrane biofouling. In preliminary research, the strain of *Halomonas aquamarina* was isolated from Arabian Gulf seawater and was identified using Matrix Assisted Laser Desorption Ionization – Time of Flight Mass Spectrometry (MALDI-TOF MS) technique. The strain was identified with a score of 2.02, which is interpreted as reliable genus level identification and probable species level identification as per the manufacturer (Bruker Daltonics, Germany) instructions. The strain was tested for the ability to use antiscalants as a carbon/energy source by providing growth medium containing only one of the targets antiscalant as a carbon source. The antiscalants focused on that research included monomers of acrylic and maleic acids and poly acrylic acid. It was found that the *H. aquamarina* strain was able to grow in an antiscalant containing medium with specific growth rates ( $h^{-1}$ ) of 0.076 (acrylic acid), 0.088 (maleic acid) and 0.115 (poly acrylic acid), which concluded that the strain was able to use these antiscalants as a carbon/energy source for its growth. Furthermore, it has also been shown

in the literature that the antiscalants can enhance membrane biofouling either through their assimilation as a source of carbon (Vrouwenvelder et al. 2000) or phosphorus (Sweity et al. 2013) by microorganisms or through altering membrane surface properties (hydrophobicity) that favors biofouling (Sweity et al. 2015). Thus, it can be concluded from these researches that there is a need to develop certain screening methods to quickly evaluate the antiscalants and obtain early conclusion about their biofouling potential before their utilization at industrial scale.

Conventionally, membrane fouling and anti-fouling studies are conducted in membrane filtration setup. Depending upon the type of fouling under investigation, the experiments are usually conducted from few hours to weeks and the setup mandates to include high-pressure pumps, flow meters, pressure gauges and membrane filtration cells, which makes it time consuming and a costly methodology. In recent research, a method of quantifying biofilm formation using microbiology-based assays was proposed (Lutskiy et al. 2015). The suggested methodology was successfully applied to quantify early stage of biofilm formation on RO and nanofiltration (NF) membranes. The effect of antimicrobial polypeptide (nisin) on biofouling was recently studied using similar methodology (Jung et al. 2018). Therefore, it can be concluded that such assays are useful to evaluate the performance of membranes coated with anti-microbial materials to give early conclusion about the performance of modified membranes without the use of complex filtration setups. Similarly, such assays can further be utilized to study the factors (e.g. effect of antiscalants) affecting microbial growth/viability, a critical step of biofouling.

There are variety of microscopic methods that can be used to evaluate biofouling such as Epifluorescence, Confocal Laser Scanning, Atomic force, Nuclear magnetic

resonance and Electron Microscopy. However, inability to obtain information about biofilm composition, being labor intensive, and critical specimen preparation procedures are some of the disadvantages of these techniques (Nguyen et al. 2012). On the other hand, FTIR spectroscopy is a reliable, cheaper and quicker analytical technique (Amir et al. 2013; Al-Juboori and Yusaf, 2012), suitable for the detection and identification of functional groups in organic compounds or in biofilm layer on the membrane (Al-Degs et al. 2011; Gelaw et al. 2014). FTIR relies on the measurement of characteristic peaks associated with certain functional groups. The technique is designated as ‘fingerprint analytical technique’ for the identification of compounds as it is nearly impossible to obtain same spectrum for two different compounds (Al-Degs et al. 2011). It is rapid and a non-destructive technique and therefore, is good for qualitative analysis of membrane fouling. In addition, analytical information can also be extracted from overlapped FTIR spectra by using multivariate analysis (principle component analysis, PCA) and multivariate calibration (Al-Ghouti et al. 2008, 2010). Combination of FTIR and multivariate calibration has been successfully applied for various purposes such as fuel adulteration (Al-Ghouti et al. 2008), determining viscosity index and base number of motor oils (Al-Ghouti et al. 2010). However, its application in membrane sciences is seldom reported. Gelaw et al. (2014) used FTIR and multivariate analysis (Soft independent modeling of class analogy model, SIMCA) to investigate membrane fouling which helped them to differentiate between fouled and cleaned membrane and to determine best cleaning protocol for removal of organic foulants. Principle component analysis (PCA) is also a type of multivariate analysis that helps to reduce data redundancy. The technique is used for identification of a smaller number of uncorrelated variables from a larger set of data, which help to emphasize variation in the

dataset. These uncorrelated variables are known as principal components (PCs). The PCs are the new coordinates and are numbered as per the percentage of variance in the real data they explain, and they help to maximize variances between the clusters and minimize within the clusters. Thus, the tool of PCA can be combined with FTIR to differentiate between the fouling layers on the membrane receiving different treatments.

The goal of the present study was to evaluate the effect of antiscalants on biofilm formation on RO membranes using relatively faster and efficient methodology. Therefore, FTIR spectroscopy with multivariate analysis (PCA) and microbiological based assay were employed in this research. It is expected that the results of this research will help to develop the application of FTIR with PCA in membrane sciences and to propose simple, rapid and cost-effective methods to investigate membrane biofouling.

## 5.2.2 Results

### 5.2.2.1 Qualitative analysis of Bio-fouled membrane

5.2.2.1.1 *FTIR analysis.* Figure 37 shows the FTIR results of RO membranes exposed to media containing different carbon sources and *H. aquamarina* as a bacterial strain. Higher similarity among all FTIR spectra and absence of any peak shifts shows that there was no interaction between the RO membrane and the biofilm layer and thus biofouling did not cause any obvious structural changes on the RO membrane surface. However, through comparison with the negative controls and virgin RO membrane (pure RO membrane surface), decrease in percentage transmittance at specific wavenumbers shows that the formation of biofilm increased after the addition of antiscalants. Because,

the biofilm present on the RO membrane is subjected to IR radiations; the molecules present in the biofilm will absorb the radiations. The amount of radiation absorbed by the molecules is directly proportional to the number of molecules present in the biofilm or the intensity of the biofilm (Wolf et al. 2002). This result can also be explained through Beer-Lambert law, which states that the absorbance is directly proportional to the thickness and concentration of the sample (Salido et al. 2017; Stuart, 2004) as shown in Equation (29).

$$A = \epsilon cl \text{ -----(29)}$$

Where, A is the absorbance,  $\epsilon$  is molar absorptivity, c is the concentration and l is the path length of the sample, and the absorbance (A) is related to transmittance (T) through the Equation (30)

$$A = -\log T \text{ -----(29)}$$

Therefore, lower the % transmittance is, higher the absorbance will be and consequently, the concentration/thickness of the biofilm will be high. Similar changes in the intensity of the FTIR spectra of biofilm has also been obtained from different regions of the bio-fouled RO membranes (feed, middle and brine regions) and the increase in peak intensity for the RO membrane obtained from the brine region was also correlated with relatively higher intensity of biofouling (Khan et al. 2015).



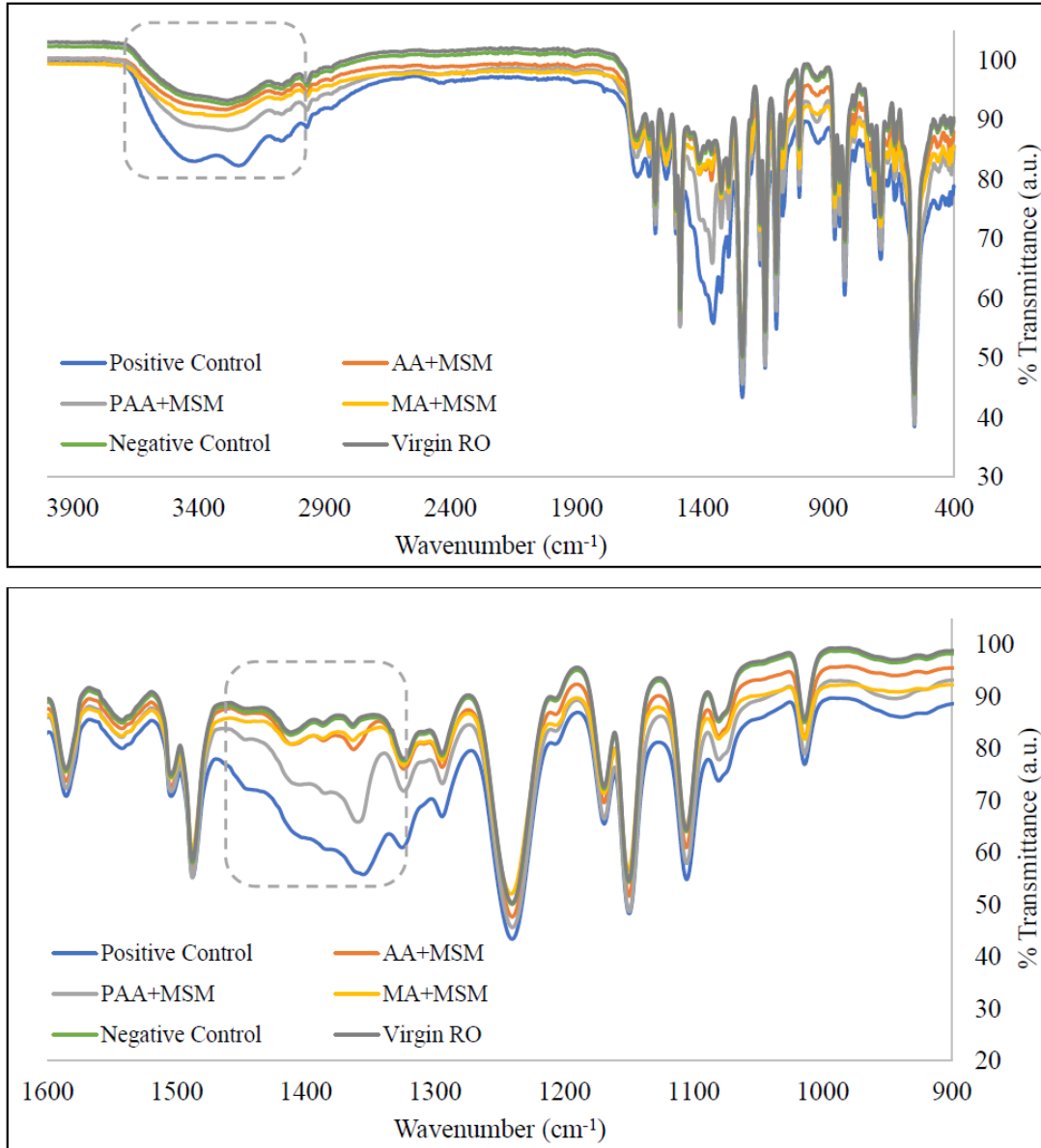


Figure 36. FTIR spectra of RO membranes after exposure to different media in the presence of *H. aquamarina* (incubation for 48 hours at 30°C, Concentration – 1g/L) (Virgin RO – Pure RO membrane surface, Negative control – MSM (no carbon source) with bacteria and MSM + Carbon source (acrylic/maleic/poly acrylic acid/glucose) without bacteria, Positive

control – Glucose in MSM, AA+MSM – Acrylic acid in MSM, PAA+MSM – Poly acrylic acid in MSM, MA+MSM – Maleic acid in MSM) (Ashfaq et al., 2019b)

Table 16 shows various peaks and their assignments from the literature. The broad region from 2900 – 3300 and 900 – 1200  $\text{cm}^{-1}$  represents polysaccharides region. In this region, vibrations result from stretching of C-OH and C-O-C bond (glycoside bond) (Jin et al. 2013). Absorbance in these peaks were also observed in the biofilm produced by *Pseudomonas aeruginosa* strain (Nivens et al. 2001). In addition, stretching vibrations of C-O of carbohydrates, P-O-P and C-O-P of polysaccharides of cell wall and symmetrical stretching of P=O of phosphate group in nucleic acids characterize this polysaccharide region (Karadenizli et al. 2007). The peaks at 2955 and 2930  $\text{cm}^{-1}$  corresponds to C-H asymmetric stretching of  $-\text{CH}_3$  and  $>\text{CH}_2$  in fatty acids, whereas, peaks at 2870 and 2850  $\text{cm}^{-1}$  represents C-H symmetric stretching of  $-\text{CH}_3$  and  $>\text{CH}_2$  in fatty acids. In addition, peaks at 1240 and 1085  $\text{cm}^{-1}$  has been assigned to P=O asymmetric and symmetric stretching of DNA, RNA and phospholipids in the literature. The protein component of the biofilm can be seen through the peaks at 3200  $\text{cm}^{-1}$ , which results from N-H stretching of amide A in proteins and peaks at 1650, 1540, and 1310-1240  $\text{cm}^{-1}$  represents Amide I, II and III components of proteins respectively. The C = O bond in the peptide group resulted in Amide I peak, whereas, both N-H bending and C-N stretching combine to give Amide II peak (Long et al. 2009).

Table 16. Peak assignments to characterize biofilm layer (Boubakri and Bouguecha, 2008; Karime et al. 2008; Krishnamurthy et al. 2010; Xu et al. 2010; Rabiller-Baudry et al. 2012; Dixit et al. 2014) (Ashfaq et al., 2019b)

<b>Peaks (cm<sup>-1</sup>)</b>	<b>Peak assignments</b>	<b>Feature(s)</b>
2900 - 3300	Polysaccharides	Polysaccharides
3200	N-H stretching of amide A in proteins	Proteins
2955	C-H asymmetric stretching of -CH <sub>3</sub> in fatty acids	Fatty acids/Lipids
2930	C-H asymmetric stretching of >CH <sub>2</sub> in fatty acids	Fatty acids/Lipids
2898	C-H stretching of ≥C-H of aminoacids	Proteins
2870	C-H symmetric stretching of -CH <sub>3</sub> in fatty acids	Fatty acids/Lipids
2850	C-H symmetric stretching of >CH <sub>2</sub> in fatty acids	Fatty acids/Lipids
1740	>C=O stretching of lipid esters	Fatty acids/Lipids
1715	>C=O stretching of ester, in nucleic acids and carbonic acids	--
1650	Protein secondary structures (Amide I)	Proteins
1540	Protein secondary structures (Amide II)	Proteins
1468	C-H deformation of >CH <sub>2</sub> in lipids proteins	Lipids/Proteins
1415	C-O-H in-plane bending in Carbohydrates, DNA/RNA backbone, proteins	Proteins
1400	C=O symmetric stretching of COO- group in amino acids, fatty acids	Fatty acids
1310-1240	Amide III band components of proteins	Proteins
1240	P=O asymmetric stretching of phosphodiester in phospholipids	Fatty acids/Lipids
1100	Polysaccharides and alike substances	Polysaccharides
1085	P=O symmetric stretching in DNA, RNA and phospholipids	Fatty acids/Lipids
1342–952	Various cellular components	--
720	C-H rocking of >CH <sub>2</sub> in fatty acids, proteins	Fatty acids/Proteins

Based on the peak assignments in Table 16, peaks were selected that represent protein, polysaccharides and lipids/fatty acids components of the biofilm to show increase in the absorbance in FTIR spectra. Figure 38 clearly shows that the absorption increased

with the addition of antiscalants, which corresponds to the increased biofilm formation on RO membranes. The t-test was also conducted which showed that the mean absorbance of bio-fouled membranes at various wavenumbers was significantly different from the negative control at 95% confidence level. Nevertheless, the absorbance obtained for maleic acid (MA+MSM) at 1100, 1650 and 1310  $\text{cm}^{-1}$  and at 1540 and 1310  $\text{cm}^{-1}$  for acrylic acid (AA+MSM), were not significantly different from the negative control at 95% confidence level. This could be attributed to relatively lesser biofilm formation when monomer antiscalants were used. Therefore, it can be concluded that the biofilm formation increased after the addition of antiscalants, in which, poly acrylic acid caused most intense biofouling on RO membrane.

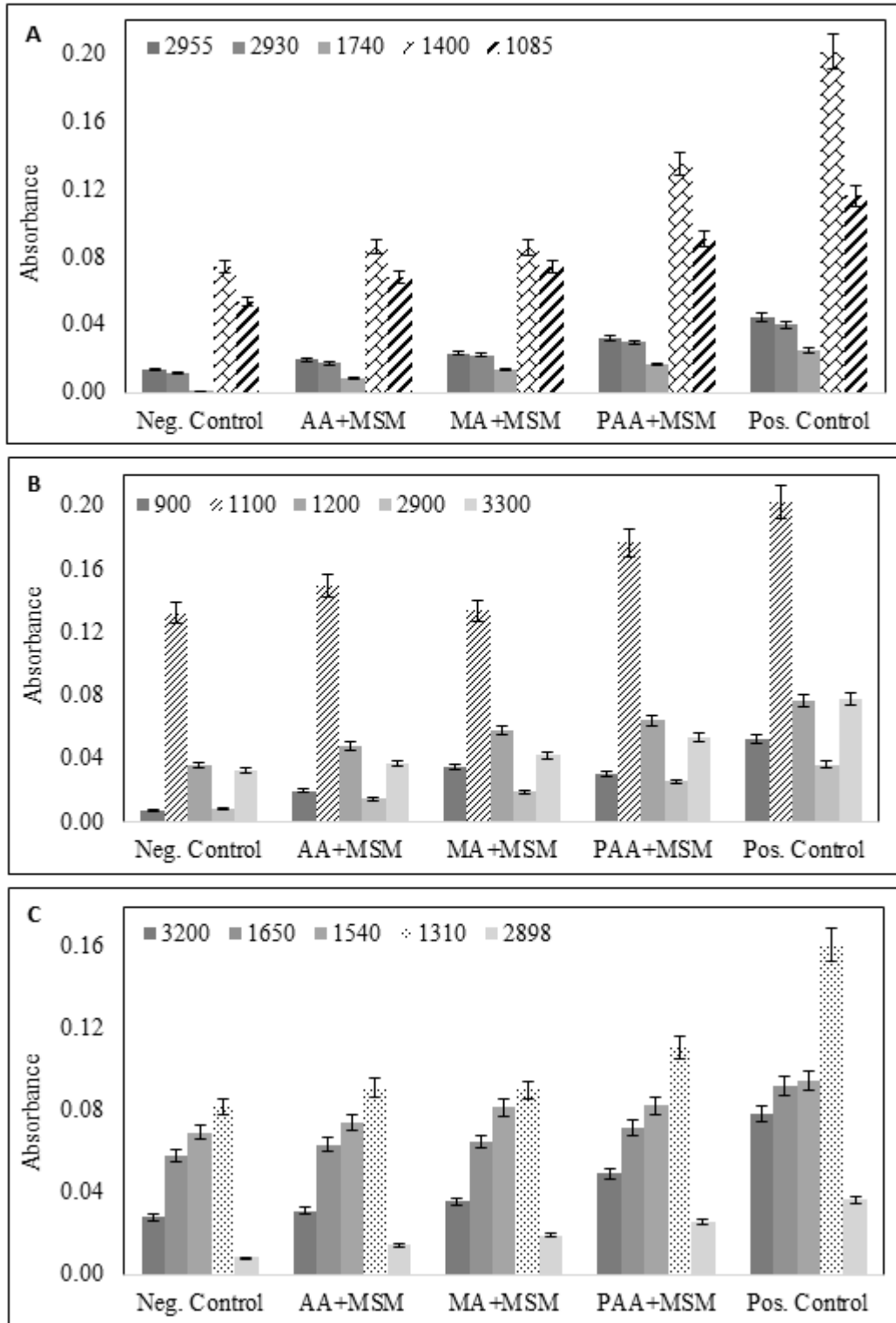


Figure 37. Increase in absorbance for selected peaks representing: A. Fatty acids and phospholipids, B. Polysaccharides, C. Protein components of Biofilm layer (Neg. control

– MSM (no carbon source) with bacteria, and MSM + Carbon source (acrylic/maleic/poly acrylic acid/glucose) without bacteria, Pos. control – Glucose in MSM, AA+MSM – Acrylic acid in MSM, PAA+MSM – Poly acrylic acid in MSM, MA+MSM – Maleic acid in MSM) (Ashfaq et al., 2019b)

*5.2.2.1.2 Classification using Principal Component Analysis.* PCA was carried out for FTIR spectra of biofilm formed on RO membranes because of addition of antiscalants and glucose (as positive control). PCA helped to cluster the variables (Positive control, AA+MSM, MA+MSM, PAA+MSM and Negative control in this case) based on their scores in PC1 and PC2. As shown in Figure 39, both PC1 and PC2 represents 96% of the data variance. Biofilm spectra obtained for poly acrylic acid and glucose was found to be positively correlated to PC1 and negatively correlated to PC2. Whereas, biofilm spectra obtained for acrylic acid and negative control was negatively correlated to both principle components. Biofilm spectra obtained for maleic acid is the only variable that was found to be positively correlated to PC2 and negatively to PC1. Briefly, three clusters can be obtained based on PCA ie Cluster 1 (PAA and Glucose), Cluster 2 (AA and negative control) and Cluster 3 (only MA) as shown in Figure 39. Hence, the biofilm spectra that corresponds to biofilm intensity as well as composition (polysaccharides/proteins/lipids or phospholipids) are similar for the variables qualifying for the same cluster, for example, poly acrylic acid and glucose under cluster 1. On the other hand, variables qualifying for different clusters are more different from each other, for example: acrylic acid (cluster 2) and maleic acid (cluster 3). Since, PCA helps to maximize the differences between the two clusters and minimize within the cluster, such clustering can help to understand the

variability among various class of antiscalants and can help to differentiate their effect on membrane biofouling.

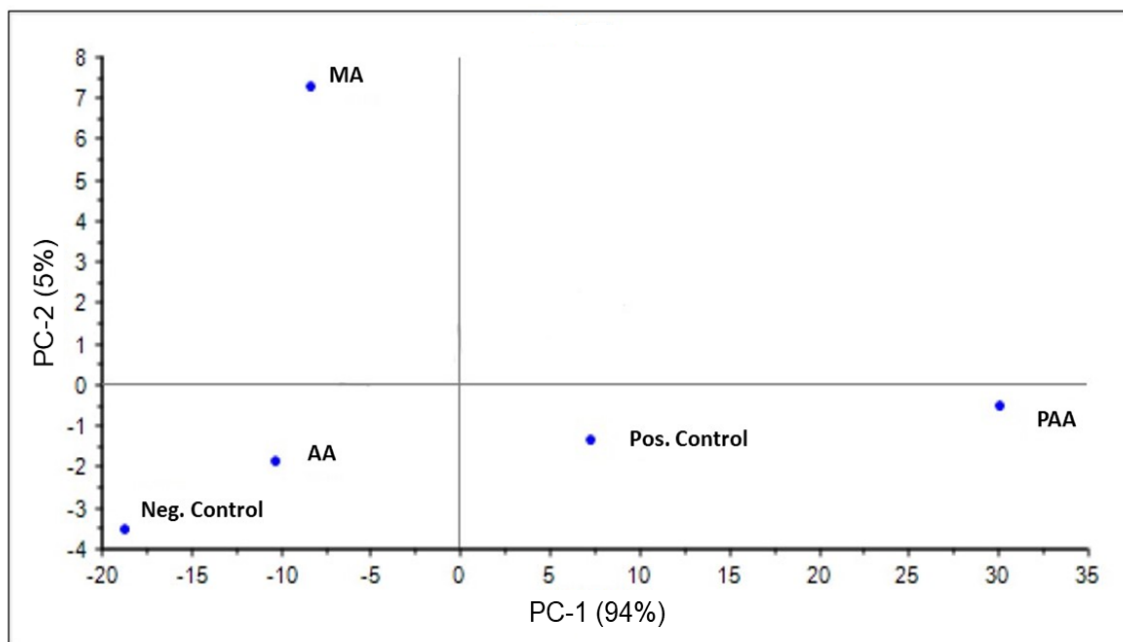


Figure 38. Clustering of variables obtained through PCA using The Unscrambler (V10.5) (Ashfaq et al., 2019b)

#### 5.2.2.2 Component wise analysis of biofilm using PCA

5.2.2.2.1 Protein component. PCA was done for the peaks representing protein component of biofilm in XLSTAT 2016. The biplot in Figure 40A shows that the two factors or PCs (F1 and F2) represent 99.9% of the variance in the data. The data showed that biofilm spectra obtained from poly acrylic acid and positive control (previously categorized as cluster 1 using SVD-PCA) is positively correlated to F1 and negatively to F2. Whereas, spectra obtained for maleic acid, acrylic acid and negative control are positively correlated to both F1 and F2 and hence can be categorized as one cluster. The

biplot shows that peaks of 3200 and 1468  $\text{cm}^{-1}$  has high loading value for negative control, acrylic acid and maleic acid spectra and corresponds to N-H stretching of amide A in proteins and C-H deformation of  $>\text{CH}_2$  in lipids proteins. On the other hand, peaks of 2898, 1650, 1540, and 720  $\text{cm}^{-1}$  have higher loading values for the biofilm obtained because of poly acrylic acid and glucose (positive control). These peaks mainly represent C-H stretching of  $\geq\text{C-H}$  of amino acids, protein secondary structures Amide I, Amide II and C-H rocking of  $>\text{CH}_2$  in fatty acids, proteins.

*5.2.2.2.2 Lipids/Phospholipids component.* The biplot obtained for peaks corresponding to lipids or phospholipids component of biofilm formed is shown in Figure 40B. The results clearly showed that the lipid component of biofilm has negligible loading values for negative control, acrylic acid and maleic acid, whereas, several peaks (2955, 2930, 2850, 2870, 1740  $\text{cm}^{-1}$ ) has high loading values for biofilm spectra obtained in the presence of poly acrylic acid and glucose (positive control).

*5.2.2.2.3 Polysaccharides component.* The biplot of polysaccharides results from PCA give somewhat contrasting results as compared to other two components. The Figure 40C shows that the peaks such as 3300, 3100, 3000 and 2900  $\text{cm}^{-1}$  has higher loading values for biofilm spectra obtained for acrylic acid and maleic acid in opposed to, both positive and negative controls and poly acrylic acid spectra.



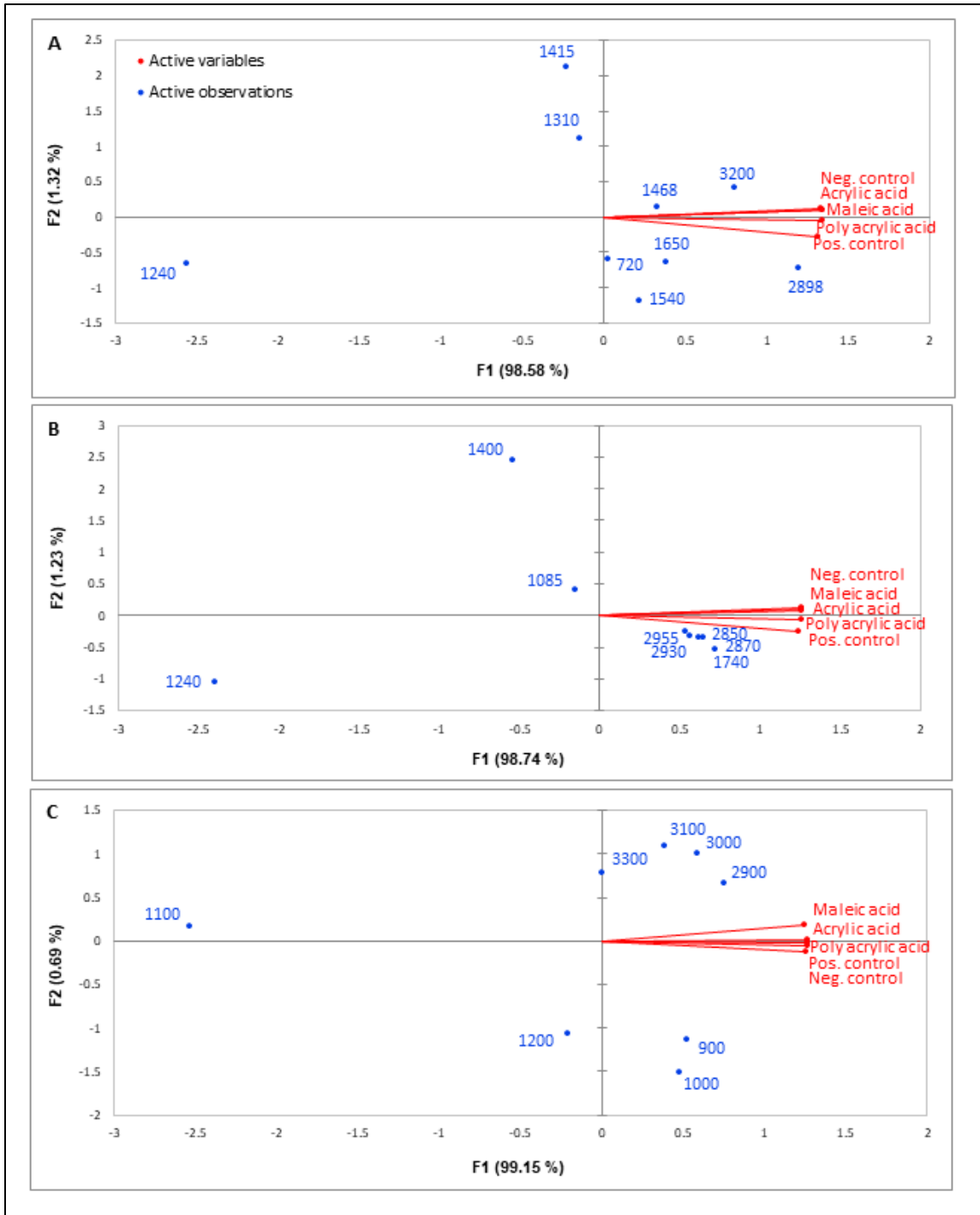


Figure 39. Biplot obtained for A. Proteins, B. Fatty acids and phospholipids, C. Polysaccharides components of Biofilm using XLSTAT (V2016) (Ashfaq et al., 2019b)

5.2.2.2.4 Biofilm – combining all components. The biplot was also obtained

combining all the three components of biofilm. Figure 41 shows that spectra obtained for negative control, maleic acid and acrylic acid are positively correlated to both F1 and F2 representing 99.85% of the variance. Whereas, poly acrylic acid and glucose (positive control) biofilm spectra are negatively correlated to F2 and positively to F1. Since, none of the variable are negatively correlated to F1, these values will have less loading values. Two classes can be observed considering positive correlation to F1, first cluster comprising 3300 (polysaccharide), 3200 and 1468  $\text{cm}^{-1}$  (proteins) have more influence on MA, AA and negative control spectra. Whereas, second cluster comprise of 2930, 2870, 1715, 1740, 2850  $\text{cm}^{-1}$  corresponding to lipid component, 900 and 2900  $\text{cm}^{-1}$  to polysaccharide component and 2898  $\text{cm}^{-1}$  to protein component which has more loading values for poly acrylic acid and glucose biofilm spectra. Thus, it can be concluded that in the case of intense biofouling ie when glucose and poly acrylic acid was used as a carbon source, biofilm was mainly comprised of lipids/phospholipids, polysaccharides and protein. On the other hand, in the case of relatively less intense biofouling formed after the addition of acrylic and maleic acids (monomers), the biofilm is comprised of only two components ie polysaccharides and proteins. The information about the biofilm composition can be used in mitigating the biofouling as some of the researchers target to reduce/degrade/remove certain components of biofilm present in abundance such as polysaccharides (Nagaraj et al. 2017).

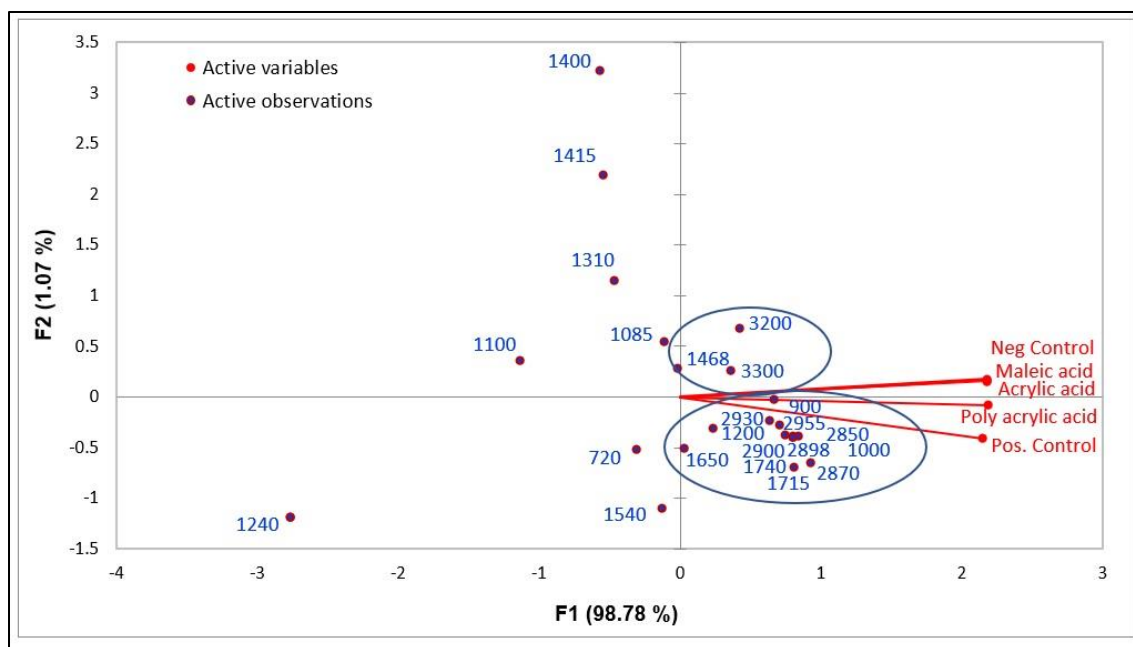


Figure 40. Clustering of biofilm components obtained in the presence of different carbon sources (Ashfaq et al., 2019b)

5.2.2.3 *Quantitative analysis of Bacterial cells in biofilm.* The membrane biofouling resulted in response to different carbon sources was also quantitatively analyzed through plate count method to estimate the number of viable bacterial cells in the biofilm layer. The results (Figure 42) showed that log CFU/mL was in the following decreasing order: glucose > poly acrylic acid > maleic acid > acrylic acid. The CFU count results are in consistent with the FTIR results as the spectral intensity also varied in the same fashion. Interestingly, the bacterial counts in the presence of only MSM (without any carbon source) were also observed which shows that bacteria were able to sustain in the absence of any carbon source. However, addition of antiscalants increased the CFU count, which shows the potential of microorganisms to use antiscalants as a carbon/energy source and enhance their growth and biofouling in membrane systems.

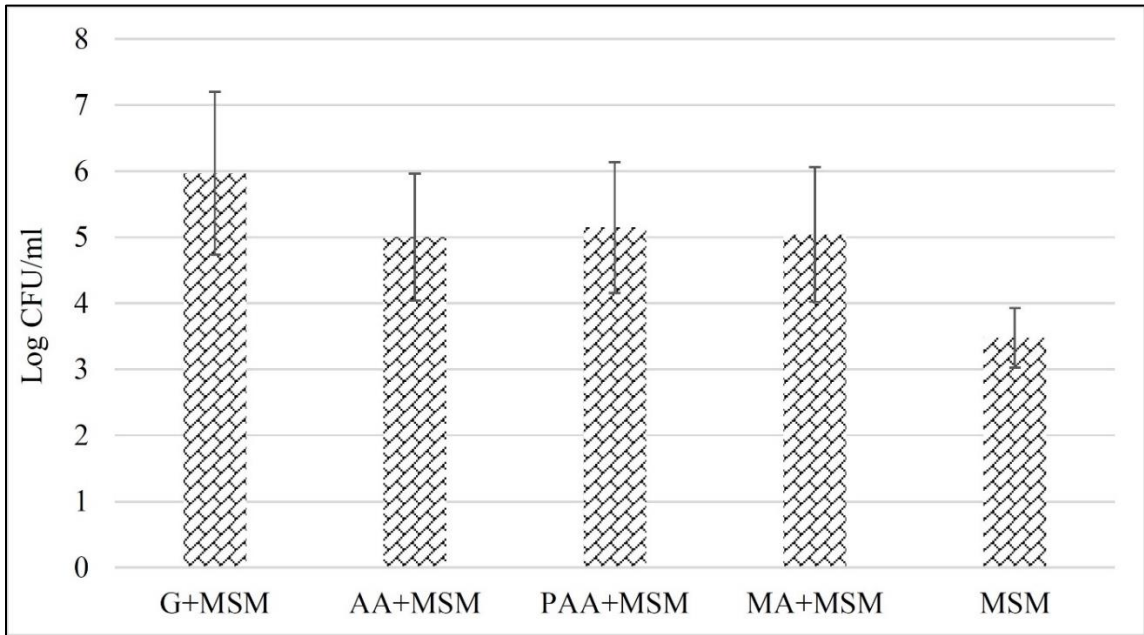


Figure 41. CFU Counts obtained from bio-fouled RO membranes (Ashfaq et al., 2019b)

### 5.2.3 Discussion

Membrane biofouling has been reported as a major problem in NF and RO membranes and contributes more than 45% among all types of membrane fouling. Biofouling starts with initial attachment of microorganisms because of formation of conditioning layer on the membrane followed by their rapid multiplication and growth by feeding on the nutrients and organic substances in the feed water. This issue is where presence of antiscalants can make the difference in the intensity of biofouling. Previous researchers have reported the effect of antiscalants on the membrane properties that enhances the microorganisms' attraction to the membrane surface as well as the formation of the conditioning layer. The presence of biodegradable antiscalants such as used in this study will act as an additional carbon source for microorganisms resulting in more intense

biofouling. Vrouwenvelder et al. (2000) noted that there is a correlation between the antiscalants' assimilable organic carbon (AOC) and the biofouling of RO membranes. Therefore, it was suggested to choose antiscalants with least or negligible AOC values to reduce their effect on biofouling. In another research (Sweity et al. 2013), it was observed that addition of poly acrylate and poly phosphonate antiscalants changed the RO membrane surface properties by increasing the contact angle to  $49 \pm 1.3$  from  $21 \pm 5.8$  which made the membrane more hydrophobic which in return promotes biofouling. Furthermore, the surface charge of RO membrane became less negative because of addition of poly phosphonate antiscalants. Other than changing the membrane surface properties that promotes biofouling, poly phosphonate antiscalants also provided additional source of phosphorus for enhanced microbial growth. Both antiscalants had higher deposition coefficient, which means that they aided in the initial attachment of microorganisms to RO membrane (Sweity et al. 2013).

Research has also shown that there was sharp decline in permeate flux as a result of more intense biofouling, when poly acrylate based antiscalants were used in feed water as compared to poly phosphonate based antiscalants (Sweity et al. 2015). Scanning electron microscopy (SEM) and Confocal laser scanning microscopy (CLSM) images also showed that the biofilm thickness was more in the presence of poly acrylate based antiscalants. It could be due to higher EPS production and secretions as a result of phosphorus – limiting conditions when these antiscalants were used. However, uptake of oxygen, phosphorus and nitrogen was more in the case of poly phosphonate based antiscalants attributed to the higher growth rates of microorganisms in these types of antiscalants (Sweity et al. 2015). While, previous work deals with nutritional contribution of antiscalants to biofouling and

influence of antiscalants on membrane properties and biofouling enhancement. In this work, method of quick screening of antiscalants for their effect on biofouling and its characterization has been tested and proposed. Since, the use of antiscalants in membrane-based technologies is important to obtain better performance. Nevertheless, their use needs to be monitored to minimize their impacts on biofouling.

Extracellular polymeric substances (EPS) are secreted by microorganisms, which help them to further enhance additional microbial attachment and growth on the surface of the membrane (Al-Juboori and Yusaf, 2012). EPS are mainly composed of polysaccharides, nucleic acids, lipids/phospholipids and proteins. EPS also exhibits certain functional groups such as carboxylic, phenolic, hydroxylic, and phosphoric groups and several non-polar groups like hydrophobic groups in carbohydrates, aromatics and aliphatics in proteins. The presence of these functional groups aided in characterization of biofouling on RO membrane using FTIR in this research. It has been reported that the EPS comprised of 50 to 80% of the total organic matter and protein in biofilms. Many researchers have attempted to characterize EPS in biofilms. Jiao et al. (2010) used FTIR to characterize EPS extracted from mid-development and mature stage biofilm. The presence of peaks at 1300 – 900 and 1700 – 1500  $\text{cm}^{-1}$  showed the presence of polysaccharides, nucleic acids and proteins. The variation in spectral shape as well as intensity helped in obtaining information about the composition and quantity of EPS produced at different stages of biofilm formation. Thus, it was noted that the amount of protein and carbohydrates were higher for the biofilm reaching mature stages. The ratio of carbohydrate to protein was found to be between 3 – 6 which was considered very high as compared to ratios of 0.2 – 1.7 cited in the literature (Bura et al. 1998; Prolund et al. 1996;

Liu and Fang, 2002; Sheng et al. 2005). These results show that the composition of EPS and biofilm layer may vary to the great extent, which will have its implications on the performance of membrane system, cleaning efficiency and other factors. These factors include type of substrate (source of carbon and ratio of carbon to nitrogen), growth phase of involved microorganisms, solution composition and chemistry (ie dissolved oxygen, pH, ionic strength etc.), physico-chemical conditions (like shear rates, retention times) and presence of toxic substances (drugs or heavy metals) (Jia et al. 1996; Rinzema et al. 1998; Drews et al. 2006; Sheng and Yu, 2006; Ozturk et al. 2010). Sheng et al. (2006) reported that the production of cell mass was highest in the presence of succinate followed by malonate, propionate, acetate, butyrate, and benzoate. However, the EPS production was almost in the opposite order ie it was highest for benzoate and acetate followed by butyrate, propionate, succinate, and malonate. Therefore, EPS secretion is increased by microorganisms during stress conditions (Sheng et al. 2006). In this research, it was also noted that both biofilm composition and intensity varied with the type of carbon source in which intensity varied in the following decreasing order glucose > poly acrylic acid > maleic acid > acrylic acid.

Generally, it is considered that polysaccharides and proteins are the major components of membrane fouling (Kristensen et al. 2008). Therefore, most studies focus on determining EPS concentration through measuring carbohydrates and proteins content only. The carbohydrates being more hydrophilic in nature tend to contribute more in fouling propensity over its counterparts (Yigit et al. 2008; Li et al. 2012). The organic matter content of the biofilm formed on membrane was studied and it was found that proteins and carbohydrates were major constituents of biofilm layer (Lee et al. 2009).

Although, PCA showed that protein and polysaccharides are dominant components in biofilm layer in this research. It also showed that lipids and phospholipids are also one of the important constituents especially in the case of intense biofouling ie when glucose and poly acrylic acid are used as carbon sources. The biofilm containing lipids and phospholipids such as glycosphingolipid are known to be stronger than others (Gutman et al. 2014a). EPS containing these lipids helps in primary attachment and recalcitrance of the biofilm produced, contributing significantly to the cohesive strength of the biofilm on RO membranes (Bereschenko et al. 2010) and has also been found to produce rigid layers on polyamide RO membrane surfaces (Gutman et al. 2014b). Furthermore, the microorganisms known to produce lipids containing EPS, such as *Sphingomonas* are primary colonizers in the biofilm layer in desalination systems (Bereschenko et al. 2010). The EPS produced by secondary colonizers are usually exposed to the cleaning agents and shear stress of seawater and therefore, were washed away. Hence, the EPS containing lipids and other adhesive constituents produced by primary colonizers needs to be targeted to combat biofouling (Nagaraj et al. 2018).

The composition of EPS can also affect the physical structure of the biofilm (Ma et al. 2006; Mayer et al. 1999) like pores and water channels in internal structure of the film. The reduction in porosity and water passage channels may then affect the membrane water permeability and rejection leading to lower membrane flux and performance (Chen and Stewart, 2002; Chang and Halverson, 2003; Herzberg et al. 2009). However, it is unknown that how the composition of EPS affects the physical structures of the biofilm.

Knowledge about the composition of biofilm is also important to understand the efficiency of biofouling control and treatment strategy as it was found that certain chemicals like



sodium dodecylsulfate (SDS) and ethylenediaminetetraacetic acid (EDTA) were successful in removing more polysaccharides than proteins and many organic components of the biofilm were still found in the cleaned membranes (Al-Ashhab et al. 2017). Thus, the information about the biofilm layer and its composition can also help in developing target specific cleaning and control strategy. Interestingly, combination of FTIR with multivariate data analysis was also used for choosing best cleaning strategy for membrane biofouling. The classification results helped to differentiate between cleaned and bio-fouled membranes as well as between different cleaning strategies. Thus, combination of FTIR with multivariate data analysis can help in obtaining microscopic information about the biofilm layer components and in identifying control and cleaning measures. Furthermore, relatively less time consuming and cost-effective method can also help in quick screening and evaluation of antiscalants for their role in biofouling. Similarly, this method can also be extended to obtain quick preliminary information about the modified membranes for their efficiency in biofouling control.

#### *5.2.4 Conclusion*

Antiscalants plays a vital role in reducing membrane scaling and optimizing membrane performance. However, their presence was found to enhance membrane biofouling on RO membrane systems consistent with previous researches (Vrouwenvelder et al. 2000; Sweity et al. 2013, 2015). Therefore, initial screening of these antiscalants before their application at the industrial level is important to understand their biofouling potential. In this research, an easy and quick methodology was applied to do such screening. The suggested methodology combines FTIR with multivariate data analysis and

conventional microbiological assays to test the effect of antiscalants on biofouling. Combination of FTIR and PCA helped to classify antiscalants based on their membrane fouling potential and to characterize biofilm components. Both the spectral intensity and CFU count showed that the biofouling was more intense in the presence of poly acrylic acid followed by maleic and acrylic acid. Results of this research can help to add more in-depth information about the role of antiscalants on biofouling of membranes. Furthermore, suggested methodology can also be utilized for preliminary testing of the anti-biofouling potential of modified membranes.

## CHAPTER 6 – OBJECTIVE 03: INVESTIGATING THE INTERACTIONS BETWEEN MICROORGANISMS AND CALCIUM SULFATE IN RO SYSTEM<sup>11</sup>

### *6.1 Introduction*

Water shortage is one of the major challenges being faced by most parts of the world, and it is now further exacerbated by the increase in population and economic growth in some countries like Qatar (Ashfaq et al., 2018). Membrane technology is one of the most favorable technique to produce clean water, and it is being recommended for desalination industry over Thermal technology owing to its better environmental and economic footprint (Ashfaq et al., 2018). Nevertheless, membrane fouling is the major hurdle towards its widespread use. Membrane fouling is the complicated phenomenon governed by different mechanisms and is affected by various factors, parameters and feed water compositions. It is broadly divided into four major types based on the type of foulants i.e. biofouling (caused by attachment and subsequent growth of microorganisms mediated by extracellular polymeric substance ‘EPS’), inorganic fouling or scaling (caused by salts such as calcium carbonates and sulfates), organic fouling (organics constituents like humic acid, alginates) and colloidal fouling (suspended matter) (Qasim et al., 2019).

Most of the researches target towards investigating one of the fouling types. However, it should be noted that all types of foulants i.e.

---

<sup>11</sup> This content has already been published. Reference: (1) Ashfaq, M.Y., Al-Ghouti, M.A., Al-Disi, Z., Zouari, N. 2020. Investigating the microorganisms-calcium sulfate interaction in reverse osmosis systems using SEM-EDX technique. *J. Env. Chem. Eng.* 8, 103963. (2) Ashfaq, M.Y., Al-Ghouti, M.A., Al-Disi, Z., Zouari, N. 2020. Interaction of seawater microorganisms with scalants and antiscalants in reverse osmosis systems. *Desalination* 487, 114480.

organic/inorganic/microbial/colloidal are present in feed water. Therefore, it is important to investigate the foulant-foulant interactions and how they both affect the severity of membrane fouling. For example: it has been noted that the presence of organic macromolecules enhances the membrane scaling by shortening the nucleation time and increasing the flux decline (Liu and Mi, 2014). Moreover, microorganisms present at the Reverse Osmosis (RO) membrane surface do not only cause biofouling but also secrete carbohydrates, EPS, which in turn enhance the organic fouling. Indeed, 60% of the constituents in biofilm were found to be organic substances (Butt et al., 1997).

Biofouling refers to the formation of biofilm by the attachment and subsequent growth of microorganisms on the membrane surface (Kim et al., 2019). Biofouling is a major problem in RO systems especially in Middle East countries like Qatar where temperature of seawater entering the plants exceeds 25°C which is optimum temperature for microbial growth (Al-Ahmad et al., 2000). It has been found that biofouling is the most frequently occurring type of membrane fouling in membrane filtration plants. Thus, 82% of RO plants in USA (Ridgway and Flemming, 1996) and 70% of RO plants treating seawater worldwide suffer from the problem of biofouling (Khedr, 2002). While the other types of fouling can be controlled by reducing the concentration of their causative agents, biofouling cannot be prevented even after removal of 99.9% of the microorganisms from feed water. This is due to the ubiquitous nature of microorganisms as well as their ability to multiply at a faster rate (Nguyen et al., 2012).

It has been shown that microorganisms influence the formation of variety of minerals such as carbonates, sulfates, sulfides, oxides, phosphates and nitrates through microorganisms-mineral interactions. Bacteria can induce/mediate precipitation either

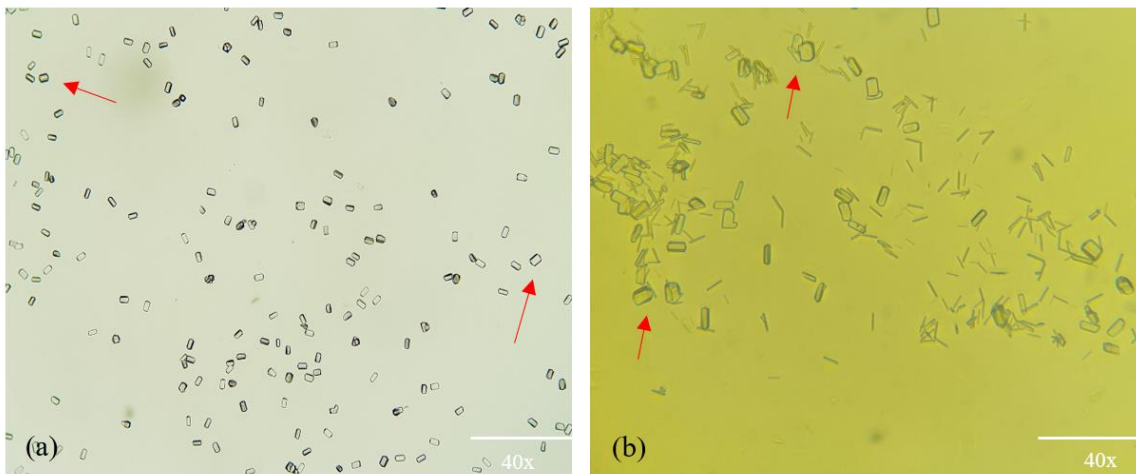
directly in which the metabolic activities of bacteria lead to supersaturation with respect to mineral or indirectly when the bacterial cells (dead/alive), and EPS act as a template for nucleation (Driessche et al., 2019). Nevertheless, the implications and applications of this microorganism-mineral interaction in general are far reaching. Thus, the biomineralization capability of bacteria has found its influence on global biogeochemical cycling such as fixation of atmospheric carbon for carbonates sediment formation (Dhimi et al., 2013) and dolomite precipitation (Al-Disi et al., 2017) and being considered for applications such as in sustainable construction industry (Achal et al., 2015), and in environmental applications like soil stabilization (Bibi et al., 2018). Therefore, it can be expected that the presence of bacteria in membrane filtration systems does not only result in biofouling, but it may also induce/mediate precipitation of minerals causing increased mineral scaling. That is why, it is important to investigate the interactions between bacteria present in feed water e.g. seawater microorganisms in case of seawater reverse osmosis (SWRO) with inorganic mineral scalants such as calcium sulfates and carbonates. Therefore, the main aim of this research was to investigate the ability of seawater microorganisms to form calcium sulfate (gypsum; a polymorph of calcium sulfate:  $\text{CaSO}_4 \cdot 2\text{H}_2\text{O}$ ) in the controlled lab-scale conditions. This work is the continuation of previously published work done to isolate, identify and differentiate various seawater microorganisms that could use antiscalants as carbon/energy source (Ashfaq et al., 2019a). Some of those strains were used to explore their application in biomineralization of calcium sulfate minerals in this research. The experiments were carried out with different selected strains of bacteria, and at different concentrations of calcium ions. Furthermore, the kinetics of biomineralization was also explored. The results of this research will help to fill knowledge gaps related to the

microorganisms-mineral interactions in membrane filtration systems.

## 6.2 Results

### 6.2.1 Formation of $\text{CaSO}_4$ crystals in solid medium (Light Microscopy investigation)

Formation of crystals in solid media was regularly monitored through light microscopy at 40x and 100x magnification level. Figure 43a shows the formation of crystals in solid LBM medium in the presence of different tested strains. Crystals were found to be short, with thick acicular structures at the high concentrations of  $\text{Ca}^{+2}$  (i.e. LBM3,  $\text{Ca}^{+2} = 50 \text{ mM}$ ). After 21 days of incubation, the crystals size did not increase, possibly due to the attachment of bacteria or EPS onto the  $\langle 100 \rangle$ ,  $\langle 101 \rangle$ ,  $\langle 001 \rangle$  faces of the gypsum as shown in Figure 43c. Aref, (1998), showed that the attachment of organic compounds on 111 and 103 faces of lenticular shape gypsum also minimized the growth of crystals.



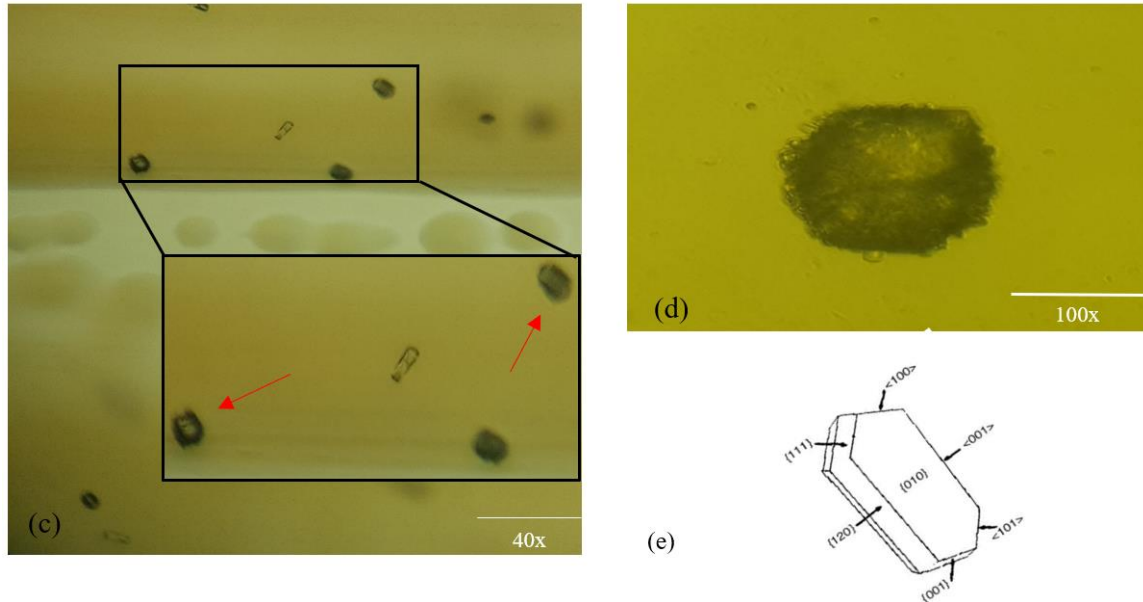
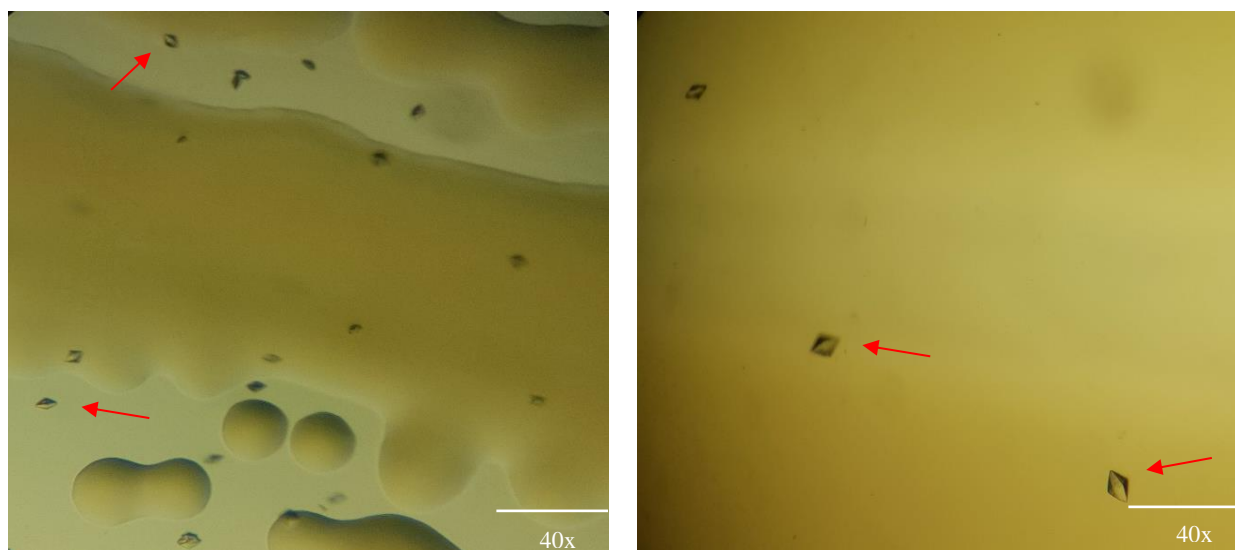


Figure 42. Formation of  $\text{CaSO}_4$  crystals in the presence of bacteria at  $\text{Ca}^{+2}$  and  $\text{SO}_4^{-2} = 50$  mM after 14 days of incubation (a) *P. fragi* (QOFSW-3 (#2)), (b) *C. maltaromaticum* (QONSW-2 (#2)), (c, d) Adhesion and growth of *H. aquamarina* (QOFSW-1 (#1)) on the surface of crystals after 21 days of incubation at 40x and 100x magnifications, and (e) Morphology of gypsum crystal (Ashfaq et al., 2020b)

At lower concentration of ions (i.e. 30 and 20 mM), the crystals were more of a pyramidal shaped as shown in Figure 44. This could show that the shapes of gypsum crystals varied with the concentration of calcium ions.



(a)

(b)

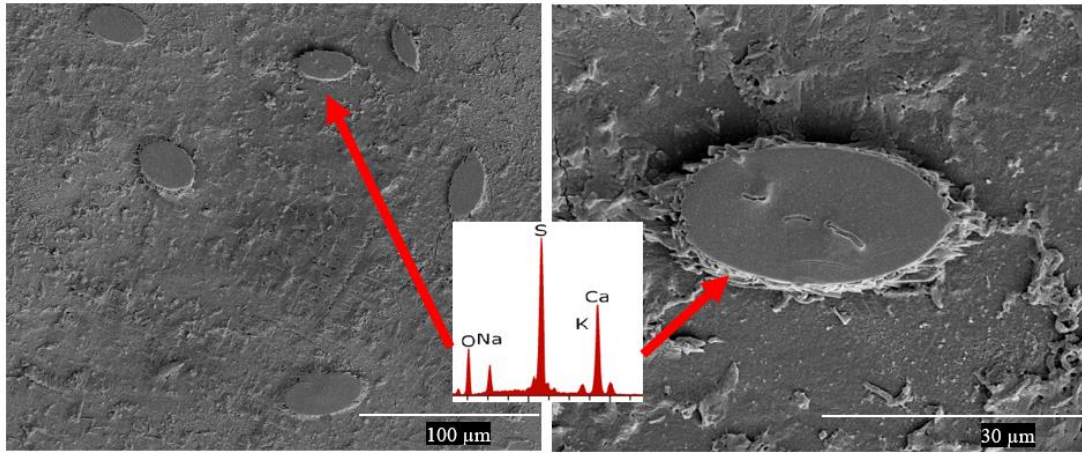
Figure 43. Formation of  $\text{CaSO}_4$  crystals at lower ions concentrations in the presence of *H. aquamarina* (QOFSW-1 (#1)) strain after 14 days of incubation (a)  $\text{Ca}^{+2}$  and  $\text{SO}_4^{-2} = 30$  mM (LBM2), (b)  $\text{Ca}^{+2}$  and  $\text{SO}_4^{-2} = 20$  mM (LBM1) (Ashfaq et al., 2020b)

### 6.2.2 Precipitation of $\text{CaSO}_4$ on the RO membrane and in the biofilm

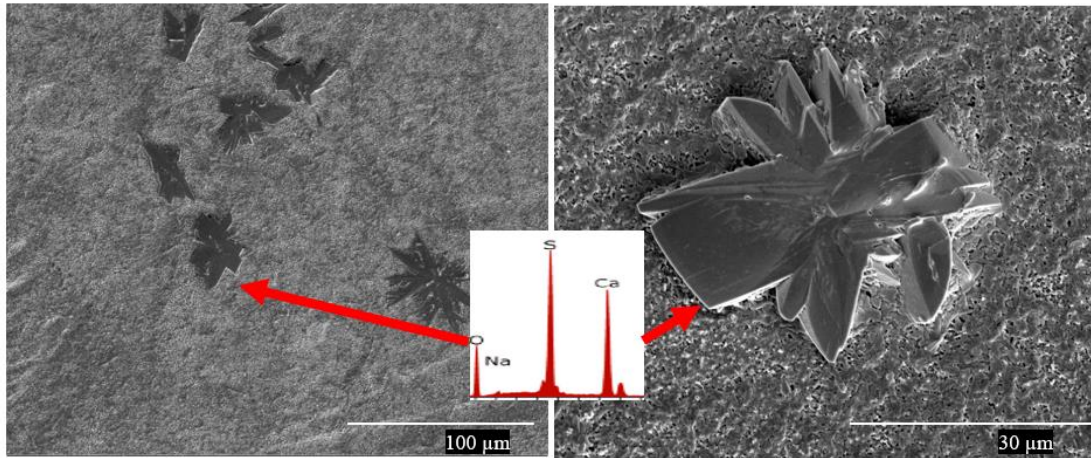
In this research, SEM coupled with EDX technique was mainly used to investigate the formation of gypsum crystals, their morphologies and composition under the influence of bacterial growth. The crystallization of gypsum on the surface of the RO membrane as well as in the liquid medium was explored. SEM analysis after 7 days of incubation showed that the calcium sulfate was formed and attached to the RO membrane. In control samples i.e. without bacteria, there were no precipitates noted on the RO membrane. Furthermore, it was noted that all strains studied in this research were able to form precipitates on the RO membrane (Figure 45). The precipitates were also observed even in the presence of dead bacteria (after autoclaving of the strains), which showed that the precipitation can



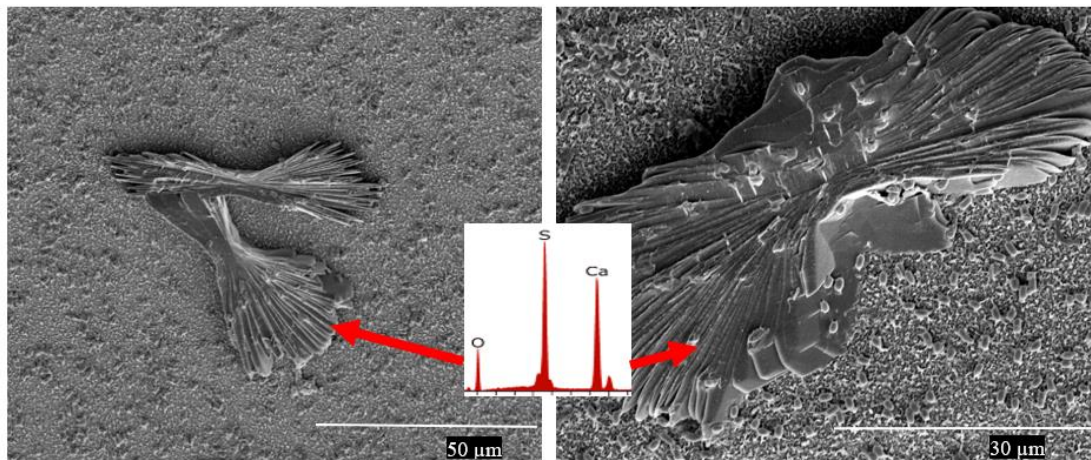
occur even in the absence of bacterial growth activity. In that case, bacterial cellular components may have participated in the formation of precipitates. Various morphologies of crystals were noted as shown in Figure 45, including typical needle like and floral like structures. In general, typical needle like structure is for gypsum precipitates as previously reported in non-biologically induced gypsum precipitation on the membrane (Ashfaq et al., 2019b; Antony et al., 2011; Rahman, 2013; Shih et al., 2005).



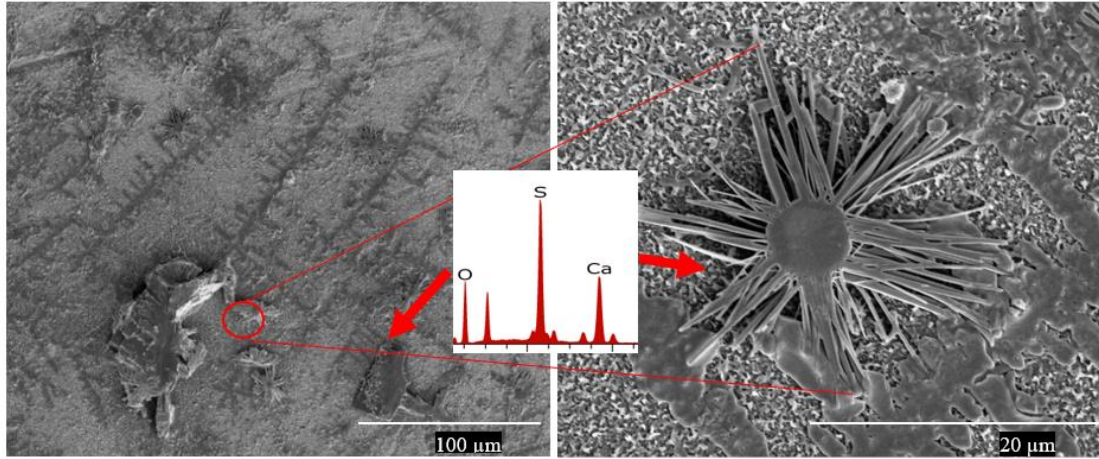
(a)



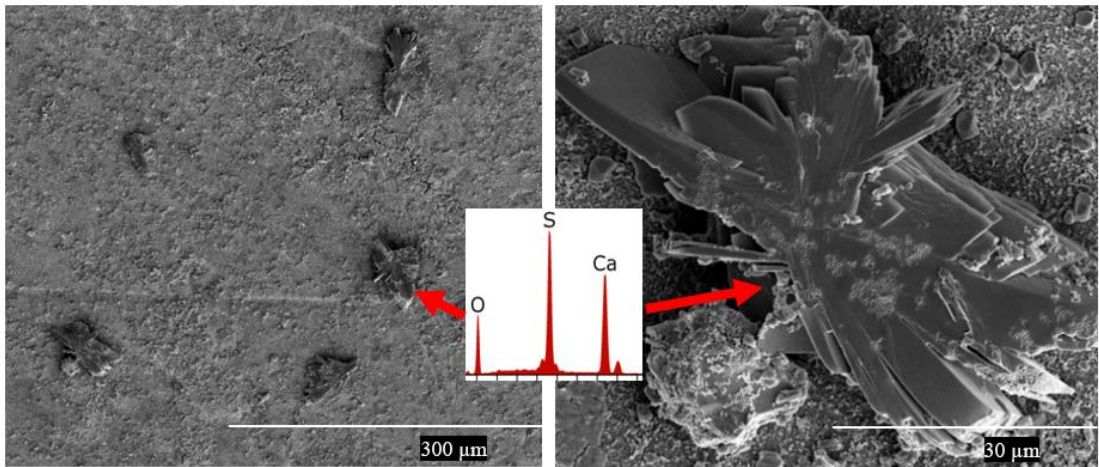
(b)



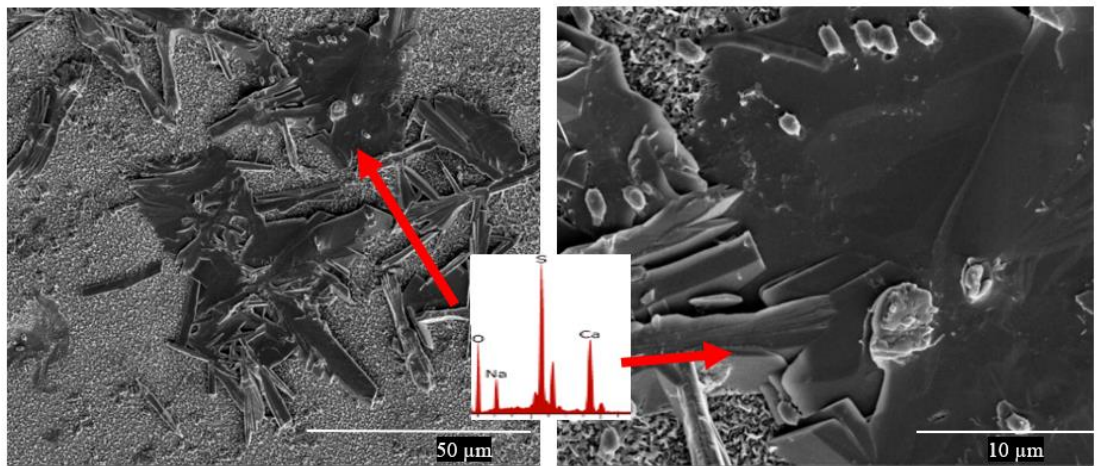
(c)



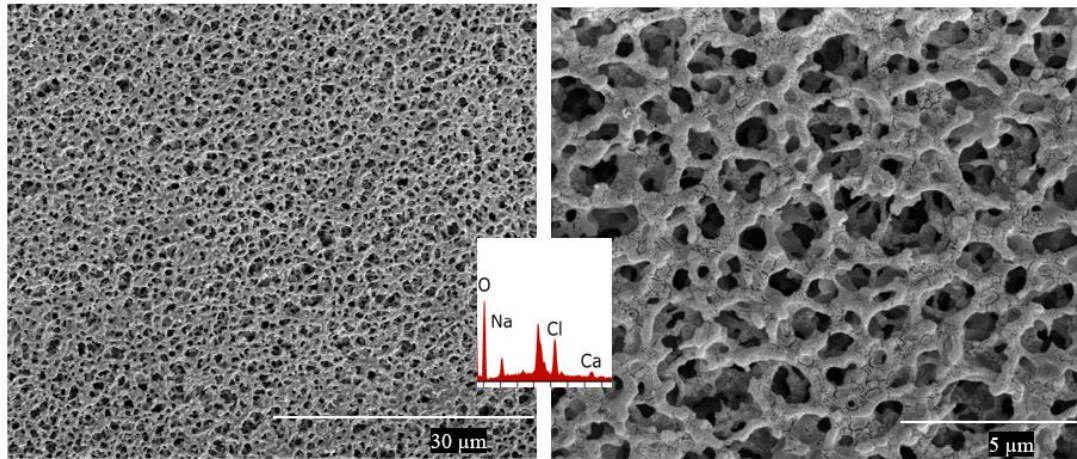
(d)



(e)



(f)



(g)

Figure 44.  $\text{CaSO}_4$  precipitates attached to the membrane in the presence of bacteria after 7 days of incubation at  $\text{Ca}^{+2}$  and  $\text{SO}_4^{-2} = 50$  mM (a) *P. stutzeri* (QOFSW-2 (#3)), (b) *P. fragi* (QOFSW-5 (#1)), (c) *H. aquamarina* (QOFSW-1 (#1)), (d) *H. aquamarina* (dead), (e) *C. maltaromaticum* (QONSW-2 (#2)), (f) *P. fragi* (dead) (QOFSW-5 (#1)), (g) Control (without bacteria – no crystals formation) (Ashfaq et al., 2020b)

After 14 days of incubation, the loss of calcium ions as a result of microbially mediated calcium sulfate precipitation was calculated. For this purpose, the representative volume of liquid medium was filtered through  $0.2 \mu\text{m}$  and the filtrate was analyzed using Ion chromatography (IC). The results also confirmed the formation of  $\text{CaSO}_4$  in the solution as the filtered samples showed significant reduction in calcium ions in the presence of microorganisms as compared to the controls at 95% confidence level (Figure 46). However, SEM results showed that the precipitation of  $\text{CaSO}_4$  occurred even in the presence of autoclaved dead cell. The results of IC confirmed that the concentration of calcium ions decreased significantly in the presence of live cells as compared to dead cells

(at 95% confidence level) for all tested strains which represents the probable involvement of bacterial activity in the biomineralization of  $\text{CaSO}_4$ .

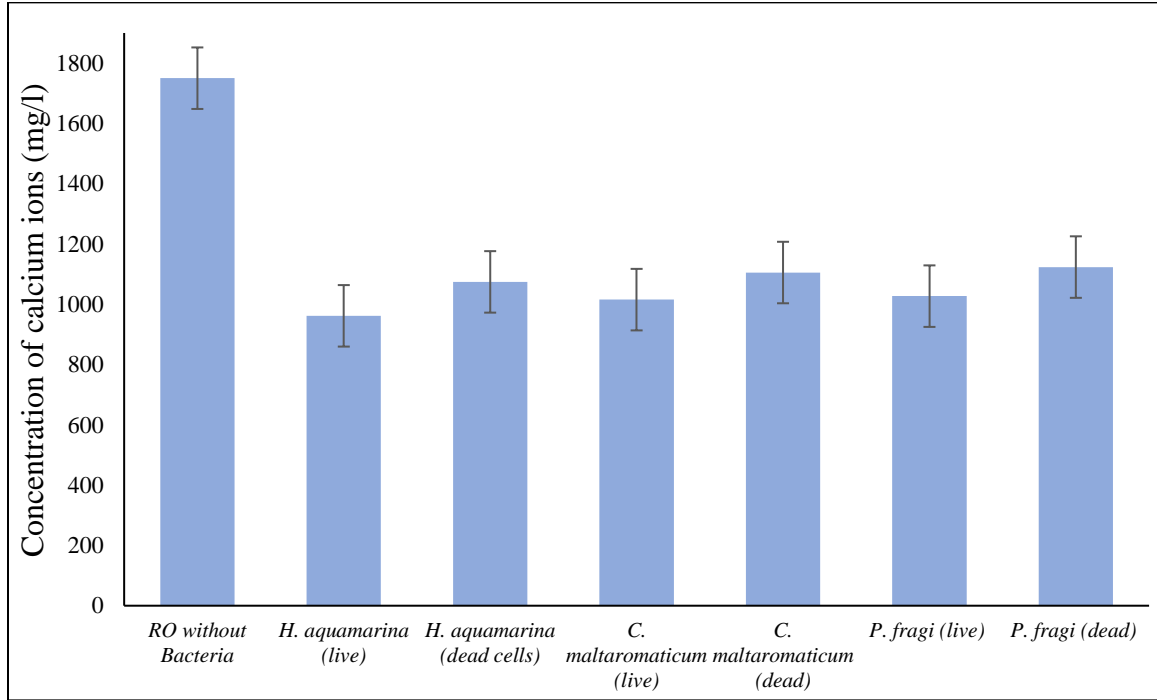
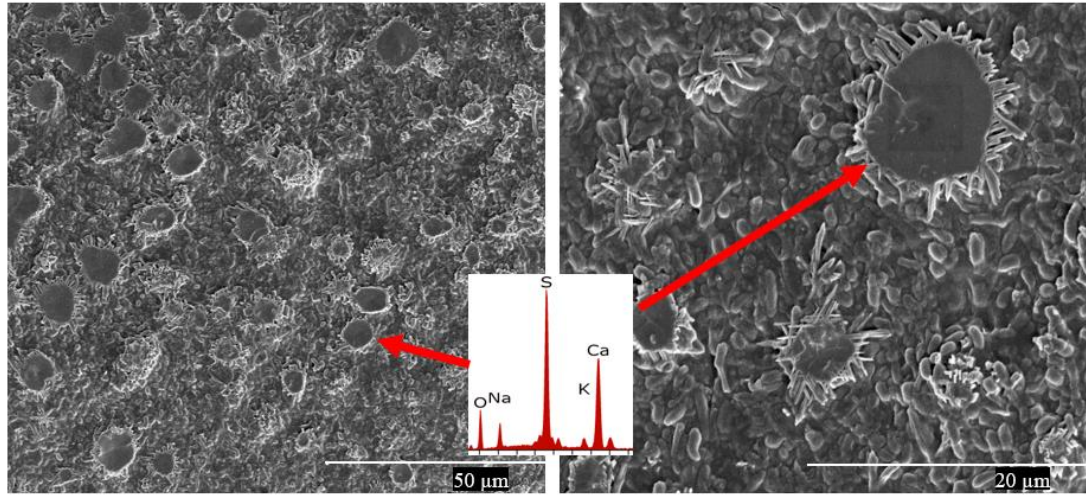
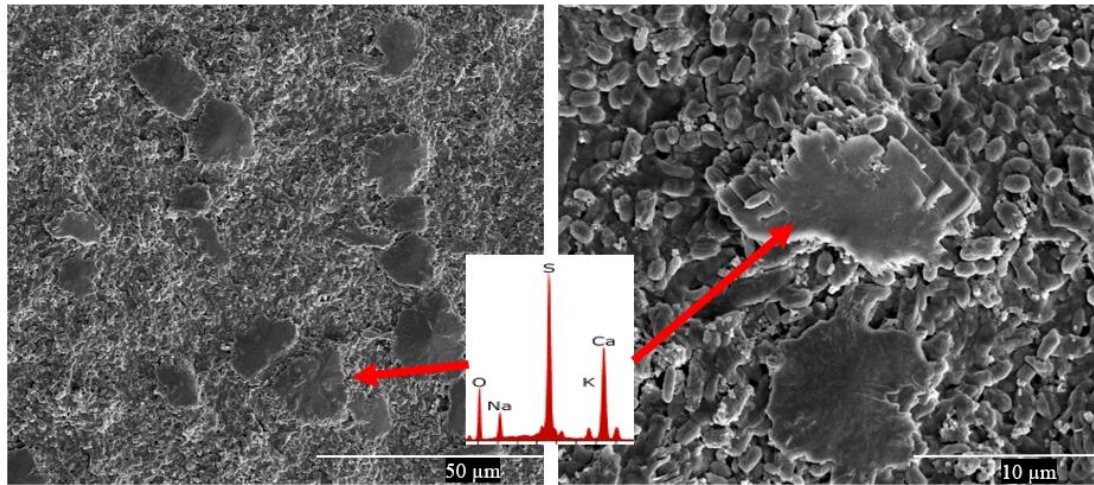


Figure 45. Concentration of calcium ions remaining in the liquid medium after 14 days of incubation (medium used: LMB3 containing  $\text{Ca}^{+2}$  and  $\text{SO}_4^{-2} = 50 \text{ Mm}$ , *H. aquamarina*:  $n = 3$ , *P. fragi*:  $n = 1$ , *C. maltaromaticum*:  $n = 1$ ) (Ashfaq et al., 2020b)

The samples containing RO membranes were found to possess biofilm at the bottom of tubes, possibly due to the detachment from membranes. This biofilm was also analyzed, and the  $\text{CaSO}_4$  precipitates were noted as shown in Figure 47. It is interesting to note that there were neither biofilm nor precipitates noted in samples without RO membrane. This shows that the precipitation of calcium sulfate requires a template and therefore, the presence of RO membrane was important for the crystal's formation.



(a)



(b)

Figure 46. SEM-EDX analysis of precipitates formed in the biofilm of (a) *P. fragi* (QOFSW-4 (#2)), (b) *H. aquamarina* (QOFSW-1 (#1)) (medium used: LMB3 containing  $\text{Ca}^{+2}$  and  $\text{SO}_4^{-2} = 50 \text{ mM}$ ) (Ashfaq et al., 2020b)

### 6.2.3 Kinetics and effect of calcium ions concentration on $\text{CaSO}_4$ biomineralization

The effect of calcium ions was studied to investigate the potential for bio-mediated precipitation of  $\text{CaSO}_4$  at low calcium and sulfate ions concentration i.e. 800 and 1200

mg/L. In addition, kinetics of biomineralization was also explored to study the formation of crystals and changes in their morphologies with time. Figure 48 shows the variation in morphology of crystals with both increase in concentration as well as an incubation time. It is evident that at higher concentration with longer incubation time ( $\text{Ca}^{+2} = 50 \text{ mM}$ , 3 and 7 days), the crystals sizes are bigger, with clear arrangements giving rise to floral morphologies. While at lower concentration and after 1 or 3 days of incubation, the crystals were irregularly arranged rod and circular structures. The kinetic model for gypsum crystallization explains this trend as follows (Lee et al., 2000; Ozkar, 2001; Shih et al., 2005).

$$\frac{dm}{dt} = k (C_m - C_s)^n \text{-----}(31)$$

$C_m$  refers to gypsum concentration and  $C_s$  denotes the calcium sulfate solubility at the experimental conditions,  $k$  is the growth rate constant and  $n$  represents the order of kinetics.

At lower saturation conditions and after incubation of 1 and 3 days, formation of NaCl crystals were also noted attached with newly formed  $\text{CaSO}_4$  in the presence of bacteria. EDX mapping in Figure 49a, shows the interesting transition and formation of both NaCl and  $\text{CaSO}_4$  crystals together after only 1 day of incubation at concentration of calcium (30 mM) under the influence of microorganisms. The distribution of carbon (representing bacteria and biofilm), calcium and sulfate ions (showing  $\text{CaSO}_4$  crystal), and sodium and chloride ions (demonstrating NaCl crystallization) on the surface of the

membranes is evident. These results clearly indicate the initiation, formation and growth of biologically mediated minerals (gypsum and sodium chloride) on the membranes.

The floral structures represent increased rate of minerals formation because at low saturation conditions, gypsum crystals are of needle-like structures. Whereas, at higher saturation conditions, gypsum crystals grow further to form rosette structures. The results of IC (Figure 49b) further confirmed the SEM-EDX results, as the concentration of calcium ions reduced consistently with increase in incubation times and concentration of calcium ions. At 95% significance level, it was noted that the concentration of calcium ions remaining under the influence of microorganism was significantly less than their respective controls (solutions without bacteria inoculated).



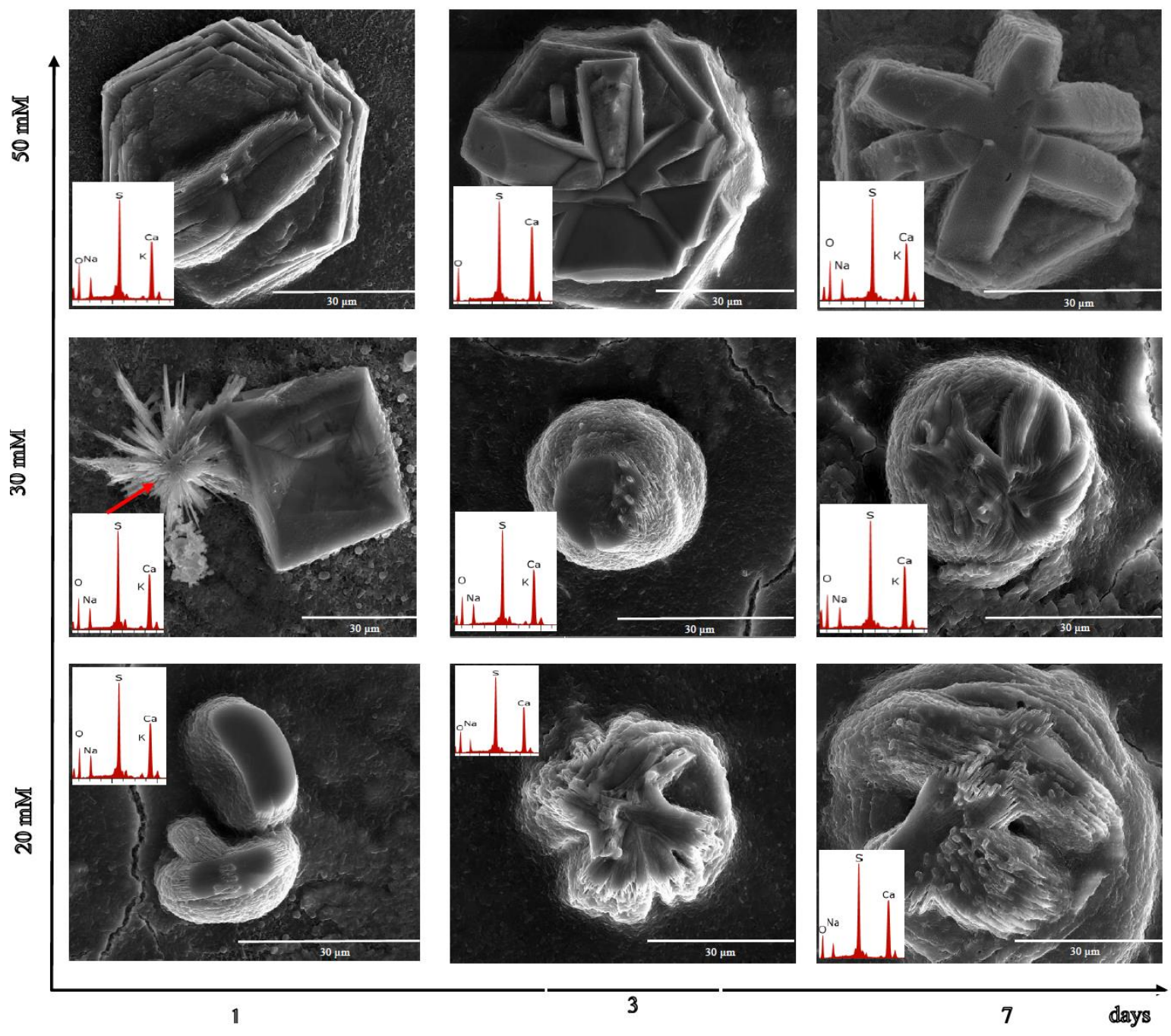
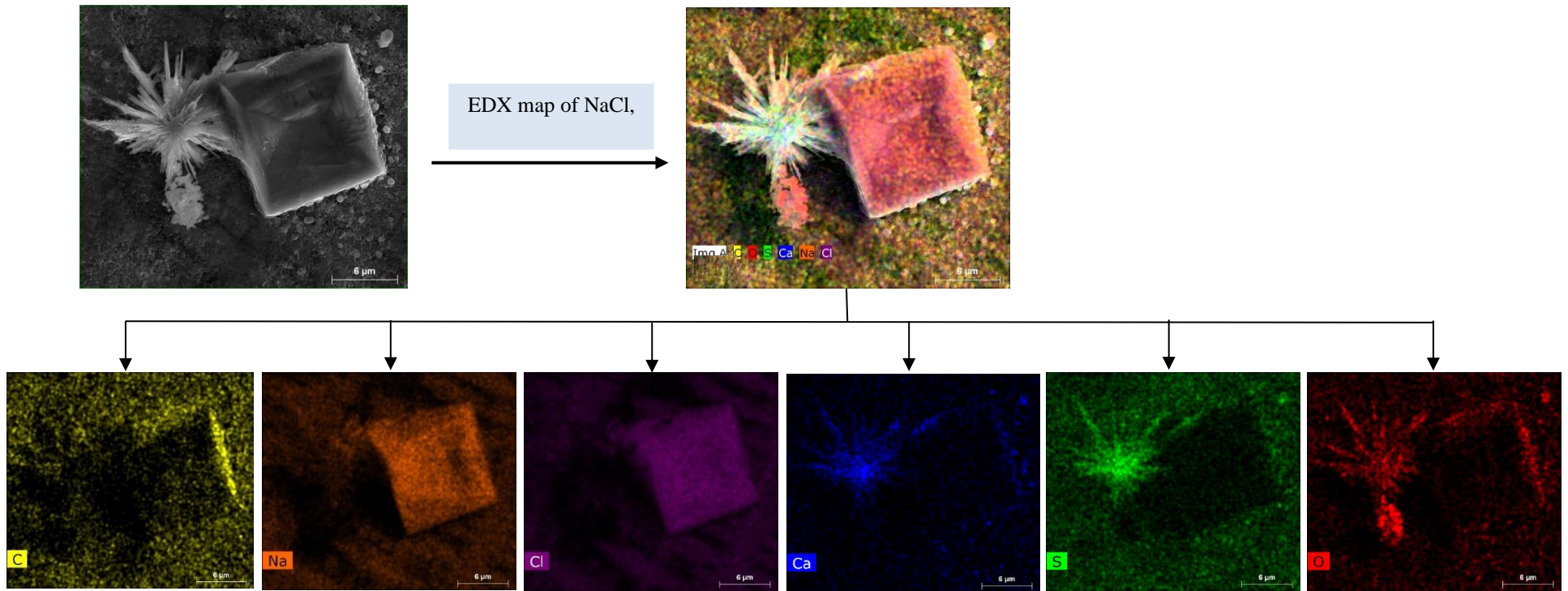
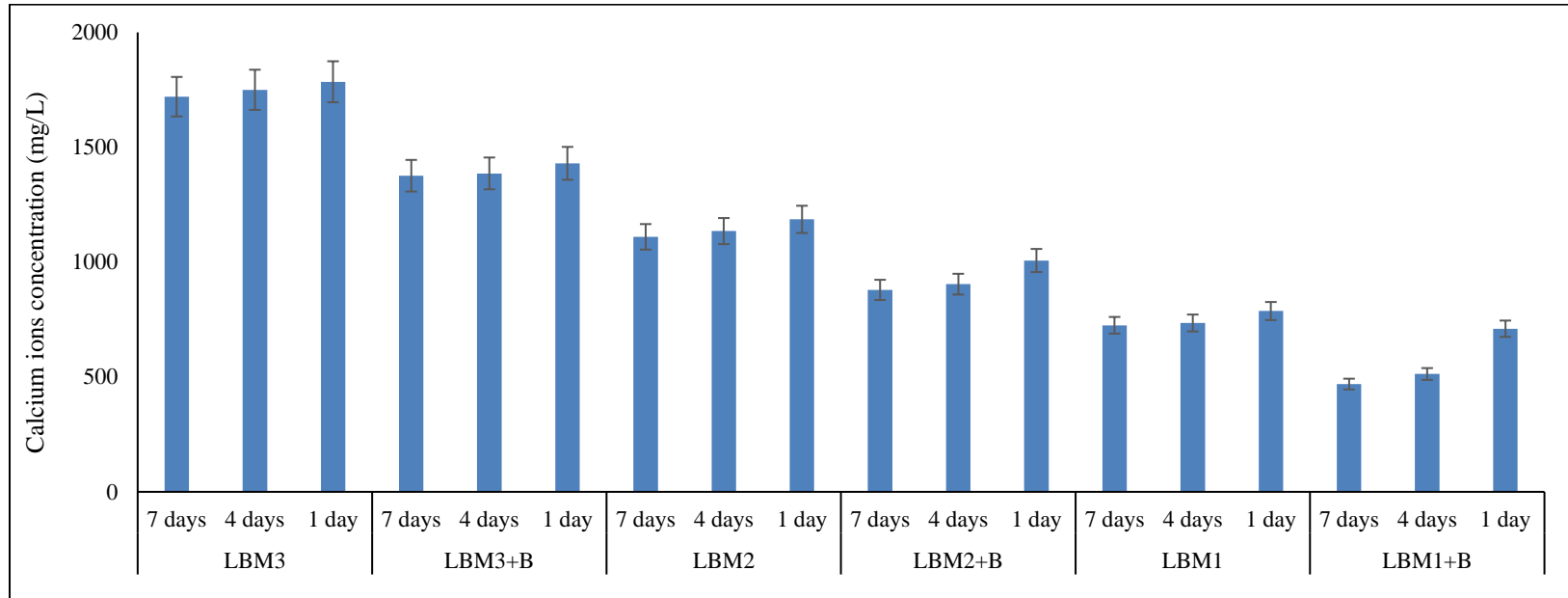


Figure 47. Kinetics and effect of calcium and sulfate ions concentration on  $\text{CaSO}_4$  bio-precipitation (Strain used: *H. aquamarina* - (QOFSW-1 (#1)) (Ashfaq et al., 2020b)



(a)

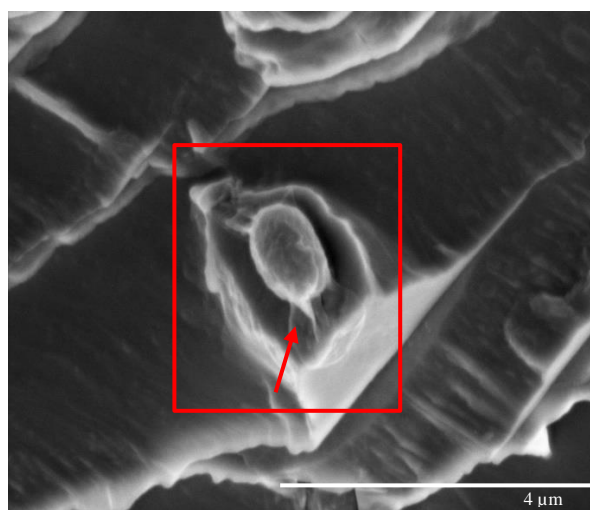


(b)

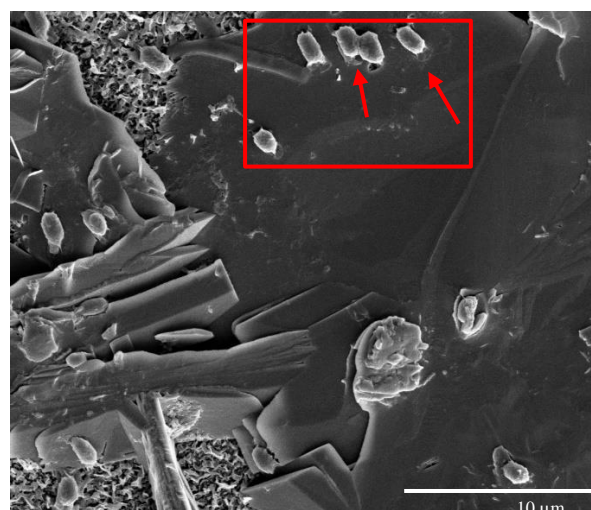
Figure 48. (A) EDX mapping of  $\text{CaSO}_4$  and  $\text{NaCl}$  crystals formed in the presence of bacteria at low concentration ( $\text{Ca}^{+2}$  and  $\text{SO}_4^{-2} = 30$  mM, LBM2) after 1-day incubation, (B) IC results showing quantitative analysis of  $\text{CaSO}_4$  precipitation – kinetics and effect of calcium ions concentration (LBM3:  $\text{Ca}^{+2}$  and  $\text{SO}_4^{-2} = 50$  mM, LBM2:  $\text{Ca}^{+2}$  and  $\text{SO}_4^{-2} = 30$  mM, LBM1:  $\text{Ca}^{+2}$  and  $\text{SO}_4^{-2} = 20$  mM, B: Bacteria i.e. *H. aquamarina* - (QOFSW-1 (#1))) (Ashfaq et al., 2020b)

#### 6.2.4 Attachment of bacteria and biofilm formation on the surface of gypsum crystals

SEM results showed the attachment of bacteria to the surface of gypsum crystals (Figure 50a-d). It is evident from Figure 50 that the bacterial cells adhered to the surface of crystals influencing the kinetics, growth and morphology of crystals. Microorganisms, in general, have been shown to adhere to the surface of the minerals to form biofilms (Li et al., 2019). Several factors control the adhesion of bacterial cells to the mineral such as surface properties of bacteria (Cai et al., 2013; Cao et al., 2011) and the mineral (Wu et al., 2014) and also the chemical characteristics of the medium (Tuson and Weibel, 2013). Hence, in this case, the cations from gypsum may have assisted in the attachment of bacterial cells (Perdrial et al., 2009). In addition, the adhesion can also result through EPS (Poorni and Natarajan, 2013; Ghashoghchi et al., 2017), protein-binding receptors (Poorni and Natarajan, 2013) and/or through the secretion of slime layer from the cells as evident from SEM images (e.g. Figure 50a).



(a)



(b)

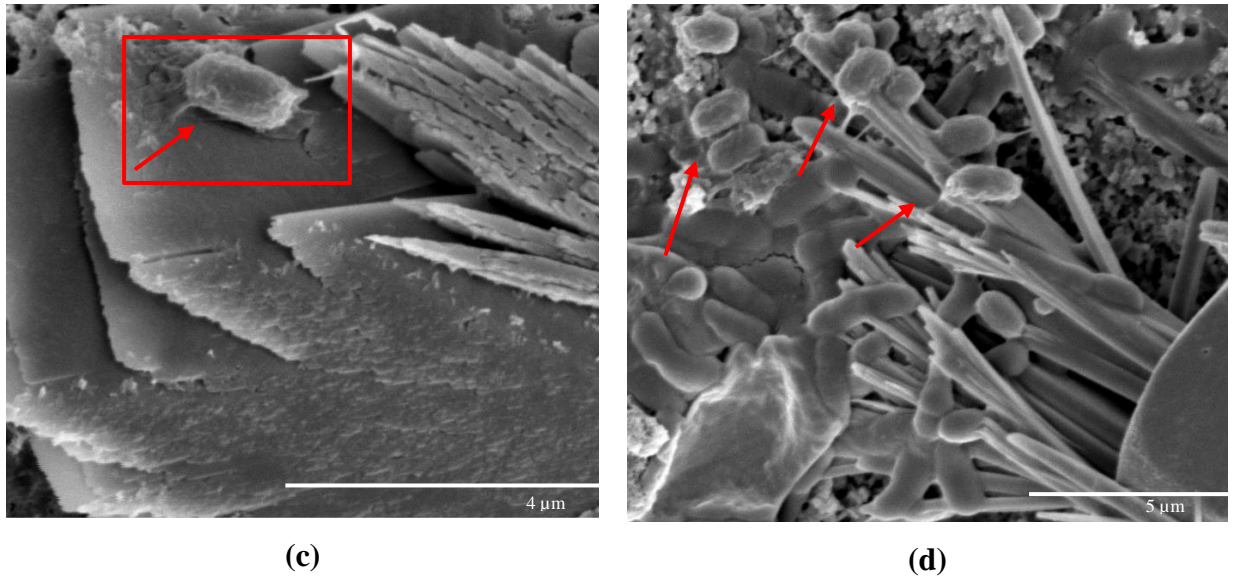
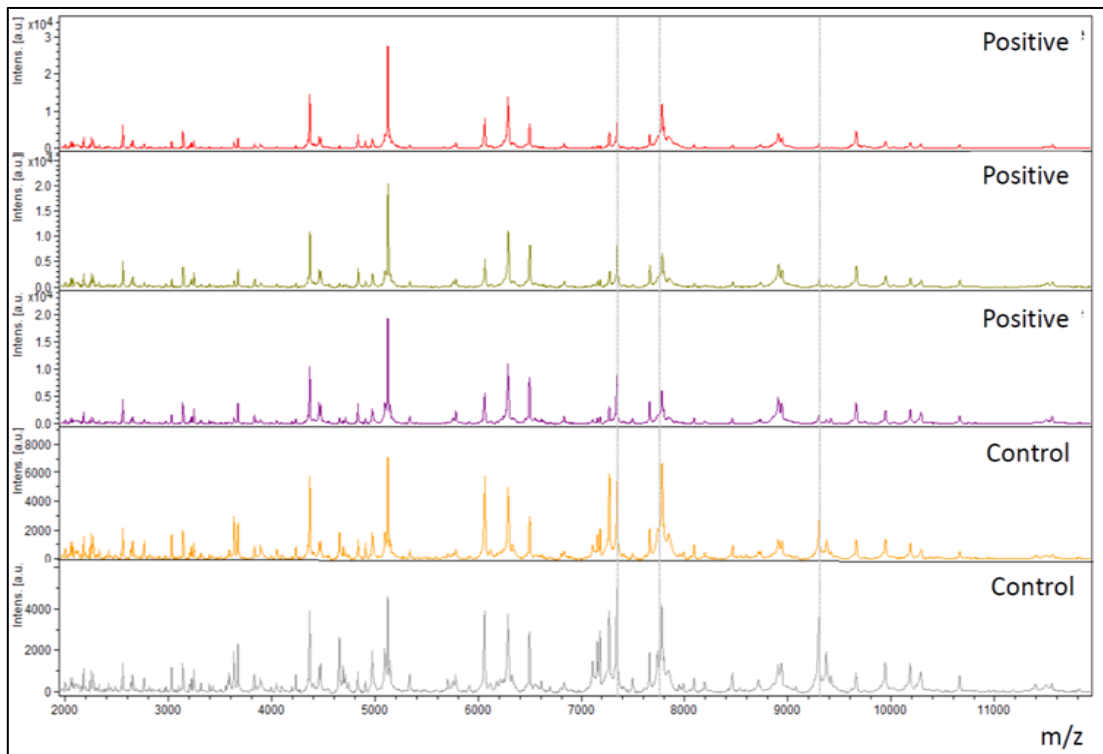


Figure 49. Attachment of bacteria to gypsum crystals and formation of biofilm in LBM3 medium (a) *H. aquamarina* (QOFSW-1 (#1)), (b) *P. stutzeri* (QOFSW-2 (#3)), (c) *P. fragi* (QOFSW-3 (#2)), (d) *H. aquamarina* (QOFSW-5 (#2)) (Ashfaq et al., 2020b)

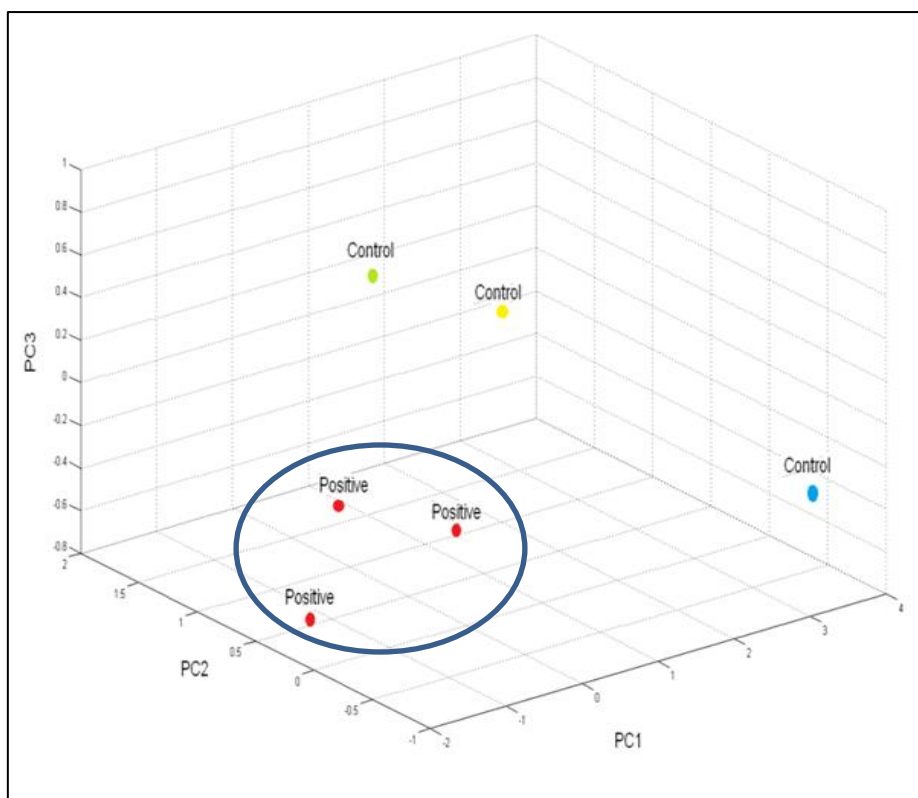
#### 6.2.5 Role of proteins in biomineralization of $\text{CaSO}_4$

Extensive production of EPS associated with the identified species of the aerobic bacteria may play a crucial role in providing the templates and/or the nucleation sites for mineral formation (Bontognali et al., 2014). Many reported researches showed the involvement of exopolysaccharides and proteins in biomineralization (Al Disi et al., 2019). In this research, we also investigated the role of proteins in  $\text{CaSO}_4$  precipitation. As shown in Figure 51a, there are visible changes in the protein spectra of the biomineralizing cells as compared to the control cells. Figure 51b shows the results of PCA in which the biomineralizing cells are clustered separately than the control cells demonstrating the significant variation in their protein spectra resulted during biomineralization. The results indicate that the overall protein expression by bacterial cells played important role in precipitation of  $\text{CaSO}_4$ . These results have significance in developing anti-fouling techniques as it showed that the protein is also one of the

important organic macromolecules involve in membrane fouling, in addition to polysaccharides and lipids.



(a)



(b)

Figure 50. Discriminating the protein profiles of cells involved in biomineralization (a) Direct visual method (b) Through PCA (Strain used: *H. aquamarina* - (QOFSW-1 (#1), Medium used: LBM3,  $\text{Ca}^{+2}$  and  $\text{SO}_4^{-2} = 50 \text{ mM}$ ) (Ashfaq et al., 2020b)

#### 6.2.6 Effect of calcium ions on bacterial growth

The cell wall of bacteria contains variety of divalent cations such as  $\text{Ca}^{+2}$ , and  $\text{Mg}^{+2}$ . These ions allow bacteria to carryout variety of functions such as metabolic regulation, enzymatic actions and maintains the integrity of the outer membranes. Therefore, it is important also to investigate the effect of calcium ions on the growth of bacteria used in this research. It was done by comparing the bacterial growth in LB medium with the growth in LB modified medium (i.e. supplemented with calcium ions). It was noted that the bacterial growth was enhanced in the medium containing additional source of calcium ions. Thus, the presence of calcium ions significantly enhanced the growth of all bacteria studied at 95% confidence level (Figure 52). It was also noted that the *H.*

*aquamarina*, a halophilic bacterium, had lowest growth rate in both LB and LBM media possibly due to the presence of less salt concentration i.e. 1%. Whereas, strains of *Pseudomonas* were found to exhibit highest growth rates in the media used. Therefore, the presence of these ions in RO systems have major implications in promoting the growth of bacteria, their attachment to the membrane surface and promote biofilm formation causing biofouling.

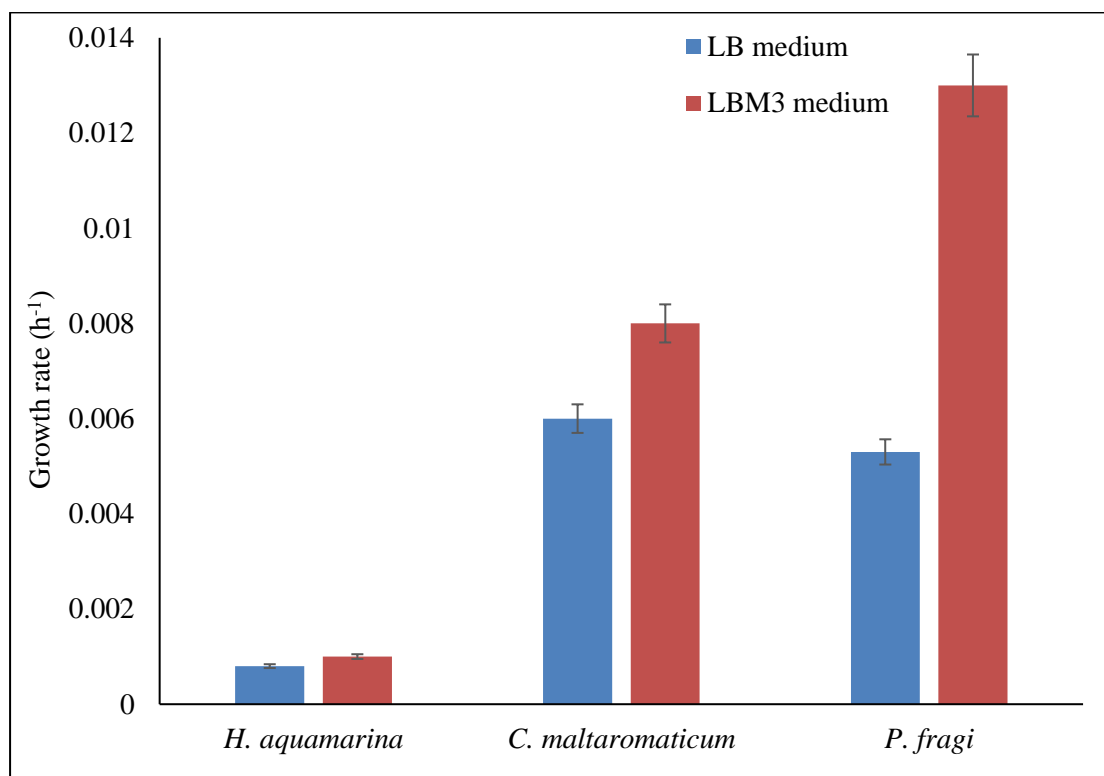


Figure 51. Growth rates of bacteria in LB and LBM medium (LB – Luria Bertani, LBM3 – Luria Bertani medium supplemented with Ca<sup>+2</sup> ions = 50 mM, 2000 mg/L) [H. aquamarina: QOFSW-1 (#1), C. maltaromaticum: QONSW-2 (#2) P. fragi: QOFSW-3 (#2)] (Ashfaq et al., 2020b)

### 6.3 Discussion

The strains utilized in this research include *H. aquamarina*, *P. fragi*, *P. stutzeri* and *C. maltaromaticum*. The ecological importance of *Halomonas* bacteria can be



found through their oil degrading capabilities (Sorkhoh et al., 2010), and biomineralization potential for calcium carbonate via ureolytic activity (Arias et al., 2017). Moreover, EPS production and ability to adhere to surfaces increases their potential to form biofilm and cause biofouling (Rodriguez-Calvo et al., 2017, Zhang et al., 2011; Ivnitsky et al., 2010; Bereschenko et al., 2010). *Pseudomonas fragi*; a Gram-negative psychrophilic bacillus, is generally present in temperate water (Wang et al., 2017) and has been shown to produce biofilm (Wirtanen and Mattila-Sandholm, 1994) and cause food spoilage especially meat, fishes and other marine organisms (Ercolini et al., 2007; Tryfinopoulou et al., 2002). Several strains of *Halomonas* and *Pseudomonas* isolated from seawater of the Arabian Gulf were also previously reported to possess antiscalant degradation potential (Ashfaq et al., 2019a). Another bacteria isolated from Qatari seawater and used in this research was *Carnobacteria maltaromaticum*, which is ubiquitous lactic acid bacteria (LAB) and has been previously isolated from both temperate and cold environments such as Antarctic lakes (Leisner et al., 2007), Arctic and Antarctic seawater as well as the deep sea (Toffin et al., 2004; Lauro et al., 2007), and freshwater habitats from the temperate zone, including rivers in the northwest region of Spain (Gonzalez et al., 1999). It appears that the temperate/polar aquatic and terrestrial environments are both natural habitats of *C. maltaromaticum*.

In this research, all the studied strains were found to produce calcium sulfate precipitates on the RO membrane. Light microscopy results showed the formation of acicular shaped crystal structures which have been designated as gypsum ( $\text{CaSO}_4 \cdot 2\text{H}_2\text{O}$ ) in the literature (Gominsek et al., 2005; Cakal et al., 2006; Al-Youssef, 2015). Moreover, needle-like and floral structures seen under SEM have also been interpreted as gypsum crystals in many researches and were confirmed through X-ray

diffraction technique (XRD) and/or Fourier Transform Infra-red (FTIR) spectroscopic techniques (Ashfaq et al., 2019b; Antony et al., 2011; Rahman, 2013; Shih et al., 2005). In this research, XRD and FTIR were not used due to lower amount of gypsum precipitates obtained in the experimental conditions employed. Changes in morphology of crystals from needle like crystals (at lower concentration and incubation times) and rosette structures (at higher concentration and incubation times) were also observed. Similar variation in morphology of crystals was also noted in our previous research as a result of increase in temperature and saturation conditions, but in the absence of bacteria (Ashfaq et al., 2019b). In human-altered environments, few cases of formation of gypsum in the presence of bacteria have been described in the literature (Driessche et al., 2019, Lepinay et al., 2018, Harouaka et al., 2016).

There are *two mechanisms* through which bacteria can induce/mediate biomineralization (Ashfaq et al., 2020b, 2020c).

(1) *Adsorption of cations* such as calcium in the case of  $\text{CaSO}_4$ , around the cell membrane surface, or cell wall and on the layers of EPS are the ways through which bacteria can serve as a nucleus for mineral precipitation (Ferris et al., 1991; Braissant et al., 2003). With the presence of sulfate ions in the medium, gypsum formation may result within the biofilm (Farias et al., 2014). For instance, evaporation could be major factor for crystallization but the ability of bacterial cell/EPS to bind to calcium ions explained the formation of gypsum at significantly higher rates in microbial mats than anywhere else in the system (Driessche et al., 2019). The  $\text{Ca}^{+2}$  pump of the bacteria has been known to be located towards the cell exterior (Rosen, 1987), and it has higher potential to adsorb on the negatively charged bacterial cell because it has greater power for ionic selectivity (Maier et al.,

2000). Similar mechanism has been proposed for calcium carbonate precipitation in which calcium ions get adsorbed and concentrated around the cell surface, while, metabolism of organic matter in the media such as acetates, peptone, and yeast extract releases carbonates required for precipitation of  $\text{CaCO}_3$  (Ehrlich, 2002; Rivadeneyra et al., 2004; Sanchez-Roman et al., 2007). However, the metabolic activity of bacteria is important for  $\text{CaCO}_3$  precipitation as it supplies necessary carbonates ions, in addition to developing appropriate microenvironment in terms of increased pH and ionic concentration. Nevertheless, the metabolic activity of bacteria is not compulsory for the formation of  $\text{CaSO}_4$  as the sulfate ions may already be present in the media solution such as in seawater. That is why,  $\text{CaSO}_4$  precipitation also occurred in the presence of inactivated autoclaved bacterial cells in this research.

(2) *Changes in solution chemistry* such as sulfur oxidizing bacteria can convert hydrogen sulfide into sulfate resulting in decrease in pH and release of calcium ions due to dissolution of carbonates. Thus, the release of sulfate and calcium ions can result in gypsum formation. This phenomenon has been described in the literature (Harouaka et al., 2016; Mansor et al., 2018). For example: below the gypsum layers on the pre-historic decorated Sorcerer's cave walls in France, dense biofilms have been discovered. The biofilm was composed of autotrophic sulfur oxidizing bacteria (such as *Actinobacteria*), which might have played significant role in biologically mediated gypsum mineralization (Lepinay et al., 2018). Similarly, the gypsum biomineralization potential of sulfur oxidizing autotrophic bacteria was also previously reported on stone buildings in tropical environments

(Driessche et al., 2019). Gypsum precipitation experiments performed in the presence of *Acidithiobacillus thiooxidans* (a sulfur oxidizing bacterium) and at low pH using isotopes of calcium also demonstrated the formation of gypsum crystals under the influence of bacteria (Harouaka et al., 2016). In addition, the precipitates formed under the influence of microorganisms were of irregular morphologies, like what was noted in this research as compared to the abiotically formed crystals. Thus, the effects on morphology and isotopic fractionation explained the combined action of organic substances (microbes and associated organics like biofilms/dead cells) on the growth of gypsum (Harouaka et al., 2016).

The formation of gypsum through adsorption can be regarded as *heterogenous nucleation* as the gypsum crystals tend to nucleate and grow on the surface of the membrane cells/ biofilm/EPS. Previous researches have already shown that the presence of a foreign surface can considerably lower the energy barrier required for nucleation, resulting in acceleration of nucleation kinetics and mineral formation on the surface (Hoang et al., 2007). In addition to provide surface for nucleation, the organic molecules can also promote nucleation through specific interactions with the now-forming inorganic phase, which include geometric, electrostatic or stereochemical matching. These interactions will further reduce the interfacial energies and the nucleation barrier (e.g. Mann et al., 1993). For instance, it has been shown that the stronger binders can increase heterogeneous nucleation rates for CaCO<sub>3</sub> precipitation because the overall interfacial energy is reduced (Driessche et al., 2019). In this research, the gypsum formation did not take place merely in the presence of RO membrane (without bacteria) during the experimental period of up to 14 days. Whereas,

in the presence of bacteria and despite at the lowest concentration of ions (i.e. 20 mM), formation of gypsum crystals was noted even after 1 day of incubation. The results show the importance of presence of bacterial cells (and associated organic macromolecules) in initiating the nucleation and enhancing the kinetics of gypsum formation. Therefore, it can be concluded that the microorganisms have the potential to mediate calcium sulfate crystallization at non-precipitating conditions.

The results of SEM also showed the *attachment of bacteria on gypsum crystals*. To explain this adhesion, the theories of DLVO (Derjaguin, Landau, Verwey and Overbeek) (Kim et al., 2010) and the Lewis acid-base interaction (Bayouhd et al., 2009) have been used in the literature. The former helps to calculate the total interaction energy between the bacterial cells and the minerals. While the latter is based on electron donor/acceptor interactions between them in the medium. Hence, in this case, the cations from gypsum may have assisted in the attachment of bacterial cells (Perdrial et al., 2009). EPS is composed of variety of organic macromolecules i.e. proteins, polysaccharides, lipids and nucleic acids (Flemming and Wingender, 2010) and its composition in biofilm may vary with the conditions (Al-Disi et al., 2019; Ashfaq et al., 2019c). The hydrophobic, electrostatic, covalent and polymer-polymer interactions can cause adsorption of bacterial EPS on to the surface of mineral (Tsuneda, 2010) affecting its growth, kinetics and morphology. The negatively charged groups of EPS (such as carboxyl and phosphate) can also assist in its interaction with calcium ions present in the medium. This type of interaction between  $\text{Ca}^{+2}$  and EPS has also been shown to enhance the attachment of bacteria to the clay minerals (Tsuneda et al., 2010).

Alternatively, the presence of these *calcium ions can also enhance bacterial growth, bacterial adhesion to solid surfaces and subsequently biofilm formation*. Previous researches have also shown that the calcium ion concentrations from 0.7 – 1.4

mM in blood and from 0.4-1.7 mM in water can influence the adhesion of bacteria and the formation of biofilm on the surfaces (De Kerchove and Elimelech, 2008; Cruz et al., 2012). Similarly, the results of Guvensen et al., (2012) also showed the potential of divalent cations ( $\text{Ca}^{+2}$ , and  $\text{Mg}^{+2}$ ) to enhance attachment and subsequent biofilm formation by *Sphingomonas paucimobilis*. Das et al., (2014) investigated the interaction of calcium ions with the extracellular DNA (eDNA), as integral part of EPS, and found that the reaction between eDNA and  $\text{Ca}^{+2}$  is favorable in terms of thermodynamics, and that the binding between the two is spontaneous and exothermic due to its highly negative enthalpy. Hence, in addition to enhance the growth rates of bacteria, the calcium ion present in the medium can also interact with the constituents of EPS enhancing the bacterial attachment and promoting biofilm formation.

The results of this research have significant implications in SWRO. The results of this research showed that the microorganisms and scalants (calcium, sulfate ions) interact with each other in two ways.

(1) Microorganisms present in water causes the precipitation of calcium sulfate even when the concentration of calcium/sulfate ions are below the supersaturation conditions resulting in ***microbially mediated enhanced mineral scaling*** (Figure 53)

(2) On the other hand, calcium ions present in water, being the important constituent of cell wall and membrane, enhances the microbial growth. In addition, it interacts with the EPS and microbial cells and aide in the attachment of bacteria to the surfaces. This will ultimately result in ***enhanced membrane biofouling*** (Figure 53).

Since, both the microorganisms and scalants are usually present in feedwater in SWRO systems even at low concentrations, they tend to enhance the effect of each other. This mutual interaction will result in enhanced biofouling and mineral scaling in

SWRO (Figure 53). Thus, the combined effect on membrane fouling due to these microorganism-mineral interactions can result in severe membrane fouling problems which will cause severe permeate flux decline, reduction in solute rejection, shortening of membrane lifespan, reducing its overall efficiency and causing increase in operating and maintenance cost. Hence, future researches should aim to target the foulant-foulant interactions between the two major foulant types in SWRO to tackle the membrane fouling problems in membrane desalination.

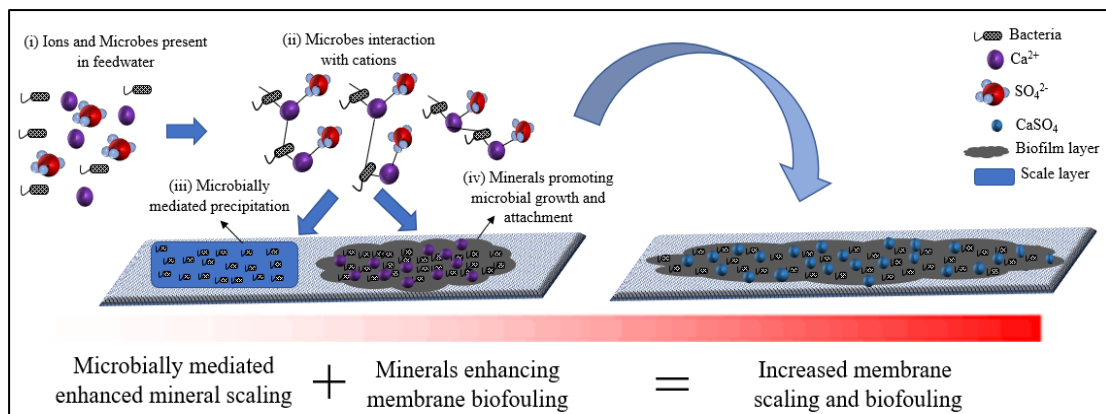


Figure 52. Effect of microbes and minerals' foulant-foulant interactions on membrane fouling (Ashfaq et al., 2020b)

#### 6.4 Conclusion and Future Perspectives

In this research, several strains previously isolated from seawater of the Arabian Gulf were investigated for their ability to induce calcium sulfate precipitation on RO membranes. It was found that all the tested strains were able to form gypsum precipitates at non-crystallizing conditions. The precipitates were not noted in the controls i.e. only in the presence of RO membrane but without bacteria. The results of SEM showed that the formation of various morphologies of crystals resulted demonstrating the influence of microorganisms. With the increase in incubation time and concentration of calcium ions, the size of crystals was bigger, with clear

arrangements and floral shapes. While at lower concentration and less incubation times (1 or 3 days), the crystals were irregularly arranged rod and circular structures. Quantitative analysis for the precipitation also confirmed that the calcium ions remaining in the medium containing bacteria were significantly lower than the controls (i.e. without bacteria) at 95% significance level. EDX mapping of both sodium chloride and calcium sulfate crystals formed by bacteria also showed interesting transition and distribution of various participating elements (carbon, calcium, sulfur, sodium, chloride) on the membrane surface. SEM technique was also useful in investigating the attachment of bacteria to gypsum crystals elucidating the precipitation mechanisms. Furthermore, it was also found that the presence of calcium ions significantly increases the growth rates of bacteria demonstrating their potential to enhance biofouling rates. Therefore, results of this research showed that the microorganisms-minerals interactions can result in both enhanced mineral scaling and biofouling on the membrane surface.

Future research is needed to investigate such microorganisms-minerals interaction under the influence of pressure and turbulent conditions within the RO units. It is important to understand the influence of this interaction on permeate flux decline, membrane solute rejection, and other parameters. Furthermore, use of other techniques such as X-ray diffraction (XRD) and Raman spectroscopy needs to be employed to confirm the polymorphs of calcium sulfate precipitating due to microbial activity. Such results will further help in developing suitable anti-fouling techniques with inherent capabilities to simultaneously reduce both mineral scaling and biofouling and discourage such microorganisms-mineral interactions in SWRO desalination.



## CHAPTER 7 – OBJECTIVE 04: DETERMINE WHETHER NEW COATINGS (GO-PAA, GO-PMA) WILL PREVENT BIOFOULING AND SCALING

### *7.1 Introduction*

Freshwater scarcity is a global issue further exacerbated by population and economic growth. Seawater desalination offers viable alternative to clean water resources. Membrane systems such as seawater reverse osmosis (SWRO) is an economically efficient and environment friendly technology for desalination (Al Najar et al., 2020; Ashfaq et al., 2018). However, it is often susceptible to fouling caused by minerals (inorganic fouling/scaling), organic macromolecules like humic acids (organic fouling), microorganisms (biofouling) and colloidal substances (colloidal fouling). Most of these foulants are often present in feedwater at the same time and interact with each other to cause membrane fouling which then leads to the decrease in performance and increase in operating cost of SWRO (Goh et al., 2019). While, SWRO simultaneously suffers from more than one type of fouling, most of the researchers still tend to focus on mitigating one of the fouling types (Ashfaq et al., 2018). Although, the prevention of one type of membrane fouling may not result in significant improvement of membrane performance due to its sensitivity to suffer from other foulants.

Modifying the membrane surface properties to develop antifouling characteristics is one of the commonly explored approach in membrane fouling research. There are two methods used for surface modification i.e. physical method like blending, and coating and chemical method such as polymers functionalization, graft polymerization and plasma treatment. Graft polymerization is one of the best techniques for grafting of monomers, protecting the membrane surface from various agents and to give distinctive properties to the membranes (Ayyavoo et al., 2016).

Graft polymerization using radiation like UV or microwave is being used widely now for the surface modification of membranes to develop composite membranes with better antifouling properties. Major advantages of this technique include; (i) variety of monomers can be used to polymerize on membrane surface, (ii) the grafting reaction can be controlled in terms of density of graft chains and exact localization to the surface i.e. without affecting the overall properties/composition of membrane, and (iii) formation of covalent bond ensuring long-term chemical stability of membranes (Kochkodan et al., 2014). Previously, UV grafting technique was used for polymerization of methacrylic acid on polysulfone membrane. Moreover, some other hydrophilic monomers like acrylic acid, NVP (N-2-vinyl-pyrrolidone), and HEMA (2-hydroxyethyl methacrylate) have also been grafted on the surface of membrane (Taniguchi and Belfort, 2004). However, the technique is considered sometimes undesirable due to the presence of UV radiations (Ayyavoo et al., 2016). Therefore, microwave radiations can be used as an alternate technique for polymerization of membranes. It is a powerful method for organic synthesis, which helps to enhance the rates of reactions and distributes heat rapidly and evenly on the surface (Shao et al., 2003; Cao et al., 2001). Microwave radiation was used as an energy initiator in which acrylic acid was used as a modifier on chitosan coated polyethersulfone membranes (PES). It was found that acrylic acid concentration of about 3 (%w/v) was good enough to improve membrane surface properties, salt rejection capability and antifouling properties against organic foulant studied in that research (Mansourpanah et al., 2015).

In the literature, several nanomaterials such as titanium oxide, multiwalled carbon nanotubes and graphene oxide (GO) etc. have been used to functionalize RO membranes in order to reduce biofouling (Saleem et al., 2020; Safarpour et al., 2015;

Inukai et al., 2015). Graphene oxide (GO) has been catching special attention in the field of research and industries due to its unique properties such as antimicrobial activity, hydrophilicity, smoothness, negative charge, and its functionalization with carboxyl, hydroxyl, epoxy, and ether groups (Saleem et al., 2020). It has been used as nanomaterials for its potential against biofouling (Chae et al., 2015). On the other hand, to control mineral scaling, antiscalants like poly acrylic acid (PAA), poly maleic acid (PMA) and poly methacrylic acid (PMAA) are added to the feedwater. However, recent researches have shown their sensitivity to biodegradation which results in their inefficiency to control mineral scaling and their side effects on enhancement of biofouling (Ashfaq et al., 2019a; Ashfaq et al., 2019b, Sweity et al., 2015). Therefore, it is important to develop RO membranes capable of controlling both mineral scaling and biofouling.

Thus, in this research, the polyamide RO membrane was functionalized with GO to impart anti-biofouling characteristics followed by polymerization of monomer antiscalants to produce polymer modified graphene oxide coated RO membranes. The effect of functionalization on membrane surface properties was investigated through Fourier transform infra-red (FTIR), and Raman spectroscopic technique, contact angle measurements, scanning electron microscopy – energy dispersive X-ray spectroscopy (SEM-EDX), and atomic force microscopy (AFM) techniques. The performance of modified membranes against mineral scaling was investigated in the presence of laboratory prepared calcium sulfate feed water and performance indicators such as decline in permeate flux with time and percentage salt rejection were measured. Moreover, the scale layer formation after the scaling experiment was characterized using SEM-EDX, XRD and FTIR technique. The biofouling tests were performed through determining bacteriostasis rates of the modified membranes. In addition, the

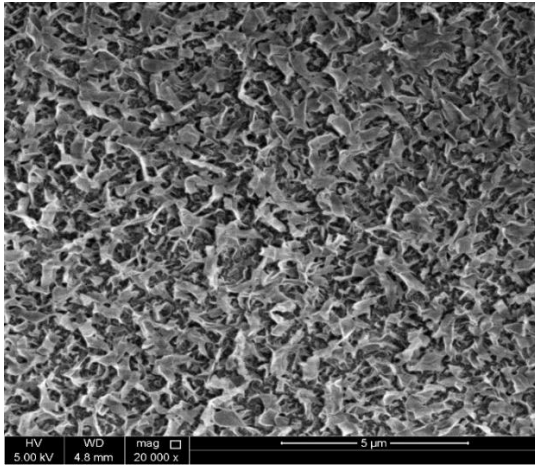
inhibition of both scaling and biofouling, simultaneously was also investigated.

## *7.2 Results and Discussion*

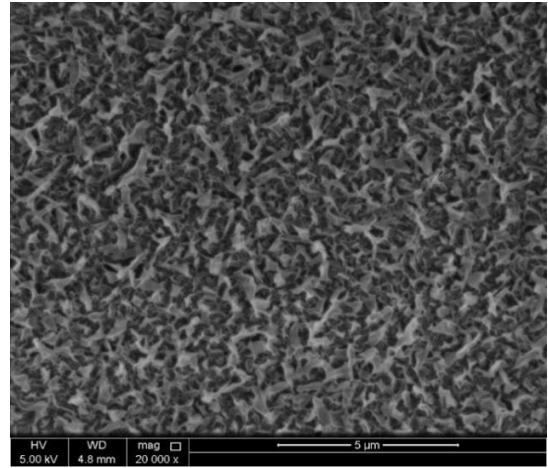
### *7.2.1 Membrane surface characterization*

*7.2.1.1 Scanning electron and Atomic force microscopy.* The leaf-like ridge and valley structure of the unmodified polyamide RO membrane is visible in SEM images (Figure 54). Due to the “edge effect”, the ridges are represented by brighter parts, whereas, the protruding ridges are generally shown by the brighter regions (Chae et al., 2015). In consistent with the literature (Ali et al., 2019; Croll et al., 2017; Ma et al., 2017), the presence of GO on the RO membrane can be seen through the darker regions on the surface (Figure 54b and 54c). With the increase in content of GO, these regions tend to appear denser in SEM images (Ali et al., 2019).

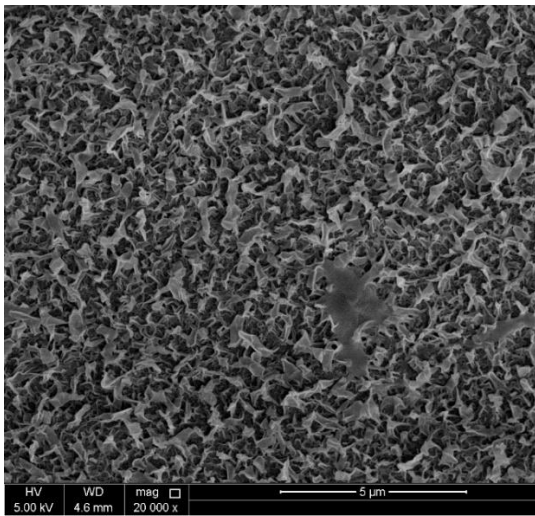
In consistent with SEM results, the AFM analysis showed that the membrane surface roughness decreased after functionalization from 74.709 nm of unmodified RO membrane to 61.555 and 61.752 for PAA-GO@RO and PAA-GO@RO\*, respectively. As seen in the AFM images, the functionalization of membranes resulted in reduction of valleys' depths leading to overall reduction in surface roughness of the membrane. Previous researches have also shown reduction in membrane surface roughness after coating with GO (Ashfaq et al., 2020a; Cao et al., 2018) and after polymerization of acrylic acid (Mansourpanah et al., 2015). Similarly, the membrane surface roughness also reduced after functionalization with PMA-GO.



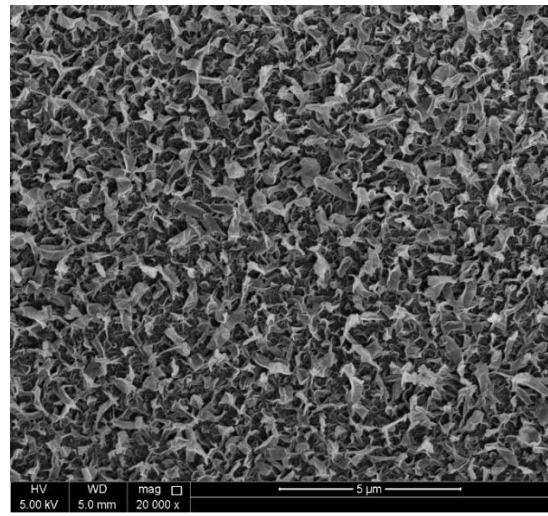
(a)



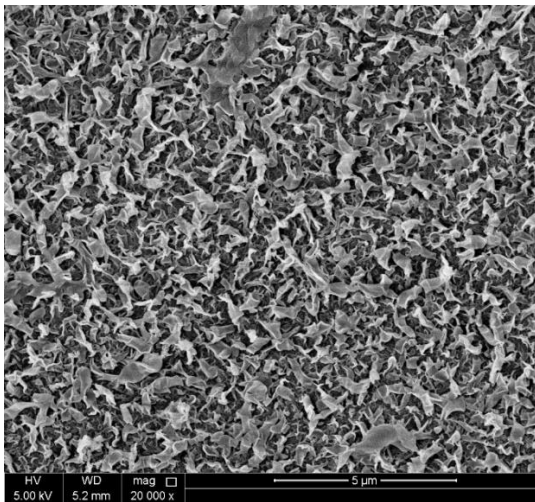
(b)



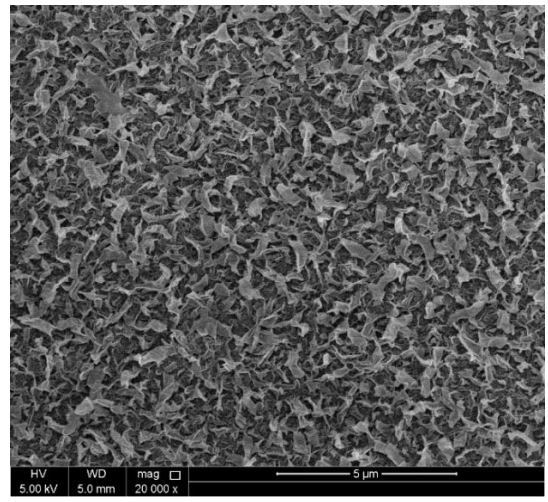
(c)



(d)



(e)



(f)

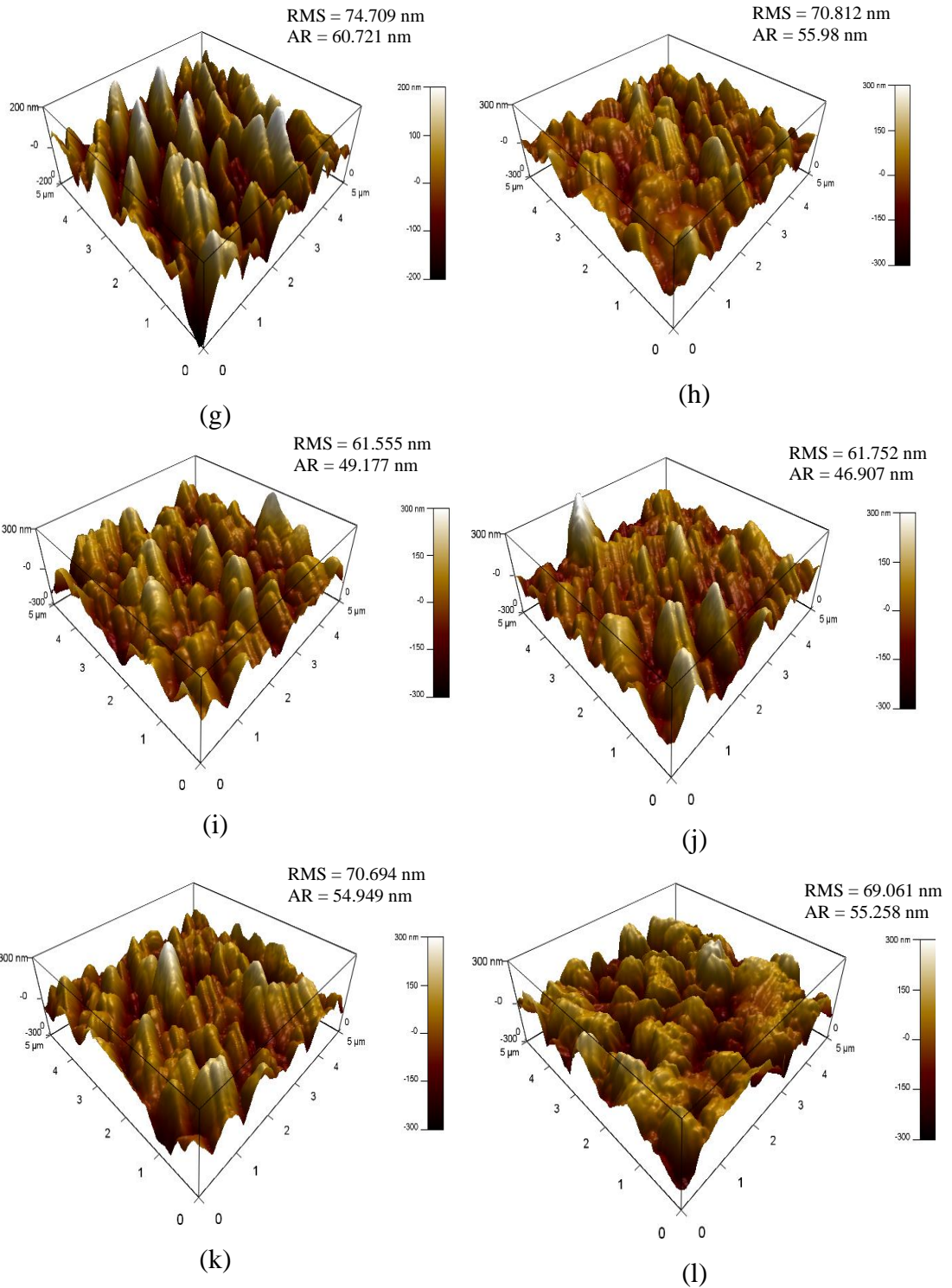
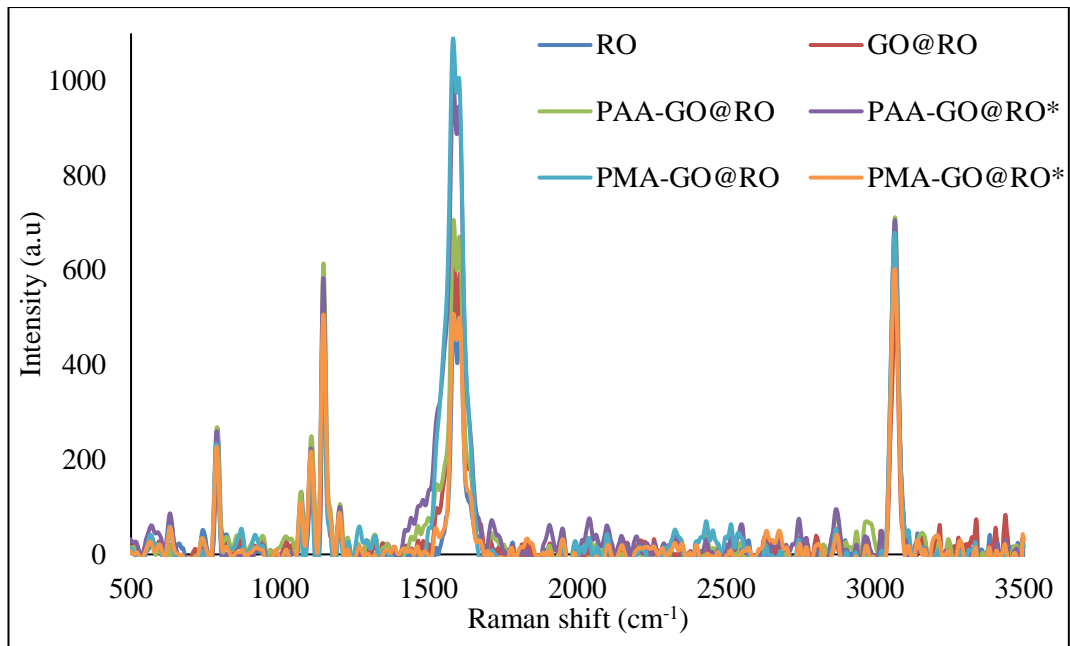
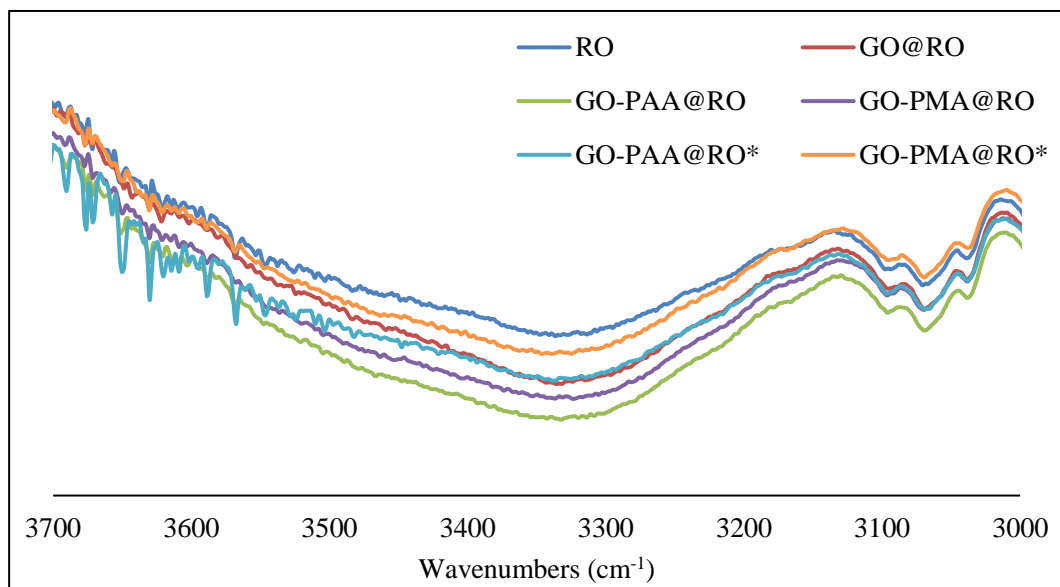


Figure 53. SEM images of the membrane surface (a) RO; (b) GO@RO; (c) PAA-GO@RO; (d) PAA-GO@RO\*; (e) PMA-GO@RO; (f) PMA-GO@RO\*; and AFM images of (g) RO; (h) GO@RO; (i) PAA-GO@RO; (j) PAA-GO@RO\*; (k) PMA-GO@RO; (l) PMA-GO@RO\*

*7.2.1.2 Raman and FTIR Spectroscopy.* Raman spectroscopic technique is useful to confirm the binding of coating materials like GO with the surface of RO membrane. For the case of GO functionalization, it can be confirmed by comparing the ratio of peak at  $1147\text{ cm}^{-1}$  to the peak at  $1585\text{ cm}^{-1}$  (Faria et al., 2017; Perrault et al., 2015). At  $1147\text{ cm}^{-1}$ , the symmetric C-O-C stretching of the polyamide is represented, while, at  $1585\text{ cm}^{-1}$ , the phenyl ring appears in Raman spectrum. Moreover, GO also exhibits its characteristic peak at  $1590\text{ cm}^{-1}$ . Thus, the binding of GO to polyamide membrane will result in decrease of ratio (I<sub>1147</sub>/I<sub>1585</sub>). In this research, it is clearly visible that the peak intensity of  $1585\text{ cm}^{-1}$  increased significantly after functionalization leading to decrease in the ratio from  $1.14 \pm 0.01$  for unmodified RO to  $0.78 \pm 0.1$  after functionalization (Figure 55a) which confirmed the successful coating of GO on the membrane, consistent with SEM observations. Furthermore, the presence of C-H and hydroxyl (-OH) groups from acrylic acid can be seen at peak around  $3027\text{ cm}^{-1}$  and increase in intensity at this peak for modified membranes showed increase in the density of these functional groups as a result of acrylic acid polymerization (Figure 55a). Similar results were also obtained for RO membranes modified with poly maleic acid and graphene oxide (PMA-GO@RO).



(a)



(b)

Figure 54. Spectroscopic analysis of the membrane surface (a) Raman spectra; (b) FTIR spectra

It has been reported that not significantly differences result in FTIR spectra after GO functionalization (Ghaseminezhad et al., 2019; Kim et al., 2016). This is due to the no obvious changes in the overall structure of the membrane surface after GO coating and also because of difficulty to detect small amount of GO dispersed in the matrix.

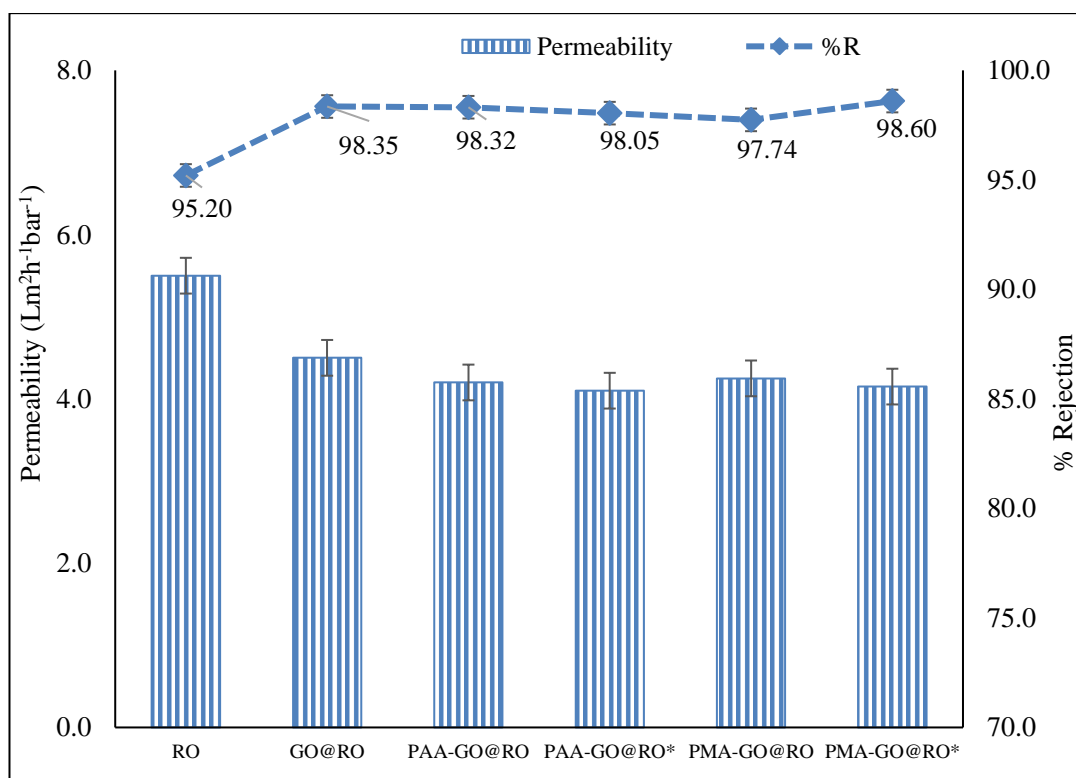


However, the presence of acrylic acid and other polymers of similar structure can be seen through the presence of carboxyl groups at around  $1730\text{ cm}^{-1}$ , given that the concentration of the polymers is significantly high. During our preliminary research, there was appearance of sharp intense peak at  $1730\text{ cm}^{-1}$  demonstrating carboxyl groups and around  $3000\text{ cm}^{-1}$  representing C=C vibration in FTIR spectra when 3.0 wt % monomer concentration was used. However, these peaks did not appear at lower concentration of 0.01 and 0.02 wt %. Nevertheless, some variation specifically in the complex region around  $3300\text{ cm}^{-1}$  were noted. This broad peak centered around  $3300\text{ cm}^{-1}$  is a complex peak because of overlapping of stretching vibration of N-H and carboxylic (-COOH) groups of the polyamide layer (Tang et al., 2009). The increase in intensity for modified membranes could have due to the over-abundance of hydroxyl (-OH) functional groups from GO and poly acrylic acid. Similar observations have also been noted previously (Seyedpour et al., 2018; Zhao et al., 2013; Wang et al., 2012).

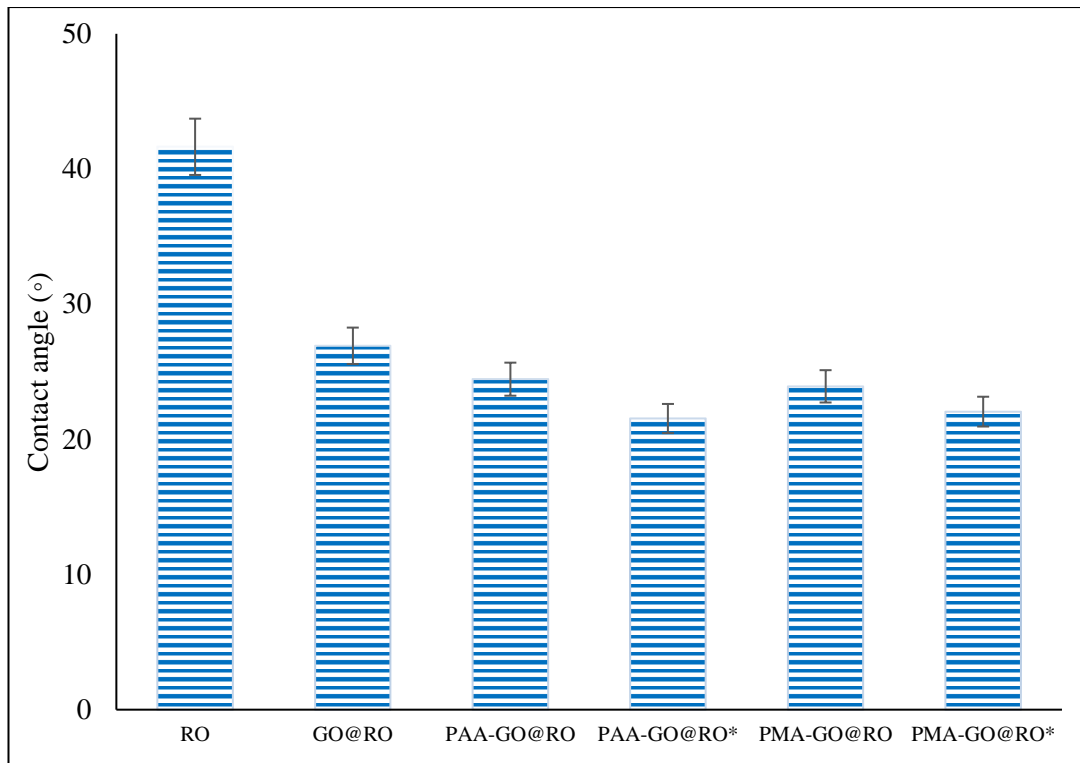
*7.2.1.3 Membrane hydrophilicity and permeation properties.* To investigate the effect of coating on membrane hydrophilicity, water contact angle was measured. The results showed that the membranes became more hydrophilic after functionalization as the water contact angle ( $^{\circ}$ ) of the PAA-GO@RO (0.02) membrane reduced significantly from  $41.7 \pm 4.5^{\circ}$  (RO unmodified membrane) to  $24.4 \pm 1.3^{\circ}$  (Figure 56b). This is consistent with the FTIR results, as the presence of additional carboxylic and hydroxyl groups of GO and PAA could have resulted in the improvement of membrane hydrophilicity. Previous researches have also reported similar results (Cao et al., 2018). Besides the effect of antiscalant (PAA), and antimicrobial GO, the improvement in membrane surface properties such as hydrophilicity and surface smoothness (as shown by AFM and SEM results) could play important role in reducing fouling on modified

membranes (Kochkodan et al., 2014).

Moreover, it was noted that the functionalization of PAA and GO resulted in minor reduction in membrane permeability (Figure 56a), since it is difficult to ensure retention of membrane intrinsic permeability during modification procedure (Faria et al., 2017). The slight loss in permeability could have resulted due to narrowing of pores as a result of polymerization adding further resistance to water flow. The SEM and AFM results also showed the variation in membrane surface topography indicating the changes in membrane porosity may have occurred. Nevertheless, the permeability did not reduce significantly fortunately. When the higher concentration was tested i.e. 3.0% (during preliminary research), up to 90% permeability reduction was obtained. The loss of membrane permeability has also been reported previously for membranes modified through graft polymerization technique (Mao et al., 2018; Goh et al., 2019)



(a)



(b)

Figure 55. Results of (a) Membrane permeability and % salt rejection; (b) water contact angle.

### 7.2.2 Membrane scaling experiment

7.2.2.1 *Permeate flux decline.* To investigate if the mineral scaling is reduced after modification, the membrane was subjected to recirculation of synthetic gypsum solution and the decline of permeate flux during the time of scaling experiment. The antiscalming performance of modified membranes is evident from the results of flux decline during the time of experiment as shown in Figure 57. When the unmodified RO membrane was used, gypsum scaling resulted in severe decline in permeate flux as the 22% reduction in flux was experienced by the end of experiment. Whereas, in the case of modified RO membranes i.e. PAA-GO@RO (0.01), the membrane permeate flux declined by only 10%. With the increase in concentration of acrylic acid i.e. PAA-

GO@RO (0.02), the membrane antiscaling properties further improved as negligible decline in flux occurred during 6-hour long experimental time period (Figure 57). This showed that the polymerization of antiscalant (PAA and PMA) on GO coated RO membrane significantly reduced the extent of membrane scaling in RO membranes. These results were further confirmed through characterizing the scale layer of the membrane after scaling experiment using SEM-EDX, FTIR, and XRD techniques.

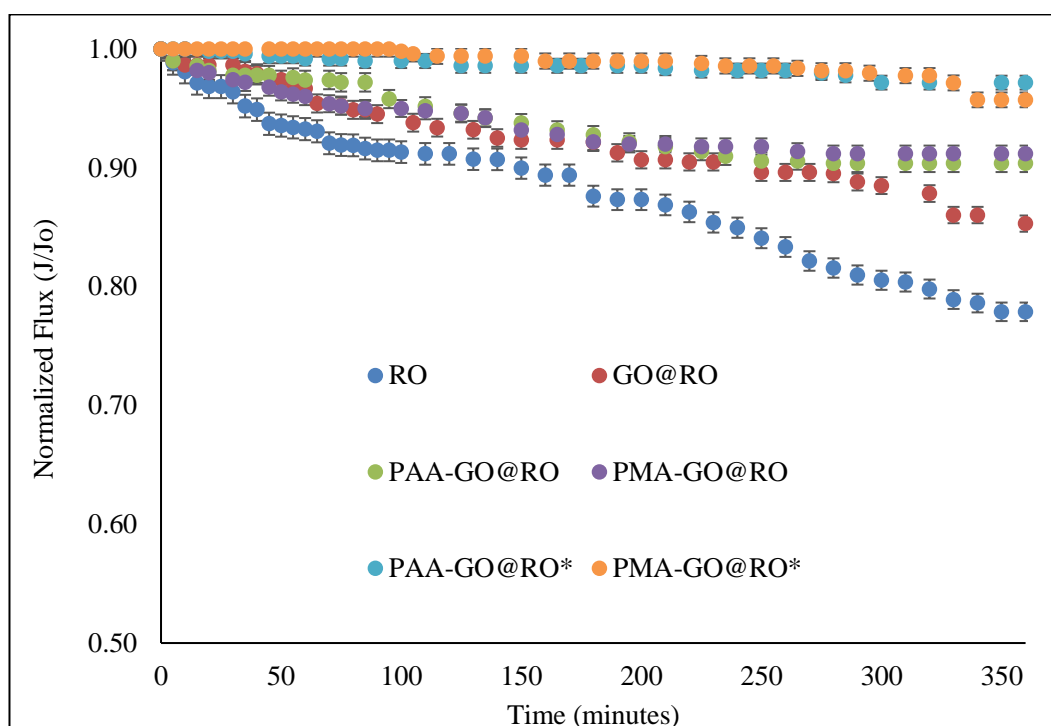
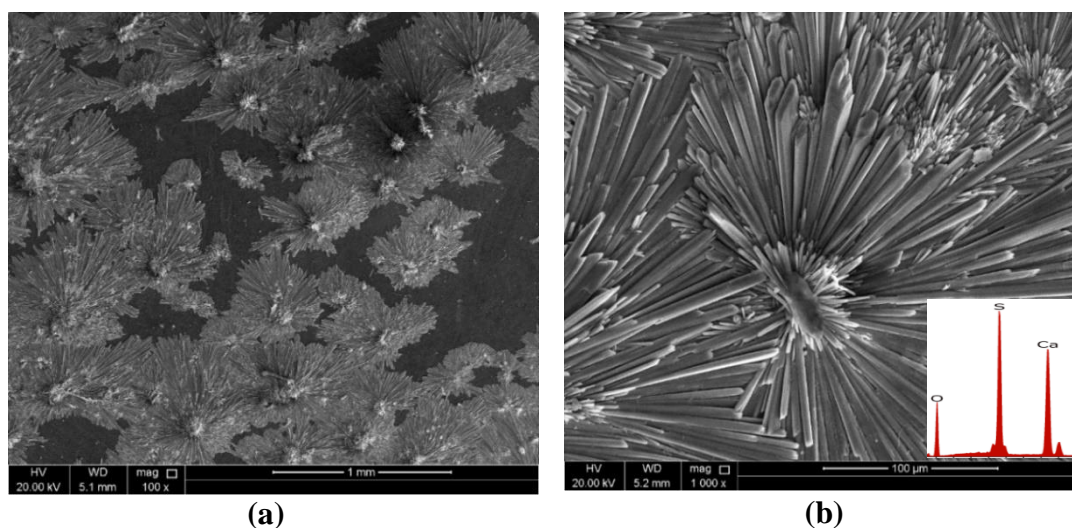


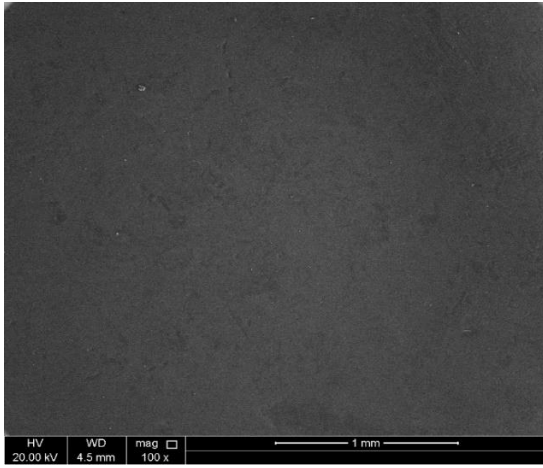
Figure 56. Normalized flux obtained during scaling experiments

*7.2.2.2 Scale layer characterization.* The membrane surface after the scaling experiment was analyzed through SEM-EDX, FTIR and XRD technologies to investigate the formation of calcium sulfate precipitates on the membrane. It is now admitted that scaling on the membrane tend to increase towards the exit region under the influence of concentration polarization (CP) (Shih et al., 2005). Therefore, to compare the performance of different membranes, samples were taken from both entrance (less saturated zone, LSZ) and exit regions (highly saturated zone, HSZ) to

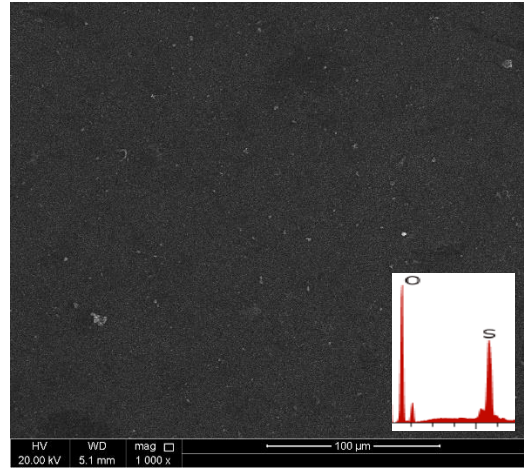
detect the scale layer formation.

The formation of needle like and floral crystals of calcium sulfate can be seen through the SEM images in Figure 58a and the EDX results further confirmed the presence of calcium, sulfur, and oxygen atoms. In the literature, similar morphologies of  $\text{CaSO}_4$  has been reported (Ashfaq et al., 2020a; Rahman, 2013; Antony et al., 2011). The precipitation of minerals on the membrane occurs due to the supersaturation conditions near the membrane surface or due to the presence of substances accountable for formation of crystals or due to the conditions that lead to nucleation (Lee et al., 1999). Generally, the needle like crystals originating from core growth region on the membrane surface as noted in Figure 58a, suggests that the surface crystallization was the RO membrane (Mi and Elimelech, 2010). However, the functionalization of PAA and GO inhibited the scaling to the extent that SEM-EDX did not detect formation of these precipitates on the modified membranes (Figure 58b and 58c).

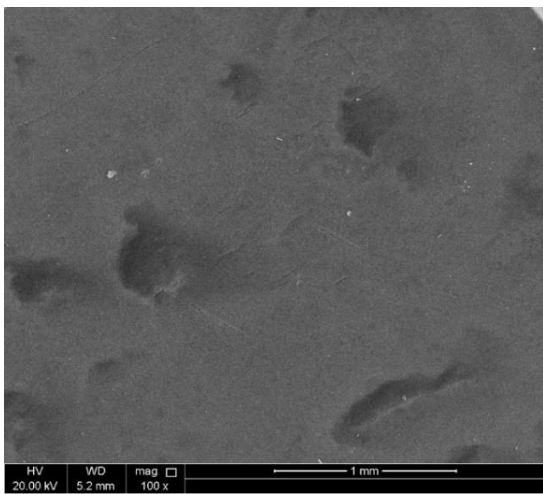




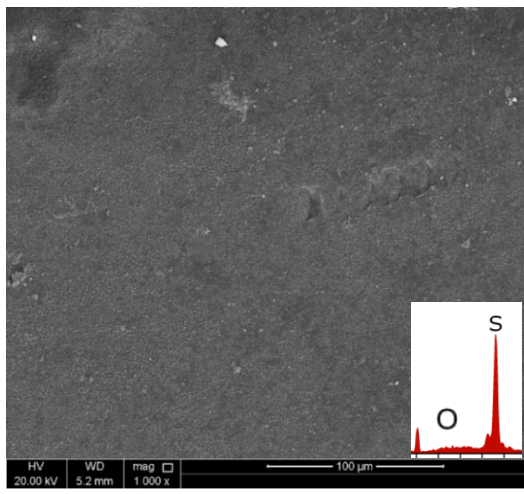
(c)



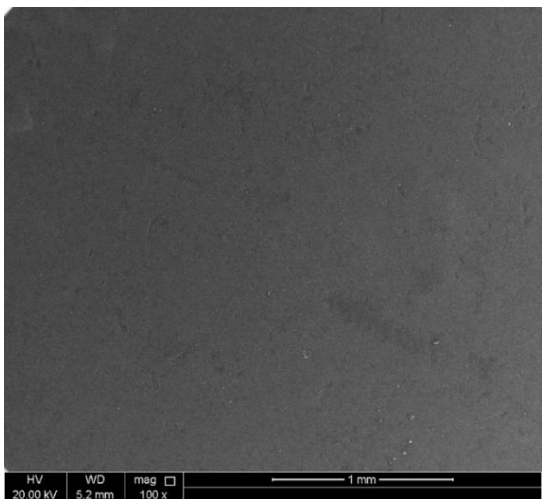
(d)



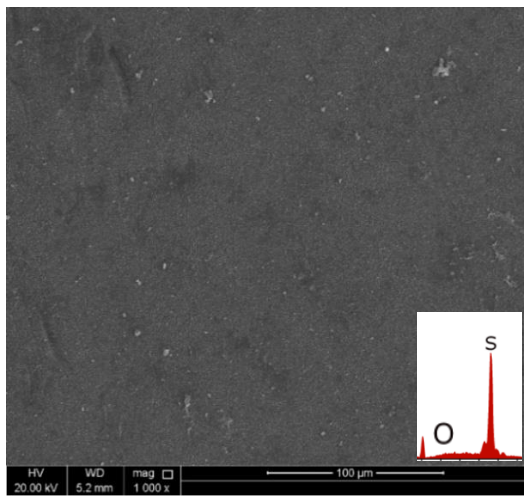
(e)



(f)



(g)



(h)

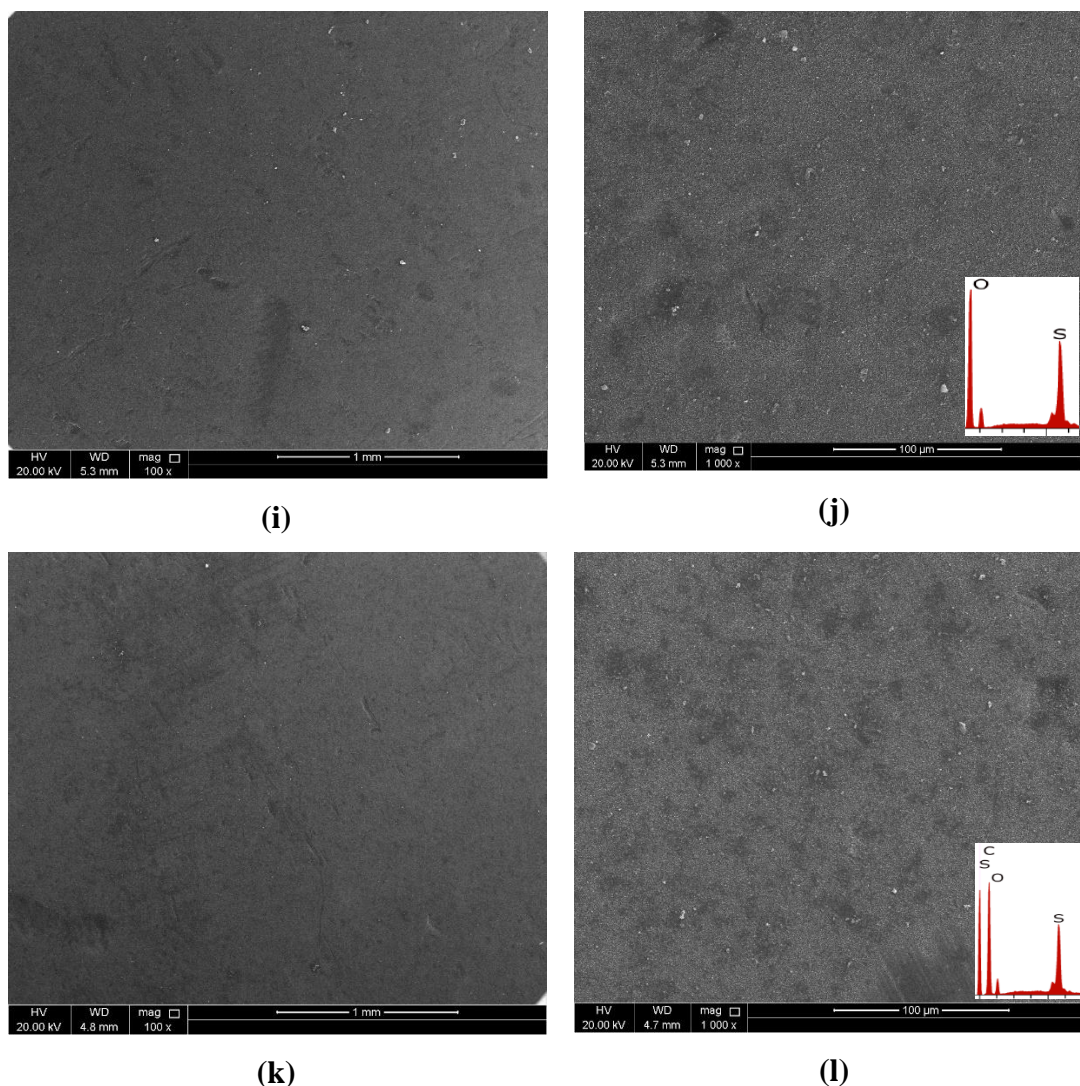
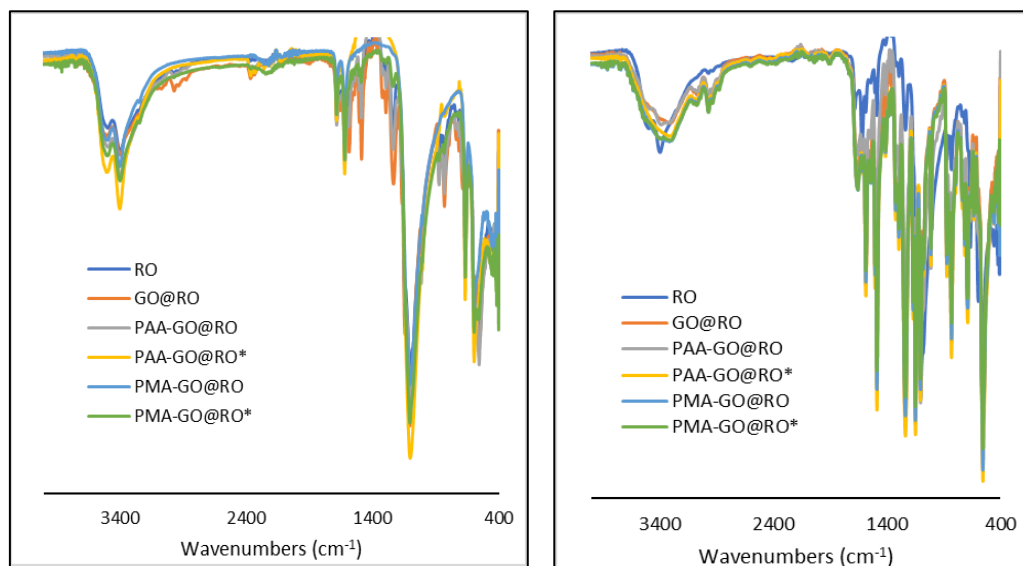


Figure 57. SEM-EDX analysis of the scaled membrane (a, b) RO; (c, d) GO@RO; (e, f) PAA-GO@RO; (g, h) PAA-GO@RO\*; (i, j) PMA-GO@RO); (k, l) PMA-GO@RO\*

FTIR technique was extensively utilized to investigate the scale layer formation at various locations across the surface of the membrane. In general, the strong bands centered around  $1140\text{ cm}^{-1}$  splitting into two components at around  $1146, 1116\text{ cm}^{-1}$  and  $669, 662\text{ cm}^{-1}$  represents stretching and bending modes of  $\text{SO}_4$  from pure gypsum (AlDabbas et al., 2014). In the case of RO membrane, similar spectra for gypsum were obtained for all the samples ( $n=5$ ) taken from both LSZ and HSZ regions. On the other hand, gypsum was detected only at very thin layer towards the most concentrated zone

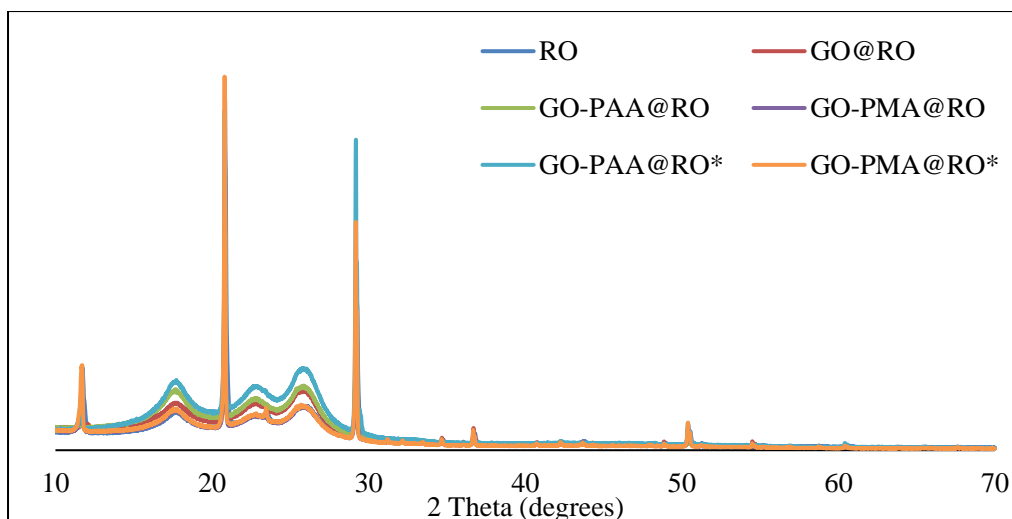
i.e. HSZ after membrane modification (Figure 59b). The XRD results (Figure 59c) provided further confirmation that the precipitates belong to gypsum polymorph of calcium sulfate as the peaks at 11.5, 20.6, 23.1, 29.0° (Farrah et al., 2004) demonstrates the presence of gypsum on the membrane, where detected. Thus, the membrane modification helped to limit the scaling only at more saturated zones in the water channel. The improvement in anti-scaling performance of the modified membranes could have resulted due to the changes in membrane surface properties in terms of hydrophilicity and surface smoothness. At more hydrophilic surface, the gypsum crystals will encounter greater energy barrier for deposition or surface nucleation.



(a)

(b)





(c)

Figure 58. (a) FTIR spectra of the scaled membrane both in high saturated zone (HSZ); (b) less saturated zone (LSZ) on membranes, (c) XRD spectra of the scale layer

### 7.2.3 Biofouling tests

To assess the anti-biofouling properties of the modified membranes, the inhibition of microbial growth was measured for both type of membranes. It was noted that the bacterial cells multiplied exponentially leading to extensive growth of microorganisms in the presence of RO membranes. However, after functionalization with antimicrobial GO, the growth was reduced significantly as more than 94% reduction in CFU/mL was observed (Figure 60).

The antibacterial activity of GO and GO coated surfaces has been extensively studied during the last decade (Akhavan et al., 2010; Nine et al., 2015; Alayande et al., 2019). The properties of GO such as its graphene size, its orientation and its ability to produce reactive oxygen species plays important role in antimicrobial activity (Zhao et al., 2013). Moreover, the electrostatic repulsion between the cell membrane of bacteria and GO sheets can also participate in its antimicrobial activity (Castrillon et al., 2015). Besides, membrane surface properties like topography and surface roughness is also

important in the interaction between GO and the bacterial cells. Generally, the adhesion of bacteria – first step in biofouling; reduces on smoother surfaces (Alayande et al., 2019). In this research, it was also noted that the membrane surface roughness reduced significantly after membrane modification. Hence, both the antimicrobial features of GO as well as improvement in membrane surface properties may have added the antimicrobial property to the membrane.

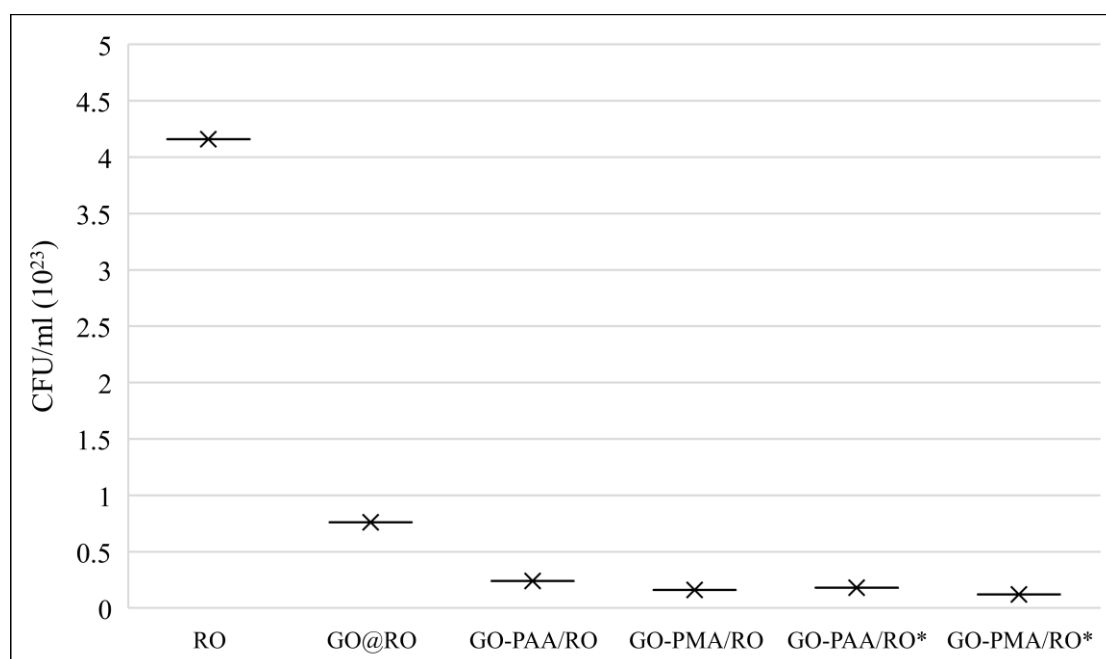


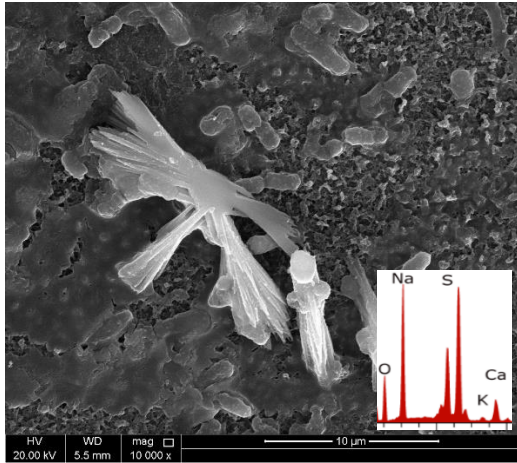
Figure 59. Anti-biofouling performance of membranes after functionalization

#### 7.2.4 Simultaneous inhibition of mineral scaling and biofouling

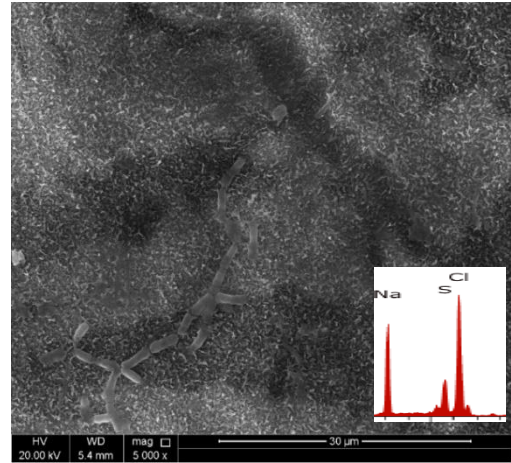
The inhibition of mineral scaling and biofouling simultaneously was also demonstrated through membrane functionalization with antiscalant polymer (poly acrylic acid) and antimicrobial nanomaterial (GO). For this purpose, experiments were performed using supplemented bacterial medium (to study bacterial growth) containing 20 mM of calcium and sulfate ions (to investigate  $\text{CaSO}_4$  precipitation) on the membranes. In this case, the technique of SEM-EDX was utilized as both the microbial

growth and formation of mineral precipitates on the membrane samples can be extensively visualized. It is also expected that the presence of bacteria may have enhanced/induced the precipitation. There are *two mechanisms* through which bacteria can induce/mediate mineralization. **(1) Adsorption of cations** such as calcium in the case of  $\text{CaSO}_4$ , around the cell membrane surface, or cell wall and on the layers of EPS are the ways through which bacteria can serve as a nucleus for mineral precipitation (Braissant et al., 2003). With the presence of sulfate ions in the medium, gypsum formation may result within the biofilm (Farias et al., 2014). **(2) Changes in solution chemistry** such as sulfur oxidizing bacteria can convert hydrogen sulfide into sulfate resulting in decrease in pH and release of calcium ions due to dissolution of carbonates. Thus, the release of sulfate and calcium ions can result in gypsum formation. This phenomenon has been described in the literature (Mansor et al., 2018; Harouka et al., 2016).

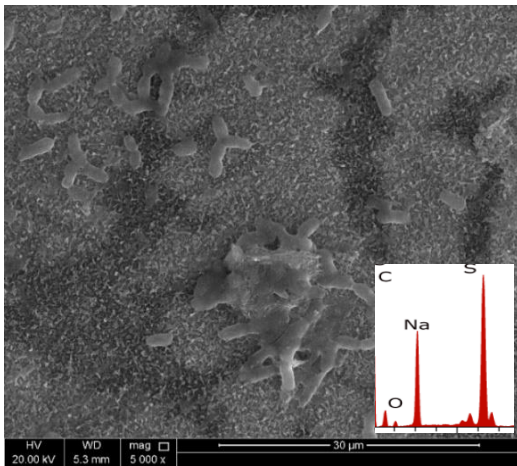
It is evident from Fig. 62c and 62d that the modified membranes were able to inhibit simultaneously both microbial growth and  $\text{CaSO}_4$  precipitation. This further confirmed that the functionalization with PAA-GO and PMA-GO enhanced the performance of RO membranes against membrane fouling and significantly reduced both scaling and biofouling simultaneously.



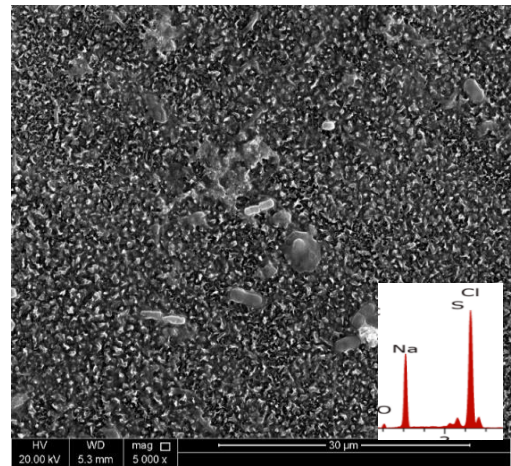
(a)



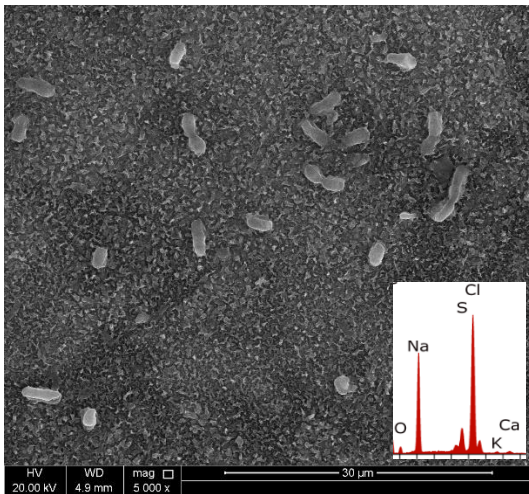
(b)



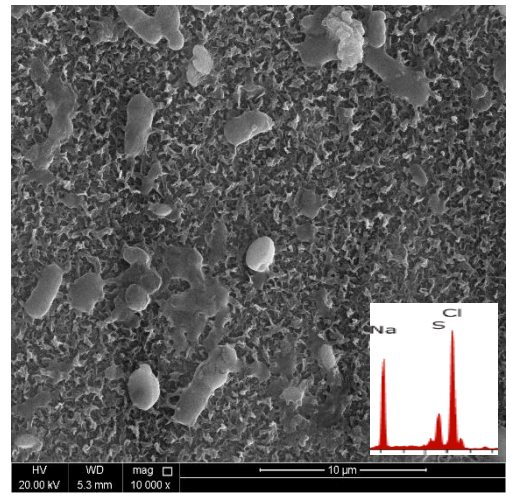
(c)



(d)



(e)



(f)

Figure 60. Simultaneous reduction of biofilm growth and CaSO<sub>4</sub> precipitation after functionalization (a) RO; (b) GO@RO; (c) PAA-GO@RO; (d) PAA-GO@RO\*; (e) PMA-GO@RO; (f) PMA-GO@RO\*

### 7.3 Conclusion

The polyamide RO membranes were coated with commercially available GO followed by polymerization of acrylic acid to confer dual anti-scaling and anti-biofouling properties to the membranes. The characterization of membrane surface after modification using water contact angle, SEM, AFM, FTIR and Raman spectroscopic techniques helped to understand the changes in surface properties in terms of hydrophilicity, surface roughness and presence of functional groups. Both the anti-scaling and anti-biofouling tests were performed to investigate the performance of membranes against both type of fouling. The scaling test results showed that the decline in permeate flux was inhibited by the modified RO membranes as only around 10% and 3% flux decline occurred in the presence of modified membranes. Thus, increase in concentration of acrylic acid or maleic acid helped to improve the anti-scaling performance of modified RO membranes. This was further confirmed by SEM-EDX, FTIR and XRD techniques used to investigate the formation of precipitates on membranes after the scaling runs. The results showed that the precipitation only occurred at highly saturated zone i.e. towards the water flow exit region. Whereas, unmodified RO membrane was found to be fully covered with gypsum precipitates. Moreover, surface modification of RO also inhibited microbial growth up to 97% in comparison to the control membrane. Additional experiments performed on the inhibition of both gypsum precipitation and biofilm formation helped to confirm that the polymer modified graphene oxide coated RO membranes have the potential to

simultaneously reduce both membrane scaling and biofouling in SWRO systems. Thus, further research is being conducted to test the long-term performance of these membranes at pilot-scale and to perform cost-benefit analysis in terms of their application in SWRO.

## CHAPTER 8: CONCLUSION AND FUTURE PERSPECTIVES

Overall, the results of this research helped to understand various unknown interactions between calcium sulfate (as scalant), seawater microorganisms, antiscalants (poly acrylic acid and poly maleic acid) and antibacterial nanocomposites (graphene oxide).

It was found that the intensity of membrane scaling increased with the increase in concentration and temperature of feedwater as reflected by the increase in intensity of flux decline over time as well as mass of crystals formed on the membrane surface, which caused increase in membrane resistance. The morphology of the crystals varied from thin needle like structures to broader floral structures when the scaling got intense. The water contact angle analysis showed that the gypsum scaling on the membrane enhanced its hydrophilicity which may enhance its inter- / intra- foulant interactions with other ions present in water. Since, the presence of other foulants such as microorganisms may also alter the mechanism and extent the membrane scaling as a result of foulant – foulant interactions between them, further research was done on the effect of microorganism on gypsum scaling.

The microorganisms isolated from Qatar seawater were identified as *H. aquamarina*, *H. elongata*, *P. fragi*, *P. stutzeri*, *V. alginolyticus* and *V. fluvalis* using MALDI-TOF MS. By combining the techniques of MALDI-TOF MS with PCA, the isolated strains of *H. aquamarina* and *P. fragi* were categorized into several groups based on their differences in protein spectra showing the biodiversity of such antiscalant degrading bacteria in seawater. It was also noted that the growth rates vary with type of antiscalant and bacteria used. Therefore, initial screening of these antiscalants before their applications at industrial level is important to understand their biofouling

potential. In this research, an easy and quick methodology was also applied to do such screenings. The suggested methodology combined FTIR with multivariate data analysis and conventional microbiological assays to test the effect of antiscalants on biofouling. Thus, the proposed technique helped to classify antiscalants based on their membrane fouling potential and to characterize biofilm components. Both the spectral intensity and CFU count showed that the biofilm was more intense in the presence of poly acrylic acid followed by maleic and acrylic acid.

The selected strains were also tested for their ability to induce calcium sulfate precipitation on RO membranes. It was found that all the tested strains were able to form gypsum precipitates at non-crystallizing conditions. The precipitates were not noted in the controls i.e. only in the presence of RO membrane but without bacteria. The results of SEM showed that the formation of various morphologies of crystals resulted, which demonstrated the influence of microorganisms. Quantitative analysis for the precipitation also confirmed that the calcium ions remaining in the medium containing bacteria were significantly lower than the controls (i.e. without bacteria) at 95% significance level. Furthermore, it was also found that the presence of calcium ions significantly increases the growth rates of bacteria demonstrating their potential to enhance biofouling rates. Therefore, results of this research showed that the microorganisms-minerals and microorganisms-antiscalant interactions can result in both enhanced mineral scaling and biofouling on the membrane surface.

Thus, it is important to develop and modify membrane to control both scaling and biofouling. That is why, in this research, the polyamide RO membranes were coated with commercially available GO followed by polymerization of acrylic acid to confer dual anti-scaling and anti-biofouling properties to the membranes. The characterization of membrane surface after modification using water contact angle, SEM, AFM, FTIR



and Raman spectroscopic techniques helped to understand the changes in surface properties in terms of hydrophilicity, surface roughness and presence of functional groups. Both the anti-scaling and anti-biofouling tests were performed to investigate the performance of membranes against both type of fouling and the results showed that the newly modified membranes had the potential to suppress both scaling and biofouling.

Hence, future research is needed to investigate microorganisms-minerals and microorganisms-antiscalant interactions using sea water under the influence of pressure and turbulent conditions within the RO units. It is important to understand the influence of these interaction on permeate flux decline, membrane solute rejection, and other parameters. Moreover, the methodology for the development of such anti-fouling membranes needs to be optimized in terms of antiscalant concentration, irradiation type and times of irradiation. For this purpose, response surface methodology as a statistical tool is suggested to be utilized. In practice, to solve the problem of membrane fouling, such membranes should also be tested at both Lab-scale (crossflow filtration setups) and Pilot-scale. During such tests, the performance of modified membranes against both scaling and biofouling for longer period, their lifetime and release of nanomaterials into the permeate during desalination should be investigated. Such results will further help in developing suitable anti-fouling techniques with inherent capabilities to simultaneously reduce both mineral scaling and biofouling and discourage such foulant-foulant interactions in SWRO desalination.

## REFERENCES

- Achal, V., Mukherjee, A., Kumari, D., Zhang, Q. 2015. Biomineralization for sustainable construction – A review of processes and applications. *Earth-Science Reviews* 148, 1–17.
- Akhavan, O., Ghaderi, E. 2010. Toxicity of graphene and graphene oxide nanowalls against bacteria. *ACS Nano* 4, 5731–5736.
- Akin, O., Temelli, F. 2011. Probing the hydrophobicity of commercial reverse osmosis membranes produced by interfacial polymerization using contact angle, XPS, FTIR, FE-SEM and AFM. *Desalination* 278 (1–3), 387–396.
- Al-Ahmad, M., AbdulAleem, F.A., Mutiri, A., Ubaisy, A. 2000. Biofouling in RO membrane systems Part 1: Fundamentals and control. *Desalination* 132, 173-179.
- Al-Amoudi, A., Lovitt, R.W. 2007. Fouling strategies and the cleaning system of NF membranes and factors affecting cleaning efficiency. *J. Membr. Sci.* 303 (1-2), 4-28.
- Al-Ashhab, A., Sweity, A., Bayramoglu, B., Herzberg, M., Gillor, O. 2017. Biofouling of reverse osmosis membranes: effects of cleaning on biofilm microbial communities, membrane performance, and adherence of extracellular polymeric substances. *Biofouling* 33 (5), 397–409.
- Al-Dabbas, M., Eisa, M.Y., Kadhim, W.H. 2014. Estimation of gypsum-calcite percentages using a Fourier Transform Infrared Spectrophotometer (FTIR) in Alexandria Gypsiferous Soil -Iraq. *Iraqi J. Sci.* 55 (4b), 1916-1926.
- Al Disi, Z.A., Zouari, N., Dittrich, M., Jaoua, S., Al-Kuwari, H.A., Bontognali, T.R.R. 2019. Characterization of the extracellular polymeric substances (EPS) of

- Virgibacillus strains capable of mediating the formation of high Mg-calcite and protodolomite. *Marine Chemistry* 216, 103693
- Al Disi, Z.A., Jaoua, S., Bontognali, T.R.R., Attia, E.S, Al-Kuwari H.A., Zouari, N. 2017. Evidence of a Role for Aerobic Bacteria in High Magnesium Carbonate Formation in the Evaporitic Environment of Dohat Faishakh Sabkha in Qatar. *Front. Env. Sci.* 5, 1-11.
- Al-Degs, Y.S., Al-Ghouti, M., Salem, N. 2011. Determination of Frying Quality of Vegetable Oils used for Preparing Falafel using Infrared Spectroscopy and Multivariate Calibration. *Food Anal. Methods* 4, 540–549.
- Al-Hamzah, A.A., East, C.P., William, O.S.D., Fellows, C.M. 2014. Inhibition of homogenous formation of calcium carbonate by poly (acrylic acid). The effect of molar mass and end-group functionality. *Desalination* 338 (1), 93-105.
- Al-Ghouti, M., Al-Degs, Y.S., Amer, M. 2008. Determination of motor gasoline adulteration using FTIR spectroscopy and multivariate calibration. *Talanta* 76, 1105–1112.
- Al-Ghouti, M., Al-Degs, Y.S., Amer, M. 2010. Application of chemometrics and FTIR for determination of viscosity index and base number of motor oils. *Talanta* 81, 1096–1101.
- Al-Juboori, R.A, Yusaf, T. 2012. Biofouling in RO system: Mechanisms, monitoring and controlling. *Desalination* 302, 1–23.
- Al-Najar, B., Peters, C.D., Albuflas, H., Hankins, N.P. 2020. Pressure and osmotically driven membrane processes: A review of the benefits and production of nano-enhanced membranes for desalination. *Desalination* 479, 114323.
- Al-Shammiri, M., Safar, M., Al-Dawas, M. 2000. Evaluation of two different antiscalants in real operation at the Doha research plant. *Desalination* 128, 1-16.

- Al-Youssef, M. 2015. Gypsum Crystals Formation and Habits, Dukhan Sabkha, Qatar. *J. Earth Sci. Clim. Change* 6, 10.
- Alayande, A.B., Chae, S., Kim, I.S. 2019. Surface morphology-dependent spontaneous bacterial behaviors on graphene oxide membranes. *Sep. Purif. Technol.* 226, 68–74.
- Ali, S.A., Kazi, I.W., Rahman, F. 2015. Synthesis and evaluation of Synthesis and evaluation of phosphate-free antiscalants to control  $\text{CaSO}_4 \cdot 2\text{H}_2\text{O}$  scale formation in reverse osmosis desalination plants. *Desalination* 357, 36–44.
- Ali, F.A., Alam, J., Shukla, A.K., Alhoshan, M., Khaled, J.M., Al-Masry, W.A., Alharbi, N.S., Alam, M. 2019. Graphene oxide-silver nanosheet-incorporated polyamide thin-film composite membranes for antifouling and antibacterial action against *Escherichia coli* and bovine serum albumin. *J. Ind. Eng. Chem.* 80, 227–238.
- Alimi, F., Elfil, H., Gadrib, A. 2003. Kinetics of the precipitation of calcium sulfate dihydrate in a desalination unit. *Desalination* 157, 9–16.
- Almuzara, M., Barberis, C., Traglia, G., Famiglietti, A., Ramirez, M.S., Vay, C. 2015. Evaluation of matrix-assisted laser desorption ionization-time-of-flight mass spectrometry for species identification of nonfermenting Gram-negative bacilli. *J. Microbiol. Methods* 112, 24–27.
- Alventosa-deLara, E., Barredo-Damas, S., Alcaina-Miranda, M.I., Iborra-Clar, M.I. 2012. Ultrafiltration technology with a ceramic membrane for reactive dye removal: optimization of membrane performance. *J. Hazard. Matter.* 209–210, 492–500.
- Amir, R.M., Anjum, F.M., Khan, M.I., Khan, M.R., Pasha, I., Nadeem, M. 2013. Application of Fourier transform infrared (FTIR) spectroscopy for the identification of wheat varieties. *J. Food Sci. Technol.* 50 (5), 1018–1023.

- Amjad, Z. 2013. Gypsum scale formation on heated metal surfaces: the influence of polymer type and polymer stability on gypsum inhibition. *Desalination Water Treat.* 51, 4709-4718.
- An, G., Lin, J., Li, J., Li, X., Jian, X. 2011. Non-invasive measurement of membrane scaling and cleaning in spiral-wound reverse osmosis modules by ultrasonic time-domain reflectometry with sound intensity calculation. *Desalination* 283, 3–9.
- Ang, W.S., Lee, S., Elimelech, M. 2006. Chemical and physical aspects of cleaning of organic-fouled reverse osmosis membranes. *J. Membr. Sci.* 272, 198-210.
- Ang, W.L., Mohammad, A.W., Hilal, N., Leo, C.P. 2015. A review on the applicability of integrated/hybrid membrane processes in water treatment and desalination plants. *Desalination* 363, 2–18.
- Antony, A., Low, J.H., Gray, S., Childress, A.E., Le-Clech, P., Leslie, G. 2011. Scale formation and control in high pressure membrane water treatment systems: A review. *J. Memb. Sci.* 383, 1–16.
- Aptel, P., Armor, J., Audinos, R., Baker, R.W., Bakish, R., Belfort, G., Bikson, B., Brown, R.G., Bry, M.K., Burke, J.J., Cabasso, I., Chern, R.T., Cheryan, M., Cussler, E.L., Davis, R.H. 1996. Terminology for membranes and membrane processes. *J. Membr. Sci.* 120, 149-159.
- Aref, M.A.M. 1998. Holocene stromatolites and microbial laminites associated with lenticular gypsum in a marine-dominated environment, Ras El Shetan area, Gulf of Aqaba, Egypt. *Sedimentology* 45, 245-262.
- Arias, D., Cisternas, L.A., Rivas, M. 2017. Biomineralization of calcium and magnesium crystals from seawater by halotolerant bacteria isolated from Atacama Salar (Chile). *Desalination* 405, 1–9.

- Ashfaq, M.Y., Al-ghouti, M.A., Qiblawey, H., Zouari, N. 2020a. Investigating the effect of temperature on calcium sulfate scaling of reverse osmosis membranes using FTIR, SEM-EDX and multivariate analysis. *Sci. Total. Environ.* 703, 134726.
- Ashfaq, M.Y., Al-Ghouti, M.A., Al-Disi, Z., Zouari, N. 2020b. Investigating the microorganisms-calcium sulfate interaction in reverse osmosis systems using SEM-EDX technique. *J. Env. Chem. Eng.* 8, 103963.
- Ashfaq, M.Y., Al-Ghouti, M.A., Al-Disi, Z., Zouari, N. 2020c. Interaction of seawater microorganisms with scalants and antiscalants in reverse osmosis systems. *Desalination* 487, 114480.
- Ashfaq, M.Y., Al-ghouti, M.A., Qiblawey, H., Rodrigues, D.F., Hu, Y., Zouari, N. 2019a. Isolation, identification and biodiversity of antiscalant degrading seawater bacteria using MALDI-TOF-MS and multivariate analysis. *Sci. Total Environ.* 656, 910–920.
- Ashfaq, M.Y., Al-ghouti, M.A., Qiblawey, H., Zouari, N. 2019b. Evaluating the effect of antiscalants on membrane biofouling using FTIR and multivariate analysis. *Biofouling* 0, 1–14.
- Ashfaq, M.Y., Al-ghouti, M.A., Qiblawey, H., Zouari, N. Rodrigues, D.F., Hu, Y. 2018. Use of DPSIR Framework to Analyze Water Resources in Qatar and Overview of Reverse Osmosis as an Environment Friendly Technology. *Env. Prog. Sustain.* 38, 1–13.
- Ashfaq, M.Y., Wang, T., Qiblawey, H., Reesh, I.A., Judd, S. 2017. Recycling of hospital laundry wastewater using membrane technology. *Desalin. Water Treat.* 60, 122–128.

- Ayyavoo, J., Nguyen, T.P.N., Jun, B-M., Kim, I.C., Kwon, Y.N. 2016. Protection of polymeric membranes with antifouling surfacing via surface modifications. *Colloids and Surfaces A: Physicochem. Eng. Aspects* 506, 190–201.
- Baker, J.S., Dudley, L.Y. 1998. Biofouling in membrane systems - A review. *Desalination* 118, 81-89.
- Baker, R.W. 2004. *Membrane Technology and Applications*, 2nd ed., John Wiley and Sons, West Sussex, England, 2004.
- Banat, F., Qiblawey, H., Al-Nasser, Q. 2009. Economic evaluation of a small RO unit powered by PV installed in the village of Hartha, Jordan. *Desalin. Water Treat.* 3, 169–174.
- Bao, M., Zhu, G., Wang, L., Wang, M., Gao, C. 2013. Preparation of monodispersed spherical mesoporous nanosilica – polyamide thin film composite reverse osmosis membranes via interfacial polymerization. *Desalination* 309, 261–266.
- Barbuddhe, S.B., Maier, T., Schwarz, G., Kostrzewa, M., Hof, H., Domann, E., Chakraborty, T., Hainm, T. 2008. Rapid identification and typing of listeria species by matrix-assisted laser desorption ionization-time of flight mass spectrometry. *Appl. Environ. Microbiol.* 74, 5402-5407.
- Bayouhdh, S., Othmane, A., Mora, L., Ben, O.H. 2009. Assessing bacterial adhesion using DLVO and XDLVO theories and the jet impingement technique. *Colloids Surf. B: Biointerfaces* 73, 1–9.
- Ben-Hassan, I., Ennouri, M., Lafforgue, C., Schmitz, P., Ayadi, A., Massoud, H.S. 2013. Experimental study of membrane fouling during crossflow microfiltration of Yeast and Bacteria suspensions: Towards an analysis at the microscopic level. *Membranes* 3, 44–68.

- Benecke, J., Rozova, J., Ernst, M. 2018. Anti-scale effects of select organic macromolecules on gypsum bulk and surface crystallization during reverse osmosis desalination. *Sep. Purif. Technol.* 198, 68–78.
- Bellona, C., Drewes, J.E., Xu, P., Amy, G. 2004. Factors affecting the rejection of organic solutes during NF/RO treatment — a literature review. *Water Res.* 38, 2795–2809.
- Bereschenko, L.A., Stams, A.J.M., Euverink, G.J.W., Van, M.C.M. 2010. Biofilm Formation on Reverse Osmosis Membranes Is Initiated and Dominated by *Sphingomonas* spp. *Appl. Environ. Microbiol.* 76, 2623-2632.
- Bhattacharya, A., Misra, B.N. 2004. Grafting: a versatile means to modify polymers: techniques, factors and applications. *Prog. Polym. Sci.* 29, 767–814.
- Bibi, S., Oualha, M., Ashfaq, M.Y., Suleiman, M.T., Zouari, N. 2018. Isolation, differentiation and biodiversity of ureolytic bacteria of Qatari soil and their potential in microbially induced calcite precipitation (MICP) for soil stabilization. *RSC Advances* 8, 5854 - 5863.
- Blok, A.J., Chhasatia, R., Dilag, J., Ellis, A.V. 2014. Surface initiated polydopamine grafted poly([2-(methacryoyloxy) ethyl] trimethylammonium chloride) coatings to produce reverse osmosis desalination membranes with anti-biofouling properties. *J. Memb. Sci.* 468, 216–223.
- Blonk, J.C.G., Van, A.H. 1993. Confocal scanning microscopy in food research. *Food Res. Intern.* 28, 297-311.
- Bo, H. 2004. Quantification of  $\text{CaCO}_3 - \text{CaSO}_3 \cdot 0.5\text{H}_2\text{O} - \text{CaSO}_4 \cdot 2\text{H}_2\text{O}$  mixtures by FTIR analysis and its ANN model. *Mat. Lett.* 58, 723–726.
- Bontognali, T.R., McKenzie, J.A., Warthmann, R.J., Vasconcelos, C. 2014. Microbially influenced formation of Mg-calcite and Ca-dolomite in the presence of



- exopolymeric substances produced by sulphate-reducing bacteria. *Terra Nova* 26,72–77.
- Boubakri, A, Bouguecha, S. 2008. Diagnostic and membrane autopsy of Djerba Island desalination station, *Desalination* 220, 403–411.
- Braissant, O., Cailleau, G., Dupraz, C., Verrecchia, A.P. 2003. Bacterially induced mineralization of calcium carbonate in terrestrial environment: the role of exopolysaccharides and amino-acids. *J. Sed. Res.* 73, 485–490.
- Briggs D., Seah M.P. (Eds.). 1990. *Practical Surface Analysis, Auger and X-ray Photoelectron Spectroscopy*, John Wiley & Sons, Inc.
- Buonomenna, M.G. 2013. Nano-enhanced reverse osmosis membranes. *Desalination* 314, 73–88.
- Bura, R., Cheung, M., Liao, B., Finlayson, J., Lee, B.C., Droppo, I.G., Lepard, G.G., Liss, S.N. 1998. Composition of extracellular polymeric substances in the activated sludge floc matrix. *Water Sci. Technol.* 37, 325–333.
- Butt, F.H., Rahman, F., Baduruthamal, U. 1997. Characterization of foulants by autopsy of RO desalination membranes. *Desalination* 114, 51-64.
- Butt F.H., Rahman, F., Baduruthamal, U. 1995. Identification of scale deposits through membrane autopsy, *Desalination* 101, 219-230.
- Cai, P., Huang, Q., Walker, S.L. 2013. Deposition and survival of *Escherichia coli* O157:H7 on clay minerals in a parallel plate flow system. *Environ. Sci. Technol.* 47 (4), 1896–1903.
- Cakal, G.O., Eroglu, I., Ozkar, S. 2006. Gypsum crystal size distribution in four continuous flow stirred slurry boric acid reactors in series compared with the batch. *J. Crystal Growth* 290, 197–202.

- Cao, Y., Xing, W., Peng, C., Huang, Q., Rong, X., Wei, L. 2011. Preferential adsorption of extracellular polymeric substances from bacteria on clay minerals and iron oxide. *Colloids Surf. B: Biointerfaces* 83 (1), 122–127.
- Cao, B., Ansari, A., Yi, X., Rodrigues, D.F., Hu, Y. 2018. Gypsum scale formation on graphene oxide modified reverse osmosis membrane. *J. Memb. Sci.* 552, 132–143.
- Cao, Z.-Y., Ge, H.-C. Lai, S.-L. 2001. Studies on synthesis and adsorption properties of chitosan cross linked by glutaraldehyde and Cu (II) as template under microwave irradiation. *Eur. Polym. J.*, 37, 21-41.
- Caretto, E., Bardaro, M., Russello, G., Mirra, M., Zuelli, C., Barbarini, D. 2013. Comparison of the Staphylococcus Quick FISH BC test with the tube coagulase test performed on positive blood cultures for evaluation and application in a clinical routine setting. *J. Clin. Microbiol.* 51 (1), 131–135.
- Castrillon, S.R.-V., Perreault, F.O., Faria, A.F., Elimelech, M. 2015. Interaction of graphene oxide with bacterial cell membranes: insights from force spectroscopy. *Environ. Sci. Technol. Lett.* 2, 112–117.
- Cecilia, D.C., Riley, W.J., Maggi, F. 2019. Biochemical modeling of microbial memory effects and catabolite repression on soil organic carbon compounds. *Soil Biol. Biochem.* 128, 1–12.
- Chae, H., Lee, C., Park, P., Kim, I., Kim, J. 2017. Synergetic effect of graphene oxide nanosheets embedded in the active and support layers on the performance of thin-film composite membranes. *J. Memb. Sci.* 525, 99–106.
- Chae, H.-R., Lee, J., Lee, C.-H., Kim, I.-C., Park, P.-K. 2015. Graphene oxide-embedded thin film composite reverse osmosis membrane with high flux, anti-biofouling, and chlorine resistance. *J. Memb. Sci.* 483, 128–135.

- Chan, W., Chen, H., Surapathi, A., Taylor, M.G., Shao, X., Marand, E., Johnson, J.K. 2013. Zwitterion functionalized carbon nanotube / polyamide nanocomposite. *ACS Nano*. 7 (6), 5308-5319.
- Chang W.S., Halverson L.J. 2003. Reduced water availability influences the dynamics, development, and ultrastructural properties of *Pseudomonas putida* biofilms. *J. Bacteriol.* 185 (20), 6199-6204.
- Chai, G., Greenberg, A.R., Krantz, W.B. 2007. Ultrasound, gravimetric, and SEM studies of inorganic fouling in spiral-wound membrane modules 208, 277–293. <https://doi.org/10.1016/j.desal.2006.06.018>
- Chen J.P., Mou H., Wang L.K., Matsuura T. 2006. Membrane Filtration, in: *Advanced Physicochemical Treatment Processes*, L.K. Wang, Y.-T. Hung, N.K. Shamas (Eds.), Humana Press, 203-259.
- Chen X, Stewart P. 2002. Role of electrostatic interactions in cohesion of bacterial biofilms. *Appl. Microbiol. Biotechnol.* 59 (6), 718-720.
- Chen J., Peng H., Wang X., Shao F., Yuan Z., Han H. 2014. Graphene oxide exhibits broad spectrum antimicrobial activity against bacterial phytopathogens and fungal conidia by intertwining and membrane perturbation. *Nanoscale* 6, 1879–1889.
- Cheryan M. 1998. *Ultrafiltration and microfiltration handbook*, Technomic Publishing Company, Inc., Lancaster, PA, USA.
- Chian E.S.K., Chen J.P., Sheng P.-X., Ting Y.-P., Wang L.K. 2007. Reverse osmosis technology for desalination, in: *Advanced Physicochemical Treatment Technologies*, L.K. Wang, Y.-T. Hung, N.K. Shamas (Eds.), Humana Press, Totowa NJ, 329-366.
- Cohen-Tanugi, D., Grossman, J.C. 2012. Water desalination across nanoporous graphene. *Nano Lett.* 12, 3602–3608.

- Compere, C., Bellon-Fontaine, M.N., Bertrand, P., Costa, D., Marcus, P., Poleunis, C., Pradier, C.M., Rondot, B., Walls, M.G. 2001. Kinetics of conditioning layer formation on stainless steel immersed in seawater. *Biofouling*, 17, 129-145.
- Costerton, J.W., Lewandowski, Z., DeBeer, D., Caldwell, D., Korber, D., James, G. 1994. Biofilms, the customized microniche. *J. Bacteriol.*, 176, 2137-2142.
- Crittenden, J.C, Trussel, R.R, Hand, D.W, Howe, K.J, Tchobanoglous, G. 2005. *Water treatment: principles and design*. 2nd edition. John Wiley & sons.
- Croll, H., Soroush, A., Pillsbury, M.E., Castrillon, S.R. 2019. Graphene oxide surface modification of polyamide reverse osmosis membranes for improved N-nitrosodimethylamine (NDMA) removal. *Sep. Purif. Technol.* 210, 973–980.
- Cruz, L.F., Cobine, P.A., De La Fuente, L. 2012. Calcium increases *Xylella fastidiosa* surface attachment, biofilm formation and twitching motility. *Appl Environ Microbiol* 78, 1321–1331.
- Daniels S.L. 1980. Mechanisms involved in sorption of microorganisms to solid surfaces, in: *Adsorption of microorganisms to surface*, G. Bitton, K.C. Marshall (Eds.), John Wiley & Sons, New York, USA, 7–58.
- Darton, E.G. 2000. Membrane chemical research: centuries apart. *Desalination* 132, 121–131.
- Darwish, M., Hassabou, A.H., Shomar, B. 2013. Using Seawater Reverse Osmosis (SWRO) desalting system for less environmental impacts in Qatar. *Desalination* 309, 113–124.
- Darwish, M.A and Mohtar, R. 2012. Qatar water challenges. *Desalination and Water Treatment* 51 (1-3), 75-86.

- Das, T., Sehar, S., Koop, L., Wong, Y.K., Ahmed, S., Siddiqui, K.S., Manefield, M. 2014. Influence of Calcium in Extracellular DNA Mediated Bacterial Aggregation and Biofilm Formation. *Plos One*, 9 (3), e91935.
- De Kerchove, A.J., Elimelech, M. 2008. Calcium and magnesium cations enhance the adhesion of motile and nonmotile *Pseudomonas aeruginosa* on alginate films. *Langmuir* 24, 3392–3399.
- Dhami, N.K., Reddy, M.S., Mukherjee, A. 2013. Biomineralization of calcium carbonates and their engineered applications: a review. *Front. Microbiol.* 4, 1-13. doi: 10.3389/fmicb.2013.00314.
- Diaspro, A. 2002. *Confocal and Two photon Microscopy: Foundations, Applications and Advances*. Wiley-Liss, New York.
- Dieckmann, R., Malorny, B. 2011. Rapid screening of epidemiologically important *Salmonella enterica subsp. enterica* serovars by whole-cell matrix-assisted laser desorption ionization-time of flight mass spectrometry. *Appl. Environ. Microbiol.* 77, 4136-4146.
- Dieckmann, R., Graeber, I., Kaesler, I., Szewzyk, U., von Dohren, H. 2005. Rapid screening and dereplication of bacterial isolates from marine sponges of the Sula Ridge by Intact-Cell-MALDI-TOF mass spectrometry (ICM-MS). *Appl. Microbiol. Biotechnol.* 67 (4), 539–548.
- Dixit V, Cho BK, Obendorf K, Tewari J. 2014. Identifications of household's spores using mid infrared spectroscopy. *Spectrochim Acta A Mol Biomol Spectrosc.* 123, 490–496.
- Dreszer C., Vrouwenvelder J., Paulitsch-Fuchs A., Zwijnenburg A., Kruithof J., Flemming H. 2013. Hydraulic resistance of biofilms. *J. Memb. Sci.* 429, 436–447.

- Driessche, A.E.S.V., Stawski, T.M., Kellermeier, M. 2019. Calcium sulfate precipitation pathways in natural and engineering environments. *Chem. Geology*, 530:119274.
- Drews, A, Vocks, M., Iversen, V., Lesjean, B., Kraume, M. 2006. Influence of unsteady membrane bioreactor operation on EPS formation and filtration resistance. *Desalination* 192:1–9.
- Duan, L., Wang, Y., Zhang, Y., Liu, J. 2015. Graphene immobilized enzyme/polyether sulfone mixed matrix membrane: Enhanced antibacterial, permeable and mechanical properties. *App. Surf. Sci.* 355, 436–445.
- Dydo, P., Turek, M., Ciba, J., Wandachowicz, K., Misztal, J. 2004. The nucleation kinetic aspects of gypsum nanofiltration membrane scaling. *Desalination* 164, 41–52.
- East, C.P., Schiller T.L., Fellows C.M., Doherty W.O.S. 2015. Chapter 28 Analytical Techniques to Characterize Scales and Deposits. *Mineral Scales and Deposits*. 1<sup>st</sup> Edition, Elsevier, 682-689.
- Eddabra, R., Prevost, G., Scheftel, J.M. 2012. Rapid discrimination of environmental *Vibrio* by matrix-assisted laser desorption ionization time-of-flight mass spectrometry. *Microbiol. Res.* 167 (4), 226–230.
- Ehrlich, H.L. 2002. *Geomicrobiology*, 4th Edition. Marcel Dekker, New York, NY.
- Elimelech, M. 2010. Gypsum Scaling and Cleaning in Forward Osmosis: Measurements and Mechanisms. *Environ. Sci. Technol.* 44, 2022–2028.
- Elsehly, E.M., Chechenin, N., Makunin, A., Motaweh, H.A. 2018. Ozone functionalized CNT-based filters for high removal efficiency of benzene from aqueous solutions. *J. Water Process. Eng.* 25, 81-87.

- Emami, K., Askari, V., Ullrich, M., Mohinudeen, K., Anil C.A., Khandeparker, L., Burgess, J.G., Mesbahi, E. 2012. Characterization of Bacteria in Ballast Water Using MALDI-TOF Mass Spectrometry. *Plos one* 7 (6) e38515.
- Ercolini, D., Russo, F., Blaiotta, G., Pepe, O., Mauriello, G., Villani, F. 2007. Simultaneous Detection of *Pseudomonas fragi*, *P. lundensis*, and *P. putida* from Meat by Use of a Multiplex PCR Assay Targeting the *carA* Gene. *Appl. Environ. Microbiol.* 73, 2354 – 2359.
- Fang, H., Ohlsson, A.-K., Ullberg, M., Ozenci, V. 2012. Evaluation of species-specific PCR, Bruker MS, VITEK MS and the VITEK 2 system for the identification of clinical *Enterococcus* isolates. *Eur. J. Clin. Microbiol. Infect. Dis.* 31 (11), 3073–3077.
- Faria, A.F., Liu, C., Xie, M., Perreault, F., Nghiem, L.D., Ma, J., Elimelech, M. 2017. Thin-film composite forward osmosis membranes functionalized with graphene oxide–silver nanocomposites for biofouling control. *J. Memb. Sci.* 525, 146–156. <https://doi.org/10.1016/j.memsci.2016.10.040>
- Farias, M. E., Contreras, M., Rasuk, M. C., Kurth, D., Flores, M. R., Poire, D. G. 2014. Characterization of bacterial diversity associated with microbial mats, gypsum evaporites and carbonate microbialites in thalassic wetlands: Tebenquiche and La Brava, Salar de Atacama, Chile. *Extremophiles* 18, 311–329.
- Farrah, H.E., Lawrance, G.A., Wanless, E.J. 2004. Gypsum-anhydrite transformation in hot acidic manganese sulfate solution. A comparative kinetic study employing several analytical methods. *Hydrometallurgy* 75, 91–98. <https://doi.org/10.1016/j.hydromet.2004.07.002>

- Ferris, F.G., Fyfe, W.S., Beveridge, T.J. 1991. Bacteria as nucleation sites for authigenic minerals. *Diversity of Environmental Biogeochemistry. Developments in Geochemistry* (6), (Berthelin J, ed), Elsevier, Amsterdam, 319–326.
- Flemming, H.-C. 1997. Reverse osmosis membrane biofouling. *Exp. Therm Fluid Sci.*, 14, 382-391.
- Flemming, H.-C., Ridgway, H.F. 2009. Biofilm control: conventional and alternative approaches, in: *Marine and industrial biofouling*, (Eds.), 103-118.
- Flemming, H.-C., Wingender, J. 2010. The biofilm matrix. *Nat. Rev. Microbiol.* 8, 623-633.
- Garg, A., Jain, A., Bhosle, N.B. 2009. Chemical characterization of a marine conditioning film. *Int. Biodeterior. Biodegrad.*, 63, 7-11.
- Gelaw, T.K., Güell, C., Ferrando, M., De Lamo-Castellvi, S. 2014. Use of attenuated total reflectance infrared micro spectroscopy combined with multivariate analysis to study membrane fouling. *J. Food Eng.* 143, 69–73. <https://doi.org/10.1016/j.jfoodeng.2014.06.032>.
- Gelaw, T.K., Trentin, A., Guell, C., Ferrando, M., Rodríguez-Saona, L.E., de Lamo-Castellvi, S. 2011. Attenuated total reflectance infrared micro spectroscopy combined with multivariate analysis, a novel tool to characterize cleaning efficiency of organic microfiltration membranes. *J. Memb. Sci.* 376, 35–39. <https://doi.org/10.1016/j.memsci.2011.03.032>.
- Gelover S., Gomez L.A., Reyes K., Leal M.T. 2006. A practical demonstration of water disinfection using TiO<sub>2</sub> films and sunlight, *Water Res.* 40, 3274–3280.
- Ghaseminezhad, S.M., Barikani, M., Salehir, M. 2019. Development of graphene oxide-cellulose acetate nanocomposite reverse osmosis membrane for seawater desalination. *Composites Part B.* 161, 320–327.



- Ghashoghchi, R.A., Hosseini, M.R., Ahmadi, A. 2017. Effects of microbial cells and their associated extracellular polymeric substances on the bio-flocculation of kaolin and quartz. *Appl. Clay Sci.* 138, 81–88.
- Ghayeni, S.B.S., Beatson, P.J., Schneider, R.P., Fane, A.G. 1998. Adhesion of waste water bacteria to reverse osmosis membranes. *J. Membr. Sci.*, 138, 29-42.
- Ghyselinck, J., Van Hoorde, K., Hoste, B., Heylen, K., De Vos, P. 2011. Evaluation of MALDI-TOF MS as a tool for high-throughput dereplication. *J. Microbiol. Methods* 86 (3), 327–336.
- Gilron, J., Hasson, D. 2000. Calcium sulfate fouling of reverse osmosis membranes: flux decline mechanism, *Chemical Engineering Science* 42, 2351–2360.
- Ginic-Markovic, M., Barclay, T.G., Kristina, T. Constantopoulos, K.T., Markovic, E., Stephen, R., Clarke, S.R., Matisons, J.G. 2015. Biofouling resistance of polysulfobetaine coated reverse osmosis membranes. *Desalination* 369, 37–45.
- Goh, P.S., Zulhairun, A.K., Ismail, A.F., Hilal, N. 2019. Contemporary antibiofouling modifications of reverse osmosis desalination membrane: A review, *Desalination* 468, 114072.
- Gominsek, T., Lubej, A., Pohar, C. 2005. Continuous precipitation of calcium sulfate dihydrate from waste sulfuric acid and lime. *J Chem. Technol. Biotechnol.* 80, 939–947.
- Gonzalez, C-J, Lopez-Diaz, T.-M., Garcia-Lopez, M.L., Prieto, M., Otero, A. 1999. Bacterial microflora of wild brown trout (*Salmo trutta*), wild pike (*Esox lucius*), and aqua cultured rainbow trout (*Oncorhynchus mykiss*). *J. Food Prot.* 62, 1270–1277.

- Gonder, Z.B., Arayici, S., Barlas, H. 2011. Advanced treatment of pulp and paper mill wastewater by nanofiltration process: Effects of operating conditions on membrane fouling. *Sep. Purif. Technol.* 76, 292–302.
- Greenlee, L.F., Lawler, D.F., Freeman, B.D., Marrot, B., Moulin, P. 2009. Reverse osmosis desalination: water sources, technology, and today's challenges. *Water Res.* 43 (9), 2317–234.
- Gryta, M. 2009. Calcium sulphate scaling in membrane distillation process. *Chem. papers* 63, 146–151.
- Gryta, M. 2016. The study of performance of polyethylene chlorinetrifluoroethylene membranes used for brine desalination by membrane distillation. *Desalination* 398, 52–63.
- Gutman, J., Herzberg, M., Walker, S.L. 2014a. Biofouling of reverse osmosis membranes: positively contributing factors of *Sphingomonas*. *Environ. Sci. Technol.* 48 (23), 13941–13950.
- Gutman J, Kaufman Y, Kawahara K, Walker SL, Freger V, Herzberg M. 2014b. Interactions of glycosphingolipids and lipopolysaccharides with silica and polyamide surfaces: adsorption and viscoelastic properties. *Biomacromolecules* 15 (6), 2128–2137.
- Guvensen, N.C., Demir, S., Ozdemir, G. 2012. Effects of magnesium and calcium cations on biofilm formation by *Sphingomonas paucimobilis* from an industrial environment. *Fresen. Environ. Bull.*, 22 (12), 3685 – 3692.
- Hamrouni, B. Dhahbi, M. 2001. Thermodynamics description of saline waters prediction of scaling limits in desalination processes. *Desalination*, 137 (1-3), 275-284.

- Han, Y., Lin, Q. 2009. Effects of inorganics on RO membrane initial biofouling formation, in 3rd International Conference on Bioinformatics and Biomedical Engineering (ICBBE), Beijing-China, 1-4.
- Harouaka, K., Mansor M., Macalady J.L., Fantle, M.S. 2016. Calcium isotopic fractionation in microbially mediated gypsum precipitates. *Geochim. Cosmochim. Acta.* 184, 114–131.
- Hasson, D., Drak, A., Semiat, R. 2001. Inception of CaSO<sub>4</sub> scaling on RO membranes at various water recovery levels. *Desalination.* 139, 73–81.
- Hassan, I.B., Ennouri, M., Lafforgue, C., Schmitz, P., Ayadi, A., Massoud, H.S. 2013. Experimental Study of Membrane Fouling during Crossflow Microfiltration of Yeast and Bacteria Suspensions: Towards an Analysis at the Microscopic Level *Membranes* 10 (3), 44–68. <https://doi.org/10.3390/membranes3020044>
- Hasson, D., Drak, A., Semiat, R. 2009. Induction times induced in a RO system by antiscalants delaying CaSO<sub>4</sub> precipitation 157, 193–207.
- Hasson, D., Drak, A., Semiat, R., 2001. Inception of CaSO<sub>4</sub> scaling on RO membranes at various water recovery levels 139, 73–81.
- Hasson, D., Bramson, D., Relis, B. L., Semiat, R. (1996), “Influence of the flow system on the inhibitory action of CaCO<sub>3</sub> scale prevention additives,” *Desalination*, vol. 108, no. 1-3, pp. 67-79.
- Herzberg, M., Kang, S., Elimelech, M. 2009. Role of extracellular polymeric substances (EPS) in biofouling of reverse osmosis membranes. *Environ. Sci. Technol.* 43 (12), 4393-4398.
- Hilal N., Ogunbiyi, O.O., Miles, N.J., Nigmatullin, R. 2005. Methods employed for control of fouling in MF and UF membranes: a comprehensive review. *Sep. Sci. Technol.* 40, 1957–2005.

- Hirose, M., Ito, H., Kamiyam, Y. 1996. Effect of skin layer surface structures on the flux behavior of RO membranes, *J. Membr. Sci.* 121, 209–215.
- Hoang, T.A., Ang, H.M., Rohl, A.L. 2007. Effects of temperature on the scaling of calcium sulphate in pipes. *Powder Technol.* 179, 31–37.  
<https://doi.org/10.1016/j.powtec.2006.11.013>
- Hori K., Matsumoto S. 2010. Bacterial adhesion: from mechanism to control, *Biochem. Eng. J.* 48, 424–434.
- Horsch, P., Gorenflo, A., Fuder, C., Deleage, A., Frimmel, F.H. 2005. Biofouling of ultra- and nanofiltration membranes for drinking water treatment characterized by fluorescence in situ hybridization (FISH), *Desalination* 172, 41-52.
- Inbakandan, D., Kumar, C., Abraham, L.S., Kirubakaran, R., Venkatesan, R., Khan, S.A. 2013. Silver nanoparticles with anti microfouling effect: A study against marine biofilm forming bacteria. *Colloid. Surfaces B.* 111, 636– 643.
- Index Mundi accessed on 29.04.2017 01:00 pm.  
<http://www.indexmundi.com/facts/qatar/indicator/ER.H2O.INTR.PC>
- Inukai, S., Cruz-Silva, R., Ortiz-Medina, J., Morelos-Gomez, A., Takeuchi, K., Hayashi, T., Tanioka, A., Araki, T., Tejima, S., Noguchi, T., Terrones, M., Endo, M. 2015. High-performance multifunctional reverse osmosis membranes obtained by carbon nanotube polyamide nanocomposite, *Sci. Rep.* 5, 13562.
- Inurria, A., Cay-durgun, P., Rice, D., Zhang, H., Seo, D., Laura, M., Perreault, F. 2019. Polyamide thin-film nanocomposite membranes with graphene oxide nanosheets: Balancing membrane performance and fouling propensity. *Desalination* 451, 139–147. <https://doi.org/10.1016/j.desal.2018.07.004>.
- Iqbal, M., Saeed, A., Iqbal, S. 2009. FTIR spectrophotometry, kinetics and adsorption isotherms modeling, ion exchange, and EDX analysis for understanding the

- mechanism of Cd<sup>+2</sup> and Pb<sup>+2</sup> removal by mango peel waste. *J. Hazard. Mat.* 164, 161–171.
- Ivnitsky, H., Minz, D., Kautsky, L., Preis, A., Ostfeld, A., Semiat, R., Dosoretz, C.G. 2010. Biofouling formation and modeling in nanofiltration membranes applied to wastewater treatment. *J. Memb. Sci.* 360, 165-173.
- Jackson, J.E. 2003. A user's guide to principle components. A John Willey and Sons, Inc.
- Jamal, W.Y., Shahin, M., Rotimi, V.O. 2013. Comparison of two matrix-assisted laser desorption/ionization-time of flight (MALDI-TOF) mass spectrometry methods and API 20AN for identification of clinically relevant anaerobic bacteria. *J. Med. Microbiol.* 62, 540–544.
- Jawor, A., Hoek, E.M.V. 2009. Effects of feed water temperature on inorganic fouling of brackish water RO membranes. *Desalination.* 235, 44–57.
- Jia, X.S., Furumai, H., Fang, H.H.P. 1996. Extracellular polymers of hydrogen-utilizing methanogenic and sulfate-reducing sludges. *Water Res.* 30, 1439–1444.
- Jiang, S., Li, Y., Ladewig, B.P. 2017. A review of reverse osmosis membrane fouling and control strategies. *Sci. Total Environ.* 595, 567–583.
- Jiao, Y., Cody, G.D., Harding, A.K., Wilmes, P., Schrenk, M., Wheeler, K.E., Banfield, J.F., Thelen, M.P. 2010. Characterization of Extracellular Polymeric Substances from Acidophilic Microbial Biofilms. *Appl. Environ. Microbiol.* 76 (9), 2916-2922.
- Jin, L., Ong, S.L., Ng, H.Y. 2013. Fouling control mechanism by suspended biofilm carriers' addition in submerged ceramic membrane bioreactors. *J. Membr. Sci.* 427, 250–258.
- Jung, Y., Alayande, A.B., Chae, S., Kim, I.S. 2018. Applications of nisin for biofouling mitigation of reverse osmosis membranes. *Desalination* 429, 52–59.

- Kamijo, T., Huang, G. 2017. Enhancing the discussion of alternatives in EIA using principle component analysis leads to improved public involvement. *Environ. Impact Asses.* 65, 63-74.
- Kan, A.T., Wu, X., Fu, G., Tomas, M.B. 2005. Validation of Scale Prediction Algorithms at Oilfield Conditions. Presented at the SPE International Symposium on Oilfield Chemistry, The Woodlands, Texas, USA, 26-27 May.
- Kang, S.-T., Subramani, A., Hoek, E.M.V., Deshusses, M.A., Matsumoto, M.R. 2004. Direct observation of biofouling in cross-flow microfiltration: mechanisms of deposition and release. *J. Membr. Sci.*, 244, 151-165.
- Kang, S., Herzberg, M., Rodrigues, D.F, Elimelech, M. 2008. Antibacterial effects of carbon nanotubes: size does matter. *Langmuir* 24, 6409–6413.
- Kansiz, M., Heraud, P., Wood, B., Burden, F., Beardall, J., McNaughton, D. 1999. Fourier Transform Infrared micro spectroscopy and chemometrics as a tool for the discrimination of cyanobacterial strains. *Phytochemistry* 52, 407-417.
- Karabelas, A.J., Karanasiou, A., Mitrouli, S.T. 2014. Incipient membrane scaling by calcium sulfate during desalination in narrow spacer-filled channels. *Desalination* 345, 146–157. <https://doi.org/10.1016/j.desal.2014.04.020>
- Karabelas, A.J., Kostoglou, M., Mitrouli, S.T. 2011. Incipient crystallization of sparingly soluble salts on membrane surfaces: The case of dead-end filtration with no agitation. *Desalination* 273, 105–117. <https://doi.org/10.1016/j.desal.2010.10.057>.
- Karadenizli, A., Kolayli, F., Ergen, K. 2007. A novel application of Fourier-transformed infrared spectroscopy: classification of slime from staphylococci. *Biofouling* 23 (1), 63 – 71.

- Karime, M., Bouguecha, S., Hamrounia, B. 2008. RO membrane autopsy of Zarzis brackish water desalination plant. *Desalination* 220, 258–266.
- Kasban, H., Arafa, H., Elaraby, S.M.S. 2016. Principle component analysis for radiotracer signal separation. *Appl. Radiation isotopes*. 112, 20-26.
- Kehrmann, J., Wessel, S., Murali, R., Hampel, A., Bange, F.C., Buer, J., Mosel, F. 2016. Principal component analysis of MALDI TOF MS mass spectra separates *M. abscessus* (sensu stricto) from *M. massiliense* isolates. *BMC Microbiology* 16, 24.
- Khan, M.T., Hong, P.Y., Nada, N., Croue, J.P. 2015. Does chlorination of seawater reverse osmosis membranes control biofouling? *Water Res.* 78, 84-97.
- Khan, I. 2019. Carbon nanotube membranes for water purification: Developments, challenges, and prospects for the future. *Sep. Purif. Technol.* 209, 307–337.
- Khedr, M.G. 2002. Membrane fouling problems in reverse osmosis desalination applications. *Desalination Water Reuse* 10, 3-10.
- Kim, E., Yin, J., Kim, E., Yang, J., Deng, B. 2012. Fabrication of a novel thin-film nanocomposite membrane containing MCM-41 silica nanoparticles for water purification. *J. Memb. Sci.* 423–424, 238–246.
- Kim, J., Suh, D., Kim, C., Baek, Y., Lee, B., Joong, H., Lee, J., Yoon, J. 2016. A high-performance and fouling resistant thin-film composite membrane prepared via coating TiO<sub>2</sub> nanoparticles by sol-gel-derived spray method for PRO applications. *Desalination* 397, 157–164.
- Kim, H.J., Choi, Y.-S., Lim, M.-Y., Jung, K.H., Kim, D.-G., Kim, J.-J., Kang, H., Lee, J.-C. 2016. Graphene oxide-silver nanosheet-incorporated polyamide thin-film composite membranes for antifouling and antibacterial action against *Escherichia coli* and bovine serum albumin. *J. Memb. Sci.* 514, 25–34.

- Kim, S.H., Kwak, S.Y., Sohn, B.H., Park, T.H. 2003. Design of TiO<sub>2</sub> nanoparticle self-assembled aromatic polyamide thin-film composite (TFC) membrane as an approach to solve biofouling problem. *J. Membr. Sci.* 211, 157–165.
- Kim, H.N., Walker, S.L., Bradford, S.A. 2010. Macromolecule mediated transport and retention of *Escherichia coli* O157:H7 in saturated porous media. *Water Res.* 44 (4), 1082–1093.
- Kim, H-S., Lee, J.Y., Ham, S-Y., Lee, J.H., Park, J-H., Park, H-D. 2019. Effect of biofilm inhibitor on biofouling resistance in RO processes. *Fuel* 253, 823–832.
- Kochkodan, V., Johnson, D.J., Hilal, N. 2014. Polymeric membranes: Surface modification for minimizing (bio)colloidal fouling. *Adv. Colloid. Interface. Sci.* 206, 116–140.
- Koubek, J., Uhlík, O., Jecna, K., Junková, P., Vrkoslavová, J., Lipov, J., Kurzawová, V., Macek, T., Macková, M. 2012. Whole-cell MALDI-TOF: rapid screening method in environmental microbiology. *Int. Biodeterior. Biodegrad.* 69, 82–86.
- Kowalska, I., Majewskanowak, K., Kabsch-korbutowicz, M. 2006. Influence of temperature on anionic surface-active agent removal from a water solution by ultrafiltration. *Desalination* 198, 18–22.
- Krishnamurthy, K., Tewari, J., Irudayaraj, J., Demirci, A. 2010. Microscopic and spectroscopic evaluation of inactivation of *Staphylococcus aureus* by pulse UV light and infrared heating. *Food Bioproc. Tech.* 3 (1), 93–104.
- Kristensen, J.B., Meyer, R.L., Laursen, B.S., Shipovskov, S., Besenbacher, F., Poulsen, C.H. 2008. Antifouling enzymes and the biochemistry of marine settlement. *Biotechnol. Adv.* 26, 471–481.



- Kumar, M.S., Madhu, G.M. Roy, S. 2007. Fouling behavior regeneration options and on-line control of biomass-based power plant effluents using microporous ceramic membranes. *Sep. Purif. Technol.*, 57, 25–36.
- Kwak, S.Y, Kim, S.H., Kim, S.S. 2001. Hybrid organic/inorganic reverse osmosis (RO) membrane for bactericidal anti-fouling. Part 1. Preparation and characterization of TiO<sub>2</sub> nanoparticle self-assembled aromatic polyamide thin-film composite (TFC) membrane. *Environ. Sci. Technol.* 35, 2388–2394.
- Kwon B., Lee S., Cho J., Ahn H., Lee D., Shin H.S. 2004. Biodegradability, DBP formation, and membrane fouling potential of natural organic matter: characterization and controllability. *Environ. Sci. Technol.* 39, 732–739.
- Larson, R.J., Bookland, E.A., Williams, R.T., Yocom, K.M., Saucy, D.A., Freeman, M.B., Swift, G. 1997. Biodegradation of acrylic acid polymers and oligomers by mixed microbial communities in activated sludge. *J. Environ. Polym. Degrad.* 5 (1), 41–48.
- Lartigue, M.F., Arnaud, E.H., Haguenoer, E., Domelier, A.S., Schmit, P.O., Marquet, N.V., Lanotte, P., Mereghetti, L., Kostrzewa, M., Quentin, R. 2009. Identification of *Streptococcus agalactiae* Isolates from Various Phylogenetic Lineages by Matrix-Assisted Laser Desorption Ionization – Time of Flight Mass Spectrometry. *J Clin Microbiol.* 47 (7), 2284–2287.
- Lauro, F.M., Chastain, R.A., Blankenship, L.E., Yayanos, A.A., Bartlett, D.H. 2007. The unique 16S rRNA genes of piezophiles reflect both phylogeny and adaptation. *Appl. Environ. Microbiol.* 73, 838–845.
- Lee, J., Chae, H.R., Won, Y.J., Lee, K., Lee, C.H., Lee, H.H., Kim, I.C., Lee, J.M. 2013. Graphene oxide nanoplatelets composite membrane with hydrophilic and antifouling properties for wastewater treatment. *J. Memb. Sci.* 448, 223-230.

- Lee, J., Jung, J.Y., Kim, S., Chang, I.S., Mitra, S.S., Kim, I.S. 2009. Selection of the most problematic biofoulant in fouled RO membrane and the seawater intake to develop biosensors for membrane biofouling. *Desalination* 247, 125–136.
- Lee, K.P., Arnot, T.C., Mattia, D. 2011. A review of reverse osmosis membrane materials for desalination—Development to date and future potential. *J. Memb. Sci.* 370 (1–2), 1–22.
- Lee, S., Kim, J., Lee, C. 1999. Analysis of CaSO<sub>4</sub> scale formation mechanism in various nanofiltration modules. *J. Memb. Sci.* 163, 63–74.
- Lee, S., Lee, C., 2000. Effect of operating conditions on CaSO<sub>4</sub> scale formation mechanism in nanofiltration for water softening. *Wat. Res.* 34, 3854–3866.
- Leisner, J.J., Laursen, B.G., Prevost, H., Drider, D., Dalgaard, P. 2007. Carnobacterium: positive and negative effects in the environment and in foods. *FEMS Microbiol Rev.* 31(5), 592–613.
- Lepinay, C., Mihajlovski, A., Touron, S., Seyer, D., Bousta, F., Di Martino, P. 2018. Bacterial diversity associated with saline efflorescences damaging the walls of a French decorated prehistoric cave registered as a World Cultural Heritage Site. *Int. Biodeterior. Biodegrad.* 130, 55-64.
- Li, H., Liu, W., Qi, X. 2007. Evaluation of a novel CaSO<sub>4</sub> scale inhibitor for a reverse osmosis system. *Desalination* 214, 193–199.
- Li J, Yang F, Liu Y, Song H, Li D, Cheng F. 2012. Microbial community and biomass characteristics associated severe membrane fouling during start-up of a hybrid anoxic–oxic membrane bioreactor. *Bioresour. Technol.* 103: 43–47.
- Li, Y., Yan, C., Liu, W., Li, M. 2018. A principle component analysis-based random forest with the potential nearest neighbor method for automobile insurance fraud identification. *Appl. Soft Computing.* 70, 1000-1009.

- Li, G.L., Zhoua C.H., Fiore, S., Yu, W.H. 2019. Interactions between microorganisms and clay minerals: New insights and broader applications. *Appl. Clay Sci.* 177, 91–113.
- Lior, N. 2017. Sustainability as the quantitative norm for water desalination impacts. *Desalination* 401, 99–111.
- Liu, H, Fang, H.H. 2002. Extraction of extracellular polymeric substances (EPS) of sludges. *J. Biotechnol.* 95, 249–256.
- Liu, Y., Mi, B. 2014. Effects of organic macromolecular conditioning on gypsum scaling of forward osmosis membranes. *J. Memb. Sci.* 450, 153–161. <https://doi.org/10.1016/j.memsci.2013.09.001>
- Liu, L.F., Yu, S.C., Wu, L.G., Gao, C.H. 2006. Study on a novel polyamide-urea reverse osmosis composite membrane (ICIC-MPD) II. Analysis of membrane antifouling performance, *J. Membr. Sci.* 283, 133–146.
- Loeb, S., Sourirajan, S. 1962. Sea water demineralization by means of an osmotic membrane. *Adv. Chem.*, 38 (117), 117–132.
- Loeb, G.I., Neihof, R.A. 1975. Marine conditioning films, in: *Applied Chemistry at Protein Interfaces*, R.E. Baier (Ed.) American Chemical Society, Washington, 319–335.
- Long, G., Zhu, P., Shen, Y., Tong, M. 2009. Influence of Extracellular Polymeric Substances (EPS) on Deposition Kinetics of Bacteria. *Environ. Sci. Technol.* 43, 2308–2314.
- Louie, J.S., Pinnau, I., Ciobanu, I., Ishida, K.P., Ng, A., Reinhard, M. 2006. Effects of polyether–polyamide block copolymer coating on performance and fouling of reverse osmosis membranes. *J. Membr. Sci.* 280, 762–770.

- Lucas, N., Bienaime, C., Belloy C., Queneudec, M., Silvestre F., Nava-Saucedo, J.E. 2008. Polymer biodegradation: Mechanisms and estimation techniques – A review. *Chemosphere* 73 (4), 429-442.
- Lutskiy, M.Y., Avneri-Katz, S., Zhu, N., Itsko, M., Ronen, Z., Arnusch, C.J., Kasher, R. 2015. A microbiology-based assay for quantification of bacterial early stage biofilm formation on reverse osmosis and nanofiltration membranes. *Sep. Purif. Technol.* 141, 214-220.
- Ma, L., Jackson, K.D., Landry, R.M., Parsek, M.R., Wozniak, DJ. 2006. Analysis of *Pseudomonas aeruginosa* conditional psl variants reveals roles for the psl polysaccharide in adhesion and maintaining biofilm structure post attachment. *J. Bacteriol.* 188 (23), 8213-8221.
- Ma, W., Soroush, A., Luong, T.V., Rahaman, M.S. 2017. Cysteamine- and graphene oxide-mediated copper nanoparticle decoration on reverse osmosis membrane for enhanced anti-microbial performance. *J. Colloid Interface Sci.* 501, 330-340.
- Maier, R.M., Pepper, I.L., Gerba, C.P. 2000. *Environmental Microbiology*. Academic Press, San Diego, CA.
- Malaeb, L., Ayoub, G.M. 2011. Reverse osmosis technology for water treatment: State of the art review. *Desalination* 267 (1), 1–8.
- Malainine, S.M., Moussaoui, W., Prevost, G., Scheftel, J.-M., Mimouni, R. 2013. Rapid identification of *Vibrio parahaemolyticus* isolated from shellfish, sea water and sediments of the Khnifiss lagoon, Morocco, by MALDI-TOF mass spectrometry. *Lett. Appl. Microbiol.* 56, 379-386.
- Mann, S., Archibald, D.D., Didymus, J.M., Douglas, T., Heywood, B.R., Meldrum, F.C., Reeves, N. 1993. Crystallization at inorganic-organic interfaces: Biominerals and biomimetic synthesis. *Science* 261, 1286-1292.

- Mansor, M., Harouaka, K., Gonzales, M.S., Macalady, J.L., Fantle, M.S. 2018. Transport-induced spatial patterns of sulfur isotopes ( $\delta^{34}\text{S}$ ) as biosignatures. *Astrobiology* 18, 59-72.
- Mansouri, J., Harrisson, S., Vicki, C. 2010. Strategies for controlling biofouling in membrane filtration systems: challenges and opportunities. *J. Mater. Chem.* 20, 4567-4586.
- Mansourpanah, Y., Kakanejadifard, A., Dehrizi, F.G., Tabatabaei, M., Afarani, H.S. 2015. Increasing and enhancing the performance and antifouling characteristics of PES membranes using acrylic acid and microwave-modified chitosan. *Korean J. Chem. Eng.*, 32(1), 149-158.
- Mansoor, K., Toraj, M. 2007. Chemical cleaning of ultrafiltration membranes in the milk industry. *Desalination* 204, 213-218.
- Mao, C., Mohanraj, G., Kandiyote, N.S., Kasher, R., Arnusch, C.J. 2018. UV mediated attachment of short Arginine-Tryptophan antimicrobial peptides on reverse osmosis membrane surfaces inhibit *Pseudomonas aeruginosa* biofilm. *Desalination* 431, 73–79.
- Matin, A., Rahman, F., Zubair, S.M. 2019. Scaling of reverse osmosis membranes used in water desalination: Phenomena, impact, and control; future directions. *Desalination* 455, 135–157. <https://doi.org/10.1016/j.desal.2018.12.009>.
- Matral, P., Greenberg, R., Krantz, B. 2000. Investigation of membrane fouling and cleaning using ultrasonic time-domain reflectometry. *Desalination* 130, 45-60.
- Mayer, C., Moritz, R., Kirschner, C., Borchard, W., Maibaum, R., Wingender, J., Flemming, H.C. 1999. The role of intermolecular interactions: studies on model systems for bacterial biofilms. *Int. J. Biol. Macromol.* 26 (1), 3-16.

- McCeldowney, S., Fletcher, M. 1986. Effect of Growth Conditions and Surface Characteristics of Aquatic Bacteria on Their Attachment to Solid Surfaces. *J. Gen. Microbiol.*, 132, 513-523.
- Meex, C., Neuville, F., Descy, J., Huynen, P., Hayette, M.-P., De Mol, P., Melin, P. 2012. Direct identification of bacteria from BacT/ALERT anaerobic positive blood cultures by MALDI-TOF MS: maldi Sepsity per kit versus an in-house saponin method for bacterial extraction. *J. Med. Microbiol.* 61, 1511–1516.
- Melo, L.F., Bott, T.R., Bernardo, C.A. 1988. *Fouling Science and Technology*, Kluwer Academic Publishers.
- Melian-Martel, N., Sadhwani, J.J., Malamis, S., Ochsenkuhn-Petropoulou, M. 2012. Structural and chemical characterization of long-term reverse osmosis membrane fouling in a full-scale desalination plant. *Desalination* 305, 44-53.
- Mendret, J., Guigui, C., Schmitz, P., Cabassud, C., Duru, P. 2007. An optical method for in situ characterization of fouling during filtration. *AIChE J.* 53 (9), 2265-2274.
- Mi, B., Elimelech, M. 2013. Silica scaling and scaling reversibility in forward osmosis. *Desalination* 312, 75–81.
- Mi, B., Elimelech, M. 2010. Gypsum Scaling and Cleaning in Forward Osmosis: Measurements and Mechanisms. *Environ. Sci. Technol.* 44, 2022–2028.
- Mills, A., Hunte, S.L. 1997. An overview of semiconductor photocatalysis, *J. Photochem. Photobiol. A Chem.* 108, 1–35.
- Mitrouli, S., Karabelas, A.J., Karanasiou, A., Kostoglou, M. 2013. Incipient calcium carbonate scaling of desalination membranes in narrow channels with spacers — experimental insights. *J. Memb. Sci.* 425–426, 48–57. <https://doi.org/10.1016/j.memsci.2012.09.025>

- Monroe, D. 2007. Looking for chinks in the armor of bacterial biofilms. *PLoS Biol.* 5, 2458–2461.
- Monruedee, M., Sarp, S., Lee, Y.G., Kim, J.H. 2012. Time-series image analysis for investigating SWRO fouling mechanism. *Desalin. Water Treat.* 43, 212-220.
- Mu, S., Wang, S., Liang, S., Xiao, K., Fan, H., Han, B., Liu, C., Wang, X., Huang, X. 2019. Effect of the relative degree of foulant “hydrophobicity” on membrane fouling. *J. Memb. Sci.* 570–571, 1–8. <https://doi.org/10.1016/j.memsci.2018.10.023>
- Munoz, R., Lopez-Lopez, A., Urdiain, M., Moore, E.R.B., Rosselo-Mora, R. 2011. Evaluation of matrix-assisted laser desorption ionization time-of-flight whole cell profiles for assessing the cultivable diversity of aerobic and moderately halophilic prokaryotes thriving in solar saltern sediments. *Syst. Appl. Microbiol.* 34 (1), 69–75.
- Muryanto, S., Bayuseno, A., Diponegoro, U. 2013. Influence of flow rates and copper (II) ions on the kinetics of gypsum scale formation in pipes. *Int. J. Technol.* 3, 216–223.
- Nabe, A., Staude, E., Belfort, G. 1997. Surface modification of polysulfone ultrafiltration membranes and fouling by BSA solutions. *J. Membr. Sci.* 133, 57–72.
- Nagaraj, N., Skillman, L., Xie, Z., Jiang, S., Ho, G., Li, D. 2017. Investigation of compounds that degrade biofilm polysaccharides on reverse osmosis membranes from a full-scale desalination plant to alleviate biofouling. [Desalination 403 \(1\)](#), 88–96.

- Nagaraj, V., Skillman, L., Li, D., Ho, G. 2018. Bacteria and their extracellular polymeric substances causing biofouling on seawater reverse osmosis desalination membranes. *J. Environ. Manage.* 223, 586–599.
- Nghiem, L.D., Vogel, D., Khan, S. 2008. Characterizing humic acid fouling of nanofiltration membranes using bisphenol A as a molecular indicator, *Water Res.*, 42, 4049–4058.
- Nguyen, T., Roddick, F.A., Fan, L. 2012. Review - Biofouling of Water Treatment Membranes: A Review of the Underlying Causes, Monitoring Techniques and Control Measures. *Membranes* 2, 804-840.
- Ni, L., Mengn, J., Li, X., Zhang, Y. 2014. Surface coating on the polyamide TFC RO membrane for chlorine resistance and antifouling performance improvement. *J. Membr. Sci.* 451, 205–215.
- Nine, M.J., Cole, M.A., Tran, D.N., Losic, D. 2015. Graphene: a multipurpose material for protective coatings. *J. Mater. Chem. A*, 3, 12580–12602.
- Ning, R.Y. 1999. Reverse osmosis process chemistry relevant to the Gulf. *Desalination*, 123, 157-164.
- Nivens, D.E., Ohman, D.E., Williams, J., Franklin, M.J. 2001. Role of alginate and its O acetylation in formation of *Pseudomonas aeruginosa* microcolonies and biofilms. *J. Bacteriol.* 183 (3),1047-1057.
- Niyompanich, S., Jaresitthikunchai, J., Srisanga, K., Roytrakul, S., Tungpradabkul, S. 2014. Source-Identifying Biomarker Ions between Environmental and Clinical *Burkholderia pseudomallei* Using Whole-Cell Matrix-Assisted Laser Desorption/Ionization Time-of-Flight Mass Spectrometry (MALDI-TOF MS). *Plos one* 9 (6).
- Ogawa, H., Tanoue, E. 2003. Dissolved Organic Matter in Oceanic Waters. *J. Oceanogr.* 59, 129-147.



- Ong, C.S., Goh, P.S., Lau, W.J., Misdan, N., Ismail, A.F. 2016. Nanomaterials for biofouling and scaling mitigation of thin film composite membrane: A review. *Desalination* 393, 2–15.
- Ozaydin-Ince, G., Matin, A., Khan, Z., Zaidi, S.M.J., Karen, K., Gleason, K.K. 2013. Surface modification of reverse osmosis desalination membranes by thin-film coatings deposited by initiated chemical vapor deposition. *Thin Solid Films* 539, 181–187.
- Ozkar, S. 2001. Kinetics of gypsum formation and growth during the dissolution of colemanite in sulfuric acid. *J. Cryst. Growth*. 231, 559–567.
- Ozturk, S., Aslim B, Suludere Z. 2010. Cadmium (II) sequestration characteristics by two isolates of *Synechocystis* sp. in terms of exopolysaccharide (EPS) production and monomer composition. *Bioresource Technol.* 101, 9742–9748.
- Pang, M., Hong, H., Guo, H., Liu, W. 2005. Biofilm formation characteristics of bacterial isolates retrieved from a reverse osmosis membrane. *Environ. Sci. Technol.*, 39, 7541-7550.
- Patel, S., Finan, M.A. 1999. New antifoulants for deposit control in MSF and MED plants. *Desalination* 124, 63-74.
- Pathak, V.M., Navneet. 2017. Review on the current status of polymer degradation: a microbial approach. *Bioresour. Bioprocess.*, 4 (15), 1-31.
- Paul, D.H., Abanmy, A.M. 1990. Reverse osmosis, membrane fouling - the final frontier. *Ultra-Pure Water* 7 (3), 25-36.
- Perdrial, J.N., Warr, L.N., Perdrial, N., Lett, M.-C., Elsass, F. 2009. Interaction between smectite and bacteria: implications for bentonite as backfill material in the disposal of nuclear waste. *Chem. Geol.* 264, 281–294.

- Perreault, F., Tousley, M.E., Elimelech, M. 2013. Thin-film composite polyamide membranes functionalized with biocidal graphene oxide nanosheets, *Environ. Sci. Technol. Lett.* 1, 71-76.
- Popov, K., Oshchepkov, M., Afanas, E., Koltinova, E. 2019. A new insight into the mechanism of the scale inhibition: DLS study of gypsum nucleation in presence of phosphonates using nanosilver dispersion as an internal light scattering intensity reference. *Colloids Surfaces A* 560, 122–129.  
<https://doi.org/10.1016/j.colsurfa.2018.10.015>.
- Popovic, N.T., Kazazic, S.P., Perovic, I.S., Rakovac, R.C. 2017. Differentiation of environmental aquatic bacterial isolates by MALDI-TOF MS. *Env. Res.* 152, 7–16.
- Prolund, B., Palmgren, R., Keiding, K., Nielsen, P.H. 1996. Extraction of extracellular polymers from activated sludge using a cation exchange resin. *Water Res.* 30, 1749–1758.
- Qasim, M., Badrelzaman, M., Darwish, N.N., Darwish, N.A., Hilal, N. 2019. Reverse osmosis desalination: A state-of-the-art review. *Desalination* 459, 59-104.
- Qiblawey, H., Banat, F., Al-Nasser, Q. 2009. Laboratory setup for water purification using household PV-driven reverse osmosis unit. *Desalin. Water Treat.* 7, 53–59.  
<https://doi.org/10.5004/dwt.2009.695>
- Rabiller-Baudry, M., Gouttefangeas, F., Le Lannic, J., Rabiller, P. 2012. Coupling of SEM-EDX and FTIR-ATR to (quantitatively) investigate organic fouling on porous organic composite membranes. *Current Microscopy contributions to Advances in Sciences and Technology*, Formatex Research Center.
- Rahardianto, A. 2008. Reverse Osmosis Desalting of Inland Brackish Water of High Gypsum Scaling Propensity: Kinetics and Mitigation of Membrane Mineral Scaling 42 (12), 4292–4297.

- Rahardianto, A., Shih, W., Lee, R., Cohen, Y. 2006. Diagnostic characterization of gypsum scale formation and control in RO membrane desalination of brackish water. *J. Membr. Sci.* 279, 655–668. <https://doi.org/10.1016/j.memsci.2005.12.059>
- Rahman, F. 2013. Calcium sulfate precipitation studies with scale inhibitors for reverse osmosis desalination. *Desalination* 319, 79–84. <https://doi.org/10.1016/j.desal.2013.03.027>
- Rezaei H., Ashtiani F. Z. and Fouladitajar A. 2014. Fouling behavior and performance of microfiltration membranes for whey treatment in steady and unsteady-state conditions. *Braz. J. Chem. Eng.* 31 (2), 503 – 518.
- Rezaei, H., Zokaee Ashtiani, F., Fouladitajar, A. 2011. Effects of operating parameters on fouling mechanism and membrane flux in cross-flow microfiltration of whey. *Desalination*, 274, 262-271.
- Ridgway, H.F., Flemming, H.C. 1996. Membrane biofouling. In: *Water treatment membrane processes*, J. Mallevialle, P.E. Odendaal, M.R. Wiesne (Eds.), McGraw-Hill.
- Ridgway, H.F., Rigby, M.G., Argo, D.G. 1985. Bacterial adhesion and fouling of reverse osmosis membranes. *J. Am. Water Works Ass.*, 77, 97–106.
- Rinzema, A., Vanlier, J., Lettinga, G. 1988. Sodium inhibition of acetoclastic methanogens in granular sludge from a UASB reactor. *Enzyme Microb. Technol.* 10, 24–32.
- Rivadeneira, M.A., P´arraga, J., Delgado, R., Ramos-Cormenzana, A., Delgado, G. 2004. Biomineralization of carbonates by *Halobacillus trueperi* in solid and liquid media with different salinities. *FEMS Microbiol. Ecol.* 48, 39–46.
- Rizzardi, K., Wahab, T., Jernberg, C. 2013. Rapid subtyping of *Yersinia enterocolitica* by matrix-Assisted laser desorption ionization-time of flight mass spectrometry

- (MALDITOF MS) for diagnostics and surveillance. *J. Clin. Microbiol.* 51, 4200–4203.
- Rodriguez-Calvo, A., Silva-Castro, G.A., Uad, I., Robledo-Mahon, T., Menendez, M., Gonzalez-Lopez, J., Calvo, C.A. 2017. Comparative study of adhesion by bacterial isolates of marine origin. *Int. Biodeterior. Biodegrad.* 123, 87-95.
- Rodriguez, G., Penate, B. 2012. Current trends and future prospects in the design of seawater reverse osmosis desalination technology. *Desalination* 284, 1-8.
- Rosen, B.P. 1987. Bacterial calcium transport. *Biochi. Biophys. Acta.* 906, 101–110.
- Saeki, D., Tanimoto, T., Matsuyama, H. 2014a. Anti-biofouling of polyamide reverse osmosis membranes using phosphorylcholine polymer grafted by surface-initiated atom transfer radical polymerization. *Desalination* 350, 21–27
- Saeki, D., Tanimoto, T., Matsuyama, H. 2014b. Prevention of bacterial adhesion on polyamide reverse osmosis membranes via electrostatic interactions using a cationic phosphorylcholine polymer coating. *Colloids and Surfaces A: Physicochem. Eng. Aspects* 443, 171– 176.
- Safarpour, M., Khataee, A., Vatanpour, V. 2015. Thin-film nanocomposite reverse osmosis membrane modified by reduced graphene oxide /TiO<sub>2</sub> with improved desalination performance. *J. Memb. Sci.* 489, 43-54.
- Saleem, H., Zaidi, S.J. 2020. Nanoparticles in reverse osmosis membranes for desalination: A state of the art review. *Desalination* 475, 114171.
- Salido, E.M., Servalli, L.N., Gomez, J.C., Verrastro, C. 2017. Phototransduction early steps model based on Beer-Lambert optical law. *Vision Res.* 131, 75–81.
- Sanchez-Roman, M., Vasconcelos, C., Warthmann, R., Rivadeneyra, M., McKenzie, J.A. 2007. Microbial dolomite precipitation under aerobic conditions: results from Brejo do Espinho Lagoon (Brazil) and culture experiments. *Perspectives in*

- Sedimentary Geology: A Tribute to the Career of Robert Nathan Ginsburg (Swart PK, Eberli GP & McKenzie JA, eds), IAS Spec Publ.
- Sathya, S., Murthy, P.S., Das, A., Sankar, G.G., Venkatnarayanan, S., Pandian, R., Sathyaseelan, V.S., Pandiyan, V., Doble, M., Venugopalan, V.P. 2016. Marine antifouling property of PMMA nanocomposite films: Results of laboratory and field assessment. *Int. Biodeterior. Biodegrad.* 114, 57-66.
- Schausberger, P., Mustafa, G.M., Leslie, G., Friedl, A. 2009. Scaling Prediction Based on Thermodynamic Equilibrium Calculation -- Scopes and Limitations. *Desalination* 244 (1-3), 31-47.
- Schirmeister, F., Wiczorek, A., Dieckmann, R., Taureck, K., Strauch, E. 2014. Evaluation of molecular methods to discriminate the closely related species *Vibrio fluvialis* and *Vibrio furnissii*. *Int. J. Med. Microbiol.* 304 (7), 851–857.
- Seltzer S.M. 1993. Calculation of photon mass energy-transfer and mass energy-absorption coefficients. *Radiat. Res.* 136 (2), 147-170.
- Seyedpour, S.F. Rahimpour, A., Shamsabadi, A.A., Soroush, M. 2018. Improved performance and antifouling properties of thin-film composite polyamide membranes modified with nano-sized bactericidal graphene quantum dots for forward osmosis. *Chem. Eng. Res. Des.* 139, 321-334.
- Shafi, H., Khan, Z., Yang, R., Gleason, K.K. 2015. Surface modification of reverse osmosis membranes with zwitterionic coating for improved resistance to fouling. *Desalination* 362, 93–103
- Shao, J., Yang, Y.M., Zhong, Q.-Q. 2003. Studies on preparation of oligoglucosamine by oxidative degradation under microwave irradiation. *Polym. Degrad. Stab.* 82 (3), 395-398.

- Sheikholeslami, R. and Ng, M. 2001. Calcium sulfate precipitation in the presence of nondominant calcium carbonate: Thermodynamics and Kinetics. *Ind. Eng. Chem. Res.* 40 (16), 3570-3578.
- Sheng, G.P., Yu, H.Q. 2006. Relationship between the extracellular polymeric substances and surface characteristics of *Rhodopseudomonas acidophila*. *Appl. Microbiol. Biotechnol.* 72, 126–131.
- Sheng, G.P., Yu, H.Q., Yue, Z. 2005. Extraction of extracellular polymeric substances from the photosynthetic bacterium *Rhodopseudomonas acidophila*. *Appl. Microbiol. Biotechnol.* 67, 125–130.
- Sheng, G.P., Yu, H.Q., Yue, Z. 2006. Factors influencing the production of extracellular polymeric substances by *Rhodopseudomonas acidophila*. *Int. Biodeter. Biodegr.* 58, 89–93.
- Sheppard, C.J.R., Shotton, D.M. 1997. *Confocal Laser Scanning Microscopy*. Bios Scientific Publisher, Royal Microscopical Society, UK.
- Shih, W.Y., Gao, J., Rahardianto, A., Glater, J., Cohen, Y., Gabelich, C.J. 2006. Ranking of antiscalant performance for gypsum scale suppression in the presence of residual aluminum. *Desalination* 196, 280–292.
- Shih, W.Y., Rahardianto, A., Lee, R.W., Cohen, Y. 2005. Morphometric characterization of calcium sulfate dihydrate (gypsum) scale on reverse osmosis membranes. *J. Memb. Sci.* 252, 253–263.  
<https://doi.org/10.1016/j.memsci.2004.12.023>
- Shmulevsky, M., Li, X., Shemer, H., Hasson, D., Semiat, R. 2017. Analysis of the onset of calcium sulfate scaling on RO membranes. *J. Memb. Sci.* 524, 299–304.  
<https://doi.org/10.1016/j.memsci.2016.11.055>

- Shirazi, S., Lin, C.-J., Chen, D. 2010. Inorganic fouling of pressure-driven membrane processes — A critical review. *Desalination* 250, 236-248.
- Shon, H.K., Vigneswaran, S., Zareie, M.H., Aim, R.B., Lee, E., Lee, J., Cho, J., Kim, I.S. 2009. Physico-chemical pretreatment to seawater reverse osmosis (SWRO): organic characterization and membrane autopsy. *Desalination* 236, 282-290.
- Simon, F.X., Penru, Y., Guastalli, A.R., Esplugas, S., Llorens, J., Baig, S. 2012. NOM characterization by LC-OCD in a SWRO desalination line, *Desalin. Water Treat.* 51, 1776-1780.
- Siozos, P., Philippidis, A., Hadjistefanou, M., Gounarakis, C., Anglos, D. 2013. Chemical analysis of industrial scale deposits by combined use of correlation coefficients with emission line detection of laser induced breakdown spectroscopy spectra. *Spectrochim. Acta, Part B* 87, 86-91.
- Song, L., Li, B., Sirkar, K.K., Gilron, J.L. 2007. Direct contact membrane distillation-based desalination: novel membranes, devices, larger-scale studies, and a model. *Ind. Eng. Chem. Res.* 46, 2307–2323.
- Song L., Tay K.G. 2008. Advanced Membrane Fouling Characterization in Full-Scale Reverse Osmosis Processes, in: *Membrane and Desalination Technologies*, L.K. Wang, J.P. Chen, Y.-T. Hung, N.K. Shamma (Eds.), Humana Press, 101-134.
- Sorkhoh, N.A., Al-Awadhi, H., Al-Mailem, D.M., Kansour, M.K., Khanafer, M., Radwan, S.S. 2010. Agarolytic bacteria with hydrocarbon-utilization potential in fouling material from the Arabian Gulf coast. *Int. Biodeterior. Biodegrad.* 64, 554-559.
- Spitaels, F., Wieme, A.D., Vandamme, P. 2016. MALDI-TOF MS as a novel tool for dereplication and characterization of microbiota in bacterial diversity studies.

- Applications of Mass Spectrometry in Microbiology, In: Demirev, P. Sandrin, T.R. (Eds.).
- Spyres, G., Nimmo, M., Worsfold, P.J., Achterberg, E.P., Miller, A.E.J. 2000. Determination of dissolved organic carbon in seawater using high temperature catalytic oxidation techniques. *TrAC, Trends Anal. Chem.* 19, 498-506.
- Stawski, T.M., Van Driessche, A.E.S., Ossorio, M., Rodriguez-blanco, J.D., Besselink, R., Benning, L.G. 2016. Formation of calcium sulfate through the aggregation of sub-3 nanometer primary species. *Nat. Commun.* 6, 1–9.
- Stuart, H.B. 2004. Chapter 3, Spectral Analysis. *Infrared Spectroscopy: Fundamentals and Applications.* John Wiley and Sons Ltd. 57.
- Stumm, W., Morgan, J.J. 1981. *Aquatic Chemistry, An Introduction Emphasizing Chemical Equilibria in Natural Waters.* New York: John Wiley & Sons.
- Su, M., Bai, Y., Han, J., Chen, J., Sun, H. 2018. Adhesion of gypsum crystals to polymer membranes: Mechanisms and prediction. *J. Memb. Sci.* 566, 104–111. <https://doi.org/10.1016/j.memsci.2018.08.062>
- Subramani, A., Hoek, E.M.V. 2010. Biofilm formation, cleaning, re-formation on polyamide composite membranes. *Desalination* 257, 73-79.
- Sudak, R.G. 1990. Reverse Osmosis, in: *Handbook of Industrial Membrane Technology*, M.C. Porter (Ed.) William Andrew Publishing/Noyes, Westwood, New Jersey, U.S.A., 260-305.
- Sun, Y., Yaoyao, F., Peng, L., Xia, H. 2016. Effects of online chemical cleaning on removing biofouling and resilient microbes in a pilot membrane bioreactor. *Int. Biodeter. Biodegr.* 112, 119-127.



- Sun, M., Li, J. 2018. Nano Today Graphene oxide membranes: Functional structures, preparation and environmental applications. *Nano Today* 20, 121–137. <https://doi.org/10.1016/j.nantod.2018.04.007>
- Suratt, W.B., Andrews, D.R., Pujals, V.J., Richards, S.A. 2000. Design considerations for major membrane treatment facility for groundwater. *Desalination* 131, 37–46.
- Sweity, A., Oren, Y., Ronen, Z., Herzberg, M. 2013. The influence of antiscalants on biofouling of RO membranes in seawater desalination. *Water Res.* 47 (10), 3389-3398.
- Sweity, A., Ronen, Z., Herzberg, M. 2014. Induced organic fouling with antiscalants in seawater desalination. *Desalination* 352, 158–165.
- Sweity, A., Zere, T.R., David, I., Bason, S., Oren, Y., Ronen, Z., Herzberg, M. 2015. Side effects of antiscalants on biofouling of RO membranes in brackish water desalination. *J. Membr. Sci.* 481, 172-187.
- Tang, C.Y., Kwon, Y.-N., Leckie, J.O. 2009. The role of foulant-foulant electrostatic interaction on limiting flux for RO and NF membranes during humic acid fouling-theoretical basis, experimental evidence, and AFM interaction force measurement. *J. Membr. Sci.* 326, 526-532.
- Tang, C.Y., Chong, T.H., Fane, A.G. 2011. Colloidal interactions and fouling of NF and RO membranes: A review, *Adv. Colloid Interface Sci.* 164, 126-143.
- Tang, C.Y., Kwon, Y., Leckie, J.O. 2009. Effect of membrane chemistry and coating layer on physiochemical properties of thin film composite polyamide RO and NF membranes I. FTIR and XPS characterization of polyamide and coating layer chemistry. *Des.* 242, 149–167. <https://doi.org/10.1016/j.desal.2008.04.003>
- Tang, C.Y., Kwon, Y., Leckie, J.O. 2007. Probing the nano- and micro-scales of reverse osmosis membranes — A comprehensive characterization of physiochemical

- properties of uncoated and coated membranes by XPS, TEM, ATR-FTIR, and streaming potential measurements 287, 146–156.  
<https://doi.org/10.1016/j.memsci.2006.10.038>
- Taniguchi, M., Belfort, G. 2004. Low protein fouling synthetic membranes by UV-assisted surface grafting modification: varying monomer type. *J. Membr. Sci.* 231 (1-2), 147-157.
- Tay, F.H., Kazarian, S.G. 2009. Study of Petroleum heat-exchanger deposits with ATR-FTIR spectroscopic imaging. *Energy Fuels* 23 (8), 4059-4067.
- Telesmanich, N.R., Chaika, S.O., Vodianitskaia, S., Chemisova, O.S., Chaika, I.A. 2014. The application of mass spectrometry technique MALDI-TOF for inter-specific differentiation of closely related *Vibrio*. *Klin. Lab. Diagn.* 59 (8), 27–28.
- Thompson, J., Lin, N., Lyster, E., Arbel, R., Knoell, T., Gilron, J., Cohen, Y. 2012. RO membrane mineral scaling in the presence of a biofilm. *J. Memb. Sci.* 415–416, 181–191. <https://doi.org/10.1016/j.memsci.2012.04.051>
- Tikka, A., Gao, W., Liao, B. 2019. Reversibility of membrane performance and structure changes caused by extreme cold-water temperature and elevated conditioning water temperature. *Water Res.* 151, 260-270.
- Tong, T., Wallace, A.F., Zhao, S., Wang, Z. 2019. Mineral scaling in membrane desalination: Mechanisms, mitigation strategies, and feasibility of scaling-resistant membranes. *J. Memb. Sci.* 579, 52–69.
- Trivedi, T.J., Shukla, J., Kumar, A. 2014. Effect of nitrate salts on solubility behaviour of calcium sulphate dehydrate (gypsum) in the aqueous sodium chloride system and physicochemical solution properties at 308.15 K. *J. Chem. Eng. Data* 59, 832-838.

- Tryfinopoulou, P., Tsakalidou, E., Nychas, G.H.E. 2002. Characterization of *Pseudomonas* spp. associated with Spoilage of Gilt-Head Sea Bream Stored under Various Conditions. *Appl. Environ. Microbiol.* 68, 65–72.
- Tsai, H.A., Chen, H.C., Lee, K.R., Lai, J.Y. 2006. Study of the separation properties of chitosan / polysulfone composite hollow-fiber membranes. *Desalination* 193, 129–136.
- Tsuneda, S., Aikawa, H., Hayashi, H., Yuasa, A., Hirata, A. 2010. Extracellular polymeric substances responsible for bacterial adhesion onto solid surface. *FEMS Microbiol. Lett.* 223 (2), 287–292.
- Tuson, H.H., Weibel, D.B. 2013. Bacteria-surface interactions. *Soft Matter* 9 (18), 4368.
- Uchymiak, M., Lyster, E., Glater, J., Cohen, Y. 2008. Kinetics of gypsum crystal growth on a reverse osmosis membrane 314, 163–172.  
<https://doi.org/10.1016/j.memsci.2008.01.041>
- US-EPA, Membrane filtration guidance manual, (2005).
- UN-Water, Analytical Brief on Water Security and the GlobalWater Agenda, <http://www.unwater.org/topics/water-security/en 2013>. Accessed on 29.04.2017 at 02:15 pm.
- Van de Lisdonk C.A.C., Van Paassen J.A.M., Schippers J.C., (2000). Monitoring scaling in nanofiltration and reverse osmosis membrane systems, *Desalination*, 132 (2000) 101-108.
- Vatankhah, H., Murray, C.C., Brannum, J.W., Vanneste, J., Bellona, C. 2018. Separation and Purification Technology Effect of pre-ozonation on nanofiltration membrane fouling during water reuse applications. *J. Memb. Sci.* 205, 203–211.  
<https://doi.org/10.1016/j.seppur.2018.03.052>

- Vrijenhoek, E.M., Hong, S., Elimelech M. 2001. Influence of membrane surface properties on initial rate of colloidal fouling of reverse osmosis and nanofiltration membranes. *J. Memb. Sci.* 188, 115–128.
- Vrouwenvelder, J.S., Beyer, F., Dahmani, K., Hasan, N., Galjaard, G., Kruithof, J.C., Van Loosdrecht, M.C.M. 2010. Phosphate limitation to control biofouling. *Water Res.* 44 (11), 3454-3466.
- Vrouwenvelder, J.S., Manolarakis, S.A., Veenendaal, H.R., Van der Kooij, D. 2000. Biofouling potential of chemicals used for scale control in RO and NF membranes. *Desalination* 132 (1), 1-10.
- Vrouwenvelder, J., Buijter, J., Riviere, M., Van der Meer, W., Van, L.M., Kruithof, J. 2010. Impact of flow regime on pressure drop increase and biomass accumulation and morphology in membrane systems. *Water Res.* 44, 689–702.
- Water Statistics for the State of Qatar (2013). Published at Ministry of Development Planning and Statistics official website on April 2016. ([www.mdps.gov.qa](http://www.mdps.gov.qa)) accessed on 21.04.2017.
- Wang, G., Li, M., Ma, F., Wang, H., Xu, X., Zhou, G. 2017. Physicochemical properties of *Pseudomonas fragi* isolates response to modified atmosphere packaging. *FEMS Microbiol. Lett.* 364 (11), 1-8.
- Wang, T., Qiblawey, H., Judd, S., Benamor, A., Nasser, M.S. 2018. Fabrication of high flux nano filtration membrane via hydrogen bonding based co-deposition of polydopamine with poly (vinyl alcohol). *J. Memb. Sci.* 552, 222–233.
- Wang, S., Xiao, K., Huang, X. 2019. Characterizing the roles of organic and inorganic foulants in RO membrane fouling development: The case of coal chemical wastewater treatment. *Sep. Purif. Technol.* 210, 1008–1016. <https://doi.org/10.1016/j.seppur.2018.09.062>

- Wang, Z., Yu, H., Xia, J., Zhang, F., Li, F., Xia, Y., Li, Y. 2012. Novel GO-blended PVDF ultrafiltration membranes. *Desalination* 299, 50–54.
- Wang, J., Wang, Z., Wang, J., Wang, S. 2015. Improving the water flux and bio-fouling resistance of reverse osmosis (RO) membrane through surface modification by zwitterionic polymer. *J. Memb. Sci.* 493, 188–199.
- Wang, Y., Gitis, V., Lee, J., Herzberg, M. 2013. Effects of shear rate on biofouling of reverse osmosis membrane during tertiary wastewater desalination. *J. Memb. Sci.* 427, 390–398.
- Water Resource Institute accessed on 29.04.2017 12:00 pm.  
<http://www.wri.org/applications/maps/aqueduct-atlas/>.
- Water Facts and Trends (2006). Published by World Business Council for Sustainable Development available at: <http://www.wbcsd.org/>. Accessed on 29.04.2017 at 01:30 pm.
- WHO UNICEF Joint Monitoring Program, Water Supply, Sanitation and Hygiene Progress report, 2017.
- Wirtanen, G., Mattila-Sandholm, T. 1994. Measurement of biofilm of *Pediococcus pentosaceus* and *Pseudomonas fragi* on stainless steel surfaces. *Colloids Surf. B.* 2, 33-39.
- Wolf, G., Crespo, J.G., Reis, M.A.M. 2002. Optical and spectroscopic methods for biofilm examination and monitoring. *Rev. Environ. Sci. Biotechnol.* 1, 227–251.
- Wolters, M., Rohde, H., Maier, T., Belmar-Campos, C., Franke, G., Scherpe, S., Aepfelbachera, M., Christner, M. 2011. MALDI-TOF MS fingerprinting allows for discrimination of major methicillin-resistant *Staphylococcus aureus* lineages. *Int. J. Med. Microbiol.* 301, 64–68.


- Wu, H., Chen, W., Rong, X., Cai, P., Dai, K., Huang, Q. 2014. Soil colloids and minerals modulate metabolic activity of measured using microcalorimetry. *Geomicrobiol J.* 31 (7), 590–596.
- Xie, M., Gray, S.R. 2016. Gypsum scaling in forward osmosis: Role of membrane surface chemistry. *J. Memb. Sci.* 513, 250–259.  
<https://doi.org/10.1016/j.memsci.2016.04.022>
- Xu, G.R., Wang, J.N., Li, C.J. 2013. Strategies for improving the performance of the polyamide thin film composite (PA-TFC) reverse osmosis (RO) membranes: surface modifications and nanoparticles incorporations. *Desalination* 328, 83–100.
- Xu, P., Bellona, C., Drewes, J.E. 2010. Fouling of nanofiltration and reverse osmosis membranes during municipal wastewater reclamation: membrane autopsy results from pilot-scale investigations. *J. Memb. Sci.* 353, 111–121.
- Yang, H.-L., Lin, J.C., Huang C. 2009. Application of nanosilver surface modification to RO membrane and spacer for mitigating biofouling in seawater desalination. *Wat. Res.* 43, 3777–3786.
- Yanzhen, M., Yang, L., Xiangting, X., Wei, H. 2016. Genome announcement Complete genome sequence of a bacterium *Pseudomonas fragi* P121, a strain with degradation of toxic compounds. *J. Biotechnol.* 224, 68–69.
- Yiantsios, S.G., Sioutopoulos, D., Karabelas, A.J. 2005. Colloidal fouling of RO membranes: an overview of key issues and efforts to develop improved prediction techniques. *Desalination* 183, 257-272.
- Yigit, N.O., Harman, I., Civelekoglu, G., Koseoglu, H., Cicek, N., Kitis, M. 2008. Membrane fouling in a pilot-scale submerged membrane bioreactor operated under various conditions. *Desalination* 231, 124–132.

- Ying, W., Gitis, V., Lee, J., Herzberg M. 2013. Effects of shear rate on biofouling of reverse osmosis membrane during tertiary wastewater desalination. *J. Memb. Sci.* 427, 390-398.
- Yin, J., Kim, E.S., Yang, J., Deng, B. 2012. Fabrication of a novel thin-film nanocomposite (TFN)membrane containing MCM-41 silica nanoparticles (NPs) for water purification. *J. Memb. Sci.* 423–424, 238-246.
- Yu, L., Zhang, Y., Zhang, B., Liu, J., Zhang, H., Song, C. 2013. Preparation and characterization of HPEI-GO/PES ultrafiltration membrane with antifouling and antibacterial properties. *J. Memb. Sci.* 447, 452–462.
- Zangenah, S., Ozenci, V., Borang, S., Bergman, P. 2012. Identification of blood and wound isolates of *C. canimorsus* and *C. cynodegmi* using VITEK 2 and MALDI-TOF. *Eur. J. Clin. Microbiol. Infect. Dis.* 31, 2631–2637.
- Zhang, Z., Wang Z., Wang, J., Wang, S. 2013. Enhancing chlorine resistances and anti-biofouling properties of commercial aromatic polyamide reverse osmosis membranes by grafting 3-allyl-5,5-dimethylhydantoin and N,N'-Methylenebis(acrylamide). *Desalination* 309, 187–196.
- Zhang, M., Jiang, S., Tanuwidjaja, D., Voutchkov, N., Hoek, E.M.V., Cai, B. 2011. Composition and variability of biofouling organisms in seawater reverse osmosis desalination plants. *Appl. Environ. Microbiol.* 77, 4390-4398.
- Zhao, C., Xu, X., Chen, J., Yang, F. 2013. Effect of graphene oxide concentration on the morphologies and antifouling properties of PVDF ultrafiltration membranes, *J. Environ. Chem. Eng.* 1, 349–354.
- Zhao, J., Deng, B., Lv, M., Li, J., Zhang, Y., Jiang, H., Peng, C., Li, J., Shi, J., Huang, Q. 2013. Graphene oxide-based antibacterial cotton fabrics. *Adv. Healthcare Mater.* 2, 1259-1266.

- Zhu X., Elimelech M. 1997. Colloidal Fouling of Reverse Osmosis Membranes: Measurements and Fouling Mechanisms. *Environ. Sci. Technol.* 31, 3654-3662.
- Zydney, A.L. 1997. Stagnant film model for concentration polarization in membrane systems. *J. Memb. Sci.* 130, 275–281.



# Use of DPSIR Framework to Analyze Water Resources in Qatar and Overview of Reverse Osmosis as an Environment Friendly Technology

Mohammad Y. Ashfaq,<sup>a</sup> Mohammad A. Al-Ghouti ,<sup>a</sup> Hazim Qiblawey,<sup>b</sup> Nabil Zouari,<sup>a</sup>

Debora F. Rodrigues,<sup>b</sup> and Yandi Hu<sup>b</sup>

<sup>a</sup>Department of Biological and Environmental Sciences, College of Arts and Sciences, Qatar University, State of Qatar, Doha, Qatar; mohammad.alghouti@qu.edu.qa (for correspondence)

<sup>b</sup>Department of Civil and Environmental Engineering, Cullen College of Engineering, University of Houston, Houston Texas

Published online 00 Month 2018 in Wiley Online Library (wileyonlinelibrary.com). DOI 10.1002/ep.13081

*Qatar and other countries of Gulf Cooperation Council are among the most water scarce countries in the world and are being characterized as “high-water risk” countries by Water Resource Institute. Therefore, it is important to implement sustainable water resource management that encompass economic, societal, and environmental aspects. In this review article, the Driver-Pressure-State-Impact-Response framework was used to analyze the water resource system in Qatar in terms of drivers, pressures, change in state, impacts, and responses. It was noted that both economic and population growth together with unsustainable water consumption are major driving forces that are pressurizing the Qatar’s water resources (desalinated seawater and renewable groundwater). Currently, desalination plants using Multi-Stage Flash (MSF) techniques are predominantly being used to meet the rising water demands. However, widespread use of MSF techniques poses several environmental and economic impacts. Therefore, in addition to other management and corrective measures, reverse osmosis (RO) technique has also been suggested to be utilized in desalination industry as a “response” to mitigate those impacts. Since, the performance of RO is mainly affected by biofouling and mineral scaling, the paper also highlights the recent materials (polymers and nano-materials) used to tackle these problems. © 2018 American Institute of Chemical Engineers Environ Prog, 2018*

*Keywords: water resources, reverse osmosis, scaling, bio-fouling, DPSIR framework*

## INTRODUCTION

There is scarcity of clean and safe drinking water in the world. According to recent estimates, one in 10 individuals in the world does not have access to clean water [1] and one infant dies every minute due to waterborne diseases [2]. If no action will be taken to tackle water scarcity problems, it is also predicted that everyone in low- to middle-income countries will not be having access to clean water by 2039 [1].

Qatar is an arid country. It is characterized with elevated temperature during summer crossing 40°C with average rainfall as low as 75.2 mm during the time period of 1962–1992 [3].

However, from 2008 to 2013, it was noted that the annual rainfall was even below the 75.2 mm averaging around 46.71 mm [3]. In addition, the average annual evaporation rate is as high as 2200 mm [4]. Thus, due to its harsh and fragile environment together with limited renewable water resources, the country has been categorized among countries under “high water risk” by Aqueduct Water Risk Atlas [5].

In Qatar and other countries of Gulf Cooperation Council, the concepts of water security, water stress and water resources sustainability are interrelated and are major hurdle for the economic growth and social development. Water stress concept is defined as the situation in which water is not available enough to satisfy all needs related to agricultural, domestic and industrial activities. On the other hand, reliable access to clean and safe water for every person for healthy and productive living and for social and economic growth without polluting the environment is known as water sustainability and water security [6].

It is difficult to define the threshold for water stress in terms of available water per capita. Nevertheless, it has been proposed that the boundary line in terms of annual per capita renewable water resource availability is 1000 m<sup>3</sup>. Below this, the country is considered under water stress and it begins to hamper social and economic development [7]. In comparison, the annual water resource availability per capita in Qatar was 71 m<sup>3</sup> in 2005 [4]. This was further reduced to 25.78 m<sup>3</sup> in 2014 [8] which makes the country under severe water stress condition.

The circulation of water and regional ecology are the basis of water resource systems. The water resource systems help to balance the water cycle, sustainable development and use of water resources. Better water resource management can certainly help to improve water security issues in Qatar. The challenge here will be to adopt integrated approach that helps to allocate water resources based on demands, utilize efficient technologies and promote water reuse and conservation practices. Therefore, there is a need to develop better water resource management plan that can address this challenge. It is important to overview the water resource management of a region from sustainable perspective as it helps to include economic, environmental and societal point of view [9,10]. This is in line with Qatar National Vision 2030 (QNV, 2030) that aims to promote sustainable development.

© 2018 American Institute of Chemical Engineers

## APPENDIX B: PUBLICATION FROM OBJECTIVE 01

Science of the Total Environment 703 (2020) 134726



Contents lists available at ScienceDirect

Science of the Total Environment

journal homepage: [www.elsevier.com/locate/scitotenv](http://www.elsevier.com/locate/scitotenv)



### Investigating the effect of temperature on calcium sulfate scaling of reverse osmosis membranes using FTIR, SEM-EDX and multivariate analysis



Mohammad Y. Ashfaq<sup>a</sup>, Mohammad A. Al-Ghouthi<sup>a,\*</sup>, Dana A. Da'na<sup>a</sup>, Hazim Qiblawey<sup>b</sup>, Nabil Zouari<sup>a</sup>

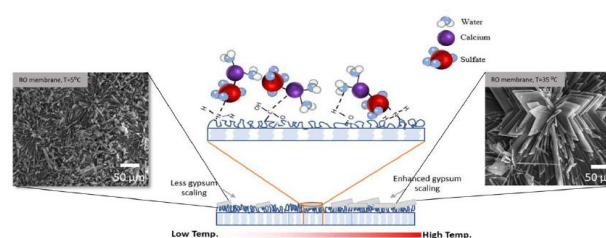
<sup>a</sup> Department of Biological and Environmental Sciences, College of Arts and Sciences, Qatar University, P.O. Box: 2713, Doha, Qatar

<sup>b</sup> Department of Chemical Engineering, College of Engineering, Qatar University, P.O. Box: 2713, Doha, Qatar

#### HIGHLIGHTS

- Membrane fouling is major hurdle for the widespread use of membrane technology.
- Increase in temperature can affect CaSO<sub>4</sub> scaling intensity, and morphology.
- At higher temperature, crystal morphology changes from rod shape to rosette structures.
- Using PCA, membrane's permeate flux can be differentiated at different conditions.
- FTIR results showed the involvement of OH, COOH and NH<sub>2</sub> groups in membrane scaling.

#### GRAPHICAL ABSTRACT



#### ARTICLE INFO

##### Article history:

Received 30 July 2019

Received in revised form 27 September 2019

Accepted 28 September 2019

Available online 31 October 2019

Editor: Yifeng Zhang

##### Keywords:

Reverse osmosis  
Graphene oxide  
Scaling  
Temperature  
Gypsum

#### ABSTRACT

Membrane fouling is one of the major hurdles in widespread use of seawater reverse osmosis (SWRO) in desalination industry. There are various factors that affect the inorganic fouling or scaling of Reverse osmosis (RO) membranes. In this research, the effect of temperature on scaling of RO and Graphene oxide (GO) coated RO membrane by calcium sulfate was investigated. It was found that the increase in temperature enhanced the membrane scaling which was evident by the severe flux decline over time leading to increase in mass of crystals precipitated ( $M_t$ ) and thickness of the scale layer. There was strong positive correlation ( $R^2 \geq 0.97$ ) noted between  $M_t$  and the temperature. The results of SEM-EDX and XRD confirmed that the crystals formed under the experimental conditions are gypsum. Results of this research showed that there was no significant difference in terms of crystal morphology, scaling intensity and mechanism after modifying RO membrane with GO. It was noted that the morphology of the crystals varied from rod shaped to rosette structures under the influence of temperature. Furthermore, the results of FTIR helped to understand the mechanism of interaction between the membranes and the gypsum. The hydrophilicity of the scaled membrane was also measured to investigate the changes in the properties of the membrane after scaling.

© 2019 Elsevier B.V. All rights reserved.

\* Corresponding author.

E-mail address: [mohammad.alghouthi@qu.edu.qa](mailto:mohammad.alghouthi@qu.edu.qa) (M.A. Al-Ghouthi).

<https://doi.org/10.1016/j.scitotenv.2019.134726>  
0048-9697/© 2019 Elsevier B.V. All rights reserved.

#### 1. Introduction

Recent estimations of World Health Organization (WHO) has shown that in every 10 individuals, one does not have access to

## APPENDIX C: PUBLICATIONS FROM OBJECTIVE 2

Science of the Total Environment 656 (2019) 910–920



Contents lists available at ScienceDirect

Science of the Total Environment

journal homepage: [www.elsevier.com/locate/scitotenv](http://www.elsevier.com/locate/scitotenv)



### Isolation, identification and biodiversity of antiscalant degrading seawater bacteria using MALDI-TOF-MS and multivariate analysis



Mohammad Y. Ashfaq<sup>a</sup>, Mohammad A. Al-Ghouthi<sup>a,\*</sup>, Hazim Qjblawey<sup>b</sup>, Debora F. Rodrigues<sup>c</sup>, Yandi Hu<sup>c</sup>, Nabil Zouari<sup>a</sup>

<sup>a</sup> Department of Biological and Environmental Sciences, College of Arts and Sciences, Qatar University, P.O. Box: 2713, Doha, Qatar

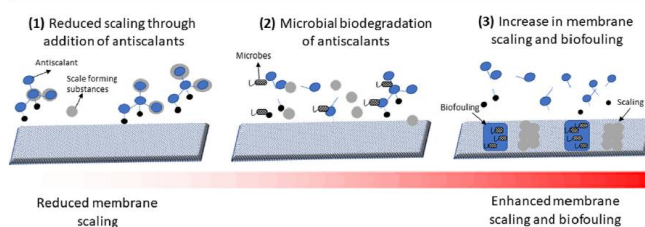
<sup>b</sup> Department of Chemical Engineering, College of Engineering, Qatar University, P.O. Box: 2713, Doha, Qatar

<sup>c</sup> Department of Civil and Environmental Engineering, Cullen College of Engineering, University of Houston, Houston, TX, USA

#### HIGHLIGHTS

- Antiscalants are commonly used to reduce scaling in seawater reverse osmosis.
- The antiscalants are prone to enhance membrane biofouling.
- There is a biodiversity of seawater bacteria that can biodegrade antiscalants.
- Bacterial biodiversity can be explored through combining MALDI-TOF MS with PCA.
- The specific growth rates vary with the type of bacteria and antiscalants.

#### GRAPHICAL ABSTRACT



#### ARTICLE INFO

##### Article history:

Received 22 October 2018

Received in revised form 30 November 2018

Accepted 30 November 2018

Available online 01 December 2018

Editor: Damia Barcelo

##### Keywords:

Antiscalant degrading bacteria

Microorganisms

Seawater reverse osmosis

MALDI-TOF-MS

Multivariate analysis

#### ABSTRACT

Seawater reverse osmosis (SWRO) is a commonly used desalination technique owing to its lesser environmental and economic impacts as compared to thermal desalination techniques. Antiscalants are used in SWRO to reduce membrane scaling caused by the supersaturation of salts present in feed water. However, to remain effective in reducing membrane scaling, antiscalants should be highly stable and resistant to biological degradation by seawater microorganisms. In this research, several bacteria from Qatar's seawater were isolated and screened for their ability to use antiscalants as a carbon and energy source. The biodiversity of antiscalant degrading seawater bacteria was demonstrated through combining the techniques of MALDI-TOF MS and principle component analysis. It was found that the bacteria isolated from Qatar's seawater such as *H. aquamarina*, *H. elongata*, *P. fragi*, *P. stutzeri* and others can degrade antiscalants and use them as a carbon and energy source. It was observed that the growth rates varied based on the type of antiscalant and the bacteria used. Among the tested strains, *H. aquamarina*, which is also known for its potential to cause biofouling, demonstrated the highest growth rates in antiscalants media. Thus, it was concluded that there is wide variety of bacteria in Qatar's seawater that can biodegrade the antiscalants; reducing their efficiency to combat membrane scaling. Since, these antiscalants will be used as a source of carbon and energy, microbial growth will increase resulting in enhanced membrane biofouling in SWRO.

© 2018 Elsevier B.V. All rights reserved.

#### 1. Introduction

As per the recent estimates of WHO (WHO UNICEF Joint monitoring program, 2017), one in every 10 individuals do not have access to clean

\* Corresponding author.

E-mail address: [mohammad.althouthi@qu.edu.qa](mailto:mohammad.althouthi@qu.edu.qa) (M.A. Al-Ghouthi).



## Evaluating the effect of antiscalants on membrane biofouling using FTIR and multivariate analysis

Mohammad Y. Ashfaq<sup>a</sup>, Mohammad A. Al-Ghouti<sup>a</sup>, Hazim Qiblawey<sup>b</sup> and Nabil Zouari<sup>a</sup>

<sup>a</sup>Department of Biological and Environmental Sciences, College of Arts and Sciences, Qatar University, Doha, Qatar; <sup>b</sup>Department of Chemical Engineering, College of Engineering, Qatar University, Doha, Qatar

### ABSTRACT

A combination of Fourier-transform infrared (FTIR) spectroscopy, multivariate analysis and conventional microbiological assays were utilized to characterize and differentiate membrane biofouling formed in the presence of antiscalants. Based on the FTIR spectra of biofouled reverse osmosis membranes obtained after incubating with antiscalants and *H. aquamarina* (as model microorganism), it was found that the biofouling intensity and composition was dependent on the type of antiscalants used. The growth of the bacterium was also highly affected by the type of antiscalants as shown by the colony forming unit (CFU) counts. By combining the techniques of principle component analysis (PCA) and FTIR, it was demonstrated that the biofouling was more intense and composed of proteins, polysaccharides and lipids, when polymer antiscalant was used. By applying PCA-FTIR with CFU counts, faster prediction of the effect of antiscalants on biofouling was made possible.

### ARTICLE HISTORY

Received 31 July 2018  
Accepted 3 December 2018

### KEYWORDS

Fourier-transform infrared (FTIR); principle component analysis; membrane deterioration; conventional microbiological assays; antiscalants; membrane biofouling

### Introduction

The membrane filtration technique is being adopted worldwide as an environmentally friendly and energy efficient technique in the desalination industry as compared to thermal desalination techniques (Tang et al. 2009, 2011; Sun et al. 2016). However, the performance of membranes, which includes permeate flux and rejection, is affected by the membrane fouling and scaling. To prevent mineral scaling on reverse osmosis (RO) membranes, antiscalants are added to suppress mineral scale formation. The most common antiscalants for calcium sulfate (CaSO<sub>4</sub>) include phosphonates and organic polymers (Shih et al. 2006). In RO systems, phosphonates, however, tend to hydrolyze to orthophosphate and react with calcium ions to form calcium orthophosphate, which is insoluble (Antony et al. 2011). Therefore, most of the commercial antiscalants for RO membranes are organic polymer-based chemicals, such as poly acrylic acid (PAA), polymethacrylic acid (PMAA), and poly maleic acid (PMA).

The use of polymer-based inhibitors has shown satisfactory performance in preventing membrane scaling (Shih et al. 2006). However, little research has been performed on their biodegradability. Due to the

presence of microorganisms in seawater, these antiscalants may act as an energy/carbon source and their biodegradation will not only reduce their efficiency to control membrane scaling, but they will also become a source of enhanced microbial growth causing membrane biofouling. In preliminary research, the strain of *Halomonas aquamarina* was isolated from Arabian Gulf seawater and identified using the matrix assisted laser desorption ionization – time of flight mass spectrometry (MALDI-TOF MS) technique. The strain was identified with a score of 2.02, which is interpreted as reliable at genus level identification and probable species level identification as per the manufacturer's (Bruker Daltonics, Bremen, Germany) instructions. The strain was tested for the ability to use antiscalants as a carbon/energy source by providing growth medium containing only one of the target antiscalants as a carbon source. The antiscalants focused on the included monomers of acrylic and maleic acids and PAA. It was found that *H. aquamarina* was able to grow in an antiscalant containing medium with specific growth rates (h<sup>-1</sup>) of 0.076 (acrylic acid; AA), 0.088 (maleic acid; MA) and 0.115 (PAA), which indicated that the strain was able to use these antiscalants as a carbon/energy source for its growth. Furthermore, it has also been shown in the

## APPENDIX D: PUBLICATIONS FROM OBJECTIVE 3

Journal of Environmental Chemical Engineering 8 (2020) 103963



Contents lists available at ScienceDirect

Journal of Environmental Chemical Engineering

journal homepage: [www.elsevier.com/locate/jece](http://www.elsevier.com/locate/jece)



### Investigating the microorganisms-calcium sulfate interaction in reverse osmosis systems using SEM-EDX technique



Mohammad Y. Ashfaq, Mohammad A. Al-Ghouthi\*, Zulfa A. Al Disi, Nabil Zouari

Department of Biological and Environmental Sciences, College of Arts and Sciences, Qatar University, Doha, P.O. Box: 2713, Qatar

#### ARTICLE INFO

Editor: Yunho Lee

#### Keywords:

Reverse osmosis  
Microorganisms  
Calcium sulfate  
Biofouling  
Scaling

#### ABSTRACT

Membrane fouling affects the performance of membrane technologies such as reverse osmosis (RO), in water treatments and desalination industries. The membrane fouling is a multifaceted phenomenon and various components of feedwater like organic and inorganic substances, and microorganisms interact with each other to further complicate and intensify the membrane fouling. In this research, the interaction between microorganisms and calcium sulfate (mineral chosen as a model scaling) was investigated. Using scanning electron microscopy – energy dispersive x-ray (SEM-EDX) technique, it was found that the variety of microorganisms present in seawater were able to form calcium sulfate crystals on the RO membrane, although no precipitation occurred under abiotic conditions (i.e. in control samples). The results of SEM-EDX were further confirmed by quantitative analysis of precipitation through ion chromatography (IC) technique, and it was found that the concentration of calcium ions remaining in the bacteria-containing medium was significantly lower than that of controls at 95 % confidence level. Furthermore, the kinetics of biomineralization and the effect of different concentrations of calcium and sulfate ions was investigated. It was found that the bacteria were able to form needle-like crystals even at the lowest concentration ( $\text{Ca}^{2+} = 20 \text{ mM}$ ) and at the lowest incubation times (i.e. 1 day) studied. On the other hand, the effect of calcium ions on bacterial growth was also investigated and it was noted that the presence of ions resulted in a statistically significant increase in growth rates of bacteria, showing their potential to enhance biofouling rates.

#### 1. Introduction

Water shortage is one of the major challenges in many countries and it is now further exacerbated because of increased population and economic growth [1]. In countries like Qatar, the growth in the gross domestic product (GDP) has strengthened the economy and has ultimately improved the income of the inhabitants but with the increase in income, the expenses of resource utilization and consumption have also increased putting stress on already limited natural resources such as water resources, aggravating water scarcity issues [1]. Membrane technology (seawater reverse osmosis, SWRO) is one of the most favorable techniques to produce clean water and is recommended for the desalination industry as compared to the thermal technology, owing to its better environmental and economic footprint [1]. Besides SWRO, Microbial fuel cell (MFC) is another advanced technology that can be used for water and wastewater treatment. Nevertheless, membrane fouling of RO and proton exchange membranes (like Nafion or clayware membranes [2]) in MFCs has affected the widespread application of membranes in the water treatment industry. Membrane fouling is a

complicated phenomenon governed by different mechanisms and gets affected by various factors, parameters, and feedwater compositions. It is broadly divided into four major types based on the type of foulants i.e. biofouling (caused by attachment and subsequent growth of microorganisms mediated by extracellular polymeric substance ‘EPS’), inorganic fouling or scaling (caused by salts such as calcium carbonates and sulfates), organic fouling (organics constituents like humic acid, alginates) and colloidal fouling (suspended matter) [3].

Most of the researches targets towards investigating one of the fouling types. However, it should be noted that all types of foulants i.e. organic/inorganic/microbial/colloidal are present in the feedwater. Therefore, it is important to investigate the foulant-foulant interactions and how they both affect the severity of membrane fouling. For example, it has been noted that the presence of organic macromolecules enhances the membrane scaling by shortening the nucleation time and increasing the flux decline [4]. Moreover, microorganisms present on the RO membrane surface do not only cause biofouling but also secrete carbohydrates and EPS, which in turn enhance the organic fouling. Indeed, 60 % of the constituents in the biofilm were found to be organic

\* Corresponding author.

E-mail address: [mohammad.alghouthi@qu.edu.qa](mailto:mohammad.alghouthi@qu.edu.qa) (M.A. Al-Ghouthi).

<https://doi.org/10.1016/j.jece.2020.103963>

Received 3 December 2019; Received in revised form 14 April 2020; Accepted 16 April 2020

Available online 21 April 2020

2213-3437/ © 2020 Elsevier Ltd. All rights reserved.



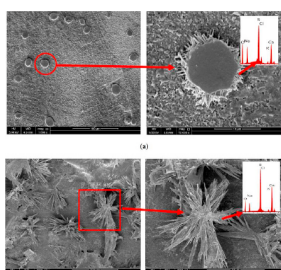
## Interaction of seawater microorganisms with scalants and antiscalants in reverse osmosis systems



Mohammad Yousaf Ashfaq, Mohammad A. Al-Ghouti<sup>\*</sup>, Zulfa A. Al Disi, Nabil Zouari

Department of Biological and Environmental Science, College of Arts and Sciences, – Qatar University, P.O. Box 2713, Doha, Qatar

### GRAPHICAL ABSTRACT



### ARTICLE INFO

**Keywords:**  
Biofouling  
Scaling  
Reverse osmosis  
Microorganisms  
Foulant-foulant interactions

### ABSTRACT

In this research, the interactions of seawater microorganisms with scalants (minerals like calcium sulfate) and antiscalants in the reverse osmosis (RO) systems were investigated. The interaction of seawater microorganisms with antiscalants was investigated by measuring the growth of bacteria in an antiscalant containing growth medium, which was added as a sole source of carbon and energy. Moreover, the interaction of microorganism with calcium sulfate (selected as a model scalant) was also investigated using scanning electron microscopy – energy dispersive x-ray spectroscopic technique. It was found that several *Pseudomonas* strains isolated from the marine water of Qatar are capable of using antiscalants as an energy or carbon source. It was noted that the growth curves of the strains vary with the type of the antiscalant studied. Furthermore, the results of microorganism-scalant interaction showed that the presence of bacteria induced/mediated precipitation of calcium sulfate on the RO membranes, whereas, no precipitation was noted on the control RO membranes (i.e. without bacteria) under the studied conditions. Therefore, the results of this research showed that the presence of microorganisms in seawater reverse osmosis not only causes biofouling but also enhances mineral scaling through biodegradation of antiscalants and precipitation of minerals (calcium sulfate).

### 1. Introduction

In desalination industry, the membrane filtration technique is being prioritized over thermal desalination technique owing to its

environmental friendliness and energy efficiency [1,2]. Nevertheless, the membrane fouling is affecting the performance and treatment efficiency of membrane filtration technique. There are different types of membrane fouling depending upon the nature of foulant such as

<sup>\*</sup> Corresponding author.

E-mail address: [mohammad.alghouti@qu.edu.qa](mailto:mohammad.alghouti@qu.edu.qa) (M.A. Al-Ghouti).

<https://doi.org/10.1016/j.desal.2020.114480>

Received 24 January 2020; Received in revised form 31 March 2020; Accepted 18 April 2020  
0011-9164/ © 2020 Elsevier B.V. All rights reserved.